Intertidal Areas as Accommodation Space for Suspended Sediments Case Study: Scheldt Estuary

Maede Gazor

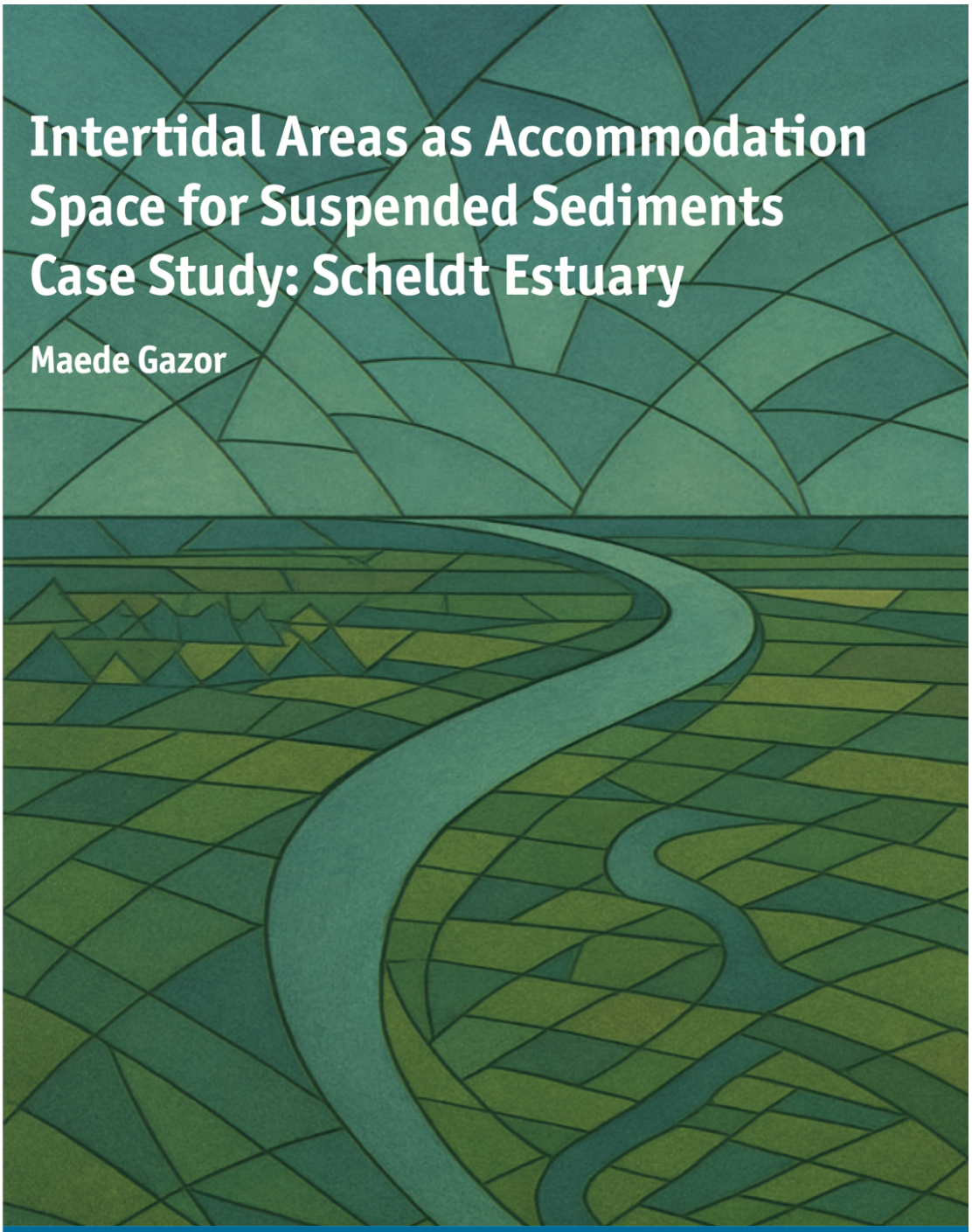

Supervisor **Prof. Dr. Patrick Meire**

Thesis submitted for the degree of Doctor of Science: Biology
Faculty of Science | Antwerp, 2025

University of Antwerp

FACULTY OF SCIENCE

DEPARTMENT OF BIOLOGY

Intertidal Areas as Accommodation Space for Suspended Sediments Case Study: Scheldt Estuary

Thesis submitted for the degree of
Doctor of Science: Biology
at the University of Antwerp to be defended by

Maede Gazor

Prof. Dr. Patrick Meire *Antwerpen, 2025*

Members of the doctoral committee:

Prof. dr. Patrick Meire	*University of Antwerp, promotor*

Independent members:

Prof. dr. Gudrun De Boeck	*University of Antwerp, chairwoman*
Prof. dr. Michael Fettweis	*Royal Belgian Institute of Natural Sciences*
Prof. dr. Ronny Blust	*University of Antwerp*
Prof. dr. Jonas Schoelynck	*University of Antwerp*

External members:

Prof. dr. ir. Ann Griensven	*Vrije Universiteit Brussel*
Prof. dr. Steve Mitchell	*University of Portsmouth*

Internal defense: 31 March 2025

Public defense: 19 June 2025

Contents

Summary

Estuaries are among the most dynamic and ecologically valuable environments, shaped by the interplay of hydrodynamics, sediment transport, and biological processes. These systems act as natural buffers between land and sea, supporting biodiversity, regulating water quality, and providing crucial ecosystem services such as flood mitigation. Sediment dynamics are essential for the ecological health and functioning of estuarine systems, influencing water quality, habitat stability, and nutrient cycling. Intertidal zones play a central role in these processes by providing critical habitats and facilitating the natural filtration of pollutants. They also serve as primary sites of carbon sequestration through the accumulation of organic-rich sediments and vegetation. However, their ability to retain sediment and maintain estuarine stability is increasingly threatened by human activities (e.g., dredging, embankments, land reclamation) and global environmental changes such as sea-level rise (SLR). Understanding whether intertidal zones function as accommodation spaces where sediments settle and stabilize, or as areas prone to frequent sediment resuspension, is crucial for effective estuary management.

The Scheldt estuary, a dynamic and complex system, faces significant challenges due to high suspended particulate matter (SPM), driven by both natural processes and human activities, which impact its ecological functions. This thesis investigates whether the estuary's intertidal zones serve as effective accommodation spaces for SPM. To achieve this, a structured approach is adopted, integrating high-resolution field observations with machine learning (ML) models to analyze sediment behavior under present and future conditions. Each chapter builds on the previous one, linking empirical data, predictive modeling, and scenario-based projections to enhance understanding of estuarine sedimentation.

The primary goal was to assess spatial and temporal variations in sedimentation and erosion. To do so, a field study is conducted at three sites representing different salinity zones of the Scheldt estuary: Branst (freshwater), Lillo (brackish), and Zuidgors (saline). The results indicate that the ability of intertidal zones in the Scheldt to function as accommodation spaces for SPM is not uniform across the estuary and cannot be generalized. Instead, it is shaped by the composition and stability of flocs, which are influenced by seasonal variations in biological activity and hydrodynamic conditions that differ not only between zones but also across seasons. For instance, at Branst, significant seasonal variability is observed, with sedimentation occurring in autumn and spring and erosion dominating in summer and winter. Notably, significant erosion during summer is unexpected, as lower energy conditions and increased biological activity would typically favor

sedimentation. Despite the presence of larger flocs, their apparent susceptibility to resuspension suggests that other factors influenced sediment stability. This variability indicates that while Branst can temporarily accommodate sediments, its role as a stable accommodation space is inconsistent and highly dependent on seasonal factors. In Lillo, sediment dynamics remained relatively stable, with sediment retention governed by floc formation and stability. In Zuidgors, sediment dynamics were primarily controlled by the formation of stable flocs, which resisted resuspension even under high-energy conditions. However, in winter, increased erosion was likely driven by slight increases in tidal energy and reduced biological activity, which limited the formation of larger, more stable flocs. These findings underscore the need for a nuanced, site-specific approach to sediment management in the Scheldt estuary.

This high degree of spatial and temporal variability highlights the challenges of predicting sediment dynamics using traditional modeling approaches. Conventional hydrodynamic and sediment transport models often struggle to capture these dynamics due to their reliance on predefined equations and simplifying assumptions. To address these limitations, ML techniques—specifically Random Forest (RF) and Artificial Neural Networks (ANN)— were applied due to their ability to handle high-dimensional datasets and capturing complex, nonlinear patterns. These models accounted for temporal fluctuations and site-specific conditions, providing valuable insights into the drivers of sedimentation and erosion, consistent with this study 's primary findings and previous research. The results demonstrated that RF models effectively captured nonlinear dependencies, while ANN models provided deeper insight into temporal fluctuations. These findings highlight the potential of ML in estuarine research, offering a robust, data-driven approach to understanding sediment behavior.

Building on these findings, the influence of changing tidal dynamics on sedimentation and erosion patterns in the Scheldt estuary is further evaluated. Historically, dredging and channel deepening have contributed to tidal range amplification in upstream reaches while enhancing energy dissipation downstream, thereby modifying sediment transport processes across the system. Projected increases in tidal range are expected to intensify these effects by altering tidal resonance, reinforcing ebb dominance, and promoting sediment export, turbidity, and overall system instability. In light of these anticipated shifts, the ability to reliably predict future sediment behavior is critical for informed estuarine management. To address this challenge, ML models were implemented to assess sediment stability by projecting key parameters—tidal range, SPM concentration, and floc size—based on empirical relationships observed under varying tidal amplification scenarios. The results demonstrated that the models effectively captured the nonlinear interactions governing sediment dynamics, with spatially and seasonally differentiated responses that aligned with both field measurements and historical patterns. Moreover, it is

concluded that while ML models do not replace physics-based process models, they can offer a valuable data-driven framework for identifying dominant controls on sediment behavior and for detecting zones of elevated vulnerability within estuarine systems.

Together, these chapters present a framework for understanding estuarine sediment dynamics, from empirical observations to predictive modeling and scenario analysis. This research underscores the importance of viewing intertidal accommodation space as a dynamic and context-dependent process rather than a fixed attribute. While SPM concentration plays a role, intertidal stability is ultimately governed by the interplay of hydrodynamics, biological processes, and floc properties. By integrating field data with ML models, this study offers a valuable approach for predicting and managing sediment behavior under changing environmental conditions. Moving forward, long-term monitoring and refinement of predictive models will be essential for sustainable estuarine management in the face of ongoing environmental change.

Chapter 1
Introduction

1.1. Estuarine Dynamics

An estuary is a dynamic, semi-enclosed coastal area where freshwater from rivers and streams merges with oceanic saltwater, establishing a salinity gradient that is crucial for diverse biological communities. This transitional environment supports complex food webs and acts as a critical nursery for numerous species (Nienhuis, 1993; Pasquaud et al., 2007). Estuaries are divided into various zones, each playing a specific role in the overall ecological balance. Firstly, the supratidal zone, typically dry except during high spring tides or storms, supports species adapted to specific environments. The subtidal zone, which remains constantly submerged, offers a stable habitat for aquatic life forms such as fish, benthos and submerged plants. In between, the intertidal zone experiences regular cycles of aerial exposure and flooding due to tidal movements and is noted for its high productivity and ecological diversity. This zone providing breeding and feeding grounds for migratory birds, fish, and marine invertebrates (Stark et al., 2017; Doeke, 2019; Kon et al., 2020).

Intertidal areas contribute significantly to ecological balance by offering services such as flood control (Hammersmark et al., 2005; Maris et al., 2007; Smolders et al., 2015; Reed et al., 2018), water purification (Middelburg et al., 1995; Damme et al., 2005; Marcovecchio et al., 2021), and carbon sequestration (Chmura et al., 2003; Van de Broek et al., 2018). They also dissipate wave energy, trap nutrients, and act as natural buffers, mitigating the effects of storms and sea-level rise by attenuating storm surges and managing river discharge (Walles et al., 2019; Leuven et al., 2019; Huismans et al., 2022).

The dynamics of sediments in intertidal zones are crucial for determining patterns of erosion and deposition, which in turn significantly influence the availability of habitat spaces essential for ecological processes (Wood & Armitage, 1997; Bergen et al., 2001). This sediment dynamic is shaped by both abiotic factors such as tidal currents, grain size and compaction, and biotic processes including floc formation, vegetation growth and decay, all of which are integral to the structural and functional integrity of estuarine ecosystems. This dynamic interplay enhances their resilience and ability to adapt to environmental changes (Chapman & Blockley, 2009; Grabowski et al., 2011; Land et al., 2012).

The multivariate juxtapositions of this interplay between sediment movement and ecological processes can have significant effects on the environment. For instance, it can set the stage for a phenomenon called the Estuarine Turbidity Maximum (ETM), where suspended sediments reach their highest concentration in estuaries. ETM, a naturally occurring pelagic habitat enabled by the

interaction between riverine and marine sediments, salinity, and tidal movements, is vital for nutrient cycling and the functioning of estuarine ecosystems. However, human activities such as dredging, dam construction, and land-use changes can intensify or disrupt ETM dynamics. These alterations may lead to excessive turbidity, reduced light penetration, and degraded water quality, severely hampering primary productivity and altering benthic habitats. Such disruptions ultimately threaten the health and function of the estuarine ecosystem (Chen et al., 2005; Burchard et al., 2018; De Neve et al., 2020). In addition, tidal actions not only facilitate physical mixing but also modulate ecological interactions within estuaries, affecting everything from sediment deposition to the distribution of juvenile fish and invertebrates (Becker et al., 2013; Azhikodan & Yokoyama, 2018).

Normally, these variables can find a natural balance and co-evolve. However, estuaries are also areas where a significant portion of human civilization—with all its environmental impact—is situated, increasing and complicating this multivariate co-evolution and potentially disrupting the balance. Estuaries face increasing degradation from overexploitation, habitat fragmentation, and pollution. Traditional forms of overfishing and unsustainable aquaculture practices not only deplete key species but also disrupt food webs and damage natural habitats, which are vital for the reproduction and early development of marine and estuarine organisms (Van den Bergh et al., 2005; Nichols et al., 2019). More recently, land development and urbanization have contributed to habitat fragmentation, disrupting species migration and the maintenance of genetic diversity (Lai et al., 2015; Fowles et al., 2018). Even more disruptive are embankments, dredging, and harbor constructions, which significantly reshape water and sediment flows, increase turbidity, and alter natural sediment dynamics, thus transforming estuarine morphology (Lesourd et al., 2001; Collins & Miller, 2012; Xu & You, 2017). Although the environmental effects of human activities cannot be entirely prevented, a detailed understanding of how to manage natural balances and maintain sustainability in critical estuaries can be developed. Moreover, climate change introduces new, impactful variables to this domain, significantly complicating the picture and making it difficult to develop an enduring, dependable, and trustworthy understanding that can serve as a long-term basis for estuary management. Specifically, sea level rise imposes additional stressors together with increasing water temperatures and altering precipitation regimes. These changes may increase the frequency and intensity of extreme weather events such as storms and floods. Consequently, enhanced erosion and sediment redistribution occur, critically impacting the dynamics within estuarine intertidal zones. These alterations also shift ecological thresholds and cause species displacement or loss in these zones (Reed, 1995; Fagherazzi et al., 2012). Another threat is pollution caused by agricultural runoff, industrial discharges, and urban wastewater, which leads to eutrophication and degrades water quality (van

der Zee et al., 2007; Brion et al., 2008; Du Laing et al., 2009). Therefore, the cumulative impact of these pressures underscores the need for proactive management and conservation strategies that emphasize the restoration of natural flows and habitats while mitigating anthropogenic stressors (Meire et al., 2005; Winterwerp et al., 2013).

1.2. Sediment Dynamics

Understanding sediment dynamics in estuarine ecosystems is crucial for comprehending how these environments function and respond to natural and anthropogenic changes. Central to these dynamics is the behavior of suspended particulate matter (SPM), a complex mixture of organic and inorganic particles that enter the estuary from sources such as river runoff, tidal action, and biological activity—such as phytoplankton growth and decomposition—within the estuary itself. The physical characteristics of SPM, such as size, shape, and density, along with processes like flocculation, determine whether these particles remain suspended in the water column or settle to form sediments on the estuary floor. This interaction significantly influences the estuary's water quality by affecting light penetration, nutrient and contaminant transport, and overall ecological health (Chen et al., 2005; Burchard et al., 2018).

A key process in the behavior of SPM within estuarine environments is flocculation, in which smaller particles aggregate into larger clusters known as flocs. This process is influenced by physical forces such as Brownian motion and fluid shear, as well as chemical interactions involving ions and organic polymers (McCave, 1984; Partheniades, 1993; Dyer & Manning, 1999). Flocculation is significant for sediment stability because larger flocs settle more quickly, contributing to the formation of stable sediment beds, especially in areas with low hydrodynamic energy. However, the stability of flocs is highly dependent on environmental conditions; while low turbulence promotes floc growth and enhances sedimentation, increased turbulence can disrupt flocs, preventing them from settling and increasing water turbidity (Dyer & Manning, 1999). As shown in Figure 1.1, these processes continuously affect sediment deposition, resuspension, and erosion.

Biological processes further modify floc behavior. In the benthic environment (sediment surface (e.g., seabed or riverbed)), microphytobenthos produce extracellular polymeric substances (EPS) that bind sediment particles together, forming cohesive biofilms. These biofilms contribute to sediment stabilization by reducing erodibility and promoting bed consolidation. In the water column (pelagic zone), phytoplankton release dissolved organic matter that is microbially transformed into transparent exopolymer particles (TEP)—a sticky, particulate subclass of EPS

that forms spontaneously in the water column. TEP plays a direct role in flocculation by aggregating suspended particles into larger, cohesive flocs (Passow, 2002). These biologically mediated processes influence the composition, size, and stability of flocs, affecting both sediment stability and transport dynamics (de Brouwer et al., 2002; Lubarsky et al., 2010; Lai et al., 2018). However, bioturbation—disturbances caused by benthic organisms—can counteract these stabilizing effects by breaking apart biofilms and flocs, loosening sediments, and making them more susceptible to erosion by hydrodynamic forces (de Brouwer et al., 2000; Widdows et al., 2004). This dynamic interplay between biological and physical processes regulates the balance between erosion, deposition, and resuspension (Droppo et al., 2000; Mikeš & Manning, 2010).

Environmental drivers such as salinity and temperature also play critical roles in flocculation. Salinity influences particle surface charge, ionic strength, and the transformation and stickiness of exopolymeric substances (particularly TEP) by altering electrostatic interactions and polymer bridging—factors that are essential to floc formation in the water column (Van Leussen, 1994; Droppo et al., 2005; Manning et al., 2010). Typically, flocculation is enhanced at moderate salinities but suppressed under very low or high salinity conditions. Temperature, in turn, affects both the viscosity of water and the biological activity underlying EPS and TEP production. Lower temperatures reduce microbial metabolism and exudation, weakening floc cohesion and slowing sedimentation rates. Warmer temperatures, by contrast, can stimulate TEP production and strengthen floc structure—provided turbulence does not exceed thresholds that destabilize flocs (Winterwerp et al., 2006; Mietta et al., 2009).

The formation and disruption of flocs not only govern short-term sediment transport but also shape the long-term morphological evolution of estuarine landscapes (Wang et al., 2013). Erosion and resuspension, driven by tidal currents and wave energy, continually reshape the estuary's physical framework. These hydrodynamic forces exert shear stress on the sediment bed, dislodging particles and reintroducing them into the water column. In more energetic zones, this results in increased erosion and resuspension, while calmer areas support deposition. Such dynamics influence channel formation, bank erosion, and habitat distribution (Widdows et al., 2004; Grabowski et al., 2011; Winterwerp et al., 2013; Schepers et al., 2018).

SPM distribution in estuaries also displays strong vertical and lateral gradients, shaped by hydrodynamic and morphological factors. Vertically, concentrations tend to increase near the bed due to gravitational settling, flocculation activity, and near-bed turbulence (Fettweis et al., 1998; Uncles et al., 2006). The extent of vertical mixing—controlled by tidal forcing and local shear—determines the suspension of different particle types: coarser particles are mobilized during high-energy events, while finer flocs dominate under calmer conditions. Laterally, SPM concentrations

vary across the estuarine width due to differences in bathymetry, channel structure, and secondary circulation. Elevated SPM levels often occur over shoals and channel margins, where slower flows allow deposition and floc growth, while deeper channels experience more active sediment turnover due to intensified flow and entrainment (Dyer, 1987; Chen et al., 2005).

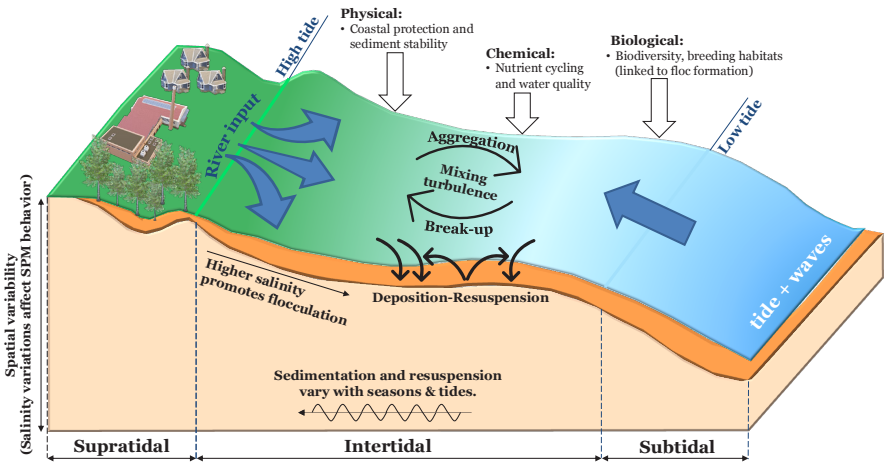

Figure 1.1: This illustration depicts the complex interactions driving sediment dynamics in estuarine environments. Physical forces such as tidal currents, wave action, and erosion shape sediment transport and resuspension. Chemical processes like nutrient recycling influence sediment composition, while biological activity—including microbial production of sticky substances and benthic organism behavior—further modulates sediment stability. Flocculation emerges as a key process influenced by the combined effects of these physical, chemical, and biological factors. Intertidal zones are shown to respond to both short-term (tidal) fluctuations and longer-term (seasonal) changes, affecting their role in estuarine sediment retention and morphology.

Importantly, human interventions such as dredging significantly influence sediment dynamics by altering both vertical mixing and bed composition. Channel deepening and smoothing of bed topography can increase tidal penetration but simultaneously reduce near-bed turbulence. This change promotes stratification within the water column, which shifts the balance from resuspension toward net deposition. Understanding how these spatial patterns are modified by dredging is essential for interpreting SPM dynamics and for assessing sediment retention capacity in intertidal accommodation zones.

Therefore, effectively managing sediment dynamics in estuarine environments requires a deep understanding of the physical processes governing sedimentation-resuspension cycles. Specifically, knowledge of flocculation and settling behavior in estuarine settings is essential for

maintaining the ecological health of estuaries and ensuring that these environments continue to provide the ecosystem services on which both human and natural communities depend.

1.3. Introduction to the Scheldt Estuary

The Scheldt estuary, a 160 km long funnel-shaped system, extends through parts of Belgium and the Netherlands (Figure 1.2) and is heavily influenced by both natural forces and human activities. It is characterized by strong tidal forces and relatively low freshwater discharge, allowing it to support a diverse range of species within a well-mixed environment (Baeyens et al., 1998; Meire et al., 2005). The estuary's hydrodynamics are shaped by the interplay of tidal forces, seasonal freshwater discharge, and estuarine circulation, which result in significant tidal ranges and dynamic sediment transport and deposition. Specifically, tidal ranges vary from approximately 3.7 m at Vlissingen to 5.4 m at Tielrode, and 2.6 m at Melle, located 150 km from the estuary's mouth (Waterinfo.be, 2019; Wang et al., 2019). Additionally, salinity varies along the estuary as saline water from the North Sea mixes with freshwater from rivers. Freshwater discharge in 2018–2019 exhibited distinct seasonality, averaging 41.58 m^3/s in summer, 96.8 m^3/s in winter, 86.25 m^3/s in spring, and 44.74 m^3/s in autumn (Waterinfo.be, 2019). Furthermore, the annual input of SPM at the upstream boundary ranged from 10^4 to 10^5 tons, correlating with freshwater discharge (Plancke et al., 2017; Dijkstra et al., 2019).

The Scheldt estuary is also one of Europe's most heavily impacted estuaries in terms of organic and chemical pollution, due to centuries of intensive industrial and agricultural use (Damme et al., 2005; Van Ael, Evy, et al., 2012). These environmental pressures have led to extensive human interventions, including dredging, land reclamation, and the construction of flood defenses, which have significantly altered the estuary's morphology (Meire et al., 2005; Dam et al., 2016; Winterwerp et al., 2013). During 2018–2019, dredging and dumping volumes in the Western Scheldt totaled approximately 9.3 Mm^3 per year, while in the Lower Sea Scheldt, around 4.7 Mm^3 per year were dredged, of which 3.4 Mm^3 consisted of mud. While these activities maintain navigable channels and reduce flood risks, the disposal of dredged material back into the estuary, particularly the fine sediments, contributes to elevated SPM loads (Plancke et al., 2017; Cox et al., 2019). Specifically, data from 2001 to 2015 show that dumping activities at km 73 and 78 in the Scheldt estuary introduced fine sediment at average rates of 60.5 and 98.5 kg/s, respectively, contributing to elevated local SPM concentrations (Dijkstra et al., 2019). This correlation between increased SPM levels and dredging practices has been confirmed by multivariate regression analysis (IMDC, 2016).

Over the past decades, the Scheldt estuary has undergone significant morphological changes due to both natural processes and sustained human intervention, especially dredging. These changes have not been uniformed along the estuary's salinity gradient. As reported in Scheldecommissie et al. (2023), the Western Scheldt—specifically around Zuidgors (Figure 1.2)—experiences natural deepening driven by strong tidal import (flood dominance), accompanied by uneven sediment redistribution that necessitates ongoing dredging to maintain navigable channels. In contrast, Lillo, located in the brackish area, exhibits strong natural sediment accumulation, requiring intensive and continuous dredging to keep channels open, thus creating a delicate, artificial equilibrium. Meanwhile, the freshwater reaches, including Branst, remain relatively self-regulating due to strong ebb currents that naturally flush sediment downstream. However, even here, localized deposition from lateral inputs and upstream transport occasionally requires maintenance dredging. While dredging does not introduce new sediment to the system, it often resuspends fine material already present in the bed, thereby increasing local SPM concentrations.

In parallel, long-term monitoring shows that tidal range has amplified most significantly in the upstream Zeeschelde, where narrowing channels and reduced bed friction—partly from dredging and embankments—have allowed more tidal energy to propagate inland (Scheldecommissie et al., 2023). These long-term shifts in hydrodynamics and morphology provide crucial context for interpreting short-term sedimentation trends, as they influence the estuary's energy balance, sediment transport pathways, and the stability of intertidal accommodation spaces.

1.3.1. Ecosystem Properties

The Scheldt estuary's ecosystem is defined by a complex interplay of physicochemical and ecological factors, particularly the interactions between SPM concentrations and salinity gradients. A pivotal study by Cox et al. (2019) identified a critical regime shift in suspended sediment dynamics around 2008–2009. Drawing on a 20-year dataset of surface SPM concentrations, the study documented an abrupt rise in turbidity and the formation of a new maximum turbidity zone (MTZ) in the freshwater upper Sea Scheldt, particularly during low summer discharges. This shift was not gradual but exhibited threshold-like behavior, including "flickering"—a phenomenon in which the system repeatedly switches between two alternative states— often interpreted as a sign of reduced resilience and an impending transition.

Several interacting factors contributed to this regime shift. Fairway deepening and widening, undertaken to improve navigation to Antwerp, enhanced salt intrusion and increased upstream sediment retention, thereby altering the system's energy balance. Simultaneously, continuous dredging and sediment disposal—the so-called "dredging pump"—likely extended the residence

time of fine sediments, fostering localized accumulation. These physical alterations coincided with long-term improvements in water quality, notably following the upgrade of Brussels' wastewater treatment facilities in 2006 (Brion et al., 2015). Additionally, reductions in nutrient loads from agricultural runoff, industrial discharges, and urban wastewater have contributed to these changes over time. Improved water quality, led to declining ammonium concentrations, increased oxygen levels, altered the abundance and composition of the zooplankton communities, reduced eutrophication, and improved overall ecosystem health.

Crucially, these ecological changes influenced sediment dynamics by modifying organic matter availability, microbial community structure, and bioflocculation processes. As a result, floc properties—such as size, strength, and settling velocity—changed, influencing sediment erodibility and transport patterns (Chen et al., 2005; Winterwerp et al., 2006; Horemans et al., 2021).

Taken together, Cox et al.'s findings underscore how long-term anthropogenic interventions, when combined with ecological recovery, can trigger nonlinear and systemic sediment responses. This highlights the importance of integrating physical and biological feedbacks into estuarine management strategies.

In addition to long-term changes, the estuary also exhibits pronounced seasonal and tidal variability in SPM concentrations. These fluctuations, tightly linked to tidal asymmetry and seasonal discharge, influence sediment dynamics through associated biogeochemical processes—particularly those that regulate sediment aggregation and erodibility (Fettweis et al., 1998; Andersen et al., 2005; Uncles et al., 2006).

Moreover, the Scheldt estuary illustrates the critical role of intertidal flats, which function as key transitional habitats. These flats, varying in sediment composition and elevation, support a wide range of flora and fauna, from benthic microalgae to migratory bird species. They also play an active role in the global carbon cycle by trapping organic matter in their sediments. These areas support plant life and various organisms, and by retaining organic material in their sediments, they help reduce the amount of carbon in the atmosphere. This process connects local ecosystems to the global carbon cycle and plays a role in reducing climate change. However, the amount of carbon these areas can store depends on factors like sediment stability, chemical processes, and the overall health of the ecosystem (Ysebaert et al., 2002; Temmerman et al., 2013).

However, these benefits are increasingly threatened by human activities such as dredging and land reclamation. These interventions have altered hydrodynamics, reduced habitat availability, and changed sediment structure—leading to degraded conditions for species that depend on mudflats and salt marshes for feeding and breeding. Increased turbidity from sediment resuspension

further limits light availability, suppressing primary productivity and altering trophic interactions (Chen et al., 2005; Winterwerp et al., 2013; Cox et al., 2019; Dijkstra et al., 2019).

1.3.2. Sediment Dynamics: Insights from Ems Estuary

Given the backdrop of increasing SPM concentrations, the potential shift toward a hyperturbid state needs to be investigated more thoroughly. To better understand the implications of such a shift, it is instructive to consider the case of the Ems estuary, located in northwest Germany and the Netherlands. This nearby estuary has undergone a transition, providing a relevant and cautionary example. In the case of Ems estuary, excessive sediment loads have led to reduced light penetration and oxygen levels, adversely affecting aquatic life and habitat quality. Notably, suspended sediment loads doubled to tripled between 1954 and 2005 and increased ten times within the turbidity maximum zone over the same period. Additionally, the turbidity maximum has moved 25 km up-estuary and expanded significantly, now extending far into the freshwater zone. This deterioration of light conditions may have reduced total primary production to only 40% compared to the 1950s/1960s (De Jonge et al., 2014).

Further, it has been reported that this regime shift can be attributed to human-induced morphological changes such as embankments and deepening, which have increased hydrodynamics, including tidal amplification and asymmetry, and estuary-upward mud transport (Winterwerp et al., 2013; De Jonge et al., 2014). It is also argued that dredging activities, particularly the removal of some non-erodible bottom layers in the lower reaches of the estuary, may have exposed new internal sources of SPM, rather than increased sediment input from the boundaries. This unstable, fluid bottom-mud layer has reduced bottom friction, thereby increasing hydrodynamic energy propagation in a feedback loop.

Similarly, there are growing concerns that the Scheldt estuary may exhibit early signs of a similar shift toward a hyperturbid state. Evidence of increasing tidal amplification, asymmetry, and recent changes in suspended sediment loads and deposition rates over the last few decades mirror some of the characteristics observed in the Ems estuary (Dijkstra et al., 2019). These changes, driven by underlying morphological alterations, could pose a significant risk to the Scheldt estuary's ecological health if not addressed promptly.

1.3.3. Accommodation Space

In estuarine systems such as the Scheldt, a key challenge lies in understanding the balance between suspended and deposited sediments—specifically, the mechanisms that govern the exchange

between the two. This concept underpins the idea of accommodation space, defined as the volume within the estuary where SPM can settle and be retained. For deposition to occur, local hydrodynamic energy must remain below a critical threshold; otherwise, sediments are re-entrained into the water column. While both subtidal and intertidal areas contribute to accommodation, subtidal zones are generally subject to stronger tidal currents and shear stress, making them more prone to erosion.

Within this context, intertidal zones emerge as especially important. These low-energy environments can act as natural buffers, enhancing sediment retention during periods of elevated SPM concentrations. In such zones, the balance between deposition and resuspension is delicately controlled by multiple factors, including hydrodynamic forcing, sediment composition, biological activity, and flocculation processes. These interactions allow intertidal flats to function as effective sediment sinks and influence the long-term morphological evolution of the estuary.

In the Scheldt estuary, SPM accommodation dynamics are shaped by both natural variability and human interventions. Rising background SPM concentrations have increased the ecological and management relevance of intertidal zones as accommodation spaces. However, their effectiveness is modulated by the estuary's hydrodynamic regime, the physical and biological characteristics of the suspended sediments, and the functional state of benthic communities. Alterations in any of these factors can shift the balance between sedimentation and erosion, particularly in intertidal regions where small-scale changes can have significant system-wide impacts.

Improved understanding of these processes is essential for anticipating how estuarine systems respond to changing boundary conditions, including seasonal variability, anthropogenic disturbance, and future sea-level rise. Despite advances in sediment modeling and monitoring, key knowledge gaps persist—especially regarding the short-term dynamics of flocculation, the site-specific effects of hydrodynamics, and the role of biological feedbacks. Many existing models rely on simplified assumptions or generalized empirical relationships that do not account for temporal variability or spatial heterogeneity across the estuary.

In particular, the role of intertidal zones as accommodation space remains insufficiently resolved, especially under fluctuating environmental conditions. This issue is critical in the Scheldt estuary, where the ecological and economic importance of the system coincides with active morphological change and sustained environmental pressure. Accurate prediction of sediment retention capacity is complicated by seasonal cycles, localized dredging operations, and the projected impacts of climate-induced sea-level rise.

To address these gaps, this study applies a data-driven approach based on high-resolution field observations across multiple estuarine zones and seasons. The aim is to identify where and when

SPM can effectively settle, and to determine how this capacity varies spatially and temporally across the estuary—thereby contributing to a more robust understanding of accommodation space in a dynamic estuarine system.

1.4. Research Approach and Objectives

This thesis employs a three-pronged approach to investigate suspended sediment accommodation in the intertidal zones of the Scheldt estuary.

First, detailed biweekly in situ observations conducted over the course of a year near the waterbed are analyzed to identify the key drivers of deposition-resuspension processes and assess their impact on the estuarine mud balance. Particular attention is given to how sediment dynamics vary across temporal, seasonal, and spatial scales, as emphasized in previous studies, including those by Cloern (1987), Fettweis et al. (1998), Chen et al. (2005), and Bolle et al. (2010). Second, a predictive machine learning model is developed to enhance understanding of sedimentation and erosion processes through observations of bed level changes in these zones. Third, the practical application of this model is demonstrated by implementing scenarios to predict bed level change under future conditions.

The subsequent sections will detail the monitoring campaigns and the methodologies behind the modeling approach.

1.4.1. Monitoring Campaigns in the Scheldt Estuary

This section outlines the specific study sites within the Scheldt estuary and the methods used for data collection. The theoretical findings are applied to this estuary in each chapter; however, the results may also be relevant to other estuaries with comparable characteristics.

From November 2018 to December 2019, continuous high-frequency sensor measurements were carried out during two-week campaigns conducted in each season at three tidal flats in the Scheldt estuary—Branst, Lillo, and Zuidgors. Sediment sampling was performed once during each campaign. These sites were strategically selected based on their positions along the estuary's salinity gradient and are located at varying distances from the Scheldt mouth (105 km, 65 km, and 20 km, respectively), representing the Upper Sea Scheldt, Lower Sea Scheldt, and Western Scheldt zones (Figure 1.2). Each site possesses distinct environmental characteristics, a sufficiently large surface area relative to its zone, and is situated along the main Scheldt channel with an adjacent tidal marsh.

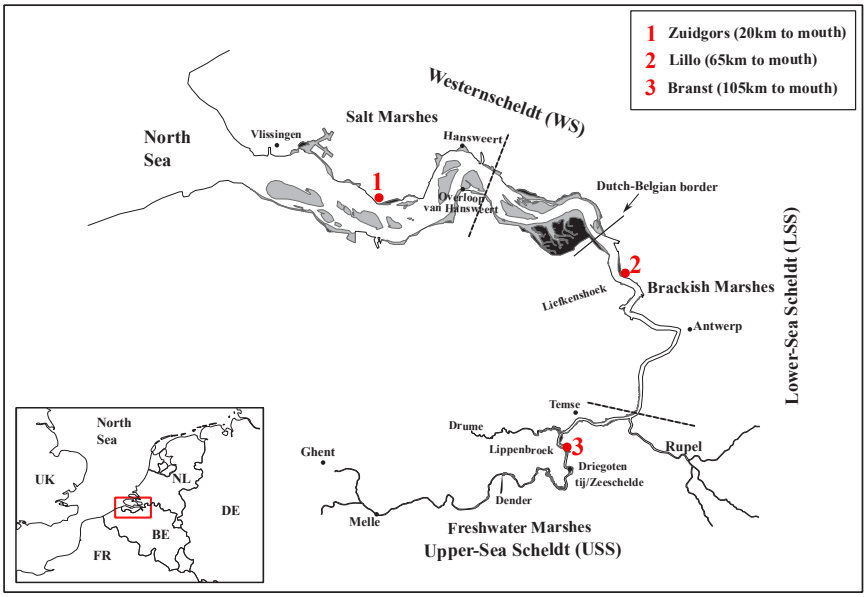

Figure 1.2: Map of the Scheldt estuary showing the main salinity zones and the locations of the three monitoring sites. Dashed lines indicate the approximate boundaries between the salt, brackish, and freshwater zones. The red dots represent the sites where biweekly sampling was conducted over a one-year period. The sites were strategically selected to capture seasonal and spatial variability along the estuarine gradient and were equipped with high-frequency sensors to monitor hydrodynamic and sediment parameters.

Building on the strategic selection of these sites, the specific environmental conditions and setup at each location are examined, as they play a crucial role in shaping the data collection process.

Branst, situated in the freshwater zone, contends with more variable river discharges and higher concentrations of suspended solids. The sampling setup here includes a natural tidal flat in front of a tidal marsh with willow vegetation, located about 10 meters from the marsh edge, on the pronounced slope of the tidal flat. It is the most sheltered of the sites, impacting its wave exposure and turbidity levels. The seasonal variation in sediment properties at Branst is shown in Table 1.1.

Table 1.1: Seasonal sediment properties in Branst, including organic matter content, bulk density, and particle size fractions. "Mud" refers to particles <63 µm, and "Sand" refers to particles in the 63–2000 µm range.

Branst	OM (%)	Bulk Density (g/cm³)	Median Grain Size of primary particles (µm)	Clay (< 2 µm) (%)	Mud (< 63 µm) (%)	Sand (< 2000 µm) (%)
Autumn	4.50 ± 0.40	0.67 ± 0.03	74.00 ± 17.00	5.00 ± 1.00	39.00 ± 8.00	57.00 ± 10.00
Winter	2.50 ± 0.70	0.95 ± 0.10	112.00 ± 6.00	2.00 ± 1.00	14.00 ± 6.00	84.00 ± 7.00
Spring	11.13 ± 12.20	0.75 ± 0.20	77.00 ± 20.00	4.00 ± 1.00	43.00 ± 6.00	52.00 ± 7.00
Summer	2.00 ± 0.80	1.30 ± 0.10	104.00 ± 4.00	2.00 ± 0.50	20.00 ± 3.00	77.00 ± 3.00

Lillo, in the mesohaline zone with a strong salinity gradient, is located in the port area and in front of a de-embanked area. The tidal flat monitored at Lillo is backed by a part of the previous dike, which forms a peninsula after de-embankment. This setup ensures that the outflow of the area does not directly affect the measurements. The instruments at Lillo are positioned approximately 60 m from the marsh edge. This site also features distinct characteristics in terms of wave exposure and turbidity levels. Table 1.2 presents the seasonal variation in sediment properties at Lillo.

Table 1.2: Seasonal sediment properties in Lillo, including organic matter content, bulk density, and particle size fractions. "Mud" refers to particles <63 µm, and "Sand" refers to particles in the 63–2000 µm range.

Branst	OM (%)	Bulk Density (g/cm³)	Median Grain Size of primary particles (µm)	Clay (< 2 µm) (%)	Mud (< 63 µm) (%)	Sand (< 2000 µm) (%)
Autumn	6.40 ± 0.95	0.90 ± 0.076	62.00 ± 18.00	4.00 ± 1.00	45.00 ± 10.00	51.00 ± 11.00
Winter	6.00 ± 4.50	0.95 ± 0.03	72.00 ± 16.00	3.00 ± 2.00	38.00 ± 13.00	59.00 ± 15.00
Spring	7.00 ± 1.50	0.90 ± 0.027	52.00 ± 15.00	4.50 ± 1.00	56.00 ± 18.00	40.00 ± 19.00
Summer	-	-	39.00 ± 9.00	5.00 ± 0.50	60.00 ± 6.00	34.00 ± 6.00

Zuidgors lies in the polyhaline zone facing south-southwest, making it more susceptible to wind and waves from the nearby large water body. Positioned about 200 m from the marsh edge, this site features a natural tidal flat in front of a saltmarsh and is situated in the dynamic multi-channel Western Scheldt, distinct in terms of hydrodynamic and sedimentary processes from the other sites. Seasonal variations in sediment properties at Zuidgors are summarized in Table 1.3.

Table 1.3: Seasonal Sediment Properties in Zuidgors, including organic matter content, bulk density, and particle size fractions. "Mud" refers to particles <63 µm, and "Sand" refers to particles in the 63–2000 µm range.

Branst	OM (%)	Bulk Density (g/cm³)	Median Grain Size of primary particles (µm)	Clay (< 2 µm) (%)	Mud (< 63 µm) (%)	Sand (< 2000 µm) (%)
Autumn	2.70 %	1.40 ± 0.20	187.00 ± 20.00	1.00 ± 0.98	13.00 ± 8.00	86.00 ± 9.00
Winter	1.30 ± 0.30	1.50 ± 0.11	207.00± 11.00	0.02 ± 0.06	1.00 ± 1.90	99.00 ± 2.00
Spring	4.00 ± 3.00	0.80 ± 0.50	204.00 ± 0.85	0.20 ± 0.15	6.00 ± 1.70	94.00 ± 2.00
Summer	2.00 ± 0.80	1.30 ± 0.12	188.00 ± 9.00	0.65 ± 0.60	8.00 ± 4.50	91.00 ± 5.00

For accurate monitoring, instruments at each site were strategically placed at specific heights within the water column, calibrated to the Tweede Algemene Waterpassing (TAW) datum —the official vertical reference system in Belgium that defines elevation relative to mean sea level. Using a standardized reference height such as TAW ensures that vertical measurements are consistent and comparable across sites and time periods. This is essential for accurately assessing elevation-dependent processes such as sedimentation, erosion, and tidal dynamics throughout the estuary. The Universal Transverse Mercator (UTM) coordinates and TAW reference heights for instrument positioning are detailed in Table 1.4.

Table 1.4: Geographical coordinates and instrument heights at the three sampling sites in the Scheldt estuary. UTM coordinates define the precise location of each site, while instrument heights (in m TAW) indicate sensor placement relative to Belgium's official vertical datum. Referencing to TAW ensures consistent elevation measurements across sites, allowing accurate comparisons of sediment and hydrodynamic processes between freshwater (Branst), brackish (Lillo), and saline (Zuidgors) zones.

Site	Easting (m E)	Northing (m N)	Instrument Height (m TAW)
Branst	579876.00	5660607.00	2.68
Lillo	596771.00	5684637.00	2.34
Zuidgors	567064.00	5700831.00	2.39

The primary instruments used in this study include the Optical Backscatter Sensor (OBS) for turbidity, the Acoustic Doppler Velocimeter (ADV) for current velocities and seabed distance, and the Laser In-Situ Scattering and Transmissometry (LISST-200X) for floc size distribution analysis. Water samples collected during biweekly campaigns at high tide were used to calibrate

sensor outputs (OBS) to SPM concentrations. Details of the measurement setup, including instrument specifications, are presented in Chapter 2.

1.4.2. A Suitable Model: Random Forest and Artificial Neural Networks

In the Scheldt estuary, sediment transport has traditionally been studied using physically based numerical models, including WAQUA-DELWAQ, Delft3D, and more recently, SCALDIS. These models integrate hydrodynamic and sediment transport components to simulate erosion, deposition, and cohesive sediment spreading under tidal and meteorological forcing. They have supported sediment management decisions and helped evaluate the impacts of dredging and morphological change (e.g., Mulder & Udink, 1991; Vanlede et al., 2015; Plancke & Vos, 2016).

However, despite their widespread application, these models often rely on simplified process formulations and empirically calibrated parameters, which can limit their accuracy—particularly in capturing site-specific, seasonally variable, and nonlinear interactions, such as those involving flocculation and biological influences. Moreover, their performance may vary across sedimentation- and erosion-dominated zones and typically requires extensive calibration efforts to ensure reliability.

To complement these traditional approaches, the present study utilizes two machine learning (ML) techniques—Random Forest (RF) Regression (Breiman, 2001) and Artificial Neural Networks (ANN) (Rosenblatt, 1958)—to explore sediment dynamics across multiple estuarine zones and seasons. ML models provide a data-driven alternative that excels at uncovering hidden patterns and capturing nonlinear dependencies in high-frequency environmental datasets. They are particularly well-suited to modeling sediment processes where conventional approaches struggle to account for spatial and temporal variability.

Generally speaking, in machine learning models, a set of input variables (features) are used to train a model that predicts an output variable. Given observational data (of data points or instances of features and output values), the model is then trained to learn the relationship between them. The architecture and algorithms for how to train models differ across various ML methods, and each can be better suited for a certain type of data or domain. As a process, after the model is trained, feeding one datapoint (feature vector) of new (previously unseen) input features will lead to a model prediction for that input. Generally, in the process of training the models in ML, one leaves aside a random subset of the data as a “test set”, to later evaluate model performance with, by comparing model predictions to the known measurements.

Some ML methods are used to "classify" output values (categorical values like "rain" or "not rain") or estimate regression values for continuous variables. In a recent surge in Artificial Intelligence (AI), a type of generative models is used to generate images or text. In this work, we needed regression models that can handle large amounts of data, and intricate balances between many variables. Two types of ML methods are most suitable with such criteria: Random Forest Regression and Artificial Neural Networks. In the following section, we describe these models. Both methods are applied in the modeling, and their strengths and shortcomings are compared throughout this thesis.

- **Random Forest Regression (RF)**

The Random Forest (RF) algorithm is a standout in the field of ensemble learning, noted for its accuracy in learning highly variable dynamics with complex dependencies. What distinguishes Random Forest is its method of creating an ensemble of decision trees that are gradually trained using subsets of the data. This approach not only boosts prediction accuracy but also mitigates the risks associated with relying on a single decision tree.

Specifically, as seen in Figure. 1.3, each tree in this ensemble of decision trees is trained on a different bootstrap sample (a randomly selected subset with replacement). Additionally, at each node in a tree, a random subset of features (variables we are learning from) is considered for splitting, which adds diversity among the trees and contributes to the model's overall robustness and accuracy. For regression tasks, the model's output as the final prediction is yielded from averaging the outcomes of all individual trees, thereby increasing result reliability. Performance metrics such as mean absolute error (MAE) and mean square error (MSE) are crucial for evaluating the precision of a Random Forest model, as they measure the discrepancies between predicted values and actual observations.

Another notable feature of Random Forest is its Out-of-Bag (OOB) error estimation, which during training, utilizes unused data from certain trees' training processes as a built-in validation mechanism. This provides an unbiased performance evaluation without needing a separate test set. Moreover, Random Forest models can provide a "feature importance" distribution which shows the relative contribution of each input feature to the training of the model for predicting the output. For this study, we employed the Scikit-Learn Python library for RF Regression, which is a widely available tool and known for its accuracy and compatibility. This facilitated a robust pipeline for model development and testing.

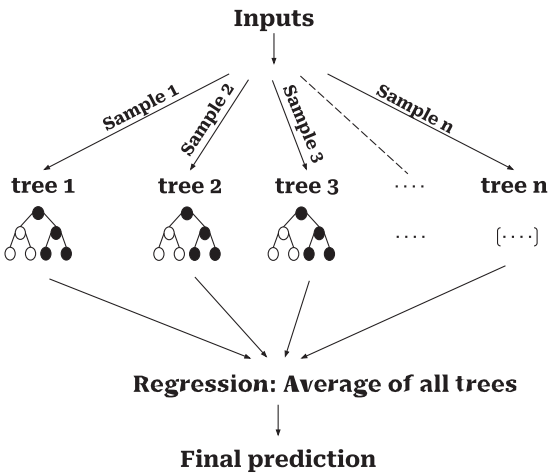

Figure 1.3: Conceptual architecture of the RF model. Input variables are passed through multiple decision trees, each trained on a random subset of the data. The final prediction is obtained by aggregating the outputs of all trees, enhancing model accuracy and reducing overfitting. This ensemble structure allows the model to capture complex nonlinear relationships between environmental drivers and bed level change.

While Random Forest is versatile and highly applicable in fields such as image classification and environmental science, it does have limitations. Though the algorithm manages large, varied datasets well and can be resistant to overfitting, it requires significant computational resources to train. Furthermore, the complexity of multiple decision trees can render the model less transparent and more difficult to interpret. Nonetheless, the insights and predictive power that Random Forest provides into feature importance and its consistent reliability in diverse scenarios make it an invaluable asset in predictive analytics.

- ## Artificial Neural Networks (ANNs)

Artificial Neural Networks (ANNs, also known as “neural networks”), were originally inspired by biological neural networks in the brain, and comprise interconnected nodes or “neurons”. Collectively, neurons process and learn from training data to capture and learn complex functions. Their capacity to adapt to new data makes ANNs particularly effective for deciphering the dynamic and intricate patterns of sediment behavior across various tidal zones and seasonal cycles.

Structurally, ANNs are composed of neurons that each implement a simple function and are connected via edges that have “weights,” which are used in calculating outputs and errors. As seen in Figure. 1.4, each network includes several interconnected layers of nodes: an input layer that

receives data, multiple "hidden" (middle) layers that process data through linear transformations and "activation" functions (such as ReLU, sigmoid, and tanh), and an output layer that delivers a prediction, often using task-specific activation functions.

The network generates output via "forward propagation," where information flows from the input to the output layer, with each connection's weight significantly influencing the calculations. Training occurs over multiple passes or "epochs" of forward propagation, where in each epoch, the network produces a value given the inputs, and an error is calculated based on the difference between the predicted and known output values. Then, during "backward propagation" and using the "gradient descent" algorithm, this error is propagated back through the network to adjust the weights, reducing discrepancies between the network's predictions and actual targets. This training typically spans multiple epochs, with weights continuously updated to enhance performance.

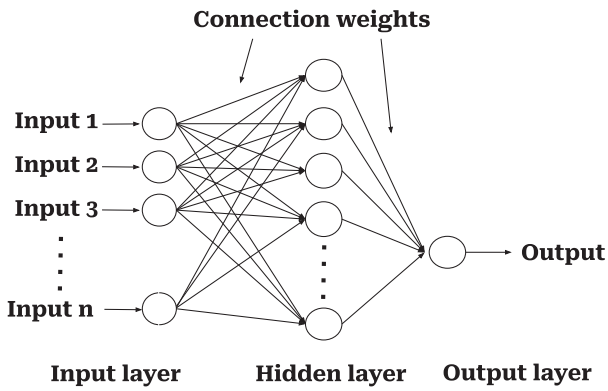

Figure 1.4: Conceptual architecture of the ANN. The model comprises an input layer, one or more hidden layers with interconnected neurons and activation functions, and an output layer that predicts bed level change. The network is trained using backpropagation and iterative weight optimization to capture complex nonlinear relationships between environmental variables and sediment dynamics in the estuarine system.

Despite their strengths, ANNs require extensive training data to effectively model complex relationships. Without ample data, these networks are prone to overfitting and may not generalize well to new scenarios. However, recent advancements have led to exciting developments like Generative Adversarial Networks (GANs) and Variational Autoencoders (VAEs), which excel at creating realistic images and simulations. ANNs have also become invaluable in environmental modeling, predicting climatic patterns, identifying biodiversity hotspots, and simulating

ecosystem interactions. Their ability to process non-linear data and learn from extensive datasets demonstrates their powerful utility in complex fields.

1.4.3. Research Questions and Outline

The primary objective of this study is to examine the influence of hydrodynamic and turbulent factors on the flocculation process in the Scheldt estuary. This process includes the aggregation and settling of suspended particles, as well as the resulting changes in bed level. The study aims to identify the forces that determine whether sediments remain settled or are redistributed within the intertidal zones of the estuary. Understanding these dynamics is essential for predicting bed level changes. The research questions are structured to align with the content of each thesis chapter. An overview of the thesis structure is presented in Figure 1.5.

RQ1. How Do Factors Influencing Deposition-Resuspension Processes Affect Intertidal Areas as Accommodation Spaces?

In Chapter 2 focuses on identifying the primary drivers influencing deposition and resuspension processes within the intertidal zones of the Scheldt estuary, with particular attention to whether these areas function as accommodation spaces for SPM or primarily as zones of frequent sediment resuspension. The analysis centers on the dynamic interactions between hydrodynamic forces and floc characteristics that govern sediment stability and mobility.

High-frequency sensor measurements and biweekly sediment sampling were conducted to investigate intertidal trends at the benthic–pelagic interface across representative tidal mudflats throughout the estuary. The collected data—comprising current velocity, turbulence, SPM concentration, mean floc size, and bed level changes—were analyzed to determine how flocculation processes, influenced by hydrodynamic conditions, affect sediment behavior.

By covering multiple seasons, the study evaluates the influence of temporal variability in floc characteristics, hydrodynamic forces, and SPM concentrations on sediment stability and transport within three distinct estuarine zones: the freshwater site at Branst, the brackish site at Lillo, and the saline site at Zuidgors. This approach aims to provide insights into suspended sediment accommodation, a key factor in managing sediment dynamics that support habitat stability and the ecological functioning of the Scheldt estuary.

Although salinity and temperature were not explicitly included as model input variables, their effects are indirectly captured through the spatial and temporal design of the study. The three

monitoring sites span a natural salinity gradient, and seasonal campaigns reflect temperature variability. These environmental conditions were accounted for during data interpretation, particularly in relation to observed differences in floc size, SPM concentration, and sediment stability across sites and seasons.

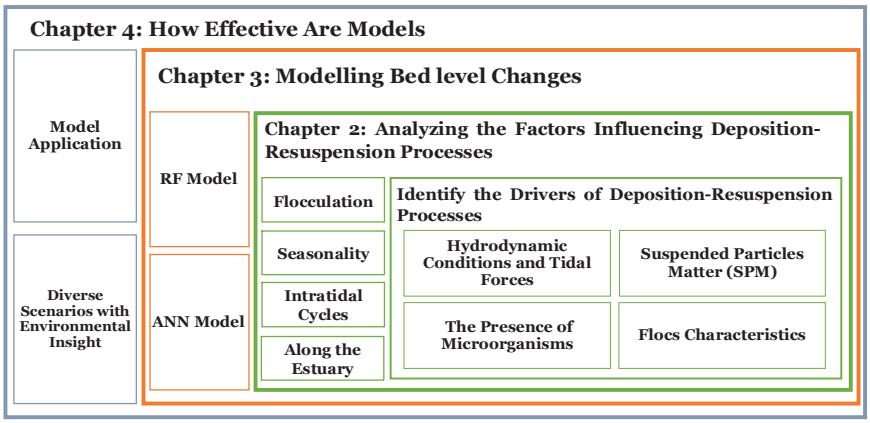

Figure 1.5: Overview of the thesis structure addressing sediment dynamics in the Scheldt estuary. Chapter 2 investigates the drivers of deposition and resuspension in intertidal zones, focusing on how hydrodynamic forces, floc characteristics, and SPM concentrations influence sediment dynamics through flocculation, while accounting for seasonal, temporal, and spatial variability in sediment stability and mobility. Chapter 3 presents the development of machine learning models to evaluate temporal fluctuations in sediment levels. Chapter 4 applies these models to future scenarios, demonstrating their potential for predicting sediment dynamics under varying conditions.

RQ2. Is There a Model to Easily Assess the Relative Impact of Temporal Fluctuations on Bed Level Changes?

Chapter 3 addresses the challenge of modeling time-dependent changes in sediment dynamics, with a particular focus on flocculation processes. Advanced machine learning techniques, including RF Regression and ANN, are applied due to their capacity to handle complex, time-varying environmental data. This approach provides a detailed perspective on sediment behavior under varying temporal conditions. The chapter demonstrates the effectiveness of these modeling techniques in predicting bed level changes, representing a methodological advancement in sediment dynamics research.

RQ3. How Effective Are Models in Predicting Bed Level Changes in Estuaries?

Chapter 4 applies the models developed in Chapter 3 to future scenarios, demonstrating their effectiveness in predicting sediment dynamics under a range of environmental conditions. This application highlights the practical utility of machine learning techniques in forecasting the impacts of factors such as climate change and human activities on sediment behavior. This forward-looking approach supports improved planning and management in intertidal zones and provides a valuable tool for environmental assessment and policy development.

Bibliography

1. Andersen, T. J., Lund-Hansen, L. C., Pejrup, M., Jensen, K. T., & Mouritsen, K. N. (2005). *Biologically induced differences in erodibility and aggregation of subtidal and intertidal sediments: a possible cause for seasonal changes in sediment deposition*. Journal of Marine Systems, 55(3-4), 123-138.
2. Azhikodan, G., & Yokoyama, K. (2018). *Sediment transport and fluid mud layer formation in the macro-tidal Chikugo river estuary during a fortnightly tidal cycle*. Estuarine, Coastal and Shelf Science, 202, 232-245.
3. Baeyens, W., Van Eck, B., Lambert, C., Wollast, R., & Goeyens, L. (1998). *General description of the Scheldt estuary. Trace metals in the Westerschelde Estuary: A case-study of a polluted, partially anoxic estuary*, 1-14.
4. Becker, M., Schrottke, K., Bartholomä, A., Ernstsen, V., Winter, C., & Hebbeln, D. (2013). *Formation and entrainment of fluid mud layers in troughs of subtidal dunes in an estuarine turbidity zone*. Journal of Geophysical Research: Oceans, 118(4), 2175-2187.
5. Bergen, M., Weisberg, S. B., Smith, R. W., Cadien, D. B., Dalkey, A., Montagne, D. E., ... & Ranasinghe, J. A. (2001). *Relationship between depth, sediment, latitude, and the structure of benthic infaunal assemblages on the mainland shelf of southern California*. Marine Biology, 138, 637-647.
6. Billen, G., Garnier, J., & Rousseau, V. (2005). *Nutrient fluxes and water quality in the drainage network of the Scheldt basin over the last 50 years*. Hydrobiologia, 540, 47-67.
7. Bolle, A., Wang, Z. B., Amos, C., & De Ronde, J. (2010). *The influence of changes in tidal asymmetry on residual sediment transport in the Western Scheldt*. Continental Shelf Research, 30(8), 871-882.
8. Breiman, L. (2001). Random forests. Machine learning, 45, 5-32.
9. Brion, N., Jans, S., Chou, L., & Rousseau, V. (2008). *Nutrient loads to the Belgian coastal zone*. Current status of eutrophication in the Belgian coastal zone, 17-43.
10. Brion, N., Verbanck, M. A., Bauwens, W., Elskens, M., Chen, M., & Servais, P. (2015). *Assessing the impacts of wastewater treatment implementation on the water quality of a small urban river over the past 40 years*. Environmental Science and Pollution Research, 22, 12720-12736.
11. Burchard, H., Schuttelaars, H. M., & Ralston, D. K. (2018). *Sediment trapping in estuaries*. Annual review of marine science, 10(1), 371-395.
12. Chapman, M. G., & Blockley, D. J. (2009). *Engineering novel habitats on urban infrastructure to increase intertidal biodiversity*. Oecologia, 161, 625-635.
13. Chen, M. S., Wartel, S., Eck, B. V., & Maldegem, D. V. (2005). *Suspended matter in the Scheldt estuary*. Hydrobiologia, 540, 79-104.
14. Chmura, G. L., Anisfeld, S. C., Cahoon, D. R., & Lynch, J. C. (2003). *Global carbon sequestration in tidal, saline wetland soils*. Global biogeochemical cycles, 17(4).

15. Cloern, J. E. (1987). *Turbidity as a control on phytoplankton biomass and productivity in estuaries*. Continental shelf research, 7(11-12), 1367-1381.
16. Collins, M. J., & Miller, D. (2012*). Upper Hudson River Estuary (USA) floodplain change over the 20th century*. River research and applications, 28(8), 1246-1253.
17. Cox, T. J. S., Maris, T., Soetaert, K., Conley, D. J., Van Damme, S., Meire, P., ... & Struyf, E. (2009). *A macro-tidal freshwater ecosystem recovering from hypereutrophication: the Schelde case study*. Biogeosciences, 6(12), 2935-2948.
18. Cox, T. J. S., Maris, T., Van Engeland, T., Soetaert, K., & Meire, P. (2019). *Critical transitions in suspended sediment dynamics in a temperate meso-tidal estuary*. Scientific reports, 9(1), 12745.
19. Dam, G., Van der Wegen, M., Labeur, R. J., & Roelvink, D. (2016). *Modeling centuries of estuarine morphodynamics in the Western Scheldt estuary*. Geophysical Research Letters, 43(8), 3839-3847.
20. Damme, S. V., Struyf, E., Maris, T., Ysebaert, T., Dehairs, F., Tackx, M., ... & Meire, P. (2005). *Spatial and temporal patterns of water quality along the estuarine salinity gradient of the Scheldt estuary (Belgium and The Netherlands): results of an integrated monitoring approach*. Hydrobiologia, 540, 29-45.
21. De Brouwer, J. F. C., Bjelic, S., De Deckere, E. M. G. T., & Stal, L. J. (2000). *Interplay between biology and sedimentology in a mudflat (Biezelingse Ham, Westerschelde, The Netherlands)*. Continental shelf research, 20(10-11), 1159-1177.
22. De Brouwer, J. F., & Stal, L. J. (2002). *Daily fluctuations of exopolymers in cultures of the benthic diatoms Cylindrotheca closterium and Nitzschia sp.(Bacillariophyceae)*. Journal of Phycology, 38(3), 464-472.
23. de Jonge, V. N., Schuttelaars, H. M., van Beusekom, J. E., Talke, S. A., & de Swart, H. E. (2014). *The influence of channel deepening on estuarine turbidity levels and dynamics, as exemplified by the Ems estuary*. Estuarine, Coastal and Shelf Science, 139, 46-59.
24. De Neve, L., Van Ryckegem, G., Vanoverbeke, J., Van de Meutter, F., Van Braeckel, A., Van den Bergh, E., & Speybroeck, J. (2020). *Hyperbenthos in the upper reaches of the Scheldt estuary (Belgium): Spatiotemporal patterns and ecological drivers of a recovered community*. Estuarine, Coastal and Shelf Science, 245, 106967.
25. Dijkstra, Y. M., Schuttelaars, H. M., Schramkowski, G. P., & Brouwer, R. L. (2019). *Modeling the transition to high sediment concentrations as a response to channel deepening in the Ems River Estuary*. Journal of Geophysical Research: Oceans, 124(3), 1578-1594.
26. Doeke, E. (2019). *Intertidal deposits: river mouths, tidal flats, and coastal lagoons*. CRC press.
27. Droppo, I. G., Walling, D. E., & Ongley, E. D. (2000). *Influence of floc size, density and porosity on sediment and contaminant transport*. IAHS Publication(International Association of Hydrological Sciences), (263), 141-147.
28. Du Laing, G., Meers, E., Dewispelaere, M., Vandecasteele, B., Rinklebe, J., Tack, F. M., & Verloo, M. G. (2009). *Heavy metal mobility in intertidal sediments of the Scheldt estuary: field monitoring*. Science of the Total Environment, 407(8), 2919-2930.

29. Dyer, K. R., & Manning, A. J. (1999). *Observation of the size, settling velocity and effective density of flocs, and their fractal dimensions*. Journal of sea research, 41(1-2), 87-95.
30. Fagherazzi, S., Kirwan, M. L., Mudd, S. M., Guntenspergen, G. R., Temmerman, S., D'Alpaos, A., ... & Clough, J. (2012). *Numerical models of salt marsh evolution: Ecological, geomorphic, and climatic factors*. Reviews of Geophysics, 50(1).
31. Fettweis, M., Sas, M., & Monbaliu, J. (1998). *Seasonal, neap-spring and tidal variation of cohesive sediment concentration in the Scheldt Estuary, Belgium*. Estuarine, Coastal and Shelf Science, 47(1), 21-36.
32. Fowles, A. E., Stuart-Smith, R. D., Stuart-Smith, J. F., Hill, N. A., Kirkpatrick, J. B., & Edgar, G. J. (2018). *Effects of urbanisation on macroalgae and sessile invertebrates in southeast Australian estuaries*. Estuarine, Coastal and Shelf Science, 205, 30-39.
33. Grabowski, R. C., Droppo, I. G., & Wharton, G. (2011). *Erodibility of cohesive sediment: The importance of sediment properties*. Earth-Science Reviews, 105(3-4), 101-120.
34. Hammersmark, C. T., Fleenor, W. E., & Schladow, S. G. (2005). *Simulation of flood impact and habitat extent for a tidal freshwater marsh restoration*. Ecological Engineering, 25(2), 137-152.
35. Horemans, D. M., Dijkstra, Y. M., Schuttelaars, H. M., Sabbe, K., Vyverman, W., Meire, P., & Cox, T. J. (2021). *Seasonal variations in flocculation and erosion affecting the large-scale suspended sediment distribution in the Scheldt estuary: the importance of biotic effects*. Journal of Geophysical Research: Oceans, 126(4), e2020JC016805.
36. Huismans, Y., van der Spek, A., Lodder, Q., Zijlstra, R., Elias, E., & Wang, Z. B. (2022). *Development of intertidal flats in the Dutch Wadden Sea in response to a rising sea level: Spatial differentiation and sensitivity to the rate of sea level rise*. Ocean & Coastal Management, 216, 105969.
37. IMDC (2016). *Monitoringprogramma Flexibel Storten. Multivariate analyse van metingen van sedimentconcentratie in de Zeeschelde*. WL Reports I /RA/11353/15.228/THL, IMDC, Antwerpen.
38. Kon, K., Shimanaga, M., & Horinouchi, M. (2020). *Marine ecology: intertidal/littoral zone*. Japanese Marine Life: A Practical Training Guide in Marine Biology, 241-254.
39. Lai, H., Fang, H., Huang, L., He, G., & Reible, D. (2018). *A review on sediment bioflocculation: Dynamics, influencing factors and modeling*. Science of the total environment, 642, 1184-1200.
40. Lai, S., Loke, L. H., Hilton, M. J., Bouma, T. J., & Todd, P. A. (2015). *The effects of urbanisation on coastal habitats and the potential for ecological engineering: a Singapore case study*. Ocean & Coastal Management, 103, 78-85.
41. Land, L. E., Kolker, A. S., & Gambrell, R. P. (2012). *Biotic and abiotic controls on sediment aggregation and consolidation: implications for geochemical fluxes and coastal restoration*. Marine environmental research, 79, 100-110.
42. Lesourd, S., Lesueur, P., Brun-Cottan, J. C., Auffret, J. P., Poupinet, N., & Laignel, B. (2001). *Morphosedimentary evolution of the macrotidal Seine estuary subjected to human impact*. Estuaries, 24, 940-949.

43. Leuven, J. R., Pierik, H. J., Vegt, M. V. D., Bouma, T. J., & Kleinhans, M. G. (2019). *Sea-level-rise-induced threats depend on the size of tide-influenced estuaries worldwide*. Nature Climate Change, 9(12), 986-992.
44. Lubarsky, H. V., Hubas, C., Chocholek, M., Larson, F., Manz, W., Paterson, D. M., & Gerbersdorf, S. U. (2010). *The stabilisation potential of individual and mixed assemblages of natural bacteria and microalgae*. PloS one, 5(11), e13794.
45. Marcovecchio, J. E., Botté, S. E., De Marco, S. G., Cazorla, A. L., Arias, A. H., Baldini, M., ... & Pereyra, M. T. (2021). *Estuarine environmental monitoring programs: long-term studies*. The Bahía Blanca Estuary: Ecology and Biodiversity, 521-547.
46. Maris, T., Cox, T., Temmerman, S., De Vleeschauwer, P., Van Damme, S., De Mulder, T., ... & Meire, P. (2007). *Tuning the tide: creating ecological conditions for tidal marsh development in a flood control area*. Hydrobiologia, 588, 31-43.
47. McCave, I. N. (1984). *Erosion, transport and deposition of fine-grained marine sediments*. Geological Society, London, Special Publications, 15(1), 35-69.
48. Meire, P., Ysebaert, T., Damme, S. V., Bergh, E. V. D., Maris, T., & Struyf, E. (2005). *The Scheldt estuary: a description of a changing ecosystem*. Hydrobiologia, 540, 1-11.
49. Middelburg, J. J., Klaver, G., Nieuwenhuize, J., & Vlug, T. (1995). *Carbon and nitrogen cycling in intertidal sediments near Doel, Scheldt Estuary*. Hydrobiologia, 311, 57-69.
50. Mikeš, D., & Manning, A. J. (2010). *Assessment of flocculation kinetics of cohesive sediments from the Seine and Gironde estuaries, France, through laboratory and field studies*. Journal of Waterway, Port, Coastal, and Ocean Engineering, 136(6), 306-318.
51. Nichols, C. R., Zinnert, J., & Young, D. R. (2019). *Degradation of coastal ecosystems: causes, impacts and mitigation efforts*. Tomorrow's Coasts: Complex and Impermanent, 119-136.
52. Nienhuis, P. H. (1993). *Nutrient cycling and foodwebs in Dutch estuaries*. Hydrobiologia, 265, 15-44.
53. Partheniades, E. (1993). *Turbulence, flocculation and cohesive sediment dynamics*. Nearshore and estuarine cohesive sediment transport, 42, 40-59.
54. Pasquaud, S., Lobry, J., & Elie, P. (2007). *Facing the necessity of describing estuarine ecosystems: a review of food web ecology study techniques*. Hydrobiologia, 588(1), 159-172.
55. Plancke, Y. M. G., Vandebroek, E., Claeys, S., & Meire, D. (2017). *Sediment transport in the Schelde-estuary: The challenge of performing good measurements in challenging conditions*. Hydraulic Measurements and Experimental Methods 2017 Conference (HMEM 2017.
56. Reed, D. J. (1995). *The response of coastal marshes to sea-level rise: Survival or submergence?*. Earth Surface processes and landforms, 20(1), 39-48.
57. Reed, D., van Wesenbeeck, B., Herman, P. M., & Meselhe, E. (2018). *Tidal flat-wetland systems as flood defenses: Understanding biogeomorphic controls*. Estuarine, Coastal and Shelf Science, 213, 269-282.
58. Rosenblatt, F. (1958). *The perceptron: a probabilistic model for information storage and organization in the brain*. Psychological review, 65(6), 386.

59. Schepers, L., Maris, T., Meire, P., & Temmerman, S. (2018). *The Scheldt estuary: an overview of the morphodynamics of intertidal areas*. Landscapes and Landforms of Belgium and Luxembourg, 281-296.
60. Smolders, S., Plancke, Y., Ides, S., Meire, P., & Temmerman, S. (2015). *Role of intertidal wetlands for tidal and storm tide attenuation along a confined estuary: a model study*. Natural Hazards and Earth System Sciences, 15(7), 1659-1675.
61. Stark, J., Meire, P., & Temmerman, S. (2017). *Changing tidal hydrodynamics during different stages of eco-geomorphological development of a tidal marsh: A numerical modeling study*. Estuarine, Coastal and Shelf Science, 188, 56-68.
62. Temmerman, S., Meire, P., Bouma, T. J., Herman, P. M., Ysebaert, T., & De Vriend, H. J. (2013). *Ecosystem-based coastal defence in the face of global change*. Nature, 504(7478), 79-83.
63. Uncles, R. J., Stephens, J. A., & Law, D. J. (2006). *Turbidity maximum in the macrotidal, highly turbid Humber Estuary, UK: Flocs, fluid mud, stationary suspensions and tidal bores*. Estuarine, Coastal and Shelf Science, 67(1-2), 30-52.
64. Van Ael, E., Covaci, A., Blust, R., & Bervoets, L. (2012). *Persistent organic pollutants in the Scheldt estuary: environmental distribution and bioaccumulation*. Environment international, 48, 17-27.
65. Van de Broek, M., Vandendriessche, C., Poppelmonde, D., Merckx, R., Temmerman, S., & Govers, G. (2018). *Long-term organic carbon sequestration in tidal marsh sediments is dominated by old-aged allochthonous inputs in a macrotidal estuary*. Global change biology, 24(6), 2498-2512.
66. Van den Bergh, E., Van Damme, S., Graveland, J., De Jong, D., Baten, I., & Meire, P. (2005). *Ecological rehabilitation of the Schelde estuary (The Netherlands–Belgium; Northwest Europe): linking ecology, safety against floods, and accessibility for port development*. Restoration ecology, 13(1), 204-214.
67. van der Zee, C., Roevros, N., & Chou, L. (2007). *Phosphorus speciation, transformation and retention in the Scheldt estuary (Belgium/The Netherlands) from the freshwater tidal limits to the North Sea*. Marine Chemistry, 106(1-2), 76-91.
68. Walles, B., Brummelhuis, E., van der Pool, J., Wiesebron, L., & Ysebaert, T. (2019). *Development of benthos and birds in an intertidal area created for coastal defence (Scheldt estuary, the Netherlands)* (No. C043/19). Wageningen Marine Research.
69. Wang, Y. P., Voulgaris, G., Li, Y., Yang, Y., Gao, J., Chen, J., & Gao, S. (2013). *Sediment resuspension, flocculation, and settling in a macrotidal estuary*. Journal of Geophysical Research: Oceans, 118(10), 5591-5608.
70. Wang, Z. B., Vandenbruwaene, W., Taal, M., & Winterwerp, H. (2019). *Amplification and deformation of tidal wave in the Upper Scheldt Estuary*. Ocean Dynamics, 69, 829-839.
71. Waterinfo.be (cited 2019). *Measurements and predictions of Waterinfo.be [data]*. [Available online at https://www.waterinfo.be/].
72. Widdows, J., Blauw, A., Heip, C. H. R., Herman, P. M. J., Lucas, C. H., Middelburg, J. J., ... & Verbeek, H. (2004). *Role of physical and biological processes in sediment dynamics of a tidal flat in Westerschelde Estuary, SW Netherlands*. Marine Ecology Progress Series, 274, 41-56.

73. Winterwerp, J. C., & Wang, Z. B. (2013). *Man-induced regime shifts in small estuaries—I: theory*. Ocean Dynamics, 63, 1279-1292.
74. Winterwerp, J. C., Manning, A. J., Martens, C., De Mulder, T., & Vanlede, J. (2006). *A heuristic formula for turbulence-induced flocculation of cohesive sediment*. Estuarine, coastal and shelf Science, 68(1-2), 195-207.
75. Wofsy, S. C. (1983). *A simple model to predict extinction coefficients and phytoplankton biomass in eutrophic waters* 1. Limnology and Oceanography, 28(6), 1144-1155.
76. Wood, P. J., & Armitage, P. D. (1997). *Biological effects of fine sediment in the lotic environment*. Environmental management, 21(2), 203-217.
77. Xu, T., & You, X. Y. (2017). *Numerical simulation of suspended sediment concentration by 3D coupled wave-current model in the Oujiang River Estuary, China*. Continental Shelf Research, 137, 13-24.
78. Ysebaert, T. J., Herman, P. M. J., Hummel, H., Schaub, B., Sistermans, W. C. H., & Heip, C. H. R. (2002). *Monitoring and predictive modelling of estuarine benthic macrofauna and their relevance to resource management problems*. VLIZ Special Publication.

Chapter 2

Accommodation Space in Turbid Estuaries: The Role of Different Estuarine Habitats as a Sink or Source for Suspended Sediment

Abstract

Sediment dynamics are vital for the ecological health and functioning of estuarine systems, influencing water quality, habitat stability, and nutrient cycling. Intertidal zones play a central role in these processes by providing essential habitats and aiding in the natural filtration of pollutants. However, in some estuaries, including the Scheldt, these ecological functions can be threatened by elevated concentrations of suspended particulate matter (SPM), driven by both natural processes and human activities. Understanding whether intertidal zones in the Scheldt estuary serve as accommodation spaces where sediments can settle and stabilize, or as areas prone to frequent sediment resuspension, is crucial for effective estuary management.

This study examines sediment behavior across three hydrodynamically distinct zones within the Scheldt estuary: the freshwater zone at Branst, the brackish zone at Lillo, and the saline zone at Zuidgors. High-frequency observations were conducted to investigate the interactions among floc characteristics, SPM concentrations, and hydrodynamic forces, with the goal of improving understanding of sediment stability and mobility across these zones.

The results demonstrate that sedimentation and erosion patterns are governed not only by SPM concentration but also by floc size, density, and composition, in combination with local hydrodynamic conditions. At Branst, sediment dynamics exhibited pronounced seasonal variability, with net sedimentation in autumn and spring and erosion in summer and winter. The presence of larger floc sizes during summer, despite ongoing erosion, suggests that these flocs were more prone to resuspension rather than contributing to stable sedimentation, potentially due to their fragile, loosely aggregated structure. At Lillo, sediment behavior was primarily influenced by SPM levels and floc stability. Unexpected erosion in summer may indicate periods when flocs lacked sufficient cohesion to support sedimentation, despite hydrodynamic conditions that were otherwise favorable. In Zuidgors, sediment dynamics were largely governed by the formation of stable flocs, which remained resistant to resuspension even under high-energy conditions. However, during winter, increased erosion was likely driven by moderate increases in tidal energy and reduced biological activity, which limited the formation of larger, more cohesive flocs. This is reflected in the smaller floc sizes observed during this period, which reduced the potential for sediment accumulation.

These findings suggest that while SPM concentration levels are important, they do not solely determine sedimentation and erosion patterns in the Scheldt estuary. The stability of sediments is intricately linked to the composition of flocs, which are influenced by seasonal biological activity

and localized hydrodynamic forces. These results emphasize the need for a nuanced, site-specific approach to sediment management in the Scheldt estuary. The variability observed across different zones highlights the importance of continued monitoring and adaptive strategies to maintain the estuary's ecological integrity.

2.1. Introduction

Intertidal zones in estuarine environments, particularly within brackish regions where freshwater and marine influences converge, are characterized by dynamic exchanges of water, sediment, and nutrients. These areas, exposed to both air and water, are constantly reshaped by tidal forces. They provide diverse and essential habitats that support a wide range of organisms and offer multiple ecosystem services.

One of the foremost ecosystem services of intertidal zones is biodiversity support. They function as nurseries and breeding grounds for various marine and terrestrial species, thereby facilitating complex food webs essential for ecological balance (Stark et al., 2017; Eisma, 2019; Kon et al., 2020). Additionally, these areas play a crucial role in water quality enhancement by naturally filtering pollutants, which contributes to the health of downstream ecosystems (Damme et al., 2005; Chainho et al., 2010; Mialet et al., 2011; do Amaral Camara Lima et al., 2023).

Furthermore, the physical structure of intertidal zones plays a vital role in shore protection. These areas act as natural buffers, absorbing the erosive forces of waves and winds, which helps mitigate the impacts of storm surges and floods. This protective function is becoming increasingly critical as climate change escalates the frequency and intensity of coastal storms (Spalding et al., 2014; Van Coppenolle et al., 2018; Maris et al., 2007; Smolders et al., 2015; Reed et al., 2018). In addition to their protective role, the sediment dynamics within intertidal zones are pivotal for maintaining ecological functions. Tidal forces drive short-term fluctuations in sediment transport and deposition, shaping sediment resuspension and redistribution, and creating diverse microhabitats. However, human activities such as dumping of dredged material can exacerbate elevated levels of suspended particulate matter (SPM) concentrations, affecting these natural processes. High turbidity reduces light penetration, hinder primary production, and degrade habitats essential for species survival. Climate and river discharge are responsible for the seasonal sediment deposition and erosion patterns, influencing habitat stability and nutrient cycling (Widdows & Brinsley, 2002; Ysebaert et al., 2005). These sediment dynamics highlight the delicate balance required to sustain estuarine productivity and ecological health, as shifts in sediment loads can have significant ecological consequences.

Integral to sediment stabilization in these zones are biological activities, including biofilm formation by microphytobenthos such as diatoms and cyanobacteria, and the presence of vegetation. These microorganisms produce extracellular polymeric substances (EPS) that bind sediment particles together, reducing erosion and enhancing sediment accretion. This capability is essential for maintaining habitat integrity, ensuring that intertidal zones continue to deliver vital ecosystem services despite environmental changes (De Brouwer & Stal, 2002; Stal, 2010; Lefebvre et al., 2014; Widdows et al., 2004). Additionally, vegetation in intertidal zones helps stabilizing the sediments, modifies hydrodynamic conditions, and provides habitats for various species, which in turn further influence sediment deposition patterns (Kakeh et al., 2016; Van Katwijk et al., 2010; Sgarabotto et al., 2021).

All these variables collectively emphasize the necessity of understanding intertidal areas as accommodation spaces for suspended sediments, highlighting their importance in sediment dynamics and transport. To understand how these sediments interact and settle, it's essential to explore flocculation—the process where the component particles aggregate and break apart to form larger particles known as flocs. This process is influenced by physical forces such as differential settling, cohesive properties of the particles, concentration and fluid shear, which facilitate particle collision and adhesion or disruption (McCave, 1984; Dyer & Manning, 1999; Winterwerp, 2002). Moreover, chemical interactions enhance flocculation, where ions from dissolved salts and minerals, along with polymers—particularly EPS produced by phytoplankton and bacteria—neutralize electrical charges on particle surfaces, forming larger particles called transparent exopolymeric particles (TEP) (Gerbersdorf et al., 2008; Lubarsky et al., 2010; Lai et al., 2018). TEPs play a key role in SPM aggregation. While TEP concentrations correlate with phytoplankton biomass in open oceans, this relationship is less clear in turbid estuarine systems due to species-specific differences and seasonal variations in TEP properties (Horemans et al., 2021; Fettweis et al., 2022).

Furthermore, settling velocity of flocs is important in understanding sediment transport and erosion. In calm conditions, flocs settle rapidly, enhancing sediment accretion. Conversely, in turbulent conditions, flocs may disintegrate or remain suspended due to factors like high turbulence, bioturbation, and water flow variations (Dyer & Manning, 1999; Lefebvre et al., 2014). These hydrodynamic conditions play pivotal roles in modulating sediment stability and aggregation, directly impacting the geomorphological stability and changes in bed level dynamics in estuaries.

Such changes in sediment dynamics alter the topography of intertidal areas, affecting habitat availability, nutrient cycling, and overall ecological health. Therefore, understanding the factors

influencing flocculation and suspended sediment dynamics is paramount in environmental management of these zones. This knowledge aids in predicting sediment behavior and distribution, which is vital for maintaining estuarine ecological balance and resilience. Such insights ensure that conservation efforts are grounded in robust scientific understanding, enhancing sustainability. Figure 2.1 illustrates the interconnected roles of hydrodynamic forces, tidal forces, suspended particle properties and biological factors on sediment dynamic. Understanding these relationships helps elucidate how variations in sediment characteristics influence the physical and ecological dynamics of intertidal zones.

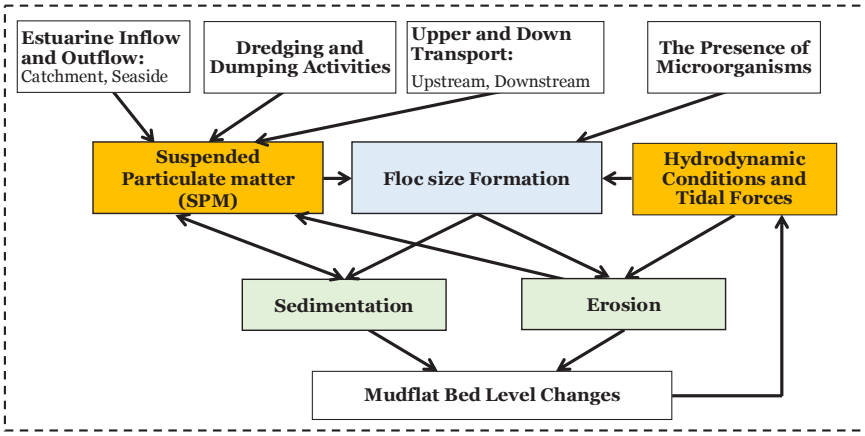

Figure 2.1. Conceptual diagram illustrating the processes influencing bed level dynamics in intertidal mudflats. SPM enters the system through multiple sources, including river inflows, dredging activities, and internal estuarine transport. It contributes directly to sedimentation, establishing a bidirectional relationship in which bed level changes also influence SPM behavior. SPM further promotes floc formation, particularly in the presence of microorganisms. The fate of these flocs, whether settling or remaining in suspension, is governed by hydrodynamic conditions such as tidal currents and turbulence. Changes in bed elevation, in turn, alter local hydrodynamics by modifying water depth, flow velocity, and turbulence, completing a feedback loop. Fully understanding mudflat evolution over time requires accounting for the combined influence of all these drivers, rather than isolating individual processes.

This research investigates sediment behavior in the Scheldt estuary's intertidal zones, focusing on whether these areas act as accommodation spaces for SPM or primarily as zones where sediments are frequently resuspended. Given the estuary's challenges—including an observed increase in SPM concentration from 2009 to 2019, as documented by Cox et al. (2019) and Maris et al. (2021), alongside, sea level rise, sediment imbalances, and human impacts—this study aims to uncover the mechanisms driving sediment stability and mobility. Previous studies have highlighted how seasonal variations, driven by climatic changes, river discharge, and biological activities,

significantly modulate sediment transport and deposition patterns throughout the year (Fettweis et al., 1998; Temmerman et al., 2003; French, 2006; Cox et al., 2019). Additionally, tidal cycles introduce short-term fluctuations that influence sediment redistribution and stability, adding to the dynamic nature of sediment behavior in intertidal zones (Dyer, 1986; Aubrey & Friedrichs, 1988; Bolle et al., 2010). Building on these insights, the study aims to provide a deeper understanding of how hydrodynamic conditions, sediment characteristics, and bed level changes interact over time and across different estuarine zones, contributing to ongoing and increasingly necessary efforts to manage and preserve the ecological integrity of the Scheldt estuary.

2.2. Material and Methods

This section first discusses some of the characteristics of the Scheldt estuary. Next, the measurement methods used to obtain the in-situ observations are introduced and the data processing approach is presented.

2.2.1. Study Area

This study investigates three tidal flats in the Scheldt estuary, located in northern Belgium and southwestern Netherlands (see Figure 2.2). The estuary exhibits well-mixed characteristics due to its relatively low freshwater discharge (Meire et al., 2005). Time-averaged freshwater discharge for 2018-2019 shows distinct seasonality, with the lowest discharge in summer at 42 $m^3.s\text{-}1$ and the highest in winter at 97 $m^3.s^{-1}$. Spring and autumn discharge rates were 86 $m^3.s\text{-}1$ and 45 $m^3.s\text{-}1$, respectively (Waterinfo.be, 2019).

Sediment budget studies estimate a net import of 0.609 Mm^3 per year of sand into the Sea Scheldt from the Western Scheldt, highlighting the high sand content in the Western Scheldt (Cleveringa, 2013; Vandenbruwaene et al., 2017). The annual fluvial input of SPM, measured in mass, is estimated to range from 10^4 to 10^5 tons per year, scaling with variations in freshwater discharge (Dijkstra et al., 2019).

The Scheldt estuary is impacted by organic and chemical pollution (De Wolf, Hans, et al., 2004; Van Ael, Evy, et al., 2012; Perrot, Vincent, et al., 2023). Its morphology has also undergone significant changes due to large-scale embankments and dredging operations aimed at maintaining the fairway to the Port of Antwerp (Meire et al., 2005; Winterwerp et al., 2013; Dam et al., 2022). Dredged material is primarily discharged back into the estuary, contributing to significantly higher SPM loads compared to the river inlet (Dijkstra et al., 2019). Dredging and

dumping volumes for 2018-2019 in the Western Scheldt were about 9.3 Mm^3/year, while in the Lower Sea Scheldt, 4.7 Mm^3/year were dredged, from which 72% mud, highlighting the muddy nature of the Sea Scheldt.

This ongoing accumulation of SPM, driven by both dredging activities and low freshwater discharge, has resulted in elevated turbidity levels, posing persistent challenges for water quality, sediment balance, and ecological health (Fettweis et al., 2019; Dam et al., 2022; Maris et al., 2024). Furthermore, the maximum turbidity zone (MTZ), where sediment tends to accumulate, has likely expanded due to the direct or indirect effects of dredging. Typically, the MTZ shifts seasonally—toward the saltwater zone in winter and the freshwater zone in summer—but its movement has become more unpredictable in recent years. Improvements in water quality have also influenced phytoplankton communities, further affecting sediment stability and behavior (Cox et al., 2019; Horemans et al., 2021; Martínez, Luz Amadei et al., 2023).

From November 2018 to December 2019, high-frequency biweekly measurements were conducted at three intertidal flats within the Scheldt estuary: Branst (freshwater zone), Lillo (brackish/mesohaline zone), and Zuidgors (saline/polyhaline zone) (Figure 2.2). Observations were carried out during each season, with one full neap–spring tidal cycle captured per season, resulting in a consistent seasonal dataset across the three locations. These sites were strategically selected to represent the estuarine salinity gradient and to capture diverse hydrodynamic and sedimentological conditions. Located approximately 105 km, 65 km, and 20 km from the estuary mouth, respectively, all sites are situated along the main Scheldt channel and are adjacent to tidal marshes. Their selection enables a cross-zonal comparison of sediment transport and flocculation processes under varying environmental influences.

Branst is located in the freshwater reach of the estuary and is influenced by seasonal river discharge fluctuations, which affect suspended sediment concentrations and deposition dynamics. The site is situated on a river bend, introducing localized current variability, and is fronted by a tidal marsh with willow (Salix spp.) vegetation. It is relatively sheltered, with minimal wave exposure, making it suitable for isolating fluvial and tidal effects on sediment processes. Measurement instruments were installed approximately 10 meters from the marsh edge.

Lillo lies within the brackish transition zone and is characterized by a pronounced salinity gradient. The site is located in the Port of Antwerp area, directly in front of a de-embanked zone, and is exposed to episodic anthropogenic disturbances, including dredging operations and ship-induced turbulence. Although relatively sheltered from wave action, these human activities periodically affect the sedimentary environment. Measurement instruments were positioned

approximately 60 meters from the marsh edge, allowing analysis of both natural and anthropogenic drivers of sediment dynamics.

Zuidgors is located in the saline region near the estuary mouth and is directly exposed to marine wave action due to its south-southwest orientation and proximity to a broad fetch area. It comprises a natural tidal flat fronting a saltmarsh, with instruments installed approximately 200 meters from the marsh edge. This site is part of a dynamic multi-channel system within the Western Scheldt, resulting in complex flow interactions and elevated current velocities in some sub-channels. These conditions contribute to localized zones of erosion and deposition, making Zuidgors representative of high-energy, wave-influenced intertidal flats.

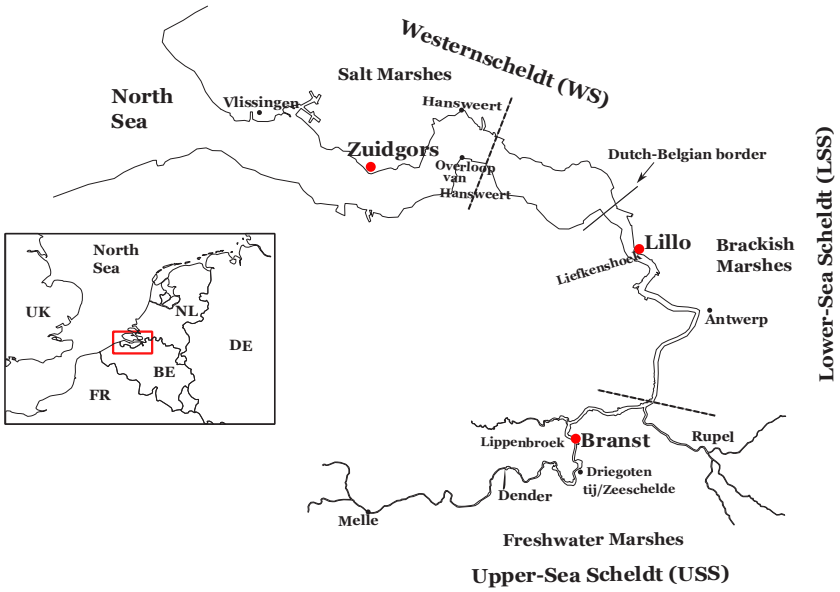

Figure 2.2: Map of the Scheldt estuary showing the locations of the three tidal marsh study sites distributed along the estuarine salinity gradient. Dashed lines represent the approximate boundaries between the salt, brackish, and freshwater zones. Red numbered dots indicate the sampling locations: Zuidgors (saline zone, 20 km from the estuary mouth), Lillo (brackish zone, 65 km), and Branst (freshwater zone, 105 km). Biweekly field sampling was conducted at each site over a one-year period.

The three sites collectively represent a gradient of salinity, hydrodynamic energy, wave exposure, and anthropogenic influence, providing a comprehensive framework for analyzing sediment dynamics across the estuary. Each site shares key features—such as a location along the main Scheldt channel, adjacency to tidal marshes, and an adequately sized intertidal zone that enables representative measurement of tidal processes. The availability of a sufficiently wide and

unobstructed intertidal surface area is critical for capturing spatial variability in sediment transport, accommodating instrument setup, and avoiding localized edge effects near marsh boundaries. These shared physical characteristics ensure that differences in sediment behavior among the sites can be attributed to environmental gradients rather than site limitations, thus supporting robust cross-site comparison of sediment transport and flocculation dynamics.

2.2.2. In-situ Observations

To ensure consistency in measurements, the same setup was employed at all three locations in the estuary. The setup included an Optical Backscatter Sensor (OBS) for measuring turbidity, an Acoustic Doppler Velocimeter (ADV) for assessing current velocities and seabed distance, and a Laser In-Situ Scattering and Transmissometry (LISST-200X) device for determining particle size distribution of the SPM. Detailed instrument specifications are provided in Table 2.1. The instruments were mounted on a framework (Figure 2.3.a), placed perpendicular to the mainstream at an elevation corresponding to 50% of the flood time. The specific elevations were 2.68 m TAW for Branst, 2.34 m TAW for Lillo, and 2.39 m TAW for Zuidgors. Data was recorded over 15-day periods, after which the frame was retrieved for maintenance, calibration, and data download. Measurement dates are listed in Table 2.A.1 in Appendix 2.A.

Table 2.1: Overview of the deployed instrumentation, including model specifications, sampling configuration, sensor height above the seabed, and key data outputs used in the analysis. All sensors were positioned approximately 12–13 cm above the bed to capture near-bed sediment dynamics relevant to deposition and erosion processes.

Instrument	Model/Type	Sample rate/Burst interval	Position above seabed	Related obtained elements
OBS (Optical Backscatter Sensor)	YSI model 6920 V2	Interval: 5 min	13 cm	• Measures water turbidity indicating SPM concentration
ADV (Acoustic Doppler Velocimeter)	Nortek Vector, 6 MHz	14400 samples per burst: 16 (Hz) x 15 (min) x 60 (sec)	12 cm	• Monitors current velocities and records distance from seabed (DSP) • Use for calculation of shear rate G
LISST (Laser In-Situ Scattering and Transmissometry)	Sequoia Scientific LISST-200X	Interval: 5 min; Volume distribution across 36 size classes (1-500 μm)	13 cm	• Assesses particle size distribution • Calculation of mean floc size

These biweekly measuring periods across different seasons of SPM properties (concentration, floc size) enabled a detailed understanding of environmental impacts, including potential changes driven by seasonal weather conditions and environmental shifts. Seasons were categorized as winter (characterized by low biological activity), early growing season (spring), full growing season (summer), and late growing season (autumn, where biological activity begins to decline, and organic matter becomes increasingly influenced by decomposition processes). The distinction between early and full growth seasons hinges on the grazing activity of zoobenthos. In early spring (April), strong phytobenthos growth potentially stabilizes the substrate, while grazing pressure increases as the season progresses, possibly destabilizing the sediment bed.

Additionally, water samples were collected at high tide to calibrate OBS readings into SPM concentrations (Figure 2.3.b). Due to variability in particle sizes, each campaign required specific calibration. Post-collection, samples were analyzed within 48 hours, categorized by turbidity, and used to derive a calibration curve correlating NTU and SPM values. Further details are provided in Section 2.2.3.2.

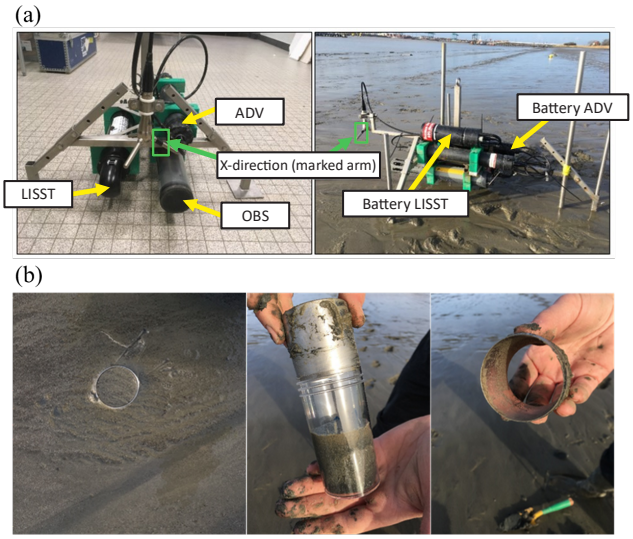

Figure 2.3: (a) Field measurement setup used across all study sites, showing the instrument frame equipped with an ADV, OBS, and LISST-200X for capturing high-frequency hydrodynamic and sediment data. Battery packs are shown on the right. The frame was positioned at elevations corresponding to 50% inundation time to ensure comparability. (b) Sampling procedure for bulk density analysis using a Kopecky ring, a metal cylinder designed to extract undisturbed sediment cores of known volume for accurate laboratory-based measurements of sediment bulk density and porosity.

Given the proximity of sensors to the sediment bed (12–13 cm above bottom), we considered the potential for instrument-induced disturbance or resuspension. However, the instruments were passively mounted and designed to minimize flow interference, and the consistent intratidal patterns observed in floc size and SPM suggest that any self-induced turbulence was negligible. This assumption is further supported by stable ADV and OBS signals during low-energy phases, indicating no artificial resuspension.

2.2.2.1. LISST: Laser In-Situ Scattering and Transmissometry

Suspended sediment particle size distributions (PSDs) were derived from the LISST-200X, configured in burst mode for the 15-day study period. Measurements were taken every 5 minutes, with each sample representing an average of 230 individual measurements over 5 seconds. This setup captured detailed changes in particle characteristics over time, ensuring comprehensive data collection. To maintain data reliability, optical transmission was kept between 15% and 98%. This range prevents abrupt changes in transmission or volume concentration that could indicate instrument misalignment or contamination.

The LISST-200X provides high-resolution measurements of particle size distributions across 36 logarithmically spaced size classes ranging from 1.00 to 500 μm. These measurements are crucial for characterizing both small and large particles in suspension. Understanding how particles of different sizes are transported by currents is essential for modeling sediment deposition and erosion in aquatic environments. Additionally, identifying how particles form aggregates (flocs) and how these flocs behave in natural waters influences settling rates and nutrient transport, providing critical information for monitoring water quality and the ecological impact of suspended sediments, particularly in areas affected by human activities or natural events.

2.2.2.2. YSI: Optical Backscatter Sensor

A multiparameter sonde (YSI type 6920 V2) equipped with an optical backscatter sensor (YSI 6136 Turbidity sensor) was deployed to continuously monitor water turbidity. The sensor, with a resolution of 0.1 NTU and an accuracy of ±2% of the reading or 0.3 NTU (whichever is greater), measures light scattered by particles at a 90° angle. This measurement was conducted at 5-minute intervals over the 15-day period.

The OBS quantifies turbidity in Nephelometric Turbidity Units (NTU), which reflect reductions in water clarity due to the presence of SPM. Consequently, turbidity assessments can estimate SPM levels (Smith & Davies-Colley, 2001; Kari et al., 2017). However, the OBS's response to different

particle sizes varies significantly; for example, it responds to 2 μm clay particles 50 times more than to 100 μm sand particles at the same concentration (Battisto et al., 1999). This variability can affect the accuracy of converting optical backscatter into mass concentration (SPM). To address this issue, a linear regression model was developed using in-situ SPM concentration samples ($mg.l^{-1}$) and laboratory OBS calibration data (NTU) values to estimate the regression parameters The details of this regression model and its application are provided in Section 2.2.3.2. This method minimizes the influence of physical, chemical, and thermal stressors that can alter the size distribution of calibration materials (Downing, 2006).

2.2.2.3. ADV: Acoustic Doppler Velocimeter

A Nortek Vector 6 MHz Acoustic Doppler Velocimeter (ADV) was deployed to monitor turbulent currents. This instrument, with a resolution of ±0.01 m/s and an accuracy of 0.5% of the measured value or 1 mm/s, measures turbulence within a defined sampling volume (14 mm in diameter, 14.9 mm in height) at the intersection of the receive transducers. It operates by detecting the Doppler shift in the acoustic backscatter from particles in the water after emitting an acoustic pulse. This setup captures three velocity components using receive transducers, facilitating the analysis of turbulent eddies during post-processing.

For the 15-day study period, the device was set to measure at 16 Hz in burst mode with 1800-second intervals (30 minutes), alternating between 15 minutes of continuous measurement and 15 minutes of sleep mode. This cycle resulted in 14,400 samples per burst. The probe was oriented in an XYZ configuration to align with the dominant flow direction, maximizing measurement accuracy.

The downward-looking setup of the ADV has the advantage of adding a distance measurement to the water-bed interface which will be explained in section 2.2.3.5.

2.2.3. Data Pre-Processing

To prepare the data for analysis, data points falling outside the valid ranges defined in the device manuals are first removed. Typically, this process affects less than 5% of the data, ensuring that only accurate measurements are retained. Because the devices may not have recorded data consistently—sometimes skipping a day or logging data at irregular intervals—a uniform data validity mask was applied across all datasets. This mask, based on each device's manual standards, ensures that all data adheres to the same quality criteria, regardless of recording frequency. Specifically, ADV measurements must have a pressure greater than 0.9 and amplitude over 100;

OBS transmission levels should be between 0.1 and 0.995; and LISST turbidity must be greater than 0. This step mitigates inconsistencies in data recording and enhances the overall reliability of the analysis.

To further improve accuracy and consistency, the raw data were processed to eliminate observational artifacts and inconsistencies. Two statistical measures—Standard Deviation (SD) and Median Absolute Deviation (MAD)—are used to identify and remove outliers. Some alternative techniques, which assume static trends in time series data, often fail when applied to dynamic datasets, where local trends frequently shift in range, mean, and deviation at various resolutions. To address this issue, a moving window analysis is applied, allowing continual adaptation to these variations and preserving the accuracy of the data analysis.

Within each window, data points that deviate significantly from the local trend are identified using predefined thresholds to mark outliers. This approach ensures that outlier detection remains context-sensitive, capturing true anomalies while disregarding transient fluctuations that do not reflect longer-term environmental patterns. However, not all outliers are removed. Sequences of data points that, despite being classified as outliers, extend beyond a certain length (e.g., N = 20) are preserved under the assumption that they represent genuine environmental events rather than noise. This method minimizes the loss of meaningful data and captures the full complexity of environmental dynamics.

The findings show that while both SD and MAD methods are effective, the choice between them depends on the specific data characteristics and the nature of the environmental phenomena under study. For ADV data, where reliability and sensitivity to outliers are paramount, the MAD method is preferred due to its aggressive outlier removal, eliminating about 5% of the data. In contrast, for OBS and LISST data, which often exhibit skewed distributions, the SD method is more effective. Its detrending capability corrects for skewness and maintains a broader range of valuable data points.

After applying the quality control procedures—including device-specific operational filters and statistical outlier removal—the number of data points retained for analysis varied by sensor, season, and station. These final data counts represent only high-quality, usable observations and form the basis for the analyses presented in this chapter. The exact number of retained data points is provided in Appendix 2.B, alongside the corresponding time series plots.

2.2.3.1. Velocity Data Alignment and Turbulence Analysis

After aligning the ADV velocity and backscatter data, it is essential to ensure that the primary flow component ('u') corresponds to the x-axis. This step minimizes discrepancies between the sensor's orientation and the main flow direction. To achieve this alignment, a double-axis rotation is applied around the transversal (v) and vertical (w) axes, following the methodologies of Lorke et al. (2013) and Wilczak et al. (2001). Once the data have been aligned and rotated, a linear trend is fitted to the adjusted velocity observations to extract turbulent fluctuations within 15-minute intervals, referred to as 'bursts'. These turbulent fluctuations are then analyzed sequentially to calculate velocity magnitudes, providing a detailed understanding of flow dynamics. The relationship between turbulence and floc formation is assessed by evaluating the shear rate (G), which is a function of the turbulent kinetic energy dissipation rate (ε) (Dyer and Manning, 1999; Van Leussen, 2011; Camp, 1943). The shear rate is calculated using the following equation:

$$G = \sqrt{\left(\frac{\varepsilon}{\nu}\right)} \quad \text{Eq. (1)}$$

where ε is the turbulent dissipation rate per unit mass ($Nm.s^{-1}.kg^{-1}$) and ν is the kinematic viscosity of the water ($0.96 \times 10\text{-}6.m^2.s^{-1}$). The turbulent dissipation rate ε can be related to the variables u_* and z/H according to Nezu and Nakagawa (1993) as:

$$\varepsilon \approx \frac{{u_*}^3}{kH} \times \frac{1-z/H}{z/H} \quad \text{Eq. (2)}$$

where k is the "von Karman" constant (0.41), z is the height above the bed of the sensor (m), and H is the total water depth (m). The shear velocity u_* ($m.s^{-1}$) can be determined by using the Reynolds stress correction (Voulgaris and Meyers, 2004):

$$u_* = \sqrt{-\overline{u'w'}} \quad \text{Eq. (3)}$$

where u ´and w ´represent turbulent fluctuations calculated as residuals after averaging the horizontal and vertical currents which underwent preprocessing including de-spiking, axis rotations, and alignment adjustments (section Data cleaning). respectively. Substituting Equation (1) into Equation (2) yields an expression for G as a function of z, H, and u*:

$$G(z,H,u_*) = \sqrt{\frac{{u_*}^3 \times (1-z/H)}{\vartheta kz}} \quad \text{Eq. (4)}$$

2.2.3.2. OBS-SPM Calibration

To determine SPM concentration, data from the OBS sensor are utilized. To translate NTU readings into SPM concentrations (mg/l), a calibration curve was established using lab-obtained NTU values and SPM concentrations from water samples.

First, water samples were collected using a Van Dorn sampler at three locations, each situated downstream from the respective monitoring setups at Branst, Lillo, and Zuidgors—700 m, 500 m, and 550 m, respectively, following the river flow. Sampling occurs during the rising tide, focusing on maximum flood currents to capture water with high suspended particle loads. A total of 18 samples are collected in 1L PE containers over approximately one hour.

After collection, samples are kept cool, dark, and undisturbed until analyzed in the lab within 48 hours. For calibration, the samples are divided into fractions to create a dilution series with varying turbidity levels, facilitating the development of an NTU-to-SPM conversion. The fractions are mixed to generate different turbidity conditions, and NTU readings are recorded in real-time with OBS for two minutes. Suspended solids were then quantified by filtering the samples through pre-combusted glass fiber filters and drying them at 105°C to determine their mass. This procedure captures the natural variability in particle size and concentration.

A linear regression model was developed using the logged NTU data and the measured SPM concentrations, producing a calibration curve that reliably correlates OBS readings to actual SPM values. This method accounts for variability in OBS response to changing concentrations and provides a robust conversion from optical backscatter to suspended sediment mass (Figure 2.4).

As shown in Figure 2.4, the high R^2 values across most models confirm that turbidity is a strong predictor of SPM. However, variations in slope and intercept values provide insights into how different sites are influenced by their unique environmental conditions. For instance, in autumn, the slopes across all sites range from 1.45 to 1.62, showing a stable relationship between turbidity and SPM. The intercepts vary slightly: Branst at -12.5, Lillo at -4.29, and Zuidgors at -9.7, suggesting different SPM levels when turbidity is near zero due to site-specific factors.

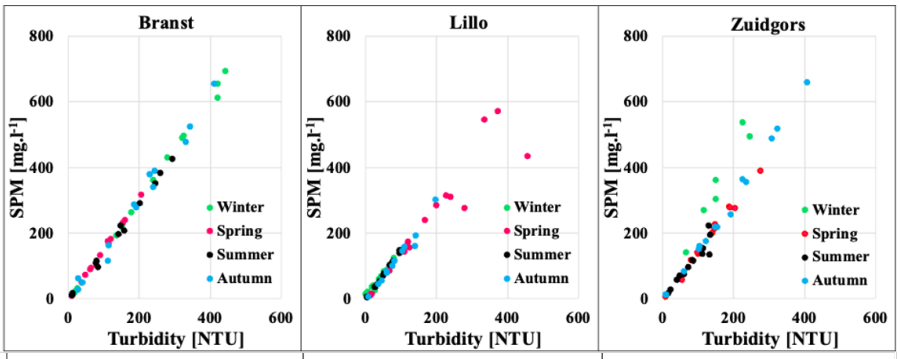

Season	Branst	Lillo	Zuidgors
Autumn	SPM=1.59 × Turbidity - 12.5 R^2=0.994	SPM=1.45 × Turbidity – 4.29 R^2=0.98	SPM=1.62 × Turbidity – 9.7 R^2=0.994
Winter	SPM=1.58 × Turbidity – 10.15 R^2=0.997	SPM=1.35 × Turbidity – 12.85 R^2=0.98	SPM=2.95 × Turbidity – 74.64 R^2=0.993
Spring	SPM=1.58 × Turbidity – 5.25 R^2=0.997	SPM=1.24 × Turbidity – 13.68 R^2=0.88	SPM=1.24 × Turbidity – 13.68 R^2=0.88
Summer	SPM=1.48 × Turbidity – 5.75 R^2=0.996	SPM=1.51 × Turbidity – 0.129 R^2=0.996	SPM=1.39 × Turbidity – 1.55 R^2=0.916

Figure 2.4: Calibration curves showing the relationship between OBS measurements (NTU) and SPM concentrations (mg/l) for each site (Branst, Lillo, and Zuidgors) across the four seasons. Each plot presents a linear regression model based on laboratory analyses of water samples collected during peak flood conditions, with corresponding R² values indicating the strength of the correlation. Variability in slope and intercept reflects site-specific environmental factors, such as particle size, composition, and turbidity response. These calibration equations were applied to transform continuous OBS data from sensors deployed near the bed into SPM time series.

In winter, the models remain highly predictive, with Zuidgors standing out with a slope of 2.95 and a negative intercept of -74.64. This suggests potential variability in the OBS-SPM relationship, possibly influenced by changes in sediment composition or particle size distribution during the sampling period. In spring, the model's strength decreases at Lillo and Zuidgors, where the slope drops to 1.24, suggesting that factors such as biological or finer sediment particles may have impacted SPM concentrations. Conversely, Branst maintains a strong relationship, reflecting a stable SPM-turbidity relationship across all seasons. In summer, slopes are stable across most sites, while Zuidgors shows slight variability with an intercept of -1.55.

These variations in intercept and slope demonstrate that the optical response of suspended particles—on which OBS measurements rely—is not temporally stable. Applying a single, year-round calibration curve would introduce systematic seasonal bias in SPM estimation. Therefore, season-specific calibration equations were used to improve the accuracy and site-representativeness of NTU-to-SPM conversion, enhancing the reliability of the SPM time series

under varying hydrodynamic and biological conditions. To estimate SPM concentrations from raw OBS data, which is measured every 5 minutes over 15 days, regression parameters specific to each season and station were applied.

2.2.3.3. The Median Particle Size (D50)

The PSD of SPM in estuarine environments is often multimodal, due to the combined processes of aggregation and fragmentation caused by hydrodynamic forces, sediment transport, and flocculation. As described by Lee et al. (2012), the PSD of SPM reflects a continuum of particle sizes, including primary particles, small aggregates, and larger flocs. This multimodality occurs because particles frequently collide, aggregate, and break apart under changing environmental conditions, creating a dynamic range of particle sizes suspended in the water column.

SPM can be categorized into several particle size groups based on aggregation state (Lee et al., 2012). Primary particles typically measure less than 4 μm and consist of clay minerals and fine organic matter. These may aggregate to form flocculi (4–40 μm), which are compact and dense early-stage flocs. Flocculi can further aggregate into microflocs (40–200 μm), and ultimately into macroflocs (>200 μm), which are loosely bound, porous, and structurally complex. Macroflocs exhibit high water content and low effective density, making them highly sensitive to turbulence and prone to fragmentation.

In this study, PSD was measured using a LISST-200X (Sequoia Scientific), which estimates particle size through laser diffraction over a 1–500 μm range. The instrument does not distinguish between primary particles and aggregates; thus, the detected particle sizes reflect both individual particles and flocculated structures. The median particle size (D50) is calculated from the volume-based PSD and is used as a proxy for floc size.

D50 is derived using Sequoia Scientific's recommended method, which accounts for the non-equidistant bin sizes by applying midpoint-based weighting (Sequoia Scientific, 2010). The resulting value represents the particle size at which 50% of the total volume lies below and 50% lies above. As a single descriptor, D50 serves as an integrative metric for assessing prevailing floc size and comparing aggregation states across conditions.

However, interpretation of D50 requires caution. By definition, D50 reflects the size at which half of the total volume is composed of smaller particles and half of larger ones; it does not represent the most frequent (modal) size class or the average particle size.

In floc-rich estuarine environments, PSDs are often right-skewed, meaning that a small number of large particles—such as macroflocs (>200 μm)—can disproportionately contribute to the total

volume. Due to their large size and low abundance, these macroflocs can dominate the volume distribution without raising the D50 above 200 μm. Indeed, D50 values between 130–160 μm may still indicate macrofloc-dominated systems. This occurs because D50 is a cumulative volume-based metric, and the 50% volume threshold may be reached before the largest size classes contribute.

Additionally, D50 reflects volume rather than mass. Larger flocs tend to be porous and water-rich, contributing more to total volume than to mass. Conversely, smaller, denser particles—such as flocculi and primary particles—may represent a smaller volume fraction while accounting for a larger share of total mass. As noted by Fall et al. (2021), estuarine systems often concentrate most of their mass in these lower size classes. This distinction is critical when interpreting PSD data in the context of sediment transport and deposition.

In summary, D50 and floc class distributions offer complementary insights into the characteristics of suspended particles. While D50 captures the central tendency of the volume-based PSD, class-based breakdowns reveal the structure and aggregation state of the suspended matter. This distinction is particularly important in flocculation-dominated environments such as estuarine intertidal zones, where floc size, structure, and stability influence settling behavior, resuspension potential, and bed level changes. Understanding both metrics is therefore essential for interpreting sediment transport processes and for evaluating how environmental drivers—such as turbulence and organic content—shape the fate of suspended sediments.

2.2.3.4. Estimation of Mud and Sand Fractions from Coupled OBS–ADV

To qualitatively assess whether suspended material was dominated by mud/flocs or sand, the Sediment Composition Index (SCI) method was applied, following the approach of Tran et al. (2024). SCI is defined as:

$$SCI = 10 \,.\, log_{10}\left(OBS_{signal}\right) - ADV_{signal} \quad \text{Eq. (5)}$$

where the OBS signal (optical backscatter) was recorded in nephelometric turbidity units (NTU), and the ADV signal (acoustic backscatter) was originally recorded as amplitude (AMP) values. To align with the SCI methodology, AMP values were first converted to a pseudo-decibel (dB) scale using the following transformation:

$$ADV\ (dB) = 10 \,.\, log_{10}(AMP) \quad \text{Eq. (6)}$$

This conversion ensured consistency with the unit conventions used by Tran et al. (2024). The resulting SCI is a dimensionless indicator that captures the relative dominance of mud or sand in suspension.

According to Tran et al. (2024), positive SCI values indicate a suspension dominated by mud or flocculated particles (typically < 63 μm, low-density aggregates), while negative SCI values suggest a suspension dominated by sand-sized particles (typically > 63 μm, higher-density grains). This interpretation is based on the differing sensitivities of optical and acoustic backscatter sensors: optical sensors respond more strongly to fine mud, whereas acoustic sensors are more sensitive to coarser, denser particles such as sand.

In this study, SCI was calculated for all sampling periods at each station. Rather than quantitatively estimating mud or sand fractions—an approach that would require site-specific calibration—SCI was used qualitatively to support interpretation of observed floc size distributions, macrofloc proportions, and sediment transport behavior. Consistently positive SCI values were interpreted as strong evidence of mud/floc dominance, whereas negative values indicated potential contributions from sand. Slightly negative SCI values (approximately –1 to –2) may reflect compact or dense flocs that exhibit acoustic properties similar to sand, particularly in dynamic, high-energy environments.

2.2.3.5. Bed Level Change Estimation

The downward-looking orientation of the ADV not only measures water velocity but also gauges the distance to the water-bed interface, adding a valuable dimension to the dataset. The key parameter in this calculation is the distance from the seabed to the ADV probe (DSP), measured with an accuracy of ±1 mm (Pang et al., 2021). Shifts in the DSP are used to identify changes in bed elevation.

By tracking DSP values at the beginning and end of each burst, the ADV records changes in seabed elevation over time. This process involves capturing DSP measurements at the start and end of each 15-minute burst period (see Section 2.2.3.1 for details on burst mode). Analysis of these values enables detection of short-term fluctuations in bed surface elevation within each burst.

Monitoring DSP at these critical time points provides a reliable method for quantifying seabed height changes, facilitating a detailed understanding of sediment dynamics and bed morphology throughout the observation period. Specifically, by comparing DSP values at the start and end of each burst—and examining trends between the first and last bursts of each season—net bed level

changes can be identified. This approach indicates whether sediment is accumulating or eroding over time, offering insights into the long-term morphological evolution of the seabed.

2.3. Results

The primary objective of this study is to investigate the behavior of SPM and its contribution to bed level changes. Suspended particle size is a key parameter in this analysis, as it provides insight into sediment transport and settling dynamics. Across the three stations—Zuidgors, Lillo, and Branst— macroflocs (>200 μm) represent the dominant size class, with geometric mean volume contributions of 85%, 82%, and 81%, respectively (Table 2.2). This indicates highly active flocculation and the presence of large aggregates, particularly under conditions favorable to floc stability and settling.

Table 2.2: Summary of SPM size class distribution across the three stations, based on volume percentage (%). Values represent the geometric mean ± geometric standard deviation, calculated from LISST particle size distributions. The data are grouped according to flocculation-based categories: primary particles (<4 μm), flocculi (4–40 μm), microflocs (40–200 μm), and macroflocs (>200 μm). Because the geometric mean multiplies values and then takes the root—treating each value more like a ratio than a simple number—the resulting averages may not sum exactly to 100%.

Parameter	Branst	Lillo	Zuidgors
Primary Particles (<4 μm) (%)	0.0006 ± 8.60	0.0002 ± 3.90	0.0005 ± 8.30
Flocculi (4–40 μm) (%)	4.00 ± 2.10	3.00 ± 3.40	2.00 ± 4.00
Microflocs (40–200 μm) (%)	12.00 ± 2.00	11.00 ± 2.00	9.00 ± 2.00
Macroflocs (>200 μm) (%)	81.00 ± 1.00	82.00 ± 1.00	85.00 ± 1.00

Microflocs (40–200 μm) constitute the second-largest volume fraction at all sites, contributing between 9% and 12%. Flocculi (4–40 μm) are present in smaller proportions, ranging from 2% to 4%, while primary particles (<4 μm) are nearly negligible, with contributions below 0.001% at all stations.

The consistently high proportion of macroflocs suggests that estuarine conditions generally support the formation and preservation of large flocculated structures. As the LISST estimates particle size based on light scattering without distinguishing material composition, the macrofloc size range may include both large flocculated aggregates and coarser or denser particles.

The volume-weighted median floc size (D50) across the three stations is relatively consistent under overall conditions, ranging from approximately 126 to 136 μm (Table 2.3). However, notable differences emerge between flood and ebb phases. At all stations, D50 values are consistently

higher during flood tides, with increases of approximately 21% at Branst, 56% at Lillo, and 16% at Zuidgors. These increases suggest enhanced floc aggregation during flood conditions, potentially driven by longer residence times, greater SPM availability, or salinity gradients. The particularly large increase observed at Lillo may also be associated with localized human activities—such as dredging—which disturb the sediment bed and alter hydrodynamic conditions, thereby influencing the flocculation environment and promoting the formation of larger aggregates during flood tides.

Table 2.3: Summary of hydrodynamic and sediment parameters (mean ± standard deviation) measured during both flood (F) and ebb (E) tides at the three study sites. These values provide insight into site-specific and tidal-phase differences in sediment behavior across freshwater (Branst), brackish (Lillo), and saline (Zuidgors) zones.

Parameter	Branst	Lillo	Zuidgors
Floc size [D50] (µm)	136.00 ± 1.00 (**F:** 149.00 ± 1.00, **E:** 123.00 ± 1.00)	127.00 ± 1.00 (**F:** 155.00 ± 1.00, **E:** 99.00 ± 1.00)	129.00 ± 1.00 (**F:** 135.00 ± 1.00, **E:** 117.00 ± 1.00)
SPM concentration ($mg.l^{-1}$)	192.00 ± 1.50 (**F:** 340.00 ± 1.50, **E:** 140.00 ± 1.50)	169.00 ± 1.32 (**F:** 203.00 ± 1.22, **E:** 160.00 ± 1.50)	338.00 ± 1.50 (**F:** 418.00 ± 1.50, **E:** 280.80 ± 1.50)
Current velocity ($m.s^{-1}$)	0.22 ± 0.13 (**F:** 0.20 ± 0.07, **E:** 0.25 ± 0.04)	0.22 ± 0.12 (**F:** 0.20 ± 0.05, **E:** 0.25 ± 0.03)	0.28 ± 0.16 (**F:** 0.35 ± 0.08, **E:** 0.21 ± 0.04)
Shear rate G (s^{-1})	0.55 ± 0.50 (**F:** 0.37 ± 0.20, **E:** 0.73 ± 0.20)	0.87 ± 0.70 (**F:** 0.90 ± 0.35, **E:** 0.80 ± 0.30)	1.50 ± 1.00 (**F:** 1.70 ± 0.45, **E:** 1.10 ± 0.30)

In terms of bed level changes (Figure 2.5), sedimentation trends across the three stations reveal a mix of accumulation and stability, with site-specific variations. Zuidgors generally experiences sediment accumulation, indicating a depositional environment where sediment builds up over time. Lillo remains stable, with minimal bed level changes, suggesting a balance between sediment deposition and erosion. Branst shows the highest variability, with alternating phases of accumulation and erosion, reflecting a more dynamic sedimentary environment influenced by multiple hydrodynamic drivers.

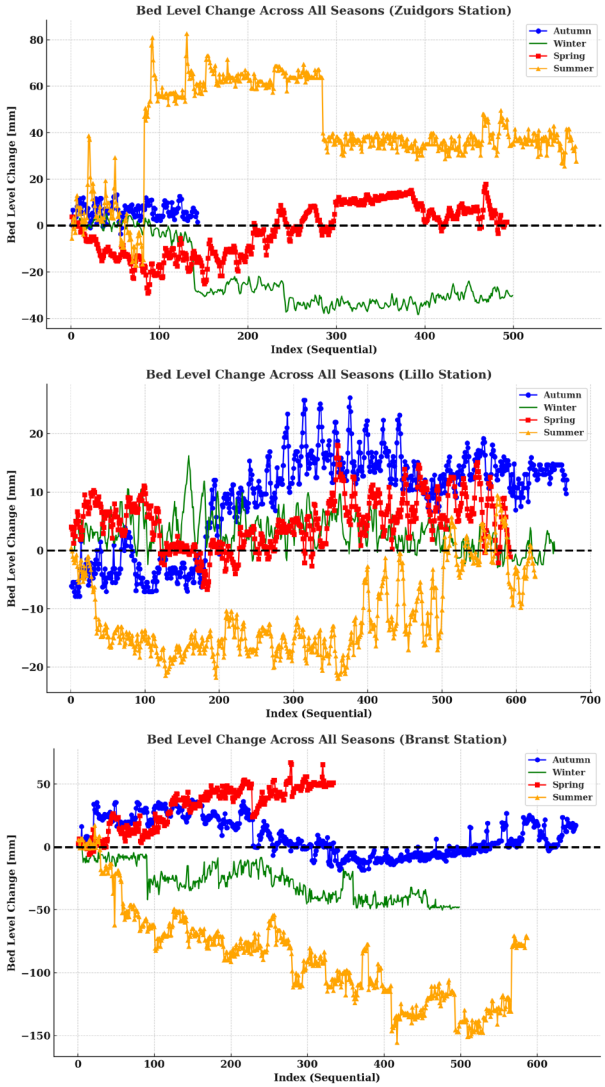

Figure 2.5: Relative bed level changes observed at Branst, Lillo, and Zuidgors during seasonal field campaigns. Positive values indicate sediment deposition, and negative values indicate erosion, both measured relative to the initial bed level at the start of each seasonal campaign. The x-axis represents the sequential order of measurements within each campaign (from Day 1 onward).

Moreover, across all seasons and stations, SPM concentrations consistently exhibit a flood-dominant pattern, with higher values during flood tides compared to ebb. This trend is most pronounced at Zuidgors, where both the highest overall SPM levels and the largest flood–ebb contrast were observed. Branst, despite having the lowest average SPM concentrations, also

demonstrated strong tidal asymmetry, with flood-phase values more than double those during ebb. Lillo followed a similar trend, though the flood–ebb contrast was more moderate. These patterns indicate a system-wide tendency toward flood-driven SPM import, with site-specific differences in magnitude likely influenced by local hydrodynamic conditions and estuarine position.

It is important to note that the SPM concentrations presented here reflect near-bed conditions in shallow intertidal flats and are substantially higher than values typically reported from the main estuarine channel, where measurements are often depth-averaged and represent broader hydrodynamic regimes. This highlights the dominant role of localized sediment resuspension and near-bed processes in mudflat environments. A more detailed comparison with main channel observations is provided in the discussion (Section 2.4).

Finally, the analysis of hydrodynamic conditions—including current velocity and shear rate (G)—provides additional insight into sediment transport dynamics at the study sites. Zuidgors recorded the highest current velocities and shear rates, particularly during flood tides. Branst and Lillo showed similar velocity patterns, with higher values during ebb, which may contribute to increased sediment resuspension and reduced floc sizes during this phase. Shear rates (G) generally followed the trends in velocity, with higher values during ebb at Branst, more balanced conditions at Lillo, and marked variation between flood and ebb at Zuidgors.

2.3.1. Seasonal Analysis: Variation Patterns Across Seasons

Following the analysis of overall trends, seasonal variations in key parameters were examined across the monitoring stations, as well as the correlation between bed level changes and other variables. A summary of parameter values across the three locations is provided in Table 2.5, while the corresponding seasonal time series for each station is presented in Appendix 2.B.

2.3.1.1. Particle Size Distribution

Across all seasons and sites, the PSD of SPM is consistently dominated by macroflocs (>200 μm). Under general conditions, macroflocs account for 75–89% of the total particle volume, microflocs (40–200 μm) contribute 7–13%, flocculi (4–40 μm) make up 1–5%, and primary particles (<4 μm) are nearly negligible. This dominance highlights a strong flocculation capacity (Table 2.4).

Despite this overall consistency, seasonal and spatial deviations in PSD patterns emerge, reflecting the influence of local hydrodynamics, sediment availability, and biological activity on floc stability. To gain deeper insight into sediment dynamics, it is useful to assess whether these general PSD patterns persist during periods of elevated SPM concentrations, often triggered by events such as tidal peaks, or increased river discharge. During these events, particle aggregation, resuspension, and deposition are influenced by elevated turbulence and shear stress. Understanding how PSD patterns respond under such conditions helps determine whether sediment behavior remains stable or is dynamically responsive to environmental forcing. Detailed comparisons between overall PSD and those observed during high-SPM periods are provided in Appendix 2.C.

Moreover, to independently assess the nature of suspended material, the SCI was calculated using paired optical and acoustic backscatter data for each station and season (Figure 2.6). Positive SCI values indicate the dominance of mud or flocculated material, while negative values suggest the presence of sand-sized particles.

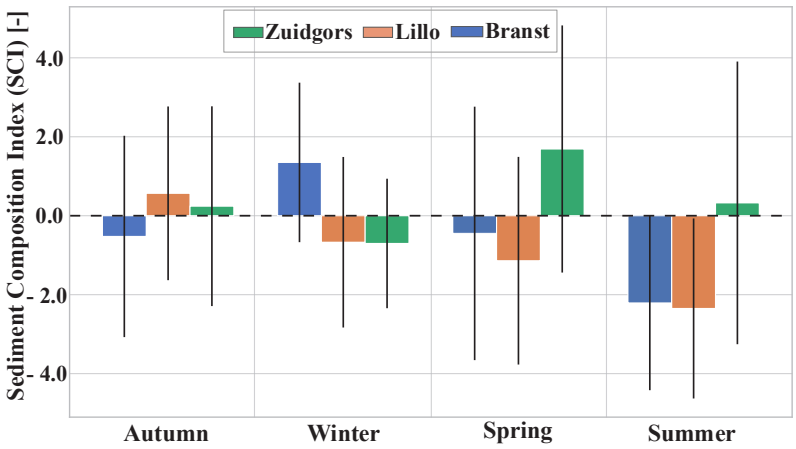

Figure 2.6: Seasonal distribution of the Sediment Composition Index (SCI) at Branst, Lillo, and Zuidgors. Each color represents a different site (Zuidgors in green, Lillo in orange, and Branst in blue), and each group of boxplots corresponds to one season. A horizontal dashed line at SCI = 0 separates mud/floc-dominated suspensions (SCI > 0) from sand-influenced suspensions (SCI < 0). Slightly negative SCI values (~–1 to –2) may reflect compacted or dense flocs that acoustically resemble sand. SCI values generally indicated floc-dominated conditions across stations and seasons, although Lillo and Branst exhibited lower and occasionally negative values during summer.

In autumn, macroflocs dominate the PSD at all stations. At Branst and Lillo, high-SPM periods reinforce the presence of coarser particles, suggesting favorable flocculation under moderate turbulence and sufficient particle supply. At Zuidgors, however, high SPM disrupts floc stability,

shifting the PSD toward smaller particles. SCI values were positive at Lillo and Zuidgors, aligning with PSD patterns. In contrast, Branst exhibited negative SCI values, suggesting influence from denser particles or occasional sand input, despite macrofloc dominance in the PSD.

Winter brings stronger turbulence, leading to minor reductions in macrofloc contributions—77% at Branst, 82% at Lillo, and 81% at Zuidgors. At Branst and Zuidgors, high SPM periods correspond with an increase in microflocs, suggesting that flocs are more prone to disaggregation. In contrast, Lillo maintains its coarse PSD and exhibits further enhancement of macrofloc proportions during high SPM periods, indicating that high sediment availability, coupled with relatively stable hydrodynamic conditions, supports sustained aggregation despite seasonal turbulence. SCI values during winter showed strong positive values at Branst, aligning with the persistence of flocs. In contrast, Lillo and Zuidgors showed negative SCI values, indicating possible temporary entrainment of coarser particles or compaction effects influencing backscatter, even though macroflocs still dominated the volume distribution.

Spring marks a recovery in macrofloc dominance. During high SPM events, all stations shift further toward coarser particles, indicating favorable conditions for floc growth and aggregation. SCI was strongly positive at Zuidgors, and near neutral at Branst. This general SCI behavior supports mud/floc dominance during spring. However, at Lillo, SCI remained negative despite strong macrofloc presence, indicating that dense flocs or minor coarse inputs may have influenced suspension characteristics.

In summer, site-specific behavior becomes more apparent. Macrofloc contributions peak at Lillo (88%) and Zuidgors (89%) and remain high at Branst (83%). Lillo continues to shift toward coarser particles during high-SPM periods, suggesting that local hydrodynamics and sediment properties promote persistent floc stability. In contrast, Branst and Zuidgors shift toward finer fractions, despite generally favorable biological conditions for floc formation. This counterintuitive trend suggests that other factors—possibly turbulence or sediment composition—affect floc structure under elevated SPM conditions. SCI values differ across sites: Zuidgors exhibits slightly positive mean values, indicating floc-dominated suspension despite its sand-rich bed. Lillo and Branst show strongly negative SCI values (SCI < -2). Given the mud-rich context at Lillo and freshwater influence at Branst, these negative values likely reflect denser or more compact flocs rather than actual sand resuspension.

Overall, macroflocs consistently dominate PSD across all sites and seasons. SCI analysis, however, reveals complex spatial and seasonal variation in suspension characteristics. The combination of PSD patterns, SCI values, and site-specific sediment settings underscores the importance of

considering floc density and structure—beyond particle size alone—when interpreting estuarine sediment dynamics.

Table 2.4: Seasonal distribution of SPM by size class across the three intertidal stations: Branst (freshwater zone), Lillo (brackish transition zone), and Zuidgors (saline zone). Values represent the geometric mean ± geometric standard deviation, calculated from LISST particle size distributions obtained under general (non-peak) conditions. Particle classes are defined as follows: primary particles (<4 µm), flocculi (4–40 µm), microflocs (40–200 µm), and macroflocs (>200 µm)

Station	Size Class (%)	Autumn	Winter	Spring	Summer
Branst	**Primary Particles (<4 µm)**	0.0004 ± 5.00	0.0004 ± 6.00	0.001 ± 13.00	0.0009 ± 13.00
	Flocculi (4–40 µm)	4.01 ± 2.00	4.70 ± 2.00	4.73 ± 1.00	3.35 ± 2.00
	Microflocs (40–200 µm)	10.30 ± 2.00	13.20 ± 2.00	11.63 ± 2.00	10.00 ± 1.00
	Macroflocs (>200 µm)	82.00 ± 1.00	77.00 ± 1.00	80.00 ± 1.00	83.00 ± 1.00
Lillo	**Primary Particles (<4 µm)**	0.0003 ± 4.00	0.0001 ± 3.00	0.0002 ± 4.00	0.0001 ± 5.00
	Flocculi (4–40 µm)	4.00 ± 3.00	3.00 ± 3.00	3.00 ± 4.00	2.00 ± 2.00
	Microflocs (40–200 µm)	13.00 ± 2.00	11.00 ± 2.00	9.00 ± 2.00	8.0 ± 2.00
	Macroflocs (>200 µm)	78.00 ± 1.00	82.00 ± 1.15	85.00 ± 1.00	88.00 ± 1.00
Zuidgors	**Primary Particles (<4 µm)**	0.0006 ± 21.00	0.0003 ± 6.00	0.0006 ± 6.00	0.0005 ± 7.50
	Flocculi (4–40 µm)	1.75 ± 5.00	3.00 ± 3.50	2.50 ± 2.30	1.50 ± 4.00
	Microflocs (40–200 µm)	9.00 ± 2.00	13.00 ± 2.00	9.00 ± 2.00	7.00 ± 2.00
	Macroflocs (>200 µm)	86.00 ± 1.00	81.00 ± 1.00	85.00 ± 1.00	89.00 ± 1.00

2.3.1.2. Bed Level Changes and Correlations

Analyzing seasonal bed level changes reveals the complex interplay between floc size, SPM concentration, and hydrodynamic conditions.

In autumn, all stations exhibited positive bed level changes, indicating widespread sediment accumulation. However, negative correlations (Figure 2.7) with current velocity, turbulent shear rate, and tidal range at Branst and Zuidgors suggest that elevated hydrodynamic energy limited further deposition. In contrast, positive correlations with floc size at both stations highlight the stabilizing effect of larger flocs. Lillo displayed an opposing pattern: bed level changes were positively correlated with hydrodynamic parameters but negatively correlated with mean floc size, indicating that physical forcing, rather than floc structure, may govern sediment stability at this site.

During winter, environmental variability resulted in erosion at Branst and Zuidgors, while Lillo remained stable. At Branst, negative correlations between bed level changes and both current velocity and floc size indicate that enhanced water movement contributed to instability. Despite erosion, Zuidgors exhibited positive correlations between bed level changes and all parameters, suggesting complex interactions in which high-energy conditions may have prevented sediment cohesion rather than simply promoting erosion. Meanwhile, Lillo maintained stable bed levels, with positive correlations to current velocity, shear rate, SPM, and tidal range, and a negative correlation with floc size, implying that alternative mechanisms beyond floc structure contributed to stability.

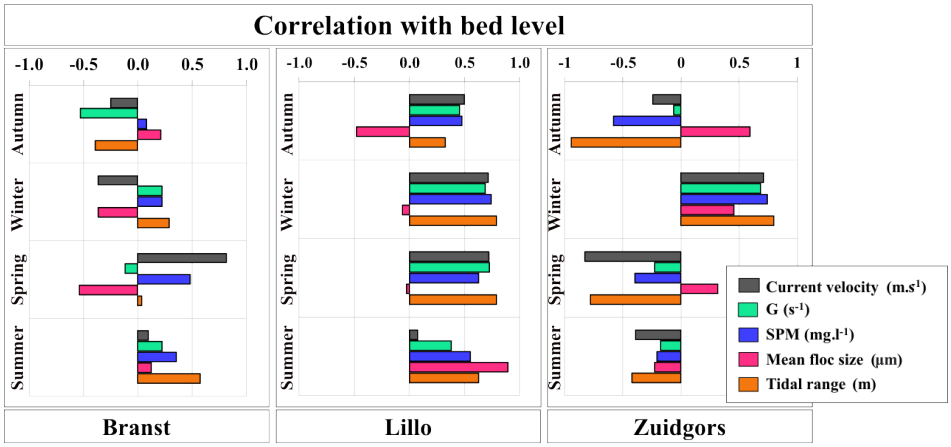

Figure 2.7: Correlation between bed level changes and key environmental parameters—current velocity (m.s $^{-1}$), turbulent shear rate G (s $^{-1}$), SPM concentration (mg.l $^{-1}$), mean floc size (µm), and tidal range (m)—at the three study sites: Branst (freshwater), Lillo (brackish), and Zuidgors (saline). Each bar represents the strength and direction of correlation between bed level variation and one parameter for a given season (Autumn, Winter, Spring, Summer), based on seasonally averaged observational data. Positive bars indicate a direct relationship with bed level rise (sedimentation), while negative bars reflect an inverse relationship (erosion tendency). The figure highlights how sedimentation and erosion processes are driven by different dominant controls across estuarine zones and seasons.

Spring marked a recovery phase, with all stations showing net sedimentation. At Branst, a negative correlation between floc size and bed level change suggests that larger flocs were less stable and more susceptible to resuspension. Positive correlations with SPM concentration, tidal range, and velocity imply that higher sediment availability and stronger tidal forcing promoted sediment deposition. The observed negative correlation with turbulence reinforces the idea that elevated shear stress near the bed can hinder sediment settling. Lillo showed a similar trend, with positive

correlations between bed level changes and SPM, tidal range, and velocity. However, floc size had little to no correlation with bed level change, indicating that hydrodynamic drivers were the primary influence on sediment behavior at this site. At Zuidgors, the positive correlation with floc size and negative correlations with other variables suggest the presence of additional stabilizing factors contributing to its sedimentation balance.

In summer, sediment dynamics varied considerably among stations. Zuidgors experienced notable sediment accumulation, while both Branst and Lillo underwent erosion. At Zuidgors, bed level changes were negatively correlated with all measured parameters, illustrating how seasonal conditions influenced sedimentation. In contrast, positive correlations at Branst and Lillo suggest that other unmeasured factors may have contributed to sediment loss during this period.

All reported correlations are statistically significant at $p < 0.001$, emphasizing that even small correlation coefficients are highly unlikely to have occurred by chance. This significance is supported by the large sample size and high variability in the dataset.

2.3.1.3. Changes in SPM, Mean Floc Size, and Hydrodynamics

The seasonal evolution of SPM concentration, floc size, and hydrodynamic conditions reveals pronounced site-specific contrasts that correspond with the direction and magnitude of observed bed level changes (Table 2.5).

In autumn, Branst—despite exhibiting the lowest SPM concentrations—recorded large mean floc sizes and low hydrodynamic energy. These conditions coincided with clear net accretion, indicating an environment favorable for sediment retention. Lillo, by contrast, showed moderate SPM levels, the smallest flocs of the season, and the highest shear rates among all sites, yet still experienced net sedimentation—suggesting the existence of a threshold beyond which transport processes do not override deposition. Zuidgors, characterized by both high SPM and elevated floc sizes, exhibited only limited net accretion despite moderate hydrodynamic forcing.

During winter, the balance between physical drivers and floc characteristics shifted. At Branst, a significant seasonal increase in SPM coupled with a marked reduction in floc size occurred alongside rising velocities and shear rates, resulting in strong net erosion. A similar trend was observed at Zuidgors, where intensified hydrodynamics, elevated SPM concentrations, and finer flocs led to continued erosion. In contrast, Lillo maintained relatively stable floc characteristics, lower SPM levels, and moderate shear, corresponding with negligible change in bed elevation—highlighting the stabilizing effect of consistent floc structure under moderate flow conditions.

In spring, the data indicate a reorganization of floc and flow regimes. At Branst, accretion resumed, supported by increasing floc sizes and only moderate hydrodynamic forcing. Lillo experienced slight accumulation under stable SPM and floc size conditions, accompanied by low velocities and shear. Zuidgors, despite recording the highest SPM concentrations and floc sizes of the year, exhibited minimal net bed level change, suggesting that sediment accumulation was counterbalanced by persistent or episodic turbulence.

Table 2.5: Seasonal summary of SPM concentration, mean floc size, current velocity, and shear rate (G) at the three intertidal stations: Branst, Lillo, and Zuidgors. Values represent geometric mean ± geometric standard deviation. Net bed level (BL) change is included to illustrate seasonal sediment accumulation or erosion, offering insight into the relationship between sediment dynamics, floc structure, and hydrodynamic forcing.

Station	Season	Net BL Change (mm)	SPM Concentration ($mg.l^{-1}$)	Floc Size (µm)	Velocity ($m.s^{-1}$)	Shear Rate G (s^{-1})
Branst	Autumn	12.10	182.00 ± 1.99	140.00 ± 2.00	0.16 ± 0.10	0.36 ± 0.25
	Winter	-50.80	307.00 ± 2.00	111.00 ± 2.00	0.22 ± 0.12	0.87 ± 0.68
	Spring	46.80	205.00 ± 2.00	156.00 ± 1.00	0.30 ± 0.11	0.57 ± 0.39
	Summer	-77.70	118.00 ± 2.00	143.00 ± 1.00	0.21 ± 0.15	0.41 ± 0.34
Lillo	Autumn	18.40	237.00 ± 2.00	107.00 ± 2.00	0.21 ± 0.13	1.00 ± 0.8
	Winter	1.33	183.00 ± 1.50	114.00 ± 1.50	0.22 ± 0.11	0.93 ± 0.63
	Spring	1.70	153.00 ± 2.00	139 ± 1.00	0.21 ± 0.13	0.85 ± 0.6
	Summer	-1.50	123.00 ± 2.00	152.00 ± 1.00	0.21 ± 0.12	0.71 ± 0.53
Zuidgors	Autumn	5.20	322.00 ± 1.50	135.00 ± 1.00	0.24 ± 0.11	0.98 ± 0.74
	Winter	-30.00	302.00 ± 2.00	99.00 ± 1.00	0.29 ± 0.17	1.65 ± 1.18
	Spring	0.63	605.00 ± 2.00	132.00 ± 1.00	0.30 ± 0.19	2.06 ± 1.20
	Summer	42.20	223.00 ± 2.50	157.00 ± 1.00	0.30 ± 0.17	1.27 ± 1.05

Summer revealed a marked decoupling between SPM levels and net deposition. At Branst, moderate SPM and floc size were accompanied by continued erosion under low current energy, indicating possible sediment instability or post-depositional reworking. Lillo recorded the largest flocs of the year under low SPM concentrations and minimal shear, yet experienced slight net erosion—implying that floc size alone may be insufficient to drive sediment accumulation in the absence of favorable transport conditions. At Zuidgors, elevated floc sizes and moderate SPM concentrations coincided with a return to net accretion, despite experiencing the highest current velocities of the season. This suggests improved floc persistence or temporarily lowered erosion thresholds under specific seasonal dynamics.

2.3.2. Temporal Analysis: Variation Patterns Across Tidal Cycles

By stacking all tidal cycles, this analysis evaluates whether key parameters exhibit consistent trends across stations. Visualizations of these results for all three stations are provided in Appendix 2.D. A general finding is that minimal bed level changes within individual tidal cycles across all stations highlight the gradual and cumulative nature of tidal forcing.

Hydrodynamic conditions show that current velocity consistently peaks during flood tides at all stations, acting as the primary driver of sediment transport. This pattern is particularly evident at Lillo and Zuidgors, where peak velocities align with the highest levels of sediment movement and SPM concentrations. The turbulent shear rate (G) follows a similar pattern—peaking during flood tide, dropping sharply at high water slack, and rising again during the ebb tide. Branst differs slightly, maintaining non-zero current velocity and shear rate even at high water slack, indicating continuous sediment motion and turbulence throughout the tidal cycle.

SPM concentrations increase during the flood phase and decrease around high water at all stations. However, ebb-tide behavior varies by site. At Branst, SPM concentrations continue to decline throughout the ebb phase. In contrast, at Lillo and Zuidgors, SPM concentrations initially decrease during ebb but increase again later in the tidal cycle.

Floc size trends also show site-specific and seasonal differences. At Branst, floc size generally decreases during the flood tide and tends to stabilize or slightly increase at high water. During the ebb tide, floc size patterns vary by season: in autumn, winter, and summer, floc size increases initially and then decreases, whereas in spring, it follows a mixed pattern of increasing, decreasing, and then increasing again. Lillo and Zuidgors exhibit more consistent floc size trends throughout the tidal cycle. At both stations, floc size increases during the early flood phase, peaks around high water, and decreases during the ebb period—likely due to rising turbulence that breaks larger aggregates into smaller particles.

2.3.2.1. Analyzing Sediment Spikes: Beyond Regular Tides

Tidal cycle variations often cause fluctuations in water levels, resulting in significant changes in sediment movement and deposition. To better understand the influence of these variations on suspended sediments, neap and spring tides were analyzed. Despite their well-documented role in sediment dynamics, no significant changes in sediment movement were observed during these periods, suggesting that typical tidal fluctuations alone do not account for major variations in sediment behavior.

To quantitatively identify and assess significant sediment movement and deposition events, a z-score analysis was applied to the bed level data across tidal cycles—a statistical method commonly used for detecting outliers in environmental datasets (Tukey, 1977; Iglewicz & Hoaglin, 1993). This approach enabled the detection of unusual bed level changes—referred to as "spikes"—likely associated with intense sediment resuspension or deposition events. Tidal cycles with z-scores greater than +3 were classified as positive spikes (indicating significant deposition), and those with z-scores less than −3 were classified as negative spikes (indicating erosion or resuspension). Tidal cycles with z-scores between −3 and +3 were considered regular, indicating no abnormal bed level change. The related plots are presented in Appendix 2.E.

By comparing environmental conditions during these spikes with those during regular tidal cycles, the analysis aimed to identify the key factors contributing to sediment instability and redistribution. This methodology enabled a clear distinction between background sediment transport and events driven by external forcing, offering a more nuanced understanding of sediment behavior in intertidal zones. Negative spikes generally reflect erosion and sediment resuspension, while positive spikes indicate sediment deposition and accumulation—underscoring the dynamic nature of estuarine sedimentary processes.

The analysis of erosion and sedimentation spikes at Branst, Lillo, and Zuidgors illustrates the complex interplay between tidal forces and site-specific environmental conditions, showing that similar hydrodynamic conditions can lead to contrasting outcomes. Several key drivers were identified:

- Firstly, high hydrodynamic energy—characterized by strong currents and turbulence—typically results in negative spikes, indicating erosion. These conditions disrupt sediment cohesion and cause particles to be resuspended in the water column.

- Secondly, high current velocities can lead to both erosion and sedimentation spikes, depending on additional factors such as SPM concentration and floc size. At Branst, during spring and summer, high velocities frequently induce sediment resuspension and erosion. However, when SPM concentrations are elevated, these same conditions can result in sedimentation spikes. The key difference lies in floc size: larger flocs in spring enhance sediment cohesion and promote deposition, whereas smaller flocs in summer increase susceptibility to erosion despite high SPM levels. Lillo shows a comparable pattern during autumn, spring, and summer, where high current velocities combined with elevated SPM levels contribute to both erosion and sedimentation spikes. In autumn and spring, smaller floc sizes during spike events compared to non-spike periods indicate that finer particles are more reactive to turbulent conditions. Although floc size data for summer are unavailable, similar dynamics are likely. At Zuidgors,

erosion and sedimentation spikes during spring and summer are also linked to high current velocities. In spring, smaller flocs enhance resuspension, while in summer, larger flocs support deposition. This highlights how seasonal variations in sediment composition affect outcomes under similar conditions.

- Lastly, the occurrence of positive spikes appears to depend on specific conditions. At Branst, positive spikes are observed under lower velocity conditions. In winter, reduced SPM concentrations and lower turbulence favor sediment settling. In autumn, higher SPM concentrations combined with increased tidal ranges promote substantial sediment accumulation. In contrast, Lillo (winter) and Zuidgors (winter and autumn) did not experience positive spikes, likely due to excessively strong current velocities that prevented particles from settling and maintained them in suspension.

2.4. Discussion

The analysis indicates that sediment dynamics at the studied sites are primarily governed by the interaction between floc characteristics and hydrodynamic forces, resulting in distinct, site-specific patterns of sedimentation and erosion. These patterns are strongly influenced by seasonal variability, SPM concentration and behavior, and the presence of organic matter which enhance floc cohesion and stability by promoting particle aggregation and binding with mineral components. Consequently, predicting SPM accommodation space becomes highly dependent on localized and dynamic changes in these parameters, underscoring the importance of site-specific assessments and sustained monitoring.

2.4.1. Floc Size and SPM Concentration Variability: Environmental and Methodological Influences

Floc size patterns in this study exhibited clear tidal-phase and seasonal variability across the three intertidal stations, reflecting the complex and dynamic interplay between biological processes, hydrodynamic forcing, and site-specific environmental conditions. Using LISST-200X measurements, median floc sizes (D50) ranged from 99 μm to 157 μm across all sites and seasons. These values fall within—and in several cases exceed—the typical floc size range of 70–150 μm previously reported for the Scheldt estuary, indicating high flocculation potential under certain local conditions. Across all stations, floc sizes generally increased in spring and summer—coinciding with the growing season when EPS/TEP production and microbial aggregation are more active. However, the degree of this seasonal response varied by site. For example, floc sizes

at Zuidgors ranged from 99 μm in winter to 157 μm in summer, while Lillo showed a similar pattern from 107 μm to 152 μm. Branst also exhibited seasonal variation (111–156 μm), though with less consistency in trend, likely reflecting a more dynamic interplay between riverine discharge, freshwater turbulence, and lower salinity, which can weaken electrochemical floc bonds. Notably, all stations experienced smaller floc sizes in winter, consistent with stronger hydrodynamic forcing and reduced biological aggregation.

To contextualize these findings, several earlier studies have reported floc sizes in the Scheldt using different instruments. Wartel and Francken (1998), using a Benthos plankton camera, reported average floc sizes of ~70 μm between km 60 and 100 (around the Lillo region), without strong longitudinal gradients. Chen et al. (2005), employing the pipette method based on settling velocity, observed flocs ranging from 30–40 μm in winter to ~90 μm in summer at km 100 (Branst) and km 20 (Zuidgors), capturing both seasonal variability and site-specific dynamics. The smaller values in these studies likely result not only from natural variation but also from differences in methodology.

Indeed, the method used to characterize flocs has a major influence on reported values. Optical instruments like the LISST-200X provide real-time, in situ particle size spectra, allowing for the detection of weakly bound and rapidly evolving aggregates that might otherwise disintegrate during sampling. In contrast, methods such as pipette or image-based techniques are more intrusive or slower, potentially underestimating fragile macroflocs. These differences do not necessarily reflect superiority of one method over another, but highlight the need to interpret floc size measurements in light of their methodological context.

Even when using the same instrument, floc sizes can vary substantially depending on hydrodynamic context. For instance, Horemans et al. (2021), who also employed the LISST-200X in the Scheldt's main channel, reported floc sizes of 100–110 μm in summer and 70–80 μm in winter at km 110 (Branst)—notably smaller than the intertidal flat values found in this study. Their Lillo values (90–100 μm in summer) were also lower than this study, likely due to differences in energy regimes.

Comparable floc size patterns have also been documented in other estuarine systems. Egan et al. (2022), using LISST-100X in the South San Francisco Bay, reported flocs ranging from 50 to 200 μm, with seasonal peaks tied to biological activity. Uncles et al. (2010), using the INSSEV-LF camera in the Tamar Estuary, recorded flocs spanning from <50 μm to >500 μm, emphasizing how floc size responds to tidal phase and sediment type. Similarly, Guo et al. (2018) observed floc sizes between 50 and 200 μm in the Kapellebank tidal flat, aligning well with the present study

and further supporting the influence of local hydrodynamics and organic content on floc formation.

Overall, the observed range of floc sizes across studies reflects not only environmental variability but also differences in sampling location, measurement technique, and local energy conditions. These factors must be carefully considered when comparing across estuarine systems or evaluating long-term trends.

An important additional insight from this study is the observed divergence between median floc size (D50), macrofloc dominance, and suspension composition as indicated by SCI. Macrofloc proportion quantifies the volumetric dominance of large aggregates (>200 μm), highlighting the system's tendency toward flocculation. Median floc size (D50) captures the central tendency of the suspended particle distribution, sensitive to shifts toward finer or coarser fractions. SCI provides complementary information on the material's optical and acoustic properties, distinguishing between mud-floc dominated and sand-influenced or compacted particle suspensions (Tran et al., 2024).

At Zuidgors, a sand-rich site, during spring, macroflocs made up 85% of the total volume, D50 reached 132 μm, and SCI values were strongly positive (+1.69). These converging observations indicate a stable, floc-dominated suspension likely favorable for sedimentation. In contrast, during winter, although macroflocs still comprised 81% of the volume, D50 dropped to 99 μm and SCI became slightly negative (mean: −0.703). According to Tran et al. (2024), slightly negative SCI values may reflect compacted or dense flocs behaving acoustically like sand, particularly in energetic environments such as Zuidgors, which is strongly influenced by tidal dynamics. While these observations suggest that the suspended material remained predominantly flocculated mud, the interpretation of negative or near-zero SCI values at Zuidgors requires caution. Especially during winter and summer, temporary entrainment of true sand particles during high-energy events cannot be excluded and warrants further investigation.

A more complex pattern emerged at Lillo during summer. Despite high macrofloc shares and relatively large D50 values, SCI values were strongly negative (−2.21 to −2.71). According to Tran et al. (2024), strongly negative SCI values are typically associated with sand resuspension. However, considering the naturally mud-rich sediment composition at Lillo and the freshwater influence at Branst, it is more likely that these values reflect the presence of dense, compacted flocs behaving acoustically like sand rather than significant entrainment of true sand grains. These observations highlight that high macrofloc shares alone do not guarantee effective sedimentation if flocs are structurally compacted, as evidenced by shifts in D50 and SCI. The combined analysis of macrofloc dominance, D50 trends, and SCI signatures provides critical insights into floc

structural integrity, suspension behavior, and the potential for sediment deposition or resuspension in dynamic estuarine environments.

While floc size distributions provide insight into particle aggregation and structural stability, SPM concentrations reflect the net outcome of sediment supply, resuspension, and transport. In this context, SPM values measured across the intertidal flats exhibited clear tidal-phase asymmetries with flood-dominant patterns, with higher values during flood tides than during ebb. This asymmetry was most pronounced at Zuidgors, where both the highest overall SPM levels and the largest flood–ebb differences were observed. Although Branst recorded the lowest overall SPM concentrations, it also showed strong flood dominance, with flood-tide concentrations more than twice those during ebb. Lillo followed a similar trend, though with a more moderate flood–ebb contrast. These patterns collectively indicate a system-wide tendency for flood-driven SPM import, modulated by site-specific factors such as local hydrodynamics, estuarine position, and sediment availability.

It is important to note that the SPM concentrations reported here reflect near-bed measurements, taken approximately 12–13 cm above the sediment surface in shallow intertidal flats. These values are substantially higher than the depth-averaged SPM concentrations reported in the main channel of the Scheldt estuary. Maris et al. (2024) documented long-term trends (2000–2020) based on depth-integrated sampling, focusing on the vertical distribution of suspended sediments and their relationship with hydrodynamic conditions. Their reported SPM values are notably lower than those observed in this study (Figure 2.8). This contrast is primarily due to differences in hydro-morphological settings. The main channel is characterized by greater depth, stronger tidal currents, and enhanced vertical mixing, which distribute suspended material more evenly throughout the water column and reduce the persistence of near-bed SPM layers. Intertidal mudflats, by contrast, experience shallower depths and localized hydrodynamic forcing. Here, weaker vertical mixing and frequent near-bed resuspension lead to higher SPM concentrations close to the bed (van Rijn & Grasmeijer, 2018; Mulligan et al., 2019). Additionally, intertidal flats naturally promote flocculation, trapping SPM and forming larger aggregates, which further contributes to elevated near-bed SPM levels.

Moreover, understanding the vertical distribution of SPM—particularly the gradient from near-bed to surface concentrations—is critical for interpreting sediment transport and deposition processes. In energetic systems like estuaries, this gradient reflects the interplay between settling, resuspension, and turbulent mixing. A steep gradient, with significantly higher concentrations near the bed, suggests active resuspension and limited upward diffusion, which can support localized deposition when turbulence decreases. In contrast, a flatter vertical profile implies

stronger mixing and broader redistribution of suspended material, reducing sediment retention near the bed. Long-term monitoring by Maris et al. (2024) in the main channel provides a useful example. Their study documented a decline in the Rouse number—a dimensionless parameter representing the balance between sediment settling and turbulent mixing—over the 2000–2020 period. This decline suggests a reduced potential for sediment suspension, possibly due to weakened turbulence or shifts in hydrodynamic drivers such as tidal forcing or freshwater discharge. As a result, the SPM profile became more uniform with depth, though the highest concentrations still occurred in the lower half of the water column, highlighting the persistent role of near-bed resuspension.

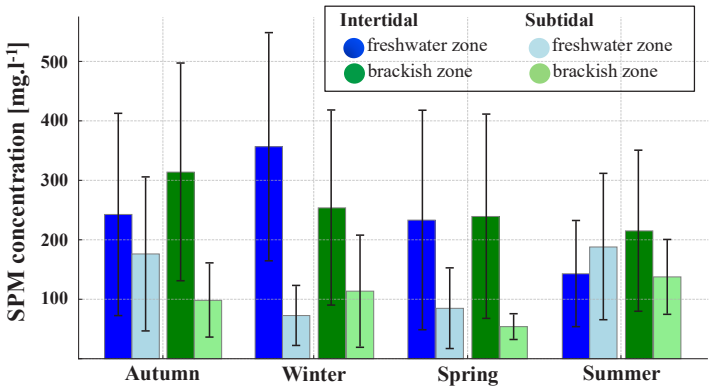

Figure 2.8: Seasonal comparison of near-bed SPM concentrations (this study) in intertidal zones of Branst and Lillo with depth-averaged SPM concentrations from the main channel (Maris et al., 2024). The figure highlights consistently higher SPM near the bed in intertidal flats, reflecting weaker vertical mixing and enhanced resuspension compared to the more uniformly mixed subtidal main channel.

Although that study focused on the deeper, well-mixed main channel, the underlying principles are equally relevant—perhaps even more so—in intertidal mudflat environments, where resuspension is highly localized and vertical diffusion is often limited. In such settings, vertical gradients in SPM concentration are sensitive indicators of sediment availability, current velocity, wave energy, and biological aggregation. While this study did not directly quantify vertical SPM gradients, future work could explore this aspect to better understand erosion and deposition dynamics in shallow estuarine zones.

In summary, these findings underscore the importance of interpreting floc size in relation to specific site conditions, including hydrodynamic forcing, biological activity, sediment availability, and measurement methodology. They also highlight the role of localized processes—such as resuspension and vertical mixing—in shaping near-bed SPM behavior across contrasting intertidal

environments, such as mudflats and main channels. Accounting for these distinct influencing factors is essential for accurately assessing sediment transport and deposition dynamics in estuarine systems.

2.4.2. Seasonal and Spatial Variations in Sediment Dynamics

Building on the previous analysis of floc structure and suspension properties, this section examines how seasonal and spatial variations influence sedimentation and erosion patterns across the three study sites. Sedimentation and erosion patterns differ markedly among Zuidgors, Lillo, and Branst, with each site exhibiting distinct seasonal dynamics driven by local hydrodynamics, sediment availability, and biological influences. In the following, the seasonal and spatial sediment behavior at each station is examined in detail.

I. Branst (Freshwater Zone)

Branst exhibited the most pronounced seasonal variability in sediment behavior among the three sites. Specifically, sedimentation occurred in spring and autumn, while erosion dominated in summer and winter. This means the bed level rose during certain periods and dropped during others, reflecting a dynamic balance between sediment settling and erosion. These shifts can be explained by the strong influence of river discharge, which changes with the seasons in freshwater zones like Branst and influence both physical and biological drivers that fluctuate seasonally (Cox et al., 2019; Horemans et al., 2021; Temmerman et al., 2023).

To understand these patterns more clearly, it is helpful to look at how SPM concentration and floc size changed through the year. At Branst, both SPM and floc size varied significantly between seasons. In winter, SPM concentrations were at their highest. This increase is linked to stronger river discharge, which stirs up and transports more sediment. Additionally, SCI values during winter at Branst were strongly positive, confirming that, the suspension dominated by flocculated mud. However, the energetic conditions created too much turbulence for flocs to settle, resulting in net erosion of the bed.

In contrast to winter, when high river discharge delivered abundant suspended sediments to the system, summer is characterized by much lower river input. This resulted in a significantly reduced supply of SPM from upstream sources. Interestingly, despite this limited sediment supply, it has both high mean floc size and high portion of macroflocs as well. However, their presence did not lead to bed-level accumulation. This is because the flocs observed were probably structurally

fragile—loosely bound and lacking the cohesive strength needed to withstand even moderate turbulence near the bed. As a result, they were easily broken apart or resuspended, preventing effective deposition (Chen et al., 2005; Lucas Pardo et al., 2015). This highlights an important insight that floc size alone doesn't guarantee sedimentation. The structure, durability, and internal cohesion of flocs are just as important.

This also helps explain why seasonal trends in sedimentation do not always align across studies. For instance, while Bas et al. (in prep.) observed summer sedimentation at Branst in 2021–2022, this study data showed erosion during the same season. Such discrepancies likely reflect interannual differences in floc properties and river discharge, but may also be influenced by biological processes—such as EPS production and benthic activity—that do not follow consistent seasonal patterns. For example, previous studies in the Scheldt estuary have reported no clear or consistent seasonality in TEP concentrations or benthic organism activity, particularly over short observational periods (Horemans et al., 2021). This suggests that floc formation driven by biological activity may not be strictly tied to seasons, but instead responds to changing factors such as light availability, nutrient input, and freshwater discharge (Gerbersdorf et al., 2008; Horemans et al., 2021).

Beyond seasonal patterns, Branst's long-term morphological changes also offer insight into system behavior, likely in response to subtle changes in upstream sediment supply, flow regime, and biological activity. Over longer timescales, Branst has remained relatively stable, and past assessments (Scheldecommissie et al., 2023) have shown that it requires much less dredging than other estuarine locations. This is largely due to its ebb-dominant flow regime, where strong outgoing currents naturally flush out sediment. This self-cleaning mechanism helps prevent long-term accumulation and minimizes the need for human intervention. However, long-term monitoring reveals that this natural flushing did not lead to continuous erosion. In fact, Branst experienced slight erosion prior to 2015, followed by a period of net sedimentation between 2016 and 2019 (Van Braeckel et al., 2019). This shift demonstrates that even naturally regulated systems can undergo decadal shifts in sediment balance. These decadal trends highlight how even relatively undisturbed intertidal systems are shaped by the cumulative effects of physical and biological processes over time.

II. Lillo (Brackish Zone)

In contrast to Branst's pronounced seasonal shifts, Lillo exhibited a more stable sedimentary regime influenced by brackish conditions and human activities. Lillo remained relatively stable throughout the year, showing only minor erosion in summer. This limited variability can be

attributed to its location in the brackish zone of the estuary, where moderate salinity reflects a balance between riverine and marine influences. In this transitional salinity range, flocculation is typically enhanced because salt ions help neutralize surface charges on fine particles, promoting aggregation into larger flocs that settle more quickly (Edzwald et al., 1974; Dyer, 1995; Winterwerp, 2002). As a result, sediment supply and hydrodynamic energy tend to remain more consistent throughout the year compared to the freshwater and saline zones (Uncles and Stephens, 1993; Manning and Dyer, 2007; Maris et al., 2024).

PSD data at Lillo support this interpretation. During periods of elevated SPM, we observed a shift toward coarser particle fractions, suggesting that resuspension processes were active, but without strong directional changes in transport. However, over longer timescales, Lillo has experienced net erosion—losing approximately 9 cm of bed elevation between 2009 and 2019 (Van Braeckel et al., 2019). This gradual trend aligns with other long-term studies showing that brackish zones, while generally depositional, are increasingly shaped by human intervention (Scheldecommissie et al., 2023).

Lillo is located near major navigation routes and is subject to frequent dredging operations, which are necessary for maintaining navigability but physically disturb the sediment bed and disrupt natural sediment dynamics. Dredging not only exports sediment that might otherwise settle, but also alters the hydrodynamic regime and interferes with floc formation by disturbing the sediment–water interface. This disruption is particularly evident in the decoupling between floc size and bed-level change: although flocs were consistently present, no clear correlation was observed between floc size and net sedimentation or erosion, suggesting that repeated physical disturbance undermines the stabilizing effect of flocculation.

In addition, dredging contributes to artificially steady hydrodynamic conditions, reducing the natural variability in flow that would otherwise support floc development through alternating turbulent and calm phases. This further inhibits the formation of large, cohesive flocs. Microbial communities responsible for EPS and TEP production may also be sensitive to repeated disturbances, with their activity reduced or irregular under such conditions. Indeed, no consistent seasonal pattern of TEP concentrations has been reported at Lillo (Horemans et al., 2021), likely reflecting a combination of physical disruption and interrupted biological cycles.

The natural sediment composition at Lillo reinforces this interpretation. Situated in the Lower Sea Scheldt, the site is dominated by fine, mud-rich sediments that are generally well-suited to floc formation. In theory, these materials should promote the development of large, stable flocs and sustained deposition. However, this potential is not fully realized. Despite floc formation, repeated dredging and biologically unfavorable conditions appear to weaken floc structure, preventing

effective sediment retention. Lillo's apparent morphological stability, therefore, conceals a dynamic system heavily shaped by human intervention—where natural depositional processes are regularly disrupted despite otherwise favorable conditions.

III. Zuidgors (Saline Zone)

Zuidgors presented a distinct case, reflecting the challenges of sediment stability in a sand-rich, marine-influenced zone. Zuidgors exhibited short-term sedimentation across most seasons during the measurement period, with the exception of an erosive phase in winter. However, long-term morphological trends tell a different story: over decadal timescales, the area has experienced net erosion. A temporary period of sediment gains between 1994 and 2005 corresponded with dredge spoil disposal, but erosion resumed thereafter (Elias et al., 2023). Channel volume records confirm a persistent deepening trend, indicating sustained sediment export. In addition, consistent dredging activity has been reported over the decades (Scheldecommissie et al., 2023). This pattern reflects the site's flood-dominant tidal asymmetry, which facilitates sediment import from the North Sea. However, the imported material does not settle uniformly. Instead, strong tidal currents redistribute it unevenly, resulting in localized deposition in some areas and scouring in others. Consequently, Zuidgors requires continuous dredging to maintain navigability, despite the apparent net influx of sediment.

Suspended sediment data provide further insight into this paradox. Analyses of PSD during periods of elevated SPM show that high SPM availability alone does not guarantee sedimentation. Rather, hydrodynamic forces—particularly tidal resuspension—play a dominant role in determining sediment fate. These forces can prevent accumulation by keeping particles in motion, highlighting the system's vulnerability to erosion (Eisma et al., 1997; Winterwerp, 2002). Correlation analyses reinforce this interpretation: even during seasons with evidence of effective flocculation (e.g., spring and summer), increased turbulence suppressed bed-level accumulation. These findings suggest that under future scenarios of intensified tidal energy or sea-level rise, Zuidgors may become even more prone to erosion—even during periods that would otherwise support sedimentation.

Floc structure metrics further support this interpretation. Although Zuidgors is a sand-rich zone, macroflocs consistently dominated the particle size distribution throughout the year, indicating strong aggregation. However, LISST data alone cannot distinguish between cohesive flocs and inert sand particles. To clarify this distinction, the SCI was applied. The slightly positive SCI observed in summer suggests that the suspension remained floc-dominated rather than sand-driven (Tran et al., 2024), implying that the large particles were likely dense flocs rather than

resuspended sand. However, such aggregates are prone to disintegration under tidal turbulence, particularly in high-energy systems like Zuidgors. Thus, despite evidence of active flocculation, the structural fragility of these aggregates under high-energy conditions further reinforces the limited potential for lasting sedimentation at Zuidgors.

Overall, these findings demonstrate that sediment dynamics in the estuary are governed by site-specific interactions among hydrodynamics, sediment supply, and biological processes. The contrasting behaviors observed across Branst, Lillo, and Zuidgors highlight the need for location-tailored sediment management, rather than generalized strategies across the system.

2.4.3. Interplay of Floc Characteristics, Biological Activity, and Hydrodynamic Forces

While the previous section described how seasonal and site-specific hydrodynamic conditions influence sedimentation and erosion, these patterns cannot be fully explained by energy conditions alone. Floc stability and deposition are governed not just by size, but by internal structure, cohesiveness, and biological composition. This section examines how biological and physical processes jointly influence the formation, transformation, and disintegration of flocs.

Across all tidal cycles, flocs exhibited distinct behaviors in response to varying hydrodynamic conditions. Specifically, under high-energy conditions—characterized by increased turbulence and shear stress—flocs tended to disintegrate, even when significant volumes of SPM were present in the system. Conversely, during low-energy periods characterized by reduced turbulence, floc size generally increased, and SPM concentrations tended to stabilize due to enhanced aggregation and reduced resuspension. However, this relationship was not always straightforward. At Branst, for example, the influx of SPM preceded the high flood phase, reflecting complex riverine influence. Even during high-water slack, Branst exhibited non-zero velocity and turbulence, and during ebb, SPM and floc size decreased despite rising turbulence, indicating external sediment supply. Also, negative correlations between current velocity and bed level change in autumn and winter, but positive correlations in spring and summer, suggest seasonally variable responses of flocs to hydrodynamic forcing.

At Lillo and Zuidgors, seasonal patterns also highlighted differing responses. In winter, stable hydrodynamic conditions and rising SPM favored floc growth at Lillo, but at Zuidgors, slight energy increases triggered floc breakage (Dyer and Manning, 1999). While these factors are significant, they do not fully account for the observed patterns. For example, in summer at Lillo, a positive correlation between hydrodynamic parameters and bed level change suggested a tendency

toward sedimentation, yet erosion was observed. Conversely, at Zuidgors, a negative correlation indicated erosion, yet sedimentation occurred.

The mismatches between expected sedimentation–erosion patterns and hydrodynamic trends indicate that physical energy alone does not fully determine sediment behavior. While turbulence and shear stress clearly influence floc disintegration and transport, they cannot explain all observed patterns—especially those that vary seasonally or between sites. This suggests that the stability of flocs under hydrodynamic stress also depends on their biological composition and internal structure, which affect how easily they break apart or remain intact (Winterwerp, 2002; Dyer and Manning, 1999).

Flocs in estuarine systems are complex aggregates composed of both inorganic mineral particles and organic material. A key biological contributor to floc formation is benthic microalgae—especially diatoms—living on sediment surfaces. These autotrophic organisms stabilize sediments by secreting EPS which act as natural 'glue' on the sediment surface and contribute to the formation of cohesive biofilm-bound flocs (Underwood and Paterson, 2003). Under favorable conditions, part of this EPS aggregates in the water column to form TEP—sticky, gel-like structures that bind together fine mineral and organic particles, promoting the formation of flocs in the water column (Passow, 2002; Morelle et al., 2017). This binding capacity is essential for the formation of large, cohesive flocs that can settle and resist resuspension. Additionally, chlorophyll-a (Chl-a), often used as a proxy for benthic algal biomass, reflects the presence of microphytobenthos (MPB)—the primary producers of EPS. These biological processes are influenced by light availability and temperature, with warmer seasons typically stimulating EPS and TEP production.

However, floc stability is not determined by EPS alone. Organic matter (OM), including the fresh EPS and algal material produced by microalgae, plays a key role in determining floc structure and stability. OM exists along a continuum—from fresh, labile biological material (e.g., living algal cells and recently produced EPS) to more refractory, degraded forms (e.g., humic substances, produced through microbial decomposition by heterotrophic bacteria). The quality and freshness of OM strongly influence its floc-forming potential. Microorganisms in sediments include both autotrophic algae (EPS producers) and heterotrophic bacteria (decomposers). While algae promote floc formation, microbial activity can break down EPS and TEP through remineralization, gradually reducing floc cohesion (Borchard and Engel, 2012). The balance between these opposing roles—production and degradation—ultimately determines whether flocs persist or disintegrate under hydrodynamic stress.

In this study, observations indicate that flocs originate through both pathways: by aggregation in the water column (e.g., via TEP production), and as cohesive structures that form at the bed

surface (e.g., biofilm-bound flocs) and are later resuspended during energetic tidal phases. At Branst and Lillo, large but fragile macroflocs were observed during periods of increasing turbulence and concurrent bed level decline—supporting the interpretation that previously settled flocs were being remobilized. In contrast, at Zuidgors, the high proportion of macroflocs in summer and slightly positive SCI values—despite the sandy-rich—suggest active flocculation in the water column, likely driven by favor biology under warmer conditions. However, strong tidal resuspension appears to prevent these flocs from contributing to stable deposition. These patterns highlight that flocs in the Scheldt estuary either form through in situ aggregation in the water column or are remobilized after deposition, depending on local hydrodynamic and biological conditions.

In addition to microbial degradation, benthic disturbances by macrofauna also play a role. Burrowing crabs (e.g., Eriocheir sinensis) and polychaete worms (Arenicola marina) destabilize sediments through bioturbation and bio-irrigation, disturbing the bed surface, enhancing oxygen penetration, and promoting both particle resuspension and microbial activity (Rossi and Chapman, 2003; Kristensen and Kostka, 2005). Their activities can both stimulate organic matter decomposition and physically disrupt floc structures, reducing floc stability.

Taken together, EPS production, microbial remineralization, and bioturbation create a dynamic balance that governs floc lifecycle processes—formation, growth, breakdown, and potential resuspension. This balance is highly sensitive to seasonal variations in environmental conditions such as light availability, temperature, and tidal exposure. Under scenarios of increased climate variability and sea level rise, changes in these environmental drivers may intensify, further modulating sediment dynamics in estuarine intertidal systems.

Although this study did not directly measure TEP concentrations, microbial remineralization rates, or benthic organism activity, the observed sediment behavior underscores the likely importance of these biological factors in regulating floc structure and stability. Future studies would benefit from integrating continuous measurements of such biological variables alongside hydrodynamic and energy-related parameters to improve predictive understanding of sediment transport. A second limitation relates to seasonality. The seasonal categories used here (spring, summer, autumn, winter) were based on calendar months rather than real-time environmental thresholds. While practical, this approach may not correspond with biologically meaningful events—such as phytoplankton blooms or peak EPS production—which vary annually based on temperature, sunlight, and hydrological factors. Additionally, field campaigns were conducted in different months at each site, meaning that the same season (e.g., “spring”) could reflect distinct environmental conditions at Branst, Lillo, and Zuidgors. Caution is therefore needed when

interpreting seasonal patterns or comparing sites based solely on calendar seasons. Future studies should consider synchronizing site measurements and incorporating real-time environmental indicators (e.g., in situ temperature and light) to define more biologically relevant phases.

2.5. Conclusion

The Scheldt estuary, a dynamic and complex system, faces significant challenges due to high concentrations of SPM, driven by both natural processes and human activities. Understanding whether the intertidal zones within the estuary act as effective accommodation spaces for this SPM—areas where sediments can settle and contribute to the long-term stability of the system—is crucial for managing its ecological health.

This study aimed to explore this question by examining sediment dynamics across three distinct zones within the estuary: the freshwater zone at Branst, the brackish zone at Lillo, and the saline zone at Zuidgors. Each of these zones presents unique conditions that influence whether sediments are likely to settle and stabilize, or remain suspended and subject to erosion.

In the freshwater zone at Branst, significant seasonal variability was observed, with sedimentation during autumn and spring, and erosion during summer and winter. The area alternated between sedimentation and erosion, driven by the dynamic interplay of riverine inputs, fluctuating hydrodynamic forces, and changes in floc composition. One of the most unexpected findings was the significant erosion observed in summer—typically a period when lower energy conditions and increased biological activity would favor sedimentation. This erosion, despite the presence of larger flocs, suggests that these aggregates may have been more prone to resuspension. Such variability indicates that while Branst can temporarily accommodate sediments, its role as a stable accommodation space is inconsistent and highly dependent on seasonal factors.

In contrast, the brackish zone at Lillo generally demonstrated more stable sedimentation patterns. The combination of relatively stable hydrodynamic conditions and more cohesive flocs supported sedimentation, particularly during periods of high SPM. However, the site exhibited unexpected behavior during summer. Although the conditions suggested a tendency toward sedimentation, erosion was observed—indicating that floc composition and stability were critical controlling factors. Anthropogenic disturbances, such as dredging or vessel-induced turbulence, may also have interfered with the flocculation process, weakening sediment cohesion. While brackish zones have the potential to stabilize sediments, they remain vulnerable to external pressures that can shift the balance toward erosion.

Zuidgors exemplifies a morphodynamically unstable, sand-rich, marine-influenced zone where high flocculation potential does not translate into long-term sediment accumulation. Although short-term sedimentation occurs—especially in spring and summer—persistent tidal energy, flood-dominant asymmetry, and strong resuspension dynamics result in net erosion over decadal timescales. The presence of macroflocs, confirmed by LISST and SCI data, indicates active floc formation; however, the structural fragility of these flocs under turbulent conditions limits their capacity to contribute to lasting deposition. Continuous dredging requirements further underscore the site's instability. Overall, Zuidgors has limited effectiveness as a long-term accommodation space for suspended sediment, and its vulnerability may increase under future scenarios of sea-level rise or intensified tidal forcing.

These observations underscore the need for a nuanced approach to sediment management in the Scheldt estuary. The ability of intertidal zones to function as accommodation spaces for SPM is not uniform and cannot be generalized. Instead, it is shaped by the composition and stability of flocs, which are governed by seasonal biological activity and hydrodynamic conditions that vary not only between zones but also across seasons. To manage sediment effectively in the Scheldt estuary, strategies must be tailored to the specific conditions of each zone. Continued monitoring and a deeper understanding of these factors will be essential for preserving the ecological integrity and long-term health of the estuary—and for developing predictive models that accurately reflect these dynamic processes.

Appendix 2.A: Measurement Periods

This appendix provides a summary of the measurement periods for Branst, Lillo, and Zuidgors stations, using ADV, LISST, and OBS instruments. ADV, LISST, and OBS instruments were deployed during each campaign to capture data on hydrodynamic and sediment characteristics at the specified locations. Each campaign lasted approximately 15 days to cover different tidal cycles.

Table 2.A.1: a summary of the measurement periods in different stations: Branst (freshwater zone), Lillo (brackish water zone), Zuidgors (saline water zone)

Location	Campaign	ADV, LISST, OBS Measurement Period
Branst	Winter	21/11/2018 - 05/12/2018
	Spring	15/05/2019 - 30/05/2019
	Summer	13/08/2019 - 28/08/2019
	Autumn	03/10/2019 - 18/10/2019
Lillo	Winter	03/01/2019 - 18/01/2019
	Spring	24/04/2019 - 09/05/2019
	Summer	23/07/2019 - 07/08/2019
	Autumn	22/10/2019 - 06/11/2019
Zuidgors	Winter	23/01/2019 - 07/02/2019
	Spring	03/04/2019 - 18/04/2019
	Summer	02/07/2019 - 17/07/2019
	Autumn	19/11/2019 - 04/12/2019

Appendix 2.B: Time Series Data for Sediment and Hydrodynamic Parameters

This appendix provides the time series data for key sediment and hydrodynamic parameters recorded at Branst, Lillo, and Zuidgors stations. These plots provide a visual representation of the data collected throughout the measurement periods. By presenting these time series, the appendix offers a baseline understanding of the natural variability and patterns observed in each parameter, laying the groundwork for further analysis and interpretation.

The following figures display the continuous time series measurements for each parameter at each station across different seasons. These plots offer a detailed view of the environmental conditions and sediment dynamics captured during the study. Parameters Included from top to bottom: Water Level (m), Current Velocity (m/s), Shear Rate (G, s^{-1}), Suspended Particulate Matter (SPM, mg/l), Floc Size (D50, μm), Bed Level (BL, mm). In the continuation you will see the Figures for Each Station and Season.

Zuidgors – Autumn: Continuous time series of hydrodynamic and sediment parameters.

Parameter	Value
Bed Level Change	+5.20 mm
SPM concentration	322.00 ± 1.50 mg/l
Mean Floc Size	135.00 ± 1.00 µm
Current Velocity	0.24 ± 0.11 m/s
Shear Rate G	0.98 ± 0.74 s^{-1}
Valid Data Points Used	ADV: 3,096,000; LISST: 3,343; OBS: 4,665
Descriptions	Moderate current velocity and shear rate accompanied with high SPM concentration combined with relatively large floc size, facilitate sediment deposition.

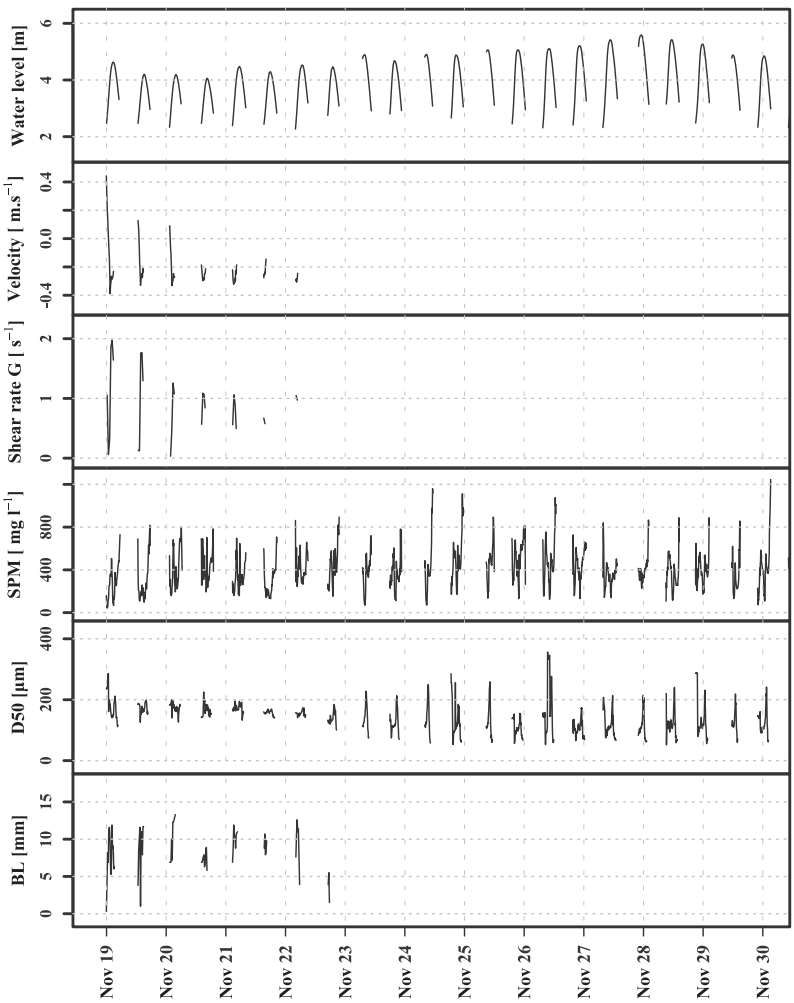

Zuidgors – Winter: Continuous time series of hydrodynamic and sediment parameters.

Parameter	Value
Bed Level Change	-30 mm
SPM concentration	302.00 ± 2.00 mg/l
Mean Floc Size	99.00 ± 1.00 µm
Current Velocity	0.29 ± 0.17 m/s
Shear Rate G	1.65 ± 1.18 s^{-1}
Valid Data Points Used	ADV: 342,780; LISST: 757; OBS: 715
Descriptions	High current velocity and shear rate disrupt the sediment and prevent settling. The reduced floc size indicates a breakdown of aggregates, likely caused by increased turbulence. Despite high SPM levels, the hydrodynamic conditions lead to sediment redistribution rather than accumulation.

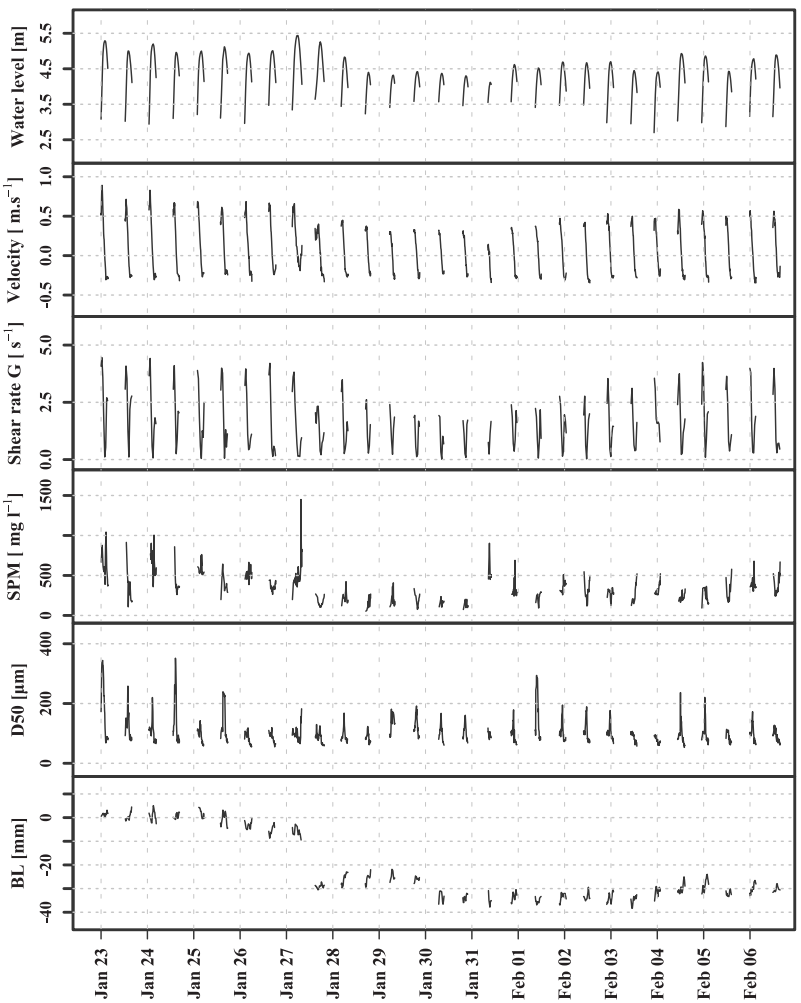

Zuidgors – Spring: Continuous time series of hydrodynamic and sediment parameters.

Parameter	Value
Bed Level Change	+0.63 mm
SPM concentration	605.00 ± 2.00 mg/l
Mean Floc Size	132.00 ± 1.00 µm
Current Velocity	0.30 ± 0.19 m/s
Shear Rate G	2.06 ± 1.20 s^{-1}
Valid Data Points Used	ADV: 86,880; LISST: 736; OBS: 988
Descriptions	The minor sedimentation shows how the system is trying to keep sedimentation balance in the presence of high SPM and shear rate and large floc size. However, the turbulence limits significant sediment accumulation.

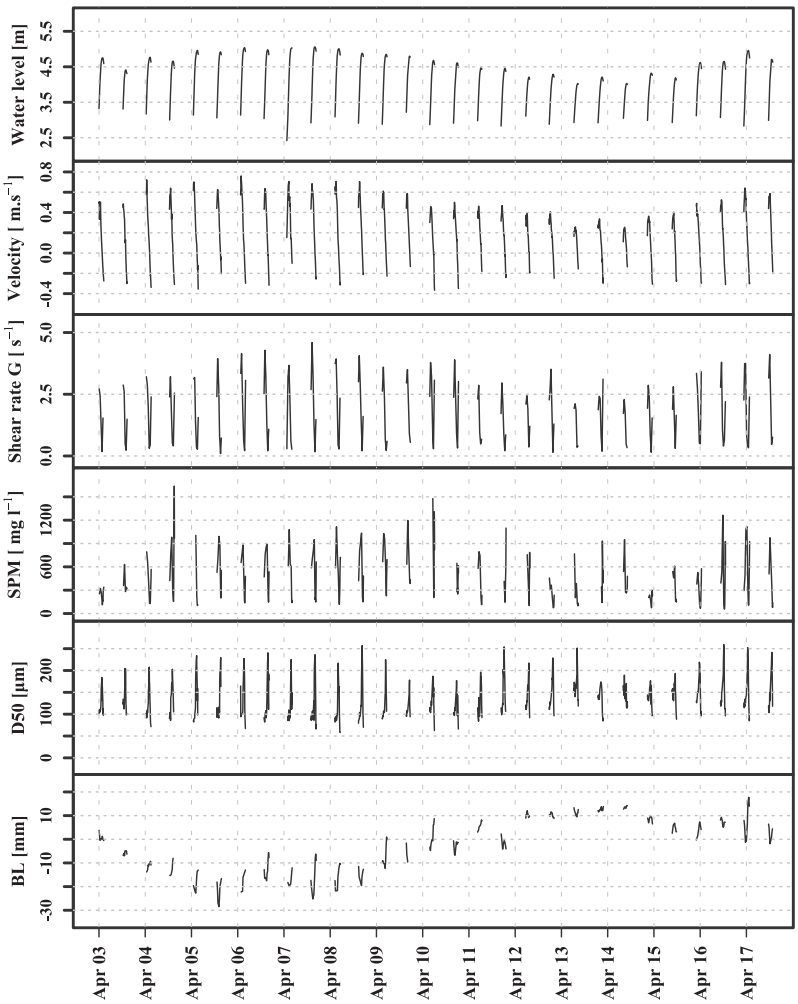

Zuidgors – Summer: Continuous time series of hydrodynamic and sediment parameters.

Parameter	Value
Bed Level Change	+42.20 mm
SPM concentration	223.00 ± 2.50 mg/l
Mean Floc Size	157.00 ± 1.00 µm
Current Velocity	0.30 ± 0.17 m/s
Shear Rate G	1.27 ± 1.05 s^{-1}
Valid Data Points Used	ADV: 86,312; LISST: 779; OBS: 761
Descriptions	The sediment accumulation is supported by large floc sizes. The stable hydrodynamic conditions, with moderate shear rate and current velocity, enable effective sediment deposition.

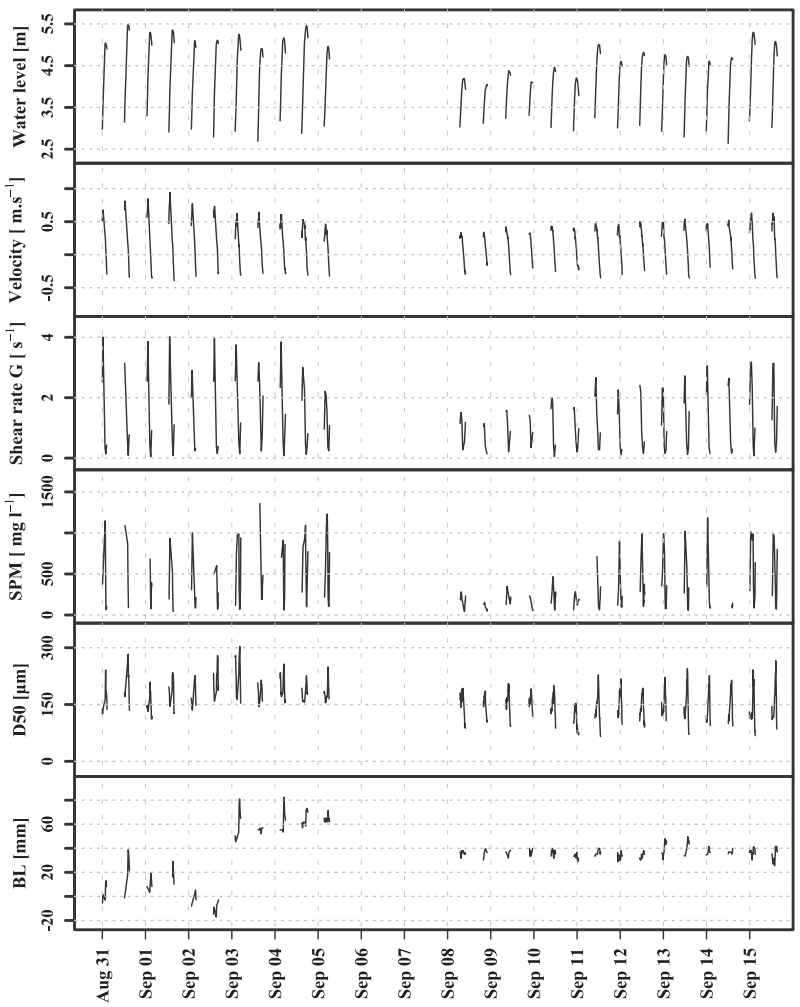

Branst – Autumn: Continuous time series of hydrodynamic and sediment parameters.

Parameter	Value
Bed Level Change	+12.10 mm
SPM concentration	182.00 ± 2.00 mg/l
Mean Floc Size	140.00 ± 2.00 µm
Current Velocity	0.16 ± 0.10 m/s
Shear Rate G	0.36 ± 0.25 s^{-1}
Valid Data Points Used	ADV: 10,526,400; LISST: 4,372; OBS: 4,380
Descriptions	Large floc size and lower shear rate create favorable conditions for sediment deposition. The low current velocity ensures minimal sediment disturbance, allowing particles to settle.

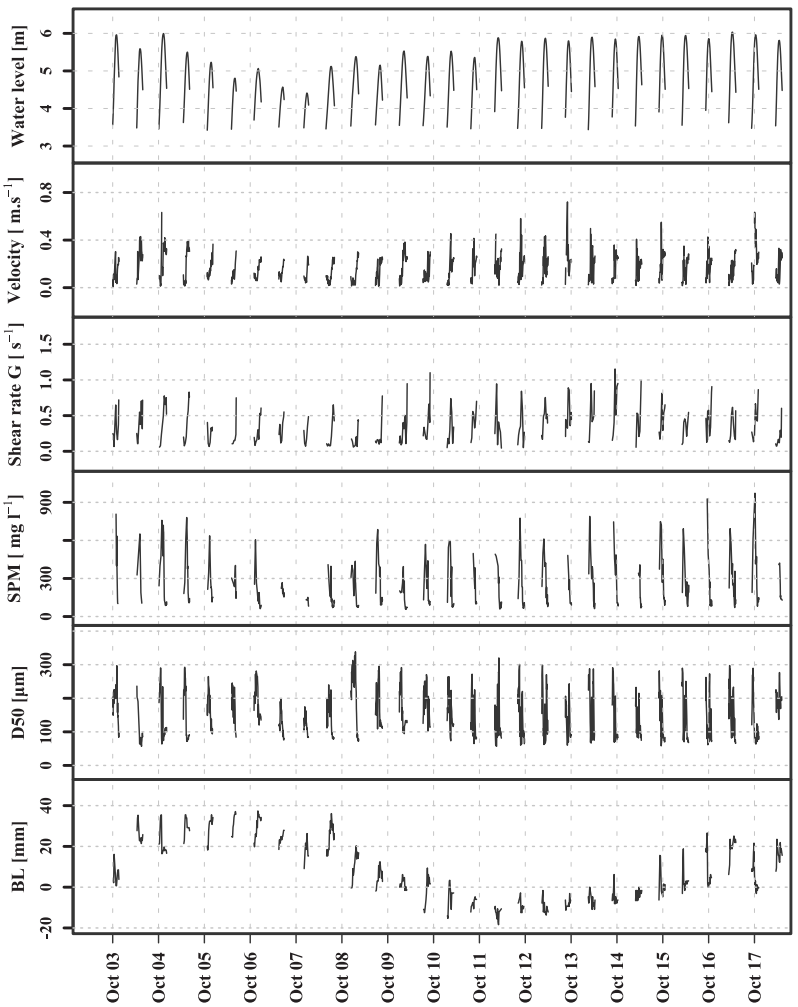

Branst – Winter: Continuous time series of hydrodynamic and sediment parameters.

Parameter	Value
Bed Level Change	-50.80 mm
SPM concentration	307.00 ± 2.00 mg/l
Mean Floc Size	111.00 ± 2.00 µm
Current Velocity	0.22 ± 0.12 m/s
Shear Rate G	0.87 ± 0.68 s^{-1}
Valid Data Points Used	ADV: 438,999; LISST: 1,013; OBS: 827
Descriptions	The most severe erosion among the stations, driven by the highest SPM levels and increased shear rate is recorded. The moderate current velocity fails to stabilize the sediment, allowing it to be swept away.

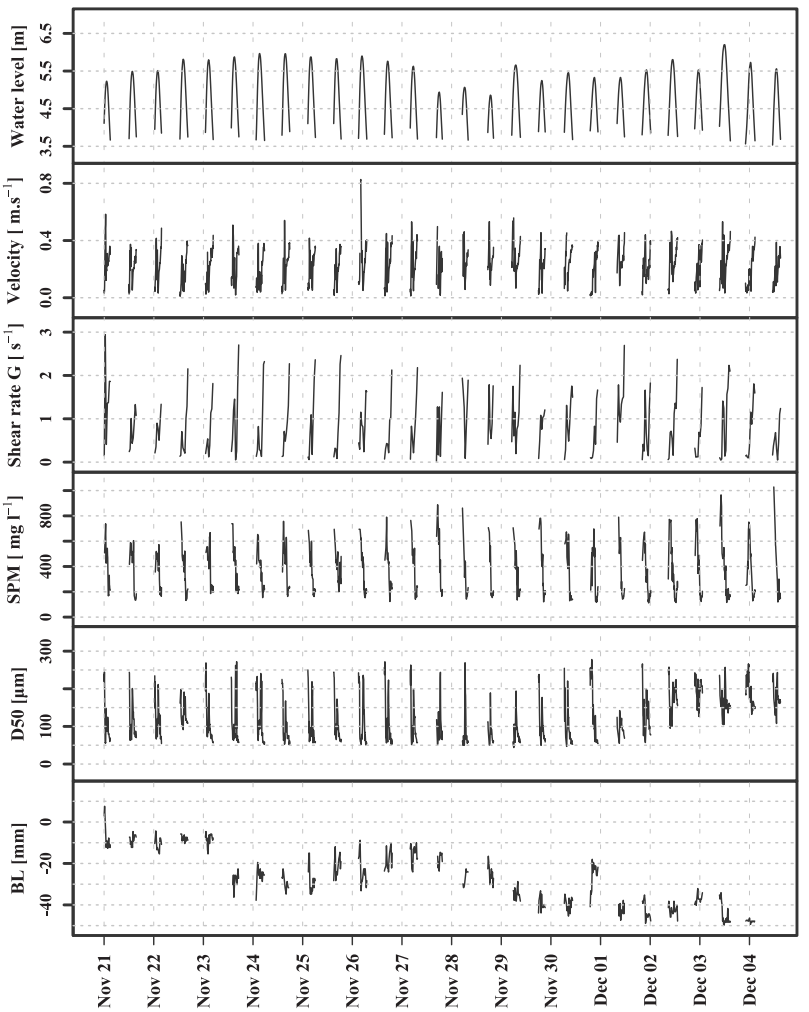

Branst – Spring: Continuous time series of hydrodynamic and sediment parameters.

Parameter	Value
Bed Level Change	+46.80 mm
SPM concentration	205.00 ± 2.00 mg/l
Mean Floc Size	156.00 ± 1.00 µm
Current Velocity	0.30 ± 0.11 m/s
Shear Rate G	0.57 ± 0.39 s^{-1}
Valid Data Points Used	ADV: 1,878,699; LISST: 4,451; OBS: 1,674
Descriptions	The high current velocity combined with moderate SPM and a reduced shear rate allows for particle settling, marking a shift towards conditions that favor deposition.

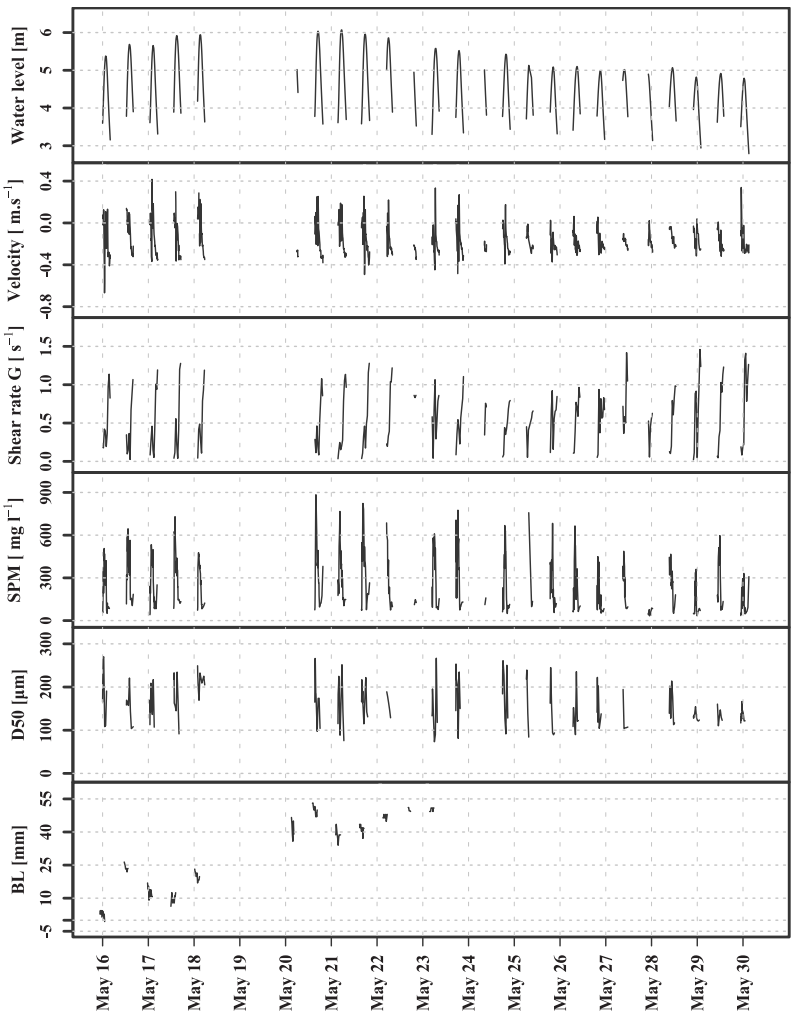

Branst – Summer: Continuous time series of hydrodynamic and sediment parameters.

Parameter	Value
Bed Level Change	-77.70 mm
SPM concentration	118.00 ± 2.00 mg/l
Mean Floc Size	143.00 ± 1.00 µm
Current Velocity	0.21 ± 0.15 m/s
Shear Rate G	0.41 ± 0.34 s^{-1}
Valid Data Points Used	ADV: 287,932; LISST: 1,102; OBS: 1,078
Descriptions	Low SPM levels and reduced shear rate, resulting in weak sediment retention. The decreased current velocity fails to support particle settling, leading to significant sediment loss.

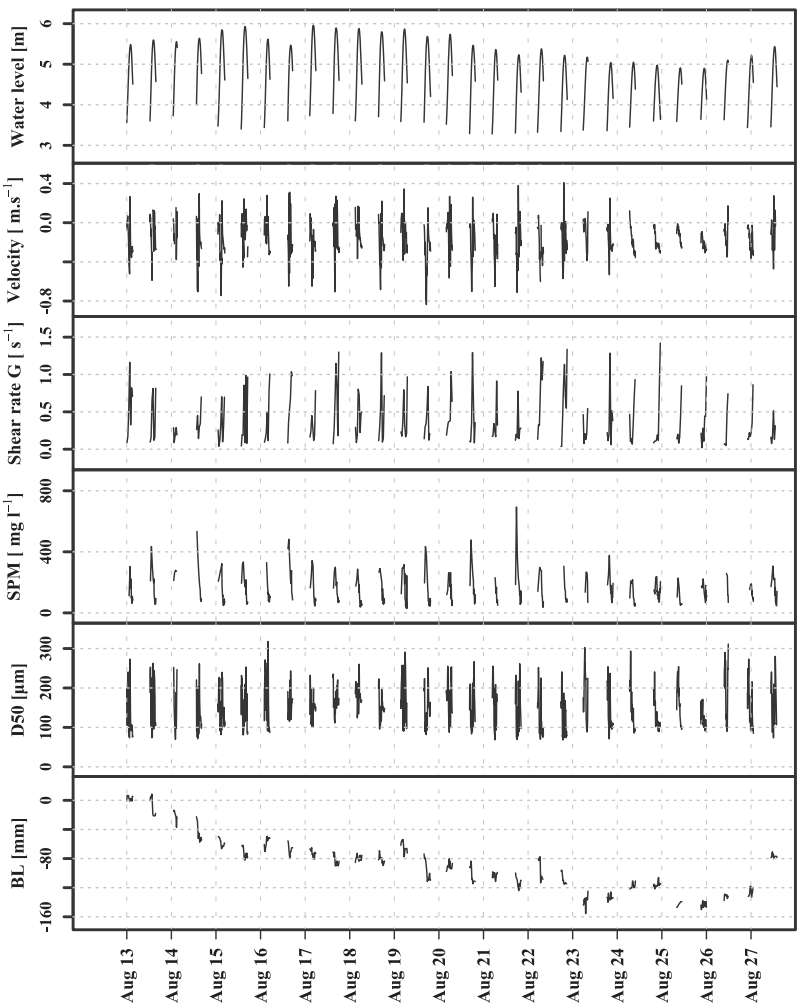

Lillo – Autumn: Continuous time series of hydrodynamic and sediment parameters.

Parameter	Value
Bed Level Change	+18.40 mm
SPM concentration	237.00 ± 2.00 mg/l
Mean Floc Size	107.00 ± 2.00 µm
Current Velocity	0.21 ± 0.13 m/s
Shear Rate G	1.00 ± 0.80 s^{-1}
Valid Data Points Used	ADV: 11,102,400; LISST: 4,465; OBS: 4,667
Descriptions	high SPM levels and a high shear rate and moderate current velocity which encourages flocculation and causes deposition.

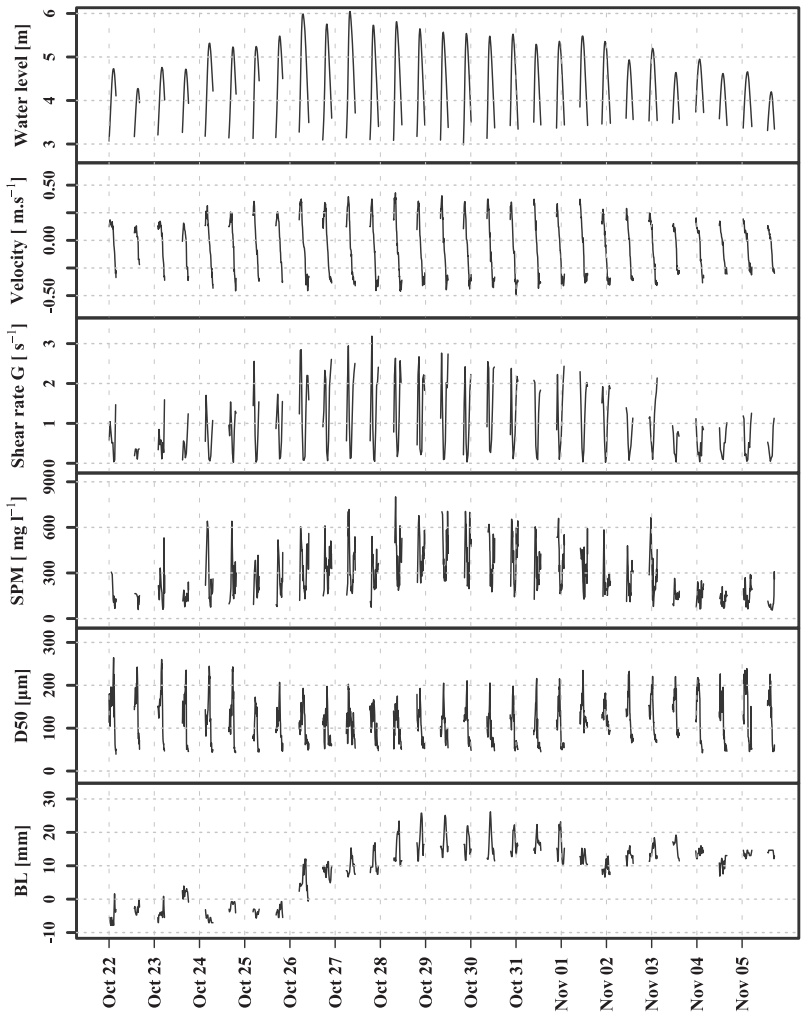

Lillo – Winter: Continuous time series of hydrodynamic and sediment parameters.

Parameter	Value
Bed Level Change	+1.33 mm
SPM concentration	183.00 ± 1.50 mg/l
Mean Floc Size	114.00 ± 1.50 µm
Current Velocity	0.22 ± 0.11 m/s
Shear Rate G	0.93 ± 0.63 s^{-1}
Valid Data Points Used	ADV: 1,075,583; LISST: 1,109; OBS: 1,077
Descriptions	The slight bed level increase is due to a balance between shear rate and current velocity. The moderate SPM suggests effective sediment retention, while the floc size supports limited aggregation and settling.

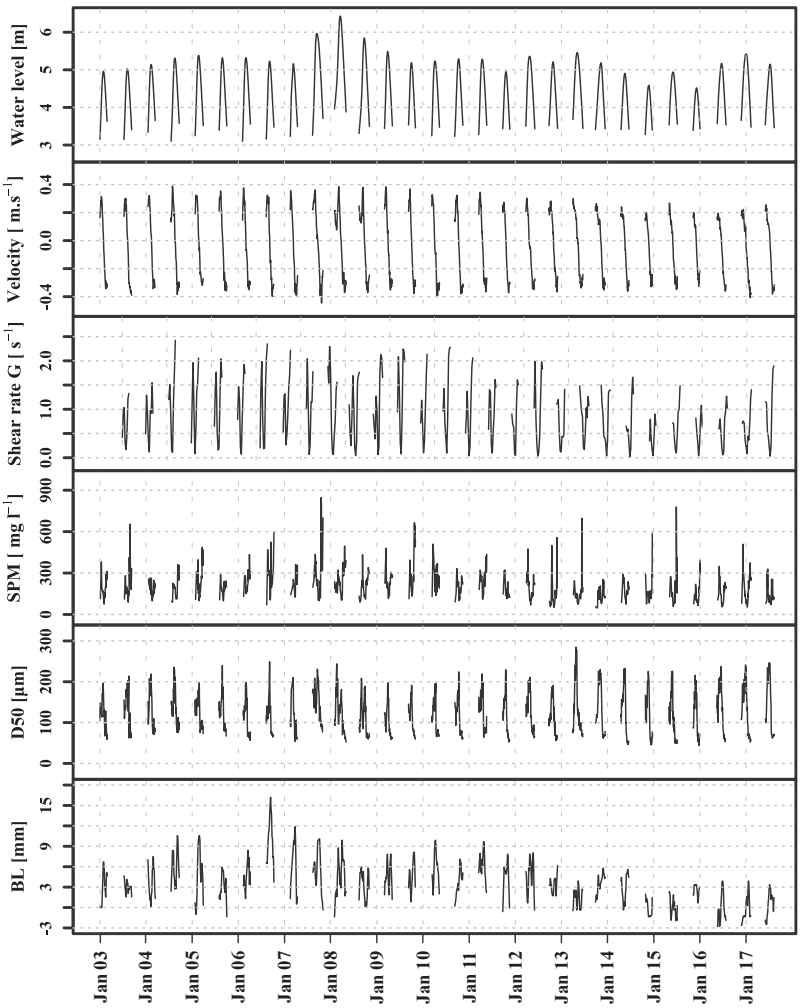

Lillo – Spring: Continuous time series of hydrodynamic and sediment parameters.

Parameter	Value
Bed Level Change	+1.70 mm
SPM concentration	153.00 ± 2.00 mg/l
Mean Floc Size	139 ± 1.00 µm
Current Velocity	0.21 ± 0.13 m/s
Shear Rate G	0.85 ± 0.60 s^{-1}
Valid Data Points Used	ADV: 873,470; LISST: 1,323; OBS: 1,295
Descriptions	The larger floc size combined with moderate hydrodynamic forces, ensure a stable sedimentary environment. The SPM level is adequate to sustain minimal accumulation.

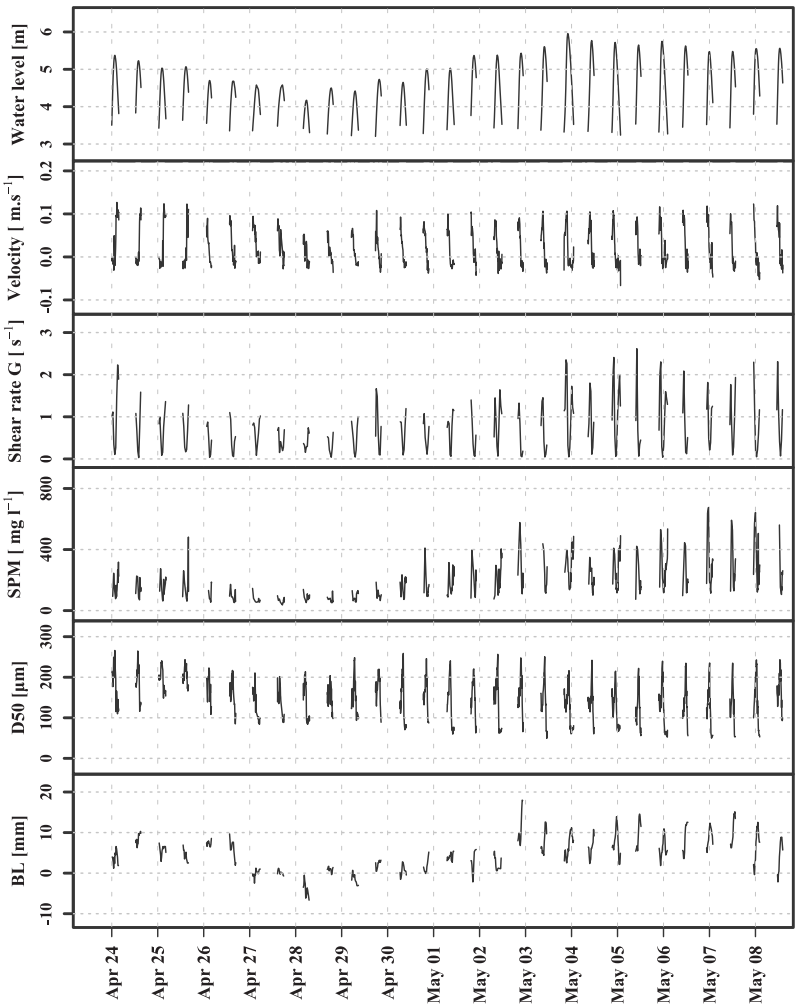

Lillo – Summer: Continuous time series of hydrodynamic and sediment parameters.

Parameter	Value
Bed Level Change	-1.50 mm
SPM concentration	123.00 ± 2.00 mg/l
Mean Floc Size	152.00 ± 1.00 µm
Current Velocity	0.21 ± 0.12 m/s
Shear Rate	0.71 ± 0.53 s^{-1}
Valid Data Points Used	ADV: 85,364; LISST: 329; OBS: 1,078
Descriptions	Despite large floc sizes, the lower SPM and shear rate create a delicate balance that slightly favors erosion indicating the presence of other environmental forces.

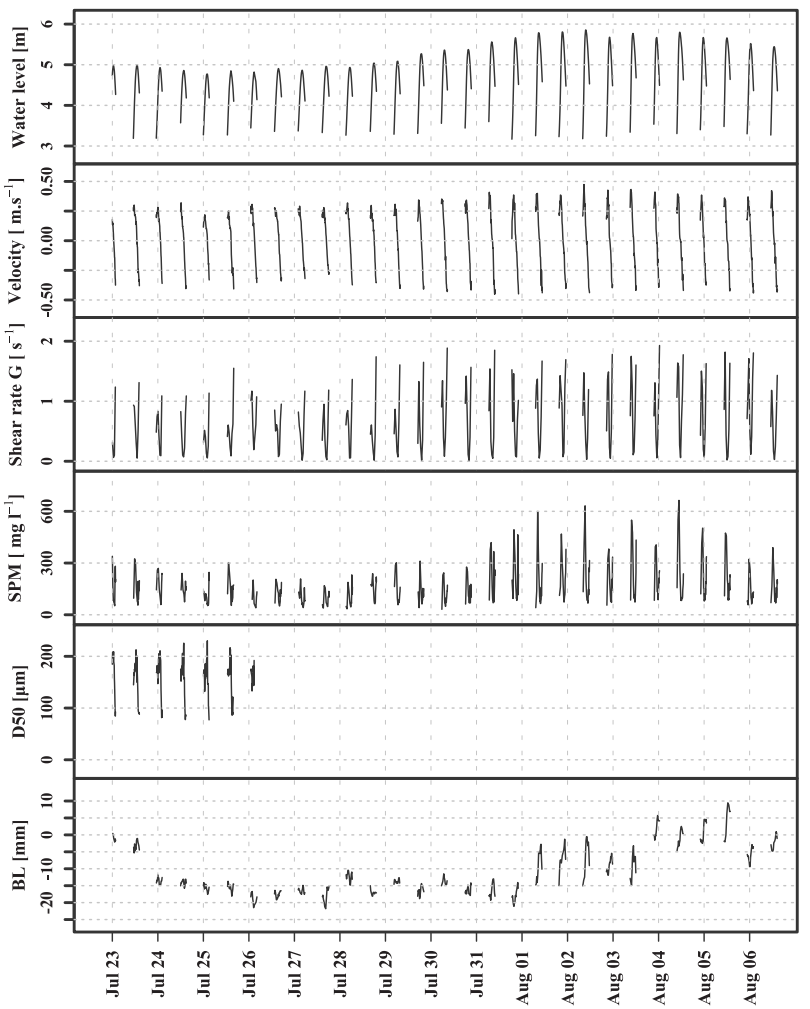

Appendix 2.C: Particle Size Distribution

This appendix presents the PSD across different seasons for the Branst, Lillo, and Zuidgors station, with a focus on variations observed during peak SPM periods. These analyses provide insights into how particle sizes fluctuate in response to changing environmental and hydrodynamic conditions. In these pictures the pink line shows average values in the measurement period and the green lines represent the PSD during periods of elevated SPM concentrations, calculated within each individual tidal cycle. Specifically, these green lines correspond to time windows in which SPM concentrations reached local maxima within the cycle, indicating phases of intensified sediment transport or floc resuspension.

Figure 2.C.1 shows particle size distribution for Branst station. Throughout the entire measurement period, Branst exhibits a bimodal distribution with peaks in coarser particles. During high SPM periods, particle size shifts towards coarser particles in Autumn and Spring, indicating enhanced flocculation. In Winter and Summer, the distribution leans toward finer particles due to increased turbulence keeping sediments suspended.

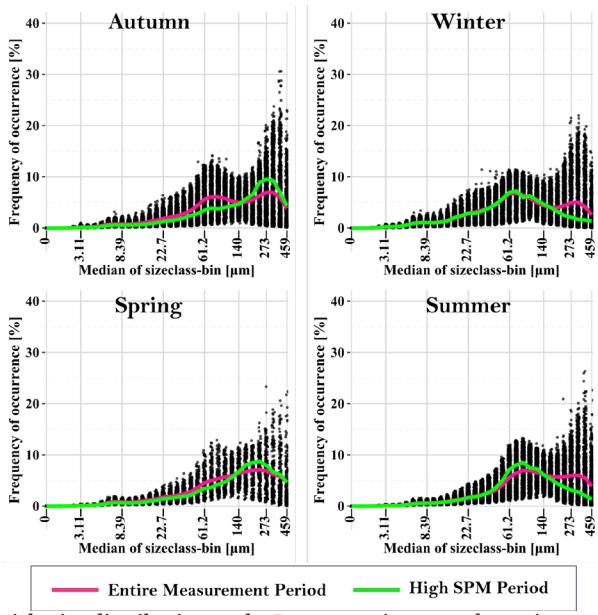

Figure 2.C.1: Particle size distribution at the Branst station over the entire measurement period (represented by the pink line) and during high SPM periods (represented by the green line).

Figure 2.C.2 shows particle size distribution for Lillo station. This station shows a bimodal distribution, primarily leaning towards coarser particles. During high SPM conditions, the shift is

consistently towards coarser particles across all seasons, highlighting strong flocculation processes that promote particle aggregation and deposition.

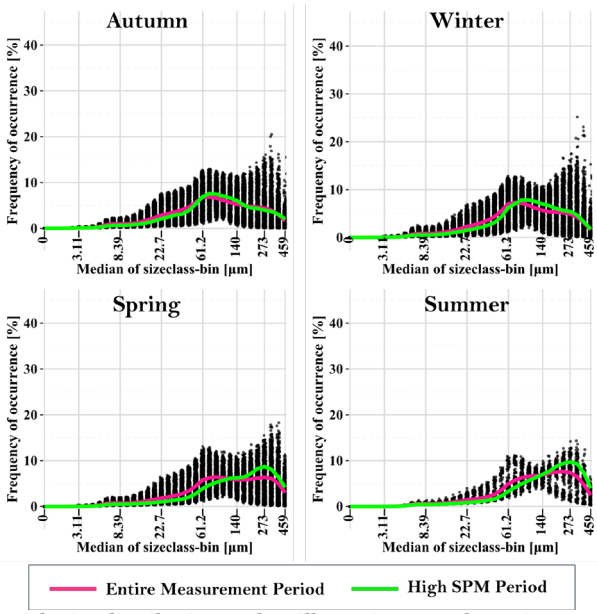

Figure 2.C.2: Particle size distribution at the Lillo station over the entire measurement period (represented by the pink line) and during high SPM periods (represented by the green line).

Figure 2.C.3 shows particle size distribution for Zuidgors station. It presents a bimodal distribution with a focus on coarser particles. Under high SPM volumes, the distribution shifts to finer particles in Autumn and Winter but moves towards coarser particles in Spring and Summer, reflecting seasonal variations in flocculation and energy dynamics.

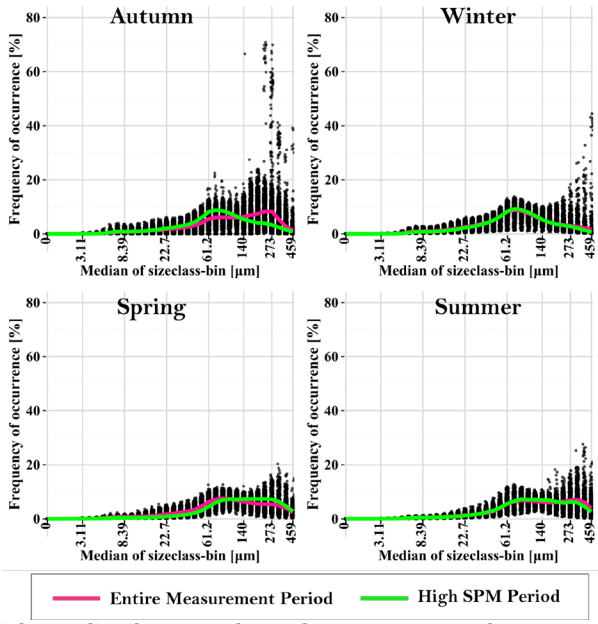

Figure 2.C.3: Particle size distribution at the Zuidgors station over the entire measurement period (represented by the pink line) and during high SPM periods (represented by the green line).

Appendix 2.D: Tidal Cycle Analysis

This appendix details the changes observed in different tidal cycles at Branst, Lillo, and Zuidgors stations. By examining key parameters such as current velocity, SPM, floc size, and bed level changes, we can gain insights into the sediment dynamics driven by tidal influences.

Figure 2.D.1 shows the changes in parameters across all tidal cycles in all seasons at Branst Station. At Branst Station, the bed level shows minimal changes during tidal cycles, indicating a gradual influence of tidal forces. Across all seasons, the current velocity and turbulent shear rate (G) increase during the flood period, peak at high water, and continue to increase during the ebb period. This continuous rise is unique to Branst, where both parameters remain non-zero even at high water slack, indicating persistent sediment movement and turbulence. SPM concentrations follow a similar pattern, rising during the flood period, peaking before high water, and decreasing at high water and during the ebb period. Floc size at Branst generally decreases during the flood tide, remains relatively steady or shows minor increase at high water. continues to decrease during the ebb period due to high turbulence and shear.

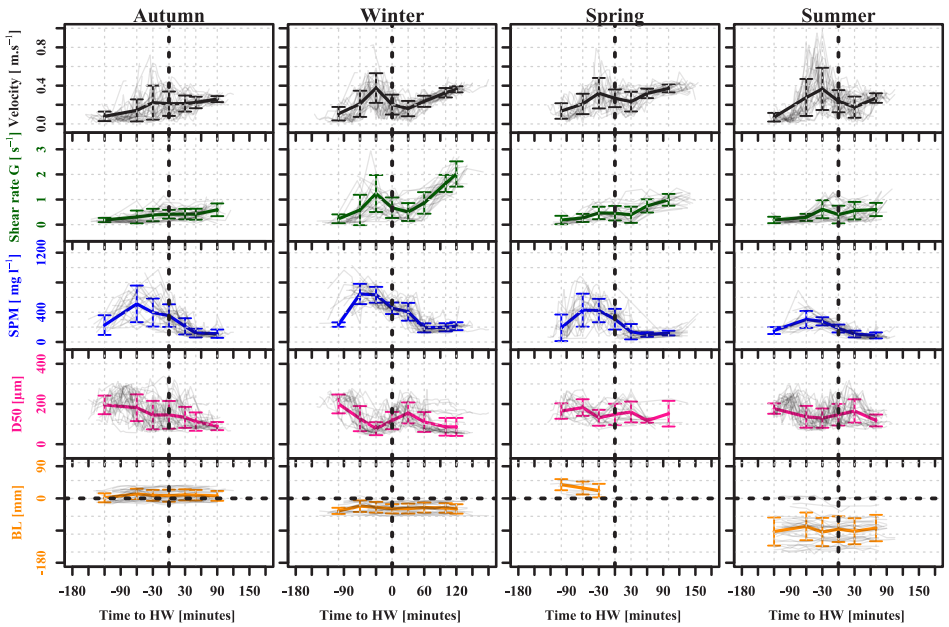

Figure 2.D.1: Graphical representation of tidal cycle changes at Branst, including current velocity, shear rate G, SPM, floc size, and bed level data.

Figure 2.D.2 shows the changes in the parameters across all tidal cycles in all seasons at Lillo Station. At Lillo Station, the current velocity and turbulent shear rate (G) increase during the flood period, peak just before high water, and decrease significantly at high water slack. During the ebb period, both parameters initially decrease but then increase again. SPM concentrations also rise during the flood period, peaking just before high water, and then decrease at high water slack. During the ebb period, SPM initially decreases but then increases again. Floc size at Lillo increases at the beginning of the flood tide, peaks at high water, and decreases during the ebb period as turbulence rises again, breaking larger aggregates into smaller particles.

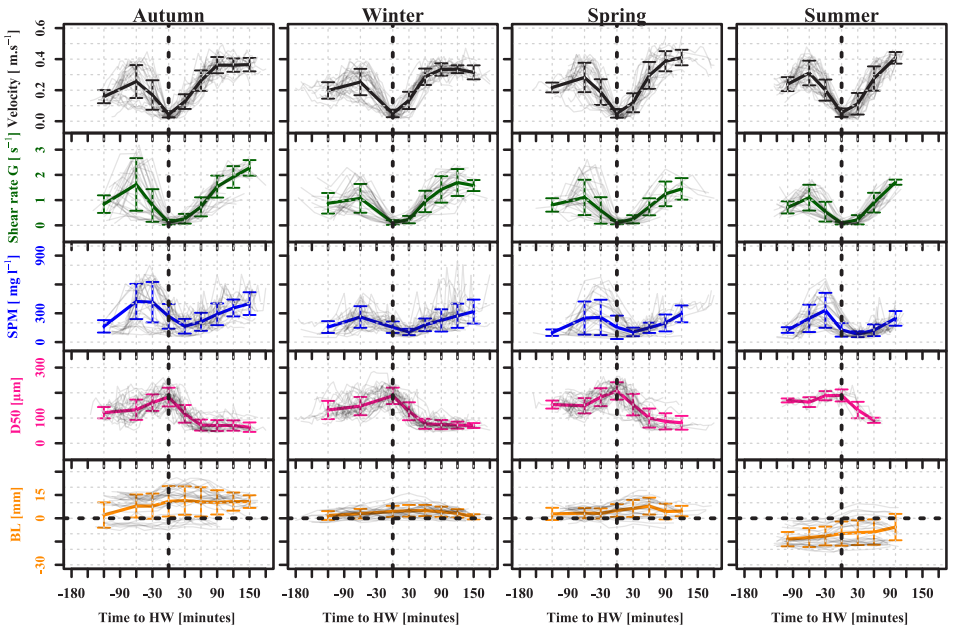

Figure 2.D.2: Graphical representation of tidal cycle changes at Lillo, including current velocity, shear rate G, SPM, floc size, and bed level data.

Figure 2.D.3 illustrates the changes in parameters across all tidal cycles and seasons at Zuidgors Station. The bed level shows minimal changes, indicating a gradual influence of tidal forces over time. At Zuidgors Station, current velocity and turbulent shear rate (G) show similar trends to Lillo, with peaks during the flood period, significant drops at high water slack, and increases during the ebb tide. SPM concentrations increase during the flood period, peak before high water, and decrease initially during the ebb period, followed by a subsequent increase. Floc size at Zuidgors increases at the start of the flood tide, peaks at high water, and decreases during the ebb period due to the higher turbulence levels, particularly in winter, which prevent significant reaggregation of particles.

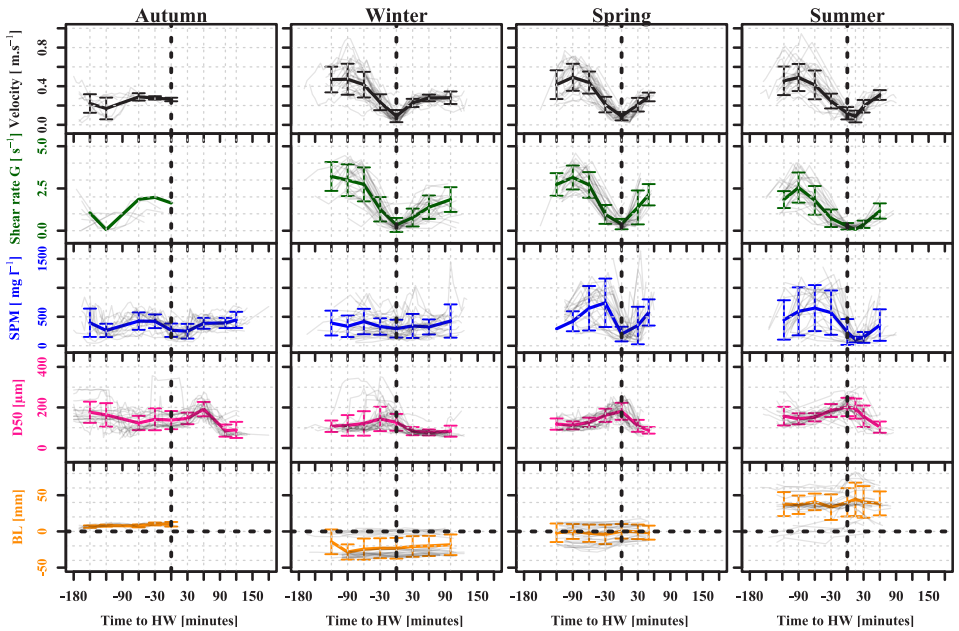

Figure 2.D.3: Graphical representation of tidal cycle changes at Zuidgors, including current velocity, shear rate G, SPM, floc size, and bed level data.

Appendix 2.E: Analyzing Sediment Spikes: Beyond Regular Tides

This appendix presents the analysis of sedimentation and erosion spikes at Branst, Lillo, and Zuidgors stations. To understand the major variations in sediment dynamics, we focused on tidal cycles with pronounced 'spikes' in bed level data. These spikes indicate unusual sediment resuspension or deposition driven by specific environmental conditions. By comparing these spikes with regular tidal cycles, we identified key factors contributing to sediment dynamics, offering insights into the processes affecting sediment stability and distribution in intertidal zones.

In the plots, you can observe the environmental conditions associated with these spikes, illustrating the interplay between tidal forces, hydrodynamic conditions, and sediment dynamics. These plots demonstrate:

- Across all stations, strong currents and turbulence typically lead to erosion. In the plots, look for negative spikes in bed level changes associated with high current velocities.
- High current velocities can result in both erosion and sedimentation spikes, depending on additional factors like SPM levels and floc size.

- **Branst:** During spring and summer, observe how high current velocities correlate with erosion spikes. Notice in the plots how higher SPM levels and larger flocs in spring lead to sedimentation spikes, while smaller flocs in summer cause increased erosion.
- **Lillo:** In autumn, spring, and summer, high current velocities combined with elevated SPM levels contribute to both erosion and sedimentation. In the plots, look for how smaller floc sizes in these seasons affect sediment dynamics.
- **Zuidgors:** In spring and summer, high current velocities drive both erosion and sedimentation spikes. The plots will show smaller flocs in spring leading to resuspension and larger flocs in summer promoting deposition.

- In winter and autumn, high-energy conditions generally prevent sedimentation at Lillo and Zuidgors, while at Branst, positive spikes occur at lower velocities.
  - **Branst:** In the plots for winter, notice the positive spikes in bed level changes associated with lower velocities and reduced SPM levels. In autumn, observe how increased SPM levels and tidal ranges promote sediment accumulation.
  - **Lillo and Zuidgors:** The plots will show the absence of positive spikes in winter due to strong currents keeping sediments suspended. In autumn, look for similar high-energy conditions that hinder sediment deposition.

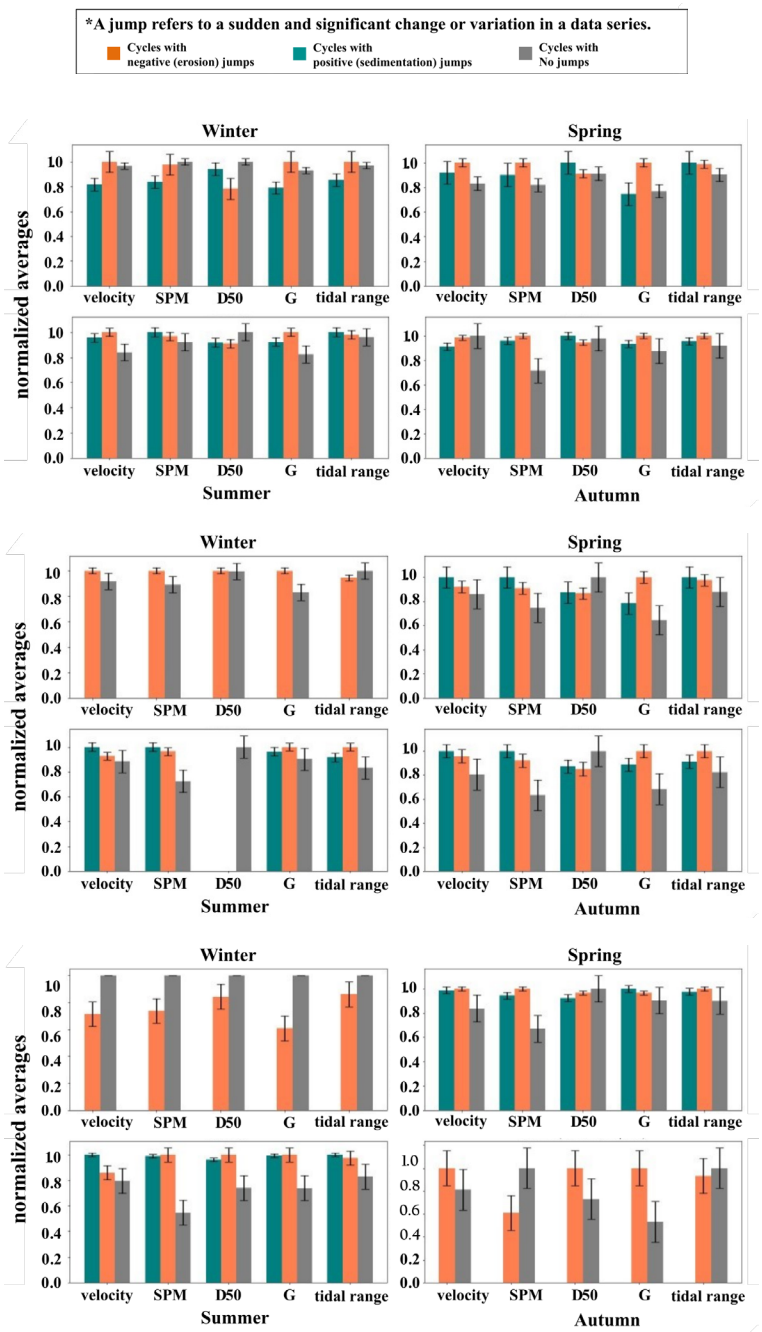
*A jump refers to a sudden and significant change or variation in a data series.
Cycles with negative (erosion) jumps
Cycles with positive (sedimentation) jumps
Cycles with No jumps
Winter
Spring
Summer
Autumn
normalized averages
0.0
0.2
0.4
0.6
0.8
1.0
velocity
SPM
D50
G
tidal range

Bibliography

1. Aubrey, D. G., & Friedrichs, C. T. (1988). *Seasonal climatology of tidal non-linearities in a shallow estuary*. In Hydrodynamics and sediment dynamics of tidal inlets (pp. 103-124). Springer New York.
2. Bar-Zeev, E., Passow, U., Romero-Vargas Castrillón, S., & Elimelech, M. (2015). *Transparent exopolymer particles: from aquatic environments and engineered systems to membrane biofouling*. Environmental Science & Technology, 49(2), 691-707.
3. Battisto, G. M. (1999). *Response of OBS to mixed grain-size suspension during SandyDuck'97.* Proc. Coastal Sed.'99, 297-312.
4. Bolle, A., Wang, Z. B., Amos, C., & De Ronde, J. (2010). *The influence of changes in tidal asymmetry on residual sediment transport in the Western Scheldt*. Continental Shelf Research, 30(8), 871-882.
5. Camp, T. R. (1943). *Velocity gradients and internal work in fluid motion*. J. Boston Soc. Civ. Eng., 30, 219-230.
6. Chainho, P., Silva, G., Lane, M. F., Costa, J. L., Pereira, T., Azeda, C., ... & Costa, M. J. (2010). *Long-term trends in intertidal and subtidal benthic communities in response to water quality improvement measures*. Estuaries and Coasts, 33, 1314-1326.
7. Chen, M. S., Wartel, S., Eck, B. V., & Maldegem, D. V. (2005). *Suspended matter in the Scheldt estuary*. Hydrobiologia, 540, 79-104.
8. Cleveringa, J. (2013). *Grootschalige sedimentbalans van de Westerschelde*. Project LTV Veiligheiden Toegankelijkheid; LTV V&T-RAPPORT K-17. Rapport 076945827:0.4 – Definitief, Arcadis.
9. Cox, T. J. S., Maris, T., Van Engeland, T., Soetaert, K., & Meire, P. (2019). *Critical transitions in suspended sediment dynamics in a temperate meso-tidal estuary*. Scientific reports, 9(1), 12745.
10. Dam, G., Van der Wegen, M., Taal, M., & Van der Spek, A. (2022). *Contrasting behaviour of sand and mud in a long-term sediment budget of the Western Scheldt estuary*. Sedimentology, 69(5), 2267-2283.
11. Damme, S. V., Struyf, E., Maris, T., Ysebaert, T., Dehairs, F., Tackx, M., ... & Meire, P. (2005). *Spatial and temporal patterns of water quality along the estuarine salinity gradient of the Scheldt estuary (Belgium and The Netherlands): results of an integrated monitoring approach*. Hydrobiologia, 540, 29-45.
12. De Brouwer, J. F. C., Bjelic, S., De Deckere, E. M. G. T., & Stal, L. J. (2000*). Interplay between biology and sedimentology in a mudflat (Biezelingse Ham, Westerschelde, The Netherlands)*. Continental shelf research, 20(10-11), 1159-1177.
13. De Brouwer, J. F., & Stal, L. J. (2002). *Daily fluctuations of exopolymers in cultures of the benthic diatoms Cylindrotheca closterium and Nitzschia sp.(Bacillariophyceae)*. Journal of Phycology, 38(3), 464-472.

14. de Lucas Pardo, M. A., Sarpe, D., & Winterwerp, J. C. (2015). *Effect of algae on flocculation of suspended bed sediments in a large shallow lake. Consequences for ecology and sediment transport processes*. Ocean Dynamics, 65, 889-903.
15. De Wolf, H., Blust, R., & Backeljau, T. (2004). *The population genetic structure of Littorina littorea (Mollusca: Gastropoda) along a pollution gradient in the Scheldt estuary (The Netherlands) using RAPD analysis*. Science of the Total Environment, 325(1-3), 59-69.
16. Dijkstra, Y. M., Schuttelaars, H. M., & Schramkowski, G. P. (2019). *A regime shift from low to high sediment concentrations in a tide-dominated estuary*. Geophysical Research Letters, 46(8), 4338-4345.
17. do Amaral Camara Lima, M., Ward, R. D., & Joyce, C. B. (2023). *Carbon sequestration and geochronology in Southern England's seagrass meadows*. Carbon Footprints, 2(4).
18. Downing, J. (2006). *Twenty-five years with OBS sensors: The good, the bad, and the ugly*. Continental Shelf Research, 26(17-18), 2299-2318.
19. Dyer, K. R., & Manning, A. J. (1999). *Observation of the size, settling velocity and effective density of flocs, and their fractal dimensions*. Journal of sea research, 41(1-2), 87-95.
20. Dyer, K. R., & New, A. L. (1986). *Intermittency in estuarine mixing*. In Estuarine variability (pp. 321-339). Academic Press.
21. Egan, G., Chang, G., Manning, A. J., Monismith, S., & Fringer, O. (2022). *On the variability of floc characteristics in a shallow estuary*. Journal of Geophysical Research: Oceans, 127(6), e2021JC018343.
22. Einstein, H. A., & Krone, R. B. (1962). *Experiments to determine modes of cohesive sediment transport in salt water*. Journal of Geophysical Research, 67(4), 1451-1461.
23. Eisma, D. (2019). *Worldwide distribution of intertidal areas*. In Intertidal Deposits (pp. 1-18). CRC Press.
24. Eisma, D., & Kalf, J. (1979). *Distribution and particle size of suspended matter in the Southern Bight of the North Sea and the Eastern Channel*. Netherlands Journal of Sea Research, 13(2), 298-324.
25. Eisma, D., Kalf, J., & Veenhuis, M. (1980). *The formation of small particles and aggregates in the Rhine estuary*. Netherlands Journal of Sea Research, 14(2), 172-191.
26. Elias, E. P., Van der Spek, A. J., Wang, Z. B., Cleveringa, J., Jeuken, C. J., Taal, M., & Van der Werf, J. J. (2023). *Large-scale morphological changes and sediment budget of the Western Scheldt estuary 1955–2020: the impact of large-scale sediment management*. Netherlands Journal of Geosciences, 102, e12.
27. Engel, A., & Passow, U. (2001). *Carbon and nitrogen content of transparent exopolymer particles (TEP) in relation to their Alcian Blue adsorption*. Marine Ecology Progress Series, 219, 1-10.
28. Engel, P. A. (2009). *Spatial and temporal variability of tide-induced salt flux in a partially mixed estuary* (Doctoral dissertation, Massachusetts Institute of Technology).
29. Fang, X., Mestdagh, S., Ysebaert, T., Moens, T., Soetaert, K., & Van Colen, C. (2019). *Spatio-temporal variation in sediment ecosystem processes and roles of key biota in the Scheldt estuary*. Estuarine, Coastal and Shelf Science, 222, 21-31.

30. Fettweis, M., & Baeye, M. (2015). *Seasonal variation in concentration, size, and settling velocity of muddy marine flocs in the benthic boundary layer*. Journal of Geophysical Research: Oceans, 120(8), 5648-5667.
31. Fettweis, M., Riethmüller, R., Verney, R., Becker, M., Backers, J., Baeye, M., ... & Vereecken, H. (2019). *Uncertainties associated with in situ high-frequency long-term observations of suspended particulate matter concentration using optical and acoustic sensors*. Progress in Oceanography, 178, 102162.
32. Fettweis, M., Sas, M., & Monbaliu, J. (1998). *Seasonal, neap-spring and tidal variation of cohesive sediment concentration in the Scheldt Estuary, Belgium*. Estuarine, Coastal and Shelf Science, 47(1), 21-36.
33. Fettweis, M., Schartau, M., Desmit, X., Lee, B. J., Terseleer, N., Van der Zande, D., ... & Riethmüller, R. (2022). *Organic matter composition of biomineral flocs and its influence on suspended particulate matter dynamics along a nearshore to offshore transect*. Journal of Geophysical Research: Biogeosciences, 127(1), e2021JG006332.
34. French, J. (2006). *Tidal marsh sedimentation and resilience to environmental change: exploratory modelling of tidal, sea-level and sediment supply forcing in predominantly allochthonous systems*. Marine Geology, 235(1-4), 119-136.
35. Gerbersdorf, S. U., Jancke, T., Westrich, B., & Paterson, D. M. (2008). *Microbial stabilization of riverine sediments by extracellular polymeric substances*. Geobiology, 6(1), 57-69.
36. Gerbersdorf, S. U., Westrich, B., & Paterson, D. M. (2009). *Microbial extracellular polymeric substances (EPS) in fresh water sediments*. Microbial ecology, 58, 334-349.
37. Geyer, W. R., & MacCready, P. (2014). *The estuarine circulation*. Annual review of fluid mechanics, 46(1), 175-197.
38. Guo, C., He, Q., van Prooijen, B. C., Guo, L., Manning, A. J., & Bass, S. (2018). *Investigation of flocculation dynamics under changing hydrodynamic forcing on an intertidal mudflat*. Marine Geology, 395, 120-132.
39. Horemans, D. M., Dijkstra, Y. M., Schuttelaars, H. M., Sabbe, K., Vyverman, W., Meire, P., & Cox, T. J. (2021). *Seasonal variations in flocculation and erosion affecting the large-scale suspended sediment distribution in the Scheldt estuary: the importance of biotic effects*. Journal of Geophysical Research: Oceans, 126(4), e2020JC016805.
40. Iglewicz, B., & Hoaglin, D. C. (1993*). Volume 16: how to detect and handle outliers*. Quality Press.
41. Kakeh, N., Coco, G., & Marani, M. (2016). *On the morphodynamic stability of intertidal environments and the role of vegetation*. Advances in Water Resources, 93, 303-314.
42. Kari, E., Kratzer, S., Beltrán-Abaunza, J. M., Harvey, E. T., & Vaičiūtė, D. (2017). *Retrieval of suspended particulate matter from turbidity–model development, validation, and application to MERIS data over the Baltic Sea*. International Journal of Remote Sensing, 38(7), 1983-2003.
43. Kon, K., Shimanaga, M., & Horinouchi, M. (2020). *Marine ecology: intertidal/littoral zone*. Japanese Marine Life: A Practical Training Guide in Marine Biology, 241-254.

44. Kristensen, E., & Kostka, J. E. (2005). *Macrofaunal burrows and irrigation in marine sediment: microbiological and biogeochemical interactions*. Interactions between macro-and microorganisms in marine sediments, 60, 125-157.
45. Kwon, B. O., Kim, H. C., Koh, C. H., Ryu, J., Son, S., Kim, Y. H., & Khim, J. S. (2018). *Development of temperature-based algorithms for the estimation of microphytobenthic primary production in a tidal flat: A case study in Daebu mudflat, Korea*. Environmental Pollution, 241, 115-123.
46. Lai, W., Pan, J., & Devlin, A. T. (2018). *Impact of tides and winds on estuarine circulation in the Pearl River Estuary*. Continental Shelf Research, 168, 68-82.
47. Lefebvre, A., Herrling, G., Becker, M., Zorndt, A., Krämer, K., & Winter, C. (2022). *Morphology of estuarine bedforms, weser estuary, Germany*. Earth Surface Processes and Landforms, 47(1), 242-256.
48. Lefebvre, J. P., Mari, X., Đo, T. P. T., & Chu, T. V. (2014). *The role of TEP in estuarine hydrosedimentary functioning: impact on settling velocity of aggregates*. COASTAL ENGINEERING, 2.
49. Lorke, A., McGinnis, D. F., & Maeck, A. (2013). *Eddy-correlation measurements of benthic fluxes under complex flow conditions: Effects of coordinate transformations and averaging time scales*. Limnology and Oceanography: Methods, 11(8), 425-437.
50. Lu, T., Wu, H., Zhang, F., Li, J., Zhou, L., Jia, J., ... & Wang, Y. P. (2020). *Constraints of salinity-and sediment-induced stratification on the turbidity maximum in a tidal estuary*. Geo-Marine Letters, 40, 765-779.
51. Lubarsky, H. V., Hubas, C., Chocholek, M., Larson, F., Manz, W., Paterson, D. M., & Gerbersdorf, S. U. (2010). *The stabilisation potential of individual and mixed assemblages of natural bacteria and microalgae*. PloS one, 5(11), e13794.
52. Manning, A. J., & Schoellhamer, D. H. (2013). *Factors controlling floc settling velocity along a longitudinal estuarine transect*. Marine Geology, 345, 266-280.
53. Maris, T., Cox, T., Temmerman, S., De Vleeschauwer, P., Van Damme, S., De Mulder, T., ... & Meire, P. (2007). *Tuning the tide: creating ecological conditions for tidal marsh development in a flood control area*. Hydrobiologia, 588, 31-43.
54. Maris, T., P. Gelsomini & J. Schoelynck, 2024. *Onderzoek naar de gevolgen van het Sigmaplan, baggeractiviteiten en havenuitbreiding in de Zeeschelde op het milieu. Geïntegreerd eindverslag van het onderzoek verricht in 2023*. ECOSPHERE 024-RES023. Universiteit Antwerpen, Antwerpen.
55. Martínez, L. A., Sabbe, K., Dasseville, R., Daveloose, I., Verstraete, T., D'hondt, S., ... & Vyverman, W. (2023). *Long-term phytoplankton dynamics in the Zeeschelde estuary (Belgium) are driven by the interactive effects of de-eutrophication, altered hydrodynamics and extreme weather events*. Science of the Total Environment, 860, 160402.
56. McCave, I. N. (1984). *Erosion, transport and deposition of fine-grained marine sediments*. Geological Society, London, Special Publications, 15(1), 35-69.

57. Meire, P., Plancke, Y., Govaerts, A., Cox, T., Gelsomi, P., Horemans, D., Meire, D., Meire, L., Zetsche, E. and Maris,T. (2021). *Synthesis note: SPM dynamics and trends in the Scheldt estuary*. ECOBE Report 021-R267 Universiteit Antwerpen, Antwerpen.
58. Meire, P., Ysebaert, T., Damme, S. V., Bergh, E. V. D., Maris, T., & Struyf, E. (2005). *The Scheldt estuary: a description of a changing ecosystem*. Hydrobiologia, 540, 1-11.
59. Mialet, B., Gouzou, J., Azémar, F., Maris, T., Sossou, C., Toumi, N., ... & Tackx, M. (2011). *Response of zooplankton to improving water quality in the Scheldt estuary (Belgium)*. Estuarine, Coastal and Shelf Science, 93(1), 47-57.
60. Mietta, F., Chassagne, C., Manning, A. J., & Winterwerp, J. C. (2009). *Influence of shear rate, organic matter content, pH and salinity on mud flocculation*. Ocean Dynamics, 59, 751-763.
61. Morelle, J., Schapira, M., & Claquin, P. (2017). *Dynamics of phytoplankton productivity and exopolysaccharides (EPS and TEP) pools in the Seine Estuary (France, Normandy) over tidal cycles and over two contrasting seasons*. Marine Environmental Research, 131, 162-176.
62. Mulligan, R. P., Smith, P. C., Tao, J., & Hill, P. S. (2019). *Wind-wave and tidally driven sediment resuspension in a macrotidal basin*. Estuaries and Coasts, 42, 641-654.
63. Pang, W., Zhou, X., Dai, Z., Li, S., Huang, H., & Lei, Y. (2021). *ADV-Based Investigation on Bed Level Changes Over a Meso-Macro Tidal Beach*. Frontiers in Marine Science, 8, 733923.
64. Passow, U. (2002). *Transparent exopolymer particles (TEP) in aquatic environments*. Progress in oceanography, 55(3-4), 287-333.
65. Perrot, V., Ma, T., Vandeputte, D., Smolikova, V., Bratkic, A., Leermakers, M., ... & Gao, Y. (2023). *Origin and partitioning of mercury in the polluted Scheldt Estuary and adjacent coastal zone*. Science of the Total Environment, 878, 163019.
66. Reed, D., van Wesenbeeck, B., Herman, P. M., & Meselhe, E. (2018). *Tidal flat-wetland systems as flood defenses: Understanding biogeomorphic controls*. Estuarine, Coastal and Shelf Science, 213, 269-282.
67. Rossi, F., & Chapman, M. G. (2003). *Influence of sediment on burrowing by the soldier crab Mictyris longicarpus Latreille*. Journal of Experimental Marine Biology and Ecology, 289(2), 181-195.
68. Savelli, R., Dupuy, C., Barillé, L., Lerouxel, A., Guizien, K., Philippe, A., ... & Le Fouest, V. (2018). *On biotic and abiotic drivers of the microphytobenthos seasonal cycle in a temperate intertidal mudflat: a modelling study*. Biogeosciences, 15(23), 7243-7271.
69. Savelli, R., Serôdio, J., Cugier, P., Méléder, V., Polsenaere, P., Dupuy, C., & Le Fouest, V. (2021). *Potential impact of photoinhibition on microphytobenthic primary production on a large intertidal mudflat*. Journal of Geophysical Research: Biogeosciences, 126(9), e2021JG006443.
70. Schartau, M., Riethmüller, R., Flöser, G., van Beusekom, J. E. E., Krasemann, H., Hofmeister, R., & Wirtz, K. (2019). *On the separation between inorganic and organic fractions of suspended matter in a marine coastal environment*. Progress in Oceanography, 171, 231-250.
71. Schwarz, C., Cox, T., Van Engeland, T., Van Oevelen, D., Van Belzen, J., Van de Koppel, J., ... & Temmerman, S. (2017). *Field estimates of floc dynamics and settling velocities in a tidal creek with*

significant along-channel gradients in velocity and SPM. Estuarine, Coastal and Shelf Science, 197, 221-235.

72. Sequoia Scienti_c. (cited 2019). *How to compute the mean particle diameter from a LISST volume distribution*. Sequoia Scienti_c. ([Available online at http://www.sequoiasci.com/article/how-to-compute-the-mean-particle-diameter-from-a-lisst-volume-distribution-2/).
73. Sgarabotto, A., D'Alpaos, A., & Lanzoni, S. (2021). *Effects of vegetation, sediment supply and sea level rise on the morphodynamic evolution of tidal channels*. Water Resources Research, 57(7), e2020WR028577.
74. Smith, D. G., & Davies-Colley, R. J. (2001). *If visual water clarity is the issue, then why not measure it*. New York City Department of Environmental Protection, Bureau of Water Supply, National Institute of Water and Atmospheric Research, Hamilton, New Zealand.
75. Smolders, S., Plancke, Y., Ides, S., Meire, P., & Temmerman, S. (2015). *Role of intertidal wetlands for tidal and storm tide attenuation along a confined estuary: a model study*. Natural Hazards and Earth System Sciences, 15(7), 1659-1675.
76. Spalding, M. D., Ruffo, S., Lacambra, C., Meliane, I., Hale, L. Z., Shepard, C. C., & Beck, M. W. (2014). *The role of ecosystems in coastal protection: Adapting to climate change and coastal hazards*. Ocean & Coastal Management, 90, 50-57.
77. Stal, L. J. (2010). *Microphytobenthos as a biogeomorphological force in intertidal sediment stabilization*. Ecological Engineering, 36(2), 236-245.
78. Stark, Jeroen, et al. "*Impact of intertidal area characteristics on estuarine tidal hydrodynamics: A modelling study for the Scheldt Estuary*." Estuarine, Coastal and Shelf Science 198 (2017): 138-155.
79. Temmerman, S., Govers, G., Meire, P., & Wartel, S. (2003). *Modelling long-term tidal marsh growth under changing tidal conditions and suspended sediment concentrations, Scheldt estuary, Belgium*. Marine Geology, 193(1-2), 151-169.
80. Temmerman, S., Horstman, E. M., Krauss, K. W., Mullarney, J. C., Pelckmans, I., & Schoutens, K. (2023). *Marshes and mangroves as nature-based coastal storm buffers*. Annual Review of Marine Science, 15(1), 95-118.
81. Tukey, J. W. (1977). *Exploratory data analysis addision-wesley*. Reading, Ma, 688, 581-582.
82. Uncles, R. J., Bale, A. J., Stephens, J. A., Frickers, P. E., & Harris, C. (2010). *Observations of floc sizes in a muddy estuary*. Estuarine, Coastal and Shelf Science, 87(2), 186-196.
83. Van Ael, E., Covaci, A., Blust, R., & Bervoets, L. (2012). *Persistent organic pollutants in the Scheldt estuary: environmental distribution and bioaccumulation*. Environment international, 48, 17-27.
84. Van Coppenolle, R. (2018). *Potential for nature-based mitigation of coastal flood risks: From regional to global scale assessments* (Doctoral dissertation, University of Antwerp).
85. Van Katwijk, M. M., Bos, A. R., Hermus, D. C. R., & Suykerbuyk, W. (2010). *Sediment modification by seagrass beds: Muddification and sandification induced by plant cover and environmental conditions*. Estuarine, Coastal and Shelf Science, 89(2), 175-181.
86. van Leussen, W. (2011). *Macroflocs, fine-grained sediment transports, and their longitudinal variations in the Ems Estuary*. Ocean dynamics, 61(2-3), 387-401.

87. van Rijn, L., & Grasmeijer, B. (2018). *Effect of channel deepening on tidal flow and sediment transport—part II: muddy channels*. Ocean Dynamics, 68(11), 1481-1501.
88. Vandenbruwaene, W., Hertoghs, R., Michielsen, S., van de Moortel, I., & Al., E. (2018). *Monitoring Effecten Ontwikkelingsschets (MONEOS) – Jaarboek monitoring 2017: Deelrapport 7 - Factua data rapportage van monitoring waterbeweging en fysische parameters in de Zeeschelde in 2017*. Versie 3.0.
89. Verney, R., Lafite, R., & Brun-Cottan, J. C. (2009). *Flocculation potential of estuarine particles: The importance of environmental factors and of the spatial and seasonal variability of suspended particulate matter*. Estuaries and coasts, 32, 678-693.
90. Wartel, S., & Francken, F. (1998). *Sedimenttransport en sedimentatieprocessen in de Schelde tussen Zandvliet en Gent*. Brussel, Koninklijk Belgisch instituut voor Natuurwetenschappen, 42.
91. Waterinfo.be (cited 2019). *Measurements and predictions of Waterinfo.be [data]*. [Available online at https://www.waterinfo.be/].
92. Widdows, J., & Brinsley, M. (2002). *Impact of biotic and abiotic processes on sediment dynamics and the consequences to the structure and functioning of the intertidal zone*. Journal of sea Research, 48(2), 143-156.
93. Widdows, J., Blauw, A., Heip, C. H. R., Herman, P. M. J., Lucas, C. H., Middelburg, J. J., ... & Verbeek, H. (2004). *Role of physical and biological processes in sediment dynamics of a tidal flat in Westerschelde Estuary, SW Netherlands*. Marine Ecology Progress Series, 274, 41-56.
94. Wilczak, J. M., Oncley, S. P., & Stage, S. A. (2001). *Sonic anemometer tilt correction algorithms*. Boundary-layer meteorology, 99(1), 127-150.
95. Winterwerp, J. C. (2002). *On the flocculation and settling velocity of estuarine mud*. Continental shelf research, 22(9), 1339-1360.
96. Winterwerp, J. C., & Van Kesteren, W. G. (2004). *Introduction to the physics of cohesive sediment dynamics in the marine environment*. Elsevier.
97. Winterwerp, J. C., Wang, Z. B., Van Braeckel, A., Van Holland, G., & Kösters, F. (2013). *Man-induced regime shifts in small estuaries—II: a comparison of rivers*. Ocean Dynamics, 63, 1293-1306.
98. Ysebaert, T., & Herman, P. M. (2002). *Spatial and temporal variation in benthic macrofauna and relationships with environmental variables in an estuarine, intertidal soft-sediment environment*. Marine Ecology Progress Series, 244, 105-124.
99. Ysebaert, T., Fettweis, M., Meire, P., & Sas, M. (2005). *Benthic variability in intertidal soft-sediments in the mesohaline part of the Schelde estuary*. Hydrobiologia, 540, 197-216.
100. Zander, F., Comans, R. N. J., & Gebert, J. (2023). *Linking patterns of physical and chemical organic matter fractions to its lability in sediments of the tidal Elbe river*. Applied Geochemistry, 156, 105760.

Chapter 3

Estimating the Effects of Existing and Future Intertidal Areas on Suspended Sediment Equilibrium in the Scheldt Estuary

Abstract

Understanding sediment transport is crucial for managing the stability of rivers, bays, and estuaries. It shapes aquatic habitats, influences water quality, and drives morphodynamic processes, all of which are critical for flood risk management, navigation, and ecosystem health. Sediment transport involves the movement of both organic and inorganic materials, essential for sustaining benthic habitats and preserving the overall geomorphological and ecological integrity of estuarine environments. However, predicting sediment dynamics is challenging due to the complex interactions between hydrodynamic forces, sediment properties, and biological factors.

This chapter aims to create an approach for predicting bed level changes in the Scheldt estuary, using Machine Learning (ML) models. Specifically, two ML methods are applied: Random Forest (RF) Regression and Artificial Neural Networks (ANN). The modeling framework incorporates key environmental variables such as current velocity, suspended particulate matter (SPM) concentration, mean floc size (D50), shear rate (G), tidal range, and seasonality as input features for training. ML also allows for the assessment of the influence of input training features on sedimentation and erosion dynamics, by feature importance distributions and model accuracy comparisons. The models are also evaluated across different scenarios and dataset selections, to assess their ability to detect and differentiate seasonal variations, as well as learn site-specific characteristics.

The results emphasize the critical role of seasonality in improving model accuracy. Both RF and ANN models perform better when adjusted for seasonal factors, with RF showing superior accuracy across various metrics due to its ability to capture the complex dynamics of sediment transport. The integration of seasonal data enhances the RF model's performance. The RF model's feature importance analysis identifies tidal range, SPM concentration, and floc size as key predictors, reinforcing RF's utility in sediment transport modeling. In contrast, ANN models demonstrate moderate predictive ability initially but show similar improvement with the inclusion of seasonal factors, making them more useful for analyzing sediment behavior. Additionally, spatial analysis indicates that both models demonstrate good accuracy in modeling sedimentation across diverse intertidal zones; however, ANN performance varies across different environmental conditions.

To this end, the results demonstrate that ML models, especially RF, are highly effective in predicting sediment dynamics, with RF excelling in accuracy and feature importance identification. ANN's adaptability makes it ideal for complex, data-rich studies. Overall, ML

approaches allow for modeling the complex interdependencies that are typical of estuarine environments, particularly when working with large datasets containing high-frequency measurements. While both RF and ANN models are highly effective, they lack the detailed, mechanistic insights that classical models provide. To address this, the integrating ML models for short-term predictions with classical models for long-term, process-based understanding offers a more complete framework for sediment transport modeling. This approach is particularly valuable as climate change and sea level rise may introduce divergences from classical understandings, exposing the more intricate dependencies across variables, an area ML models excel.

3.1. Introduction

Sediment transport is a fundamental process shaping rivers, bays, and estuaries, playing a pivotal role in morphodynamic processes, aquatic habitats, and water quality (Winterwerp & van Kesteren, 2004; Cox et al., 2009; Son & Hsu, 2011; Hillman et al., 2020). This process encompasses the movement of both organic and inorganic materials, crucial for sustaining benthic habitats and maintaining the overall geomorphological and ecological integrity of estuarine environments (Meire et al., 2005; Elliott & Whitfield, 2011). However, understanding sediment dynamics is complex due to the interplay of various physical and biological factors.

Hydrodynamic forces, such as current velocities, wave action, and tidal movement, are critical drivers of sediment transport. These forces, in conjunction with sediment characteristics affect how sediments settle, are resuspended, and are transported (Winterwerp & van Kesteren, 2004; Nichols, 2009). A key process within this dynamic is flocculation, where suspended sediment particles aggregate into larger particles (flocs) or break apart. This process is driven by hydrodynamic conditions and sediment properties, which influence particle size and, consequently, settling velocity and resuspension rates (Maggi, 2007; Winterwerp et al., 2002). In estuaries, where the interplay of these forces is highly variable, flocculation plays a crucial role in controlling the overall sediment behavior.

In addition to physical processes, biological factors—such as biofilm formation and the presence of vegetation—further complicate sediment dynamics. These biological elements can stabilize sediments in some areas or contribute to erosion in others (De Brouwer & Stal, 2002; Widdows et al., 2004). The combined effects of hydrodynamic, sedimentary, and biological factors make it extremely challenging to predict sedimentation and erosion patterns using only direct observations and measurement. This complexity necessitates the use of numerical models, which

allow for the integration of these varied factors into cohesive frameworks that simulate sediment behavior over time.

Numerical models have proven invaluable in estuarine studies, offering insights that are difficult to obtain from field measurements alone. Over time, the need to incorporate a wide range of variables—such as biological processes, hydrodynamic forces, and sediment characteristics—has become evident, in pursuit of enhanced modeling accuracy. For instance, Uchiyama's (2005) model of San Francisco Bay demonstrated how intertidal mudflats serve as significant sediment sinks but also revealed the limitations of existing models in accounting for sediment consolidation and wind-driven resuspension. Similarly, Winterwerp's (2021) research in the Ems Estuary highlighted the complexity of sediment dynamics by focusing on the variability of floc size and the influence of biological processes. However, this research also noted the difficulty in capturing seasonal variations and the role of episodic events. Similarly, Nakagawa's (2005) work in Ariake Bay underscored the importance of tidal currents in sediment redistribution but pointed out gaps in understanding long-term morphological changes driven by storms and other episodic events.

The Scheldt estuary, with its complex system of intertidal areas, seasonal variations, tidal forces, and salinity gradients, represents a particularly challenging environment for studying sediment transport. Early research, such as Mulder & Udink (1991), laid the groundwork by modeling erosion, sedimentation, and the transport of cohesive sediments in the Western Scheldt estuary, emphasizing the critical role of local sediment properties and wave action. Fettweis & Van den Eynde (2003) expanded on this work, focusing on suspended sediment processes in the Belgian-Dutch coastal zone. In 2007, Fettweis et al. further integrated satellite imagery with in-situ measurements and numerical models. This integration aimed to estimate suspended particulate matter transport in the southern North Sea. Van Kessel et al. (2011) developed a mud transport model specifically for the Scheldt estuary to support management decisions, achieving realistic hydrodynamic simulations but also highlighting the difficulties in modeling tidal wave propagation near Antwerp. Concurrently, Baeye et al. (2011) investigated the impact of tidal and wind-driven flows on sediment mobility along the Belgian inner shelf, emphasizing the variability of sediment transport influenced by hydro-meteorological conditions. Later work by Plancke & Vos (2016) and Vanlede et al. (2015) tackled sediment transport and morphological changes within the estuary. More recent studies include Dijkstra et al. (2019) on hyperturbidity potential after channel deepening, and Boelens et al. (2020), who developed a model to examine historical tidally averaged sandy sediment transport.

Despite these advances, fully grasping the complexity of estuarine sediment dynamics remains an ongoing challenge, mainly due to the limitations in datasets resolution and also the compound,

intricate dependencies as variable count increases in modeling. Accurately representing the various factors influencing sediment transport—such as flocculation, tidal currents, and seasonal variations—is difficult but critical for reliable predictions. The need for high-frequency and accurate measurements is evident, as they are essential in detecting more subtle and localized trends. Recent studies have begun to address these challenges through advanced techniques like Machine Learning (ML). Francke et al. (2008) demonstrated the limitations of traditional Sediment Rating Curves (SRCs) and showed that ML approaches like Random Forests (RF) and Quantile Regression Forests (QRF) outperform more classical approaches. Ouellet-Proulx et al. (2016) similarly validated the use of ML models with a Model Tree (MT) approach for estimating Suspended Sediment Concentration (SSC), achieving more accurate results than SRCs. Sahin et al. (2017) used Artificial Neural Networks (ANNs) to predict floc size distribution with high accuracy, while Seo et al. (2020) applied ML to analyze hydrodynamic influences on SSC, yielding results closely aligned with empirical data. These advancements reflect a growing trend towards more nuanced, data-driven models for sediment analysis.

This chapter focuses on predicting bed level changes in the Scheldt estuary using ML regression models. These models are essential for capturing the continuous nature of key environmental variables, such as current velocity, suspended particulate matter (SPM) concentration, mean floc size (D50), shear rate (G), tidal range, and seasonal variations, as they fluctuate over time, and evaluate their impact on sedimentation and erosion dynamics. To introduce a comparison of ML approaches in sediment transport modeling, two distinct approaches are employed, which operate differently in their statistical method and learning algorithm: Random Forest Regression (Breiman, 2001) and ANN (Rosenblatt, 1958). By applying both RF and ANN, the analysis demonstrates that reliable and consistent predictions can be achieved using different ML techniques, reinforcing their applicability in complex environmental systems like the Scheldt estuary, while reporting on their advantages in various conditions.

3.2. Models

This section explains the two ML models—RF Regression and ANN—used in this study, along with their key input features, outputs, and overall functionality.

3.2.1. Random Forest Regression

The Random Forest (RF) method is a widely used approach in ensemble learning, renowned for its reliability in handling complex datasets with highly inter-dependent variables. It accomplishes

this by combining multiple decision trees (individual learners), each iteratively trained on a distinct subset of the training data that together form a 'forest' (the ensemble predictor) (Figure 3.1). These subsets are generated through bootstrapping, a technique that samples with replacement, thus allowing certain instances to be duplicated, while others might be omitted (Breiman, 2001). In the RF methodology, each decision tree is independently trained on its respective bootstrapped subset. The trees evaluate their accuracy through metrics like Mean Absolute Error (MAE) or Mean Squared Error (MSE). Collectively, they form the Random Forest, a robust ensemble that mitigates anomalies in the training data. During prediction, each tree contributes a "vote" to the final outcome: the majority vote determines the result in classification tasks, while the average of outputs is used in regression.

3.2.1.1. RF Modeling Pipeline

The modeling implementation utilizes Python's Scikit-Learn in using the RF algorithms. As an open-source library, Scikit-Learn offers extensive tools for various tasks such as classification, regression, clustering, and dimensionality reduction. It is especially favored for its user-friendly interface and comprehensive documentation (Pedregosa et al., 2011). The pipeline outlines the steps involved in creating a RF Regression model using Scikit-Learn are as follows:

[1] Data preparation: The dataset, including both features (independent variables) and the target variable (dependent variable), is split into training and testing sets (a 70%, 30% random split). The training set is crucial for the training algorithm to build a model (in this case, tree) with. The test set is used after training and assesses the model's performance on previously unseen data (for which the correct value, in this case bed level change, is known and can be compared to the trained model's prediction).

[2] Determining the optimal number of trees using OOB scores: OOB error is calculated during model training by evaluating each tree on the samples that were not included in its bootstrapped training subset, i.e., the "out-of-bag" samples. This provides an unbiased estimate of the model's error rate, which is used by the learning algorithm to assess and improve the model's accuracy during training. Utilizing the OOB error, an ideal number of trees is determined. This number is optimized when the OOB error is minimized or plateaus, balancing accuracy with computational efficiency. If the number of trees is too high, the model can "overfit" and OOB decreases (overfitting is learning noise in the training data and underperforming with new test datasets).

[3] Training: After model architecture (number of trees) is determined, the forest is created, and the learning algorithm trains the model using the training dataset. Individual decision trees are trained based on random subsets of training data and selected features.

[4] Making predictions: After the model is trained, we can use new vectors of data as input variables, to make predictions. In each instance, the trees make predictions (regression numbers), and the final forest prediction is derived by averaging these individual predictions.

[5] Evaluating model performance: Overall model performance is evaluated by using the test set. We initially left a 30% random subset of the data which the model has never seen before. We then run predictions on each data point and compare models' predicted values against the measured values in the test set. Metrics such as MSE, MAE, or the Coefficient of Determination [R^2] are used to assess accuracy. While MSE, the default criterion for Random Forest Regressor, is sensitive to outliers due to its squaring of prediction errors, MAE provides a more balanced approach by calculating the absolute differences. The choice between MSE and MAE depends on the specific requirements of model sensitivity and computational efficiency (Willmott & Matsuura, 2005; Hyndman & Koehler, 2006).

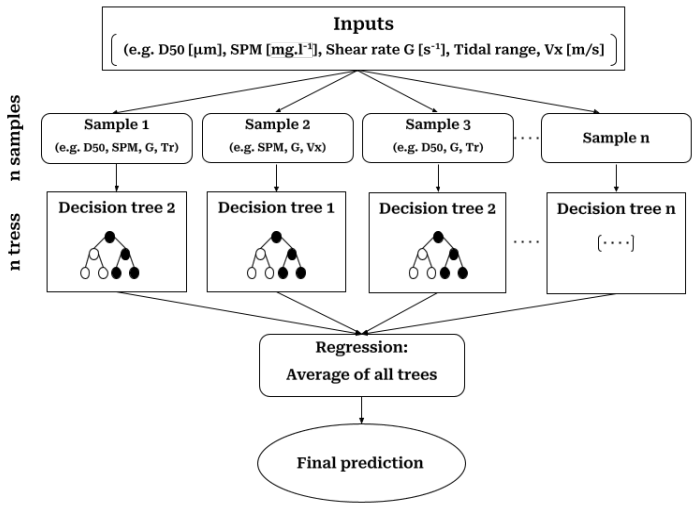

Figure 3.1: Conceptual architecture of the RF model used to predict suspended sediment deposition and erosion. The model receives multiple input features—tidal range, current velocity, shear rate (G), SPM concentration, and floc size (D50)—which are passed through an ensemble of individual decision trees. Each tree independently generates a prediction based on a subset of the data and input variables. The final model output, representing predicted bed level change, is obtained by averaging the outputs of all trees.

3.2.1.2. Predictive Strengths and Practical Applications

Random Forest models excel in handling complex datasets with multicollinearity and non-linear correlations. When multiple variables interact with each other in intricate ways, creating a non-linear web of dependencies, RF models effectively reduce dimensionality by evaluating variables at each node, covering the complex mesh of possibilities within the tree-like structure. RF models can be resistant to overfitting too, through using the OOB score. The OOB score provides an unbiased error estimate during training, which guides the training more effectively (Hastie et al., 2009). This approach allows the model to eventually generalize well to unseen data by capturing the underlying patterns and interactions in the dataset. Another strength of Random Forests is their ability to quantify feature importance, outputting a relative distribution of each input feature's contribution to the training of the forest. This insight supports understanding relationships within the data and supports feature selection or engineering for further modeling refinement.

On the other hand, Random Forest's computational complexity, resulting from the use of multiple trees, can increase training costs and time. While larger training datasets can help RF models with their advantage in capturing the nuances of variable dependencies, this also significantly increases their training complexity. Furthermore, the complexity of RF models can compromise interpretability compared to simpler machine learning methods, making it more challenging to understand how specific inputs contribute to outputs.

RF models have diverse applications across many fields, such as image classification, remote sensing, and environmental science, valued for their strong predictive performance and resistance to noise. For instance, Ghosh et al. (2014) applied them to multi-class object detection in remote sensing, improving classification accuracy, while Belgiu and Drăguț (2016) used the method to classify complex land-use patterns, enhancing environmental monitoring and disaster prediction. In environmental science, these models have proven effective in predicting biodiversity and modeling ecosystems. Cutler et al. (2007) employed RF to predict species distributions, demonstrating their strength in handling complex ecological interactions and autocorrelations. Additionally, Rodriguez-Galiano et al. (2012) used RF to identify areas vulnerable to land degradation, showcasing their value in environmental conservation and climate change mitigation. In sediment management, they have outperformed classical methods in predicting suspended sediment concentrations and assessing transport dynamics, as shown in studies by Francke et al. (2008) and Ouellet-Proulx et al. (2016), making them valuable for managing sediment dynamics in estuarine environments.

3.2.2. Artificial Neural Networks

Artificial Neural Networks (ANNs) are ML models inspired by the functioning of biological neural systems, like those in the human brain. These models are powerful tools for learning complex functions that capture the relationships between input features and target outputs. An ANN consists of interconnected layers of neurons, organized in a structure called the ANN architecture, as seen in Figure 3.2. The architecture consists of a few different layers, and the information generally moves through the network with various mathematical transformations performed on it, to reach an output, i.e. prediction. During training, the variables for the intermediate transformation (model weights) are adjusted such that the training error reduces. The architecture typically has 3 main segments:

1. **Input layer:** This is where the training or test data is fed into the network, containing nodes representing each input feature.
2. **Hidden layer(s):** Situated between the input and output layers, the hidden layers contain nodes that process information from the input layer through linear transformations and activation functions. Common activation functions include ReLU (Rectified Linear Unit), sigmoid, and tanh, enabling the network to learn and recognize patterns.
3. **Output (or target) layer:** The final layer, producing the ANN's predictions or decisions based on the processed information. Each node in this layer represents one of the potential outputs or target values. Similar to the hidden layers, this layer performs calculations but often uses different activation functions, like sigmoid for binary classification and softmax for multi-class classification problems.

3.2.2.1. ANN Modeling Pipeline

The ANN's training process is as follows:

[1] Hyperparameter tuning: Thorough experimentation with a small subset of the data, the model architecture variables, such as the number of hidden layers, the number of nodes inside each layer, the activation functions of nodes or the loss function (for calculating errors during training), are determined to form a network architecture. Moreover, a learning rate (explained leather) and an “epoch” number (the number of times the training pass is done over the entire dataset) are specified.

[2] ANN training: Model training is conducted using the training set (70% of the data). The steps involved in this process are described below.

[3] Model evaluation: Like the RF models, the trained ANN is evaluated using MSE or R^2 measures.

The ANN training process has various steps described below.

[2.A] Forward propagation: The network's layered structure, including the hidden layers, allows interconnected nodes to facilitate forward propagation of information from input to output. Connections between nodes, each with an associated weight (W), are crucial for capturing complex data patterns. Initially, these weights and biases are assigned random values. In each round, a subset of the data (called a batch) flows through the network to yield a single prediction number for each input data point in the batch (a set of regression values).

[2.B] Error calculation: This output is then compared to the actual target value, and an error is calculated using the loss function (e.g. MSE). A subset of the training data, typically around 10-20%, is used as a validation set to evaluate each epoch's performance (this is distinct from the test set, which is used after training and for model evaluation). At this stage, the learning algorithm has a measure of the error. To reduce this error, the algorithm adjusts the network weights.

[2.C] Backpropagation and Gradient Descent: Within the training process of ANNs, two fundamental methods, Back Propagation and Gradient Descent, play crucial roles. Back Propagation leverages the computed loss error at the previous stage to adjust the weights layer by layer, utilizing an optimization algorithm to fine-tune the network. Complementing this process, Gradient Descent serves as a powerful optimization technique, iteratively modifying the weights to minimize the overall loss of the network. The direction of these modifications is guided by the gradient of the loss function, which indicates the steepest descent towards the optimal solution. Throughout this optimization process, the learning rate emerges as a critical hyperparameter, carefully regulating the magnitude of weight adjustments at each step to balance convergence speed and stability.

[2.D] Epochs and continuous improvement: An epoch is a full cycle through the training dataset. The number of epochs is determined with hyperparameter tuning before training, as described earlier. The goal is for the epoch count to sufficiently train the model, while not overfitting the model (where too many epochs force the model to look for noisy patterns that are not useful information) (Brownlee, 2018).

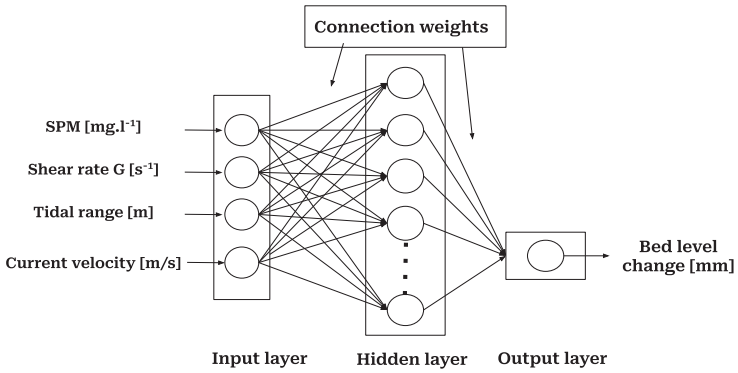

Figure 3.2: Conceptual architecture of the ANN model used to predict suspended sediment deposition and erosion. The model receives multiple input features—tidal range, current velocity, shear rate (G), SPM concentration, and floc size (D50) and seasons—and processes them through multiple hidden layers consisting of interconnected neurons. Each neuron performs weighted computations followed by activation functions, allowing the network to model complex, non-linear relationships among variables. The final output layer produces a continuous prediction of bed level change. The network train using a backpropagation algorithm and early stopping to avoid overfitting.

3.2.2.2. Predictive Strengths and Practical Applications

ANNs, particularly deep neural networks with many large hidden layers, offer numerous advantages over other ML techniques due to their capability to model incredibly complex functions. The depth of these networks is a major strength in learning varying levels of data abstraction. Through non-linear transformations induced by artificial neuron activation functions, deep networks effectively manage non-linearities inherent in real-world problems. Furthermore, they can handle intricate multivariate dependencies by adapting to diverse combinations of input features, thereby improving predictions. Their capacity to learn and adapt to unknown relationships between variables in a dataset makes them a robust tool for scenarios where the interplay between variables is either unclear or too complex to explicitly model.

ANNs are not the optimal choice for every scenario. They are most efficient when dealing with complex relationships between inputs and outputs but require an ample volume of training data to capture the complexity. This is what, for example, makes them suitable for many perception ML problems, such as machine vision, where individual data points are single pixels. However, in scenarios where these relationships are simple or can be better modeled using other methods such as linear regression or decision trees, ANNs may not offer extra advantages and could risk overfitting, leading to poor generalization to unseen data.

Recent advancements in deep learning have led to the development of sophisticated model architectures, such as Generative Adversarial Networks (GANs) or Variational Autoencoders (VAEs). These models can create new paintings and realistic images (Ramesh et al., 2021) or answering questions in text or voice – commonly known as Artificial Intelligence (AI) capabilities. ANNs have also proven invaluable in various other fields, particularly environmental modeling, due to their ability to handle nonlinearity, learn from data, and generalize patterns. For example, ANNs have been applied to predict local climatic patterns, as shown by Dibike and Solomatine (2001), and have played a crucial role in identifying biodiversity hotspots, with Kirilenko and Hanley (2008) using them to forecast the spatial distribution of bumblebee species. They have also been employed to model complex ecosystem interactions, such as in the work of Mattei et al. (2018), where ANNs were used to simulate phytoplankton primary production.

Given their flexibility, learning capabilities, and predictive power, ANNs are increasingly utilized in environmental science as well. In sediment management, for instance, ANNs have been used to predict floc size distribution and assess sediment stability and erosion potential in estuarine environments, as demonstrated by Sahin et al. (2017) and Seo et al. (2020), making them a vital tool in addressing complex sediment-related challenges.

3.3. Study Locations and Key Parameters

In this study, data collected over a one-year period from November 2018 to December 2019 by the Ecosystem Management Research Group at the University of Antwerp are used. These data, distributed across the intertidal areas of the Scheldt Estuary, were gathered from three tidal flats: The Branst site, located in the freshwater tidal region approximately 105 km from the estuary's mouth; the Lillo site, situated in the mesohaline zone about 65 km from the mouth; and the Zuidgors site, located in the polyhaline zone around 20 km from the mouth (see Figure 3.3). These sites were selected to represent distinct characteristics along the estuary's salinity gradient.

Seasonal environmental fluctuations significantly influence the sediment distribution in the Scheldt estuary, affecting its ecological balance and the health of various aquatic species (Meire et al., 2005; Fettweis & Baeye, 2015). The estuary is experiencing notable changes in its sediment dynamics, particularly due to human influences such as dredging and urban development. These changes, evident in the increased concentrations of suspended particulate matter (SPM) and the early signs of the estuary transitioning to a hyperturbid state, present new challenges for estuary management (Winterwerp et al., 2013; Cox et al., 2019; Chen et al., 2005; Dijkstra et al., 2019). Understanding how these changes impact sediment deposition and erosion in intertidal zones is

essential for assessing their capacity to support diverse ecological functions and for informing conservation and management strategies.

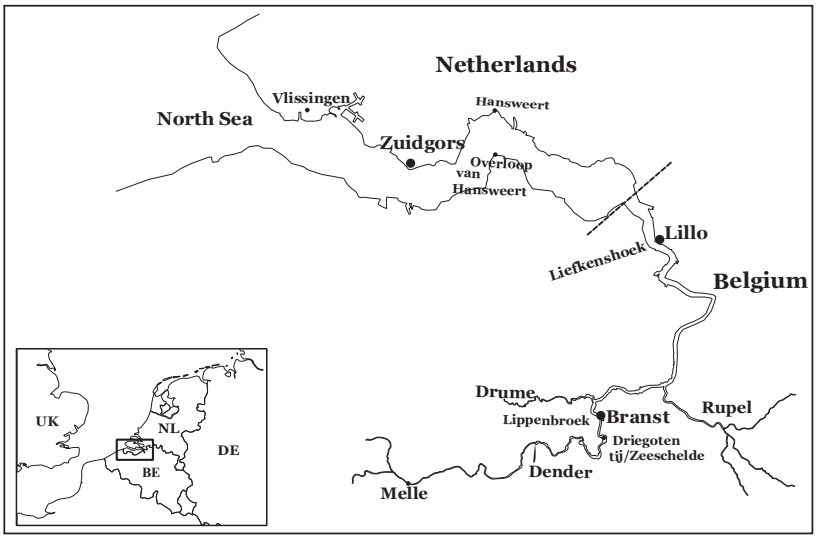

Figure 3.3: Map of the Scheldt Estuary showing the locations of the three intertidal monitoring sites. These sites were strategically selected to represent the estuary's natural salinity gradient and to capture spatial variability in sediment dynamics. Branst is located in the freshwater zone, Lillo in the mid-estuarine brackish zone, and Zuidgors near the mouth in the saline region. High-resolution data from these sites formed the input for the machine learning models developed in this study.

3.3.1. Methodology

This chapter aims to predict changes in bed levels and assess the effects of current and future intertidal areas on the equilibrium of suspended sediments in the Scheldt estuary, with a specific focus on the flocculation process and its significant impact on sediment deposition and coastal morphology. SPM concentration, turbulent shear, and current velocity influence the flocculation process, i.e., the aggregation of suspended particles (Dyer & Manning, 1999; Uncles et al., 2010; Schwarz et al., 2017). Furthermore, tidal variations affect the balance between sediment cohesion and dispersion, governing sediment transport and deposition (Winterwerp & van Kesteren, 2004; Manning & Dyer, 1999). To this end, this study incorporates tidal range data alongside other environmental parameters, such as hydrodynamics, SPM concentration, and mean floc size, to evaluate their combined influence on sediment transport and deposition in estuarine systems.

Building on the data presented in Chapter 2, this research utilizes Particle Size Distributions (PSDs) obtained from a Laser In-Situ Scattering and Transmissometry (LISST-200X) instrument

to determine the mean floc size (D50), following the Sequoia Scientific (2010) recommended method of averaging the midpoint of each bin. Hydrodynamic variables, such as current velocity, are extracted from an Acoustic Doppler Velocimeter (ADV), while the ADV's downward-facing orientation is used to measure the distance to the water-bed interface. The central variable for determining bed level changes is the distance from the seabed to the ADV probe (DSP), with an accuracy of ±1 mm (Pang et al., 2021). Shifts in DSP are indicative of changes in bed elevation. Tidal range data is obtained from tidal gauges at Driegoten tij/Zeeschelde for Branst, at Liefkenshoek for Lillo, and at Overflow van Hansweert for Zuidgors[1] (See Figure 3.3). Additionally, water turbidity is measured using an Optical Backscatter Sensor (OBS), and SPM concentrations are derived from a linear regression between OBS readings and laboratory-calibrated SPM data, addressing potential calibration errors due to physical, chemical, and thermal influences (Downing, 2006).

The methodology, described in detail in Chapter 2, includes an elaborate data cleaning process to ensure the validity of the measurements and the accuracy of subsequent analysis and modeling. This process involves removing outlier data points as specified by instrument manuals and despiking the remaining data. Moreover, the shear rate (G) is calculated to quantify the impact of turbulence on flocculation, using an equation that incorporates kinematic viscosity, turbulent dissipation rate, and shear velocity, as outlined by van Leussen (1994), Dyer and Manning (1999), and Safak et al. (2013).

For the prediction of bed level changes, RF and ANN models were employed using input features (or a subset of) mean floc size (D50), SPM concentration, turbulent shear rate (G), tidal range, current velocity, and season (Autumn, Winter, Spring, Summer). A unified dataset was constructed in Python to integrate all measured variables into a consistent analytical framework. Since the data were collected at varying frequencies, all variables were interpolated to a uniform one-minute resolution to ensure temporal alignment. Timestamps with missing values were excluded, and statistical outliers were removed to prevent skewed interpolation.

To promote stable learning, input features were normalized. This step is critical for ANN models, though not required for RF models, which use threshold-based splits; normalization was nonetheless applied uniformly across both for consistency. The output variable (bed level change) was retained in its original scale, as both models support continuous regression. This process yielded high-resolution datasets, with data point counts provided in Appendix 3.A.

[1] Available at https://www.waterinfo.be/ and https://waterinfo.rws.nl/

Once the data preparation was complete, the models were trained and evaluated across different experiments to assess sediment dynamics in the Scheldt's intertidal regions over seasons and locations.

- In the first experiment, both RF and ANN models were trained on the full dataset combining all sites and seasons. The aim was to assess whether the models could learn seasonal patterns implicitly—through variation in physical parameters—or whether including season explicitly as a one-hot encoded categorical input (i.e., converting the season into separate binary columns, each indicating whether a data point falls in spring, summer, autumn, or winter) would improve performance. In the case of RF, these binary indicators allow the model to split decision trees on season-specific behaviors if supported by the data. For the ANN, these inputs are integrated into the neural architecture as additional features, where the network can learn weighted interactions between season and the continuous physical drivers. Thus, the inclusion of season enables both models to learn not only implicit seasonal variation (reflected in changes to environmental variables over time) but also explicit seasonal effects, where specific patterns or thresholds may vary by calendar season. This dual representation ensures that both model types can capture potentially nonlinear seasonal effects on bed level change.
- The second experiment assessed the performance of season-specific models. Separate models were trained for each season, using data from all three stations, but restricted to the corresponding seasonal subset. This enabled evaluation of how well RF and ANN models could learn sediment dynamics specific to a particular seasonal regime, without relying on cross-seasonal generalization.
- Finally, in the third experiment, separate models were trained for each station, using data from all seasons, to assess the ability of both RF and ANN models to learn site-specific sediment dynamics and capture interactions between environmental drivers and seasonal context. To enable this, an additional categorical input variable representing season was included, encoded using one-hot encoding. Both RF and ANN models were trained using these season-encoded inputs alongside physical variables such as tidal range, current velocity, SPM concentration, shear rate (G), and mean floc size (D50).

Although the total number of one-minute records varied across datasets, this procedure—comprising one-minute interpolation, multi-variable merging, outlier removal, dataset partitioning, and feature normalization—was applied consistently across all four datasets used in this chapter (Datasets 3.A.1 through 3.A.4). Regardless of whether the experiment involved all stations combined (e.g., in Dataset 3.A.1), seasonally encoded data (Dataset 3.A.2), single-season

subsets (Dataset 3.A.3), or site-specific cases (Dataset 3.A.4), the 70% training and 30% testing split was maintained. The training portion was used to fit the model, while the test set was completely withheld and used exclusively for performance evaluation on unseen data. Within the training subset, a further 30% was internally allocated for model tuning—via OOB validation in the case of RF and early stopping in ANN. For instance, in the Zuidgors dataset, ~280,000 rows were used for training, ~120,000 for testing, and approximately 84,000 of the training rows were reserved for validation.

This consistent preparation and evaluation framework ensures methodological comparability across models and experiments. As a result, the performance metrics reported in Tables 3.1 to 3.4 reflect evaluation on entirely unseen data, supporting robust and reproducible model assessment.

3.4. Results

This section evaluates the performance of the models and present the results for each scenario, starting with temporal insights and progressing to spatial insights.

3.4.1. Model Performances

3.4.1.1. RF Model Performance

[I] Hyperparameter Tuning and OOB–Tree Count Chart

In optimizing the RF model structure before training, a key step is determining the ideal number of decision trees. This 'hyperparameter tuning' is conducted to assess the performance of the model with varying tree counts and choose the ideal number. As mentioned previously, a crucial goal of this tuning is to avoid overfitting, where the model performs well on training data but poorly on unseen data. To conduct this tuning efficiently, a 30% subset of the training data was used, derived from Dataset 3.A.1 (see Appendix 3.A). Dataset 3.A.1 includes the full dataset combining all stations and all seasons. Of this, 70% was allocated for training and 30% was held out for final testing. From within the training portion, a random 30% subset was used to evaluate how the model's performance changed with different numbers of trees.

For each tree count, the model was trained and evaluated using the OOB error rate, an internal validation method that estimates prediction error using samples not included in each individual tree. As shown in Figure 3.4, the OOB error decreases steeply as the number of trees increases from 10 to about 50. Beyond 50 trees, however, the error curve begins to flatten, a clear plateau indicating diminishing returns, where adding more trees does not substantially improve accuracy.

Based on this trend, 50 trees were selected as the optimal number for the final model. This choice ensures a strong balance between model performance and computational cost, while minimizing the risk of overfitting.

[II] Model Performance Metrics

The Random Forest model exhibits high predictive accuracy, as evidenced by test-set R^2 values above 0.95 across most seasons and sites. This high R^2 value indicates that the model accounts for about 95% of the variability in bed level change. Error metrics further confirm the model's precision, with low MAE values ranging from 0.10 to 0.91 and MSE values between 0.34 and 7.98 (Table 3.1). These metrics underscore the model's ability to produce accurate predictions with minimal errors, demonstrating its reliability in capturing complex dependencies in bed level change across varied spatial and temporal contexts.

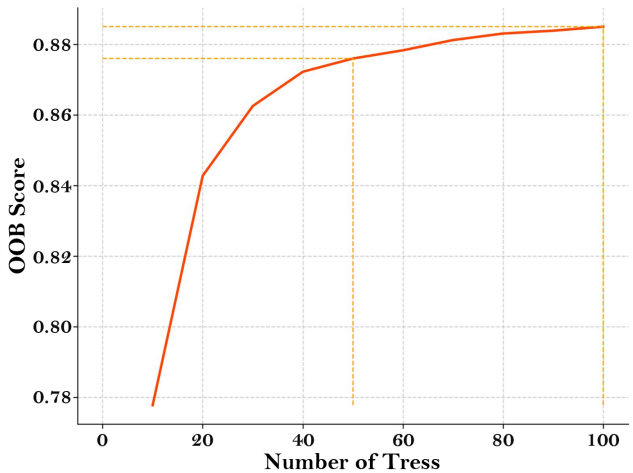

Figure 3.4: The OOB score as a function of number of trees in the Random Forest regressor. The figure illustrates the effect of increasing the number of trees on model performance. Each point represents a model trained with a specific number of trees, and evaluated using the OOB error estimate. The curve initially shows a steep decline in error, indicating rapid performance improvement, followed by a gradual plateau—suggesting diminishing returns beyond a certain tree count. The discrete nature of the curve reflects the evaluation of performance at selected tree values rather than over a continuous parameter range.

Table 3.1: Summary of predictive performance for RF and ANN models. The table lists key model configurations—number of trees for RF, and epochs for ANN—along with their respective test dataset performance metrics (R^2, MAE, MSE). The RF model consistently shows higher predictive accuracy, and lower prediction errors compared to the ANN model across the studied dataset. All metrics represent results from the independent test dataset (30% of total data), withheld entirely during model training.

RF Model	ANN Model
Number of trees: 50	Number of epochs: 50
R2 > 0.95	R2: 0.65 ~ 0.90
MAE: 0.10 ~ 0.91	MAE: 2.18 ~8.77
MSE: 0.34 ~ 7.98	MSE: 13.80 ~ 174.22

3.4.1.2. ANN Model Performance

[I] Hyperparameter tuning and Loss-Epoch Chart

Optimizing the ANN model involves careful tuning of hyperparameters, particularly the number of training epochs. The epoch count refers to the number of full passes through the training dataset and plays a critical role in balancing underfitting (insufficient learning) and overfitting (memorizing patterns without generalizing). To determine a suitable epoch limit, ANN models were tested with varying epoch counts and model performance was monitored using the MSE loss curve.

As with the RF model, this tuning was performed using a 30% subset of the 70% training portion of Dataset 3.A.1 (Appendix 3.A). As shown in Figure 3.5, the loss declines steeply within the first 30 epochs, indicating rapid learning. After approximately 50 epochs, the curve begins to plateau, showing only marginal improvement with continued training. This inflection point represents diminishing returns, where further training adds computational cost without significantly improving model accuracy. Based on this behavior, the training limit was set at 50 epochs, which was applied consistently across all ANN experiments to ensure performance stability and computational efficiency.

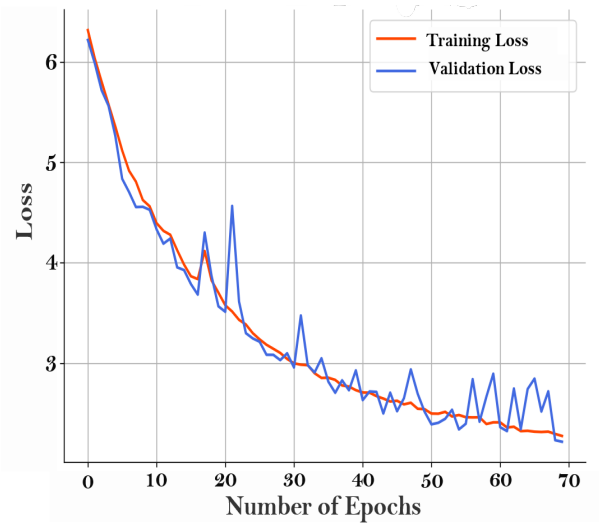

Figure 3.5: Loss minimization over epochs in ANN training. The MSE loss decreased rapidly during the initial epochs and plateaued after approximately 50 epochs. Training was limited to 50 epochs to avoid overfitting and optimize computational efficiency.

In addition to optimizing epochs, experiments were conducted with various numbers of layers and nodes in each layer of the ANN model, which dictate the model architecture. Through a manual process of trial and error, an optimal network architecture was identified (Figure 3.6). The MSE loss function and ReLU activation function were also selected. Given the similar nature and scale of the dataset across all experiments, the architecture was kept constant to enable better comparisons.

[II] Model Performance Metrics

Across various seasonal and spatial contexts, the ANN model exhibits test-set R^2 values ranging from 0.65 to 0.90, indicating varying degrees of predictive accuracy (Table 3.1). The MAE values range from 2.18 to 8.77, while the MSE values range from 13.80 to 174.22, reflecting the model's ability to predict with varying error margins. Although the ANN model shows reasonable predictive capabilities, its performance is generally lower than that of the RF model.

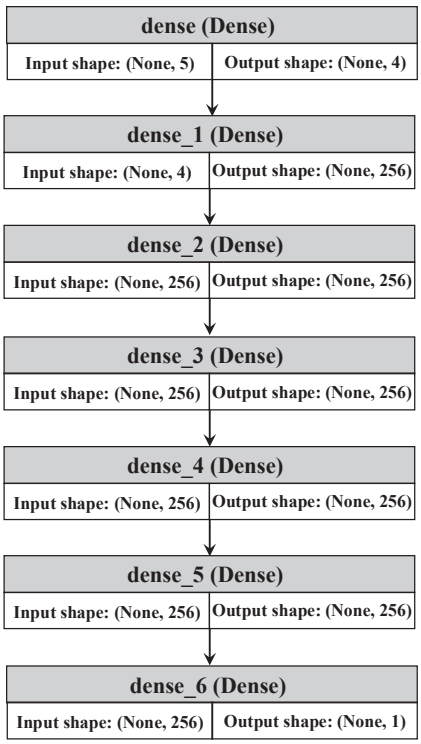

Figure 3.6. The ANN model architecture is displayed. The notation (None, x) indicates the batch size for training and the size of each layer. A specific batch size is not set, reflected by 'None', allowing flexibility in the number of data chunks processed in each training round. The model's architecture includes an input layer with 4 features and 5 subsequent layers, each consisting of 256 nodes. The output layer is composed of a single node, intended for predicting a singular (regression) value. 'Dense' in this neural network context refers to a fully connected layer type, where every node in one layer is connected to all nodes in the adjacent layers, enabling intricate pattern recognition and data processing.

3.4.2. Temporal Insights From Predictive Analysis

3.4.2.1. RF Temporal Insights

To extract temporal insights from the predictive analysis, model performance was compared in non-seasonal and seasonal contexts using Random Forest models trained on Dataset 3.A.1 (without season as a feature) and Dataset 3.A.2 (with season encoded), respectively (Appendix 3.A). In both cases, 70% of the data was used for training, and 30% was withheld for testing. As shown in Table 3.2 and Figure 3.7, the feature importance values were derived from the training set (based on Random Forest's internal structure), while all performance metrics (R^2, MAE, MSE) reflect the model's accuracy on the independent test set.

In both models, tidal range emerges as the most influential factor, underscoring its dominant role in sediment dynamics. Beyond tidal range, the significance of other variables varies slightly. In the non-seasonal model, SPM concentration and turbulent G have nearly equal importance, underscoring their considerable impact when seasonality is not considered. In contrast, the seasonal model shows that mean floc size becomes the next most influential variable, suggesting that particle characteristics gain more relevance when seasonal variations are considered. The inclusion of season as a feature also improved model accuracy on the test set: the MAE dropped from 0.91 to 0.32, and the MSE dropped from 7.98 to 2.33, reflecting more precise predictions in the seasonal model.

Table 3.2: Comparative performance and feature importance of RF models with and without "season" as an input variable. The table presents the test-set predictive performance (R^2, MAE, MSE) of two RF models evaluated on the independent test dataset. Both models used the same input variables—tidal range, current velocity, shear rate (G), SPM concentration, and mean floc size—but only the second model included "season" as an additional feature. Feature importance scores (normalized to sum to 1) were calculated from the training phase and reflect each variable's relative contribution to predicting bed level change. Including season improves prediction accuracy and slightly shifts the weighting of other variables, highlighting the influence of seasonal dynamics on estuarine sediment transport.

Model type	Tidal range	SPM concentration	Mean floc size	Turbulent shear rate G	Current velocity	R^2	MAE	MSE
Non-Seasonal	0.34	0.19	0.17	0.19	0.10	0.98	0.91	7.98
Seasonal	0.38	0.14	0.15	0.14	0.06	0.99	0.32	2.33

Moreover, the results of the season-specific RF models for predicting bed level change are shown in Figure 3.8 and Table 3.3. These models were trained separately for Autumn, Winter, Spring, and Summer using Dataset 3.A.3, which contains season-filtered observations from all stations (Appendix 3.A). Each model was trained on 70% of the relevant seasonal data and evaluated on the remaining 30% test set, enabling assessment of seasonal prediction accuracy under real-world data conditions. The RF models demonstrated strong test-set performance, with R^2 values ranging from 0.97 to 0.99 across all seasons—indicating excellent predictive power in capturing sedimentation and erosion dynamics. Feature importance values, computed during training, consistently highlight tidal range as the dominant driver across all seasons. However, the relative importance of other variables shifts seasonally: turbulent shear rate (G) is particularly influential in autumn, winter, and spring, while mean floc size gains more weight in spring and summer, suggesting seasonal changes in sediment aggregation behavior.

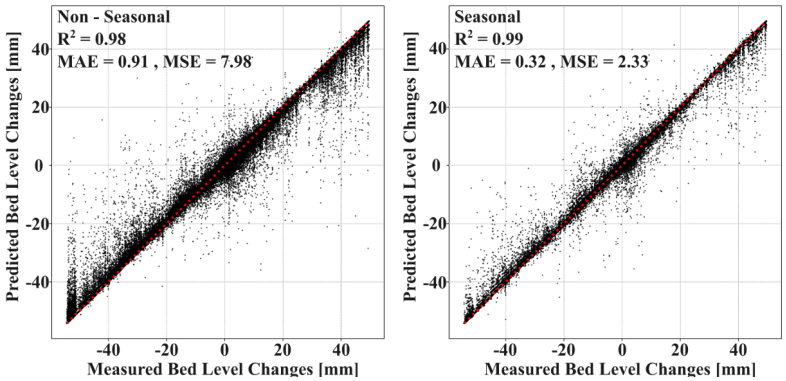

Figure 3.7: Comparative analysis of seasonal and non-seasonal RF models for bed level change prediction. The comparison is based on independent test-set performance, with R², MAE, and MSE values calculated consistently for both models. Both models used the same core set of input variables—tidal range, current velocity, shear rate (G), SPM concentration, and floc size (D50). The seasonal model included "season" as an additional input variable, encoded categorically. Including season improved predictive accuracy, indicating that temporal patterns influence sediment behavior and are better captured when season is explicitly incorporated into the model.

Error metrics reinforce these findings. The MAE values—which reflect average absolute prediction error on the test set—are low overall, with the best result in autumn (0.10). The MSE values, which penalize large deviations more heavily, remain within acceptable ranges, though the highest is observed in summer (1.42), likely due to a few high-error outliers. Despite this slight decrease in summer performance, all models exhibit robust seasonal accuracy and capture key hydrodynamic and sedimentary processes effectively.

Table 3.3: Test-set performance metrics and feature importance of RF models trained separately for each season. This table presents the test-set results (R², MAE, MSE) and feature importance values for Random Forest models trained and evaluated using data from individual seasons (autumn, winter, spring, summer). Feature importance scores (normalized to sum to 1) were computed during the training phase and reflect the relative contribution of each variable to predicting bed level change within each season.

Season	Tidal range	SPM concentration	Mean floc size	Turbulent shear rate G	Current velocity	R²	MAE	MSE
Autumn	0.41	0.16	0.15	0.21	0.07	0.97	0.10	0.34
Winter	0.41	0.16	0.16	0.20	0.07	0.98	0.18	0.72
Spring	0.39	0.15	0.18	0.18	0.10	0.99	0.13	0.7
Summer	0.46	0.17	0.23	0.11	0.03	0.99	0.14	1.42

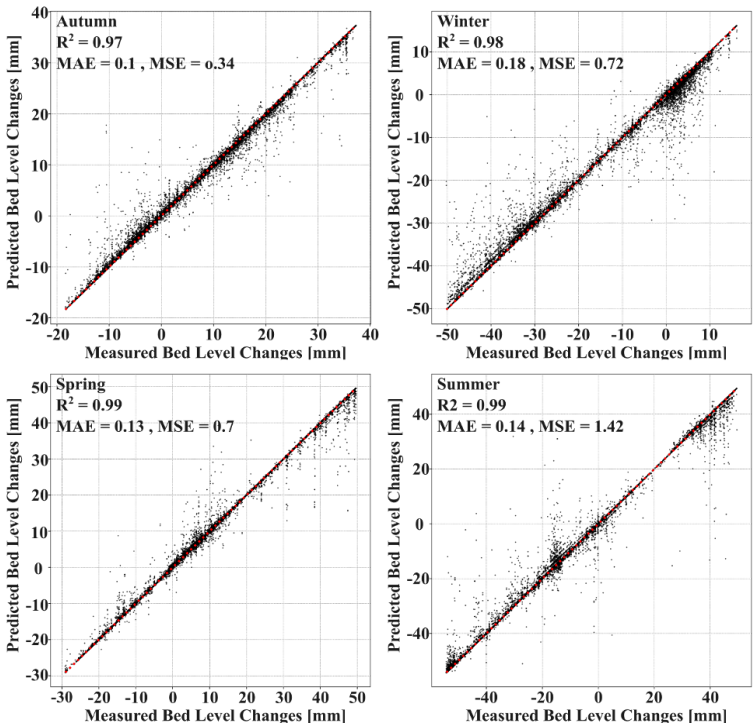

Figure 3.8: Comparative analysis of RF models across different seasons for bed level change prediction. The R², MAE, and MSE metrics shown here reflect the predictive accuracy of each model on its respective season's test data. Differences in performance across seasons highlight how sediment transport dynamics—and the model's ability to learn them—vary throughout the seasons.

3.4.2.2. ANN Temporal Insights

To replicate the approach used with the RF model, the influence of seasonality on bed level change prediction was also evaluated using Artificial Neural Network (ANN) models. Two versions of the model were trained using Dataset 3.A.1 (non-seasonal) and Dataset 3.A.2 (seasonal) as described in Appendix 3.A. Each dataset was split into 70% for training and 30% for testing, and model performance was evaluated using the test set only. Both ANN models demonstrated moderate accuracy. The non-seasonal model achieved a test-set R^2 value of 0.65, while the seasonal model improved this to 0.79, indicating better predictive ability when seasonality is included (Figure 3.9). The improvement is also reflected in the error metrics: the MAE decreased from 8.77 to 2.18, and the MSE dropped from 174.22 to 93.60, showing enhanced accuracy and reduced variance in prediction error. These results highlight the benefits of incorporating seasonal factors for enhanced predictive accuracy.

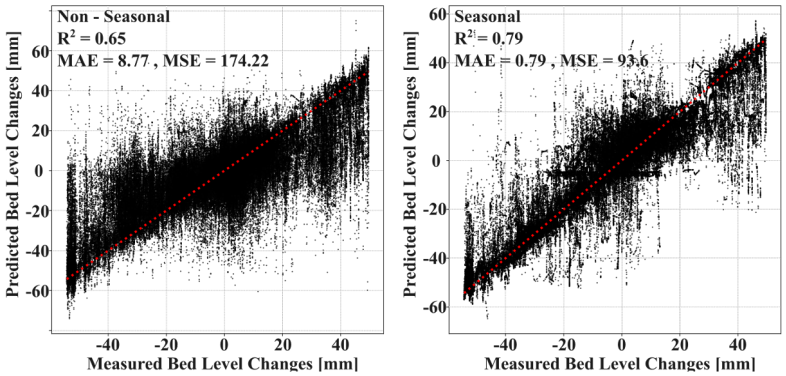

Figure 3.9: Comparative analysis of seasonal and non-seasonal ANN models for bed level change prediction. The comparison is based on testing set performance, with R², MAE, and MSE values evaluated consistently across both model types. While both models used the same physical inputs (tidal range, velocity, shear rate G, SPM, and floc size), the seasonal model achieved higher accuracy, suggesting that including season as a feature helps the model better capture seasonal differences in sediment behavior.

To evaluate the performance of the ANN in predicting bed level change, and following the approach used with the RF model, four separate models were trained using season-specific data from Dataset 3.A.3, which includes measurements for Autumn, Winter, Spring, and Summer across all stations (Appendix 3.A). Each seasonal dataset was split into 70% for training and 30% for testing, and all performance metrics reported here are based on the test set only.

Across the seasons, the ANN model demonstrated strong predictive accuracy across all seasons, with some seasonal variability (Figure 3.10). Spring yielded the best overall performance, with an R^2 of 0.88, MAE of 2.18, and MSE of 20.13, indicating highly precise predictions and low average error. Summer achieved the highest R^2 value (0.90), but also recorded the largest prediction errors (MAE: 3.33, MSE: 50.76), suggesting greater variability or presence of outliers. Autumn and Winter both delivered stable results, with R^2 values of 0.82 and 0.84, and moderate error metrics, reflecting consistent yet slightly less precise predictions than Spring. Overall, the ANN models effectively captured seasonal sediment dynamics, with Spring standing out as the most predictable season in terms of both accuracy and error minimization.

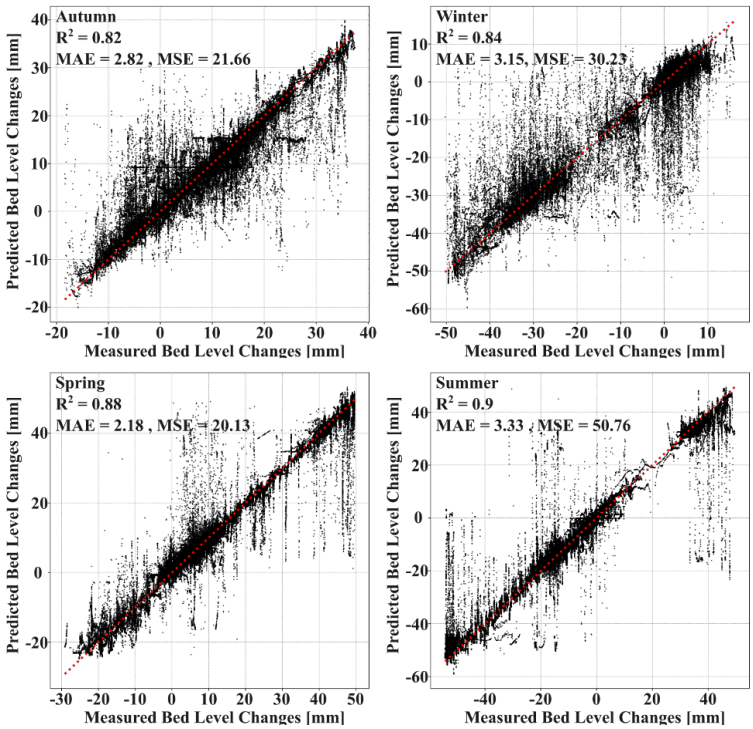

Figure 3.10. Comparative analysis of ANN models across different seasons for bed level change prediction. The R², MAE, and MSE values shown reflect model performance on the respective season's test data. Differences in accuracy between seasons illustrate how seasonal variability influences sediment transport behavior and the model's learning capacity under different environmental conditions.

3.4.3. Spatial Insights From Predictive Analysis

3.4.3.1. RF Spatial Insights

The Random Forest model was evaluated across three distinct intertidal sites in the Scheldt Estuary. Three site-specific models were trained using data from Dataset 3.A.4, which contains seasonally distributed measurements for Branst, Lillo, and Zuidgors (Appendix 3.A). Each dataset was split into 70% for training and 30% for testing, and feature importance scores were derived from the training phase, while performance was evaluated on the independent test set.

As shown in Table 3.4 and Figure 3.11, tidal range consistently emerged as the most important predictor across all sites, reflecting its dominant influence on bed level changes. Mean floc size also contributed substantially at each location. Interestingly, at Zuidgors, SPM concentration showed a noticeably higher relative importance (22%), suggesting that suspended sediment loads

play a more critical role in sediment dynamics at this marine-dominated site compared to Branst or Lillo. These differences highlight how local sediment behavior can influence model sensitivity to input features.

Table 3.4: Test-set performance and feature importance of RF models trained for each monitoring site (Branst, Lillo, Zuidgors). Each site-specific model was trained using six input variables: tidal range, current velocity, shear rate (G), SPM concentration, floc size (D50), and season (one-hot encoded). Performance metrics (R^2, MAE, MSE) reflect results on the independent test set (30% of each dataset). Feature importance values, derived from training, indicate each variable's contribution to bed level prediction. The table also shows the seasonal data composition per site, highlighting spatial and temporal variation in sediment dynamics.

Location	Tidal range	SPM concentration	Mean floc size	Turbulent shear rate G	Current velocity	Seasons				R^2	MAE	MSE
						Autumn	Spring	Summer	Winter			
Branst	0.41	0.17	0.18	0.16	0.08	0.01	0.03	0.01	0.01	0.99	0.47	5.84
Lillo	0.34	0.17	0.27	0.13	0.10	0.02	0.01	0.01	0.01	0.99	0.17	0.58
Zuidgors	0.33	0.22	0.3	0.11	0.05	0.02	0.02	0.02	0.02	0.98	0.48	5.76

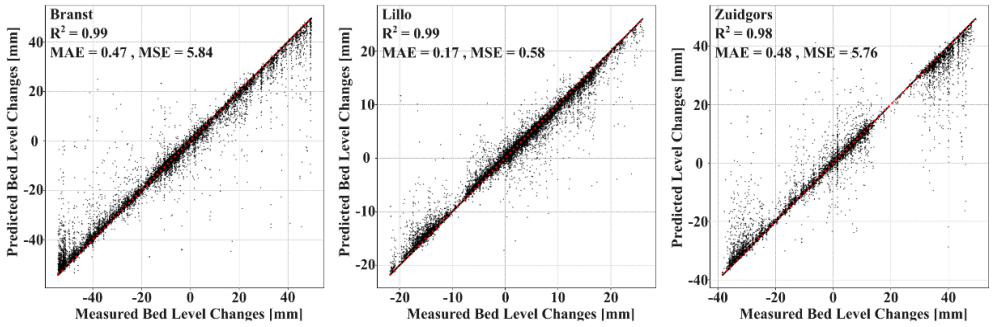

Figure 3.11: Comparative analysis of site-specific RF models for bed level change prediction. The R^2, MAE, and MSE values shown reflect predictive performance on the test data for each location. Differences in accuracy highlight the impact of site-specific environmental conditions on sediment dynamics and model learning, with greater variability at more dynamic sites like Zuidgors.

Although seasonal variation had a relatively minor effect on overall model accuracy, subtle performance differences were observed between sites. All three site-specific RF models demonstrated strong test-set performance, but error metrics varied. The model achieved its lowest errors at Lillo, with an MAE of 0.17 and MSE of 0.58, indicating high precision in this brackish zone. In contrast, Branst (freshwater) and Zuidgors (saline) exhibited higher error values,

suggesting that the model faced greater complexity or variability in those environments—likely due to differences in sediment behavior, tidal asymmetry, or input data heterogeneity.

3.4.3.2. ANN Spatial Insights

As with the RF model, three separate ANN models were trained using site-specific data from Dataset 3.A.4, which includes measurements for Branst, Lillo, and Zuidgors (Appendix 3.A). Each model was evaluated on a 30% independent test set, and the results are summarized in Figure 3.12. At Branst, the ANN achieved the highest test-set accuracy with an R^2 of 0.90, accompanied by moderate error rates (MAE: 5.02, MSE: 76.51). At Lillo, the R^2 decreased slightly to 0.84, but the model showed greater precision with lower errors (MAE: 2.34, MSE: 13.80). At Zuidgors, performance declined further, with an R^2 of 0.76, MAE of 7.02, and MSE of 138.95, suggesting higher variability or reduced model fit in this saline, more dynamic site. These results highlight how model performance varies with site-specific environmental conditions, particularly as sediment dynamics and input variability differ along the estuarine gradient.

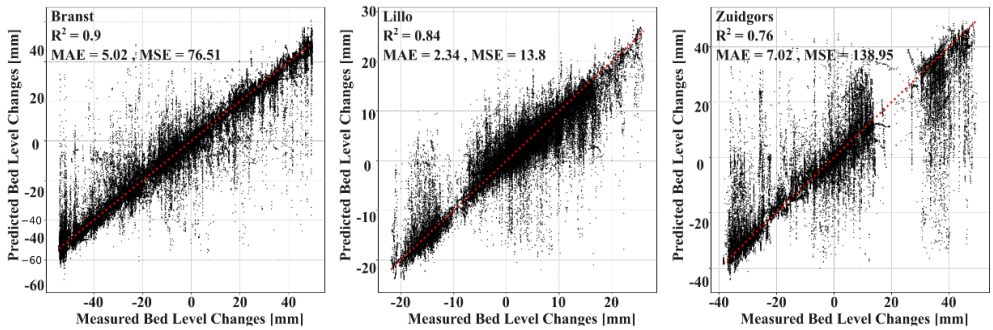

Figure 3.12: Comparative analysis of site-specific ANN models for bed level change prediction. The R^2, MAE, and MSE values reflect model accuracy on the unseen test data for each station. The variation in performance across sites illustrates how local hydrodynamic conditions and sediment characteristics influence model predictability in estuarine environments.

3.5. Discussion

The optimal number of decision trees in the RF model was selected to balance predictive accuracy with computational efficiency, following guidance from Deng et al. (2013). A plateau in the OOB error curve was observed beyond 50 trees, indicating diminishing returns in accuracy. This plateau suggested 50 as the most effective number of trees, aligning with the findings of Liaw and Wiener (2002). Beyond accuracy, computational efficiency is relevant from an environmental standpoint.

Extending training time for marginal performance gains increases electricity consumption without proportional benefit. Therefore, selecting 50 trees helped achieve a practical balance between model performance and resource use.

The RF model demonstrated consistently high predictive performance on the independent test dataset, with R^2 values exceeding 0.95 across most sites and seasons. Low MAE and MSE further confirmed the model's robustness. While R^2 values this high could raise concerns about overfitting in many machine learning contexts, it is important to emphasize that these results come exclusively from the test set, not the training data.

Nonetheless, the structure of the data introduces a known limitation. Because all input variables were interpolated to a uniform 1-minute resolution, observations are not statistically independent—values at time T are often similar to those at T+1. This temporal autocorrelation may contribute to slightly higher accuracy, as the model learns from subtle temporal patterns. To mitigate this, the training dataset covered multiple seasons and full tidal cycles, introducing a wide range of environmental variability. Still, future studies should apply time-aware validation or rolling test windows to more rigorously evaluate generalization in high-resolution time series.

In contrast, the ANN model did not reach the same performance levels. ANN predictive power is strongly influenced by hyperparameter tuning, particularly the number of training epochs (Prechelt, 1998). The loss curve showed diminishing returns beyond 50 epochs, after which further training did not significantly reduce error and risked overfitting. This choice aligns with findings by Goodfellow et al. (2016), which advocate for training duration that balances performance and computational efficiency. The ANN architecture was fixed during the tuning stage to enable consistent comparisons. The final design included five layers with 256 nodes each, which proved most effective during preliminary experimentation. Using a consistent structure ensured comparability across sites and seasons. Model evaluation followed a 70/30 train-test split, and k-fold cross-validation was applied to improve generalizability and reduce random variance, following standard practices (Kohavi, 1995; Rodriguez et al., 2009).

Although the ANN model provided reasonably accurate predictions, the RF model outperformed it across nearly all evaluation metrics. This superior performance reflects the synergy between RF's strengths and the characteristics of the environmental dataset, including its variability, non-linearity, and noise. More concretely, the following points outline the synergy between the dataset characteristics and the strengths of RFs:

1. **Complex interactions and non-linearity:** Random Forests excel at capturing the non-linear interactions between variables such as SPM, mean floc size, and velocity. While ANNs

are also highly capable of handling nonlinearity, they require significantly more data and fine-tuning to achieve this advantage, whereas RFs provide it more readily and consistently.

2. **Variability and noise:** The inherent noise and variability in environmental data are very effectively managed by Random Forests through their averaging approach across multiple decision trees.

3. **Heterogeneity of data sources:** Random Forests can better handle data inconsistencies arising from different measurement techniques and devices, as they build multiple trees based on varied data subsets. This was the case in the present study and is a common challenge across environmental modeling projects where multiple measurement devices are employed.

4. **Feature relevance and redundancy:** Random Forests automatically identify and prioritize the most relevant features for predicting bed level changes, efficiently dealing with potential redundancies in the dataset. While ANNs can do the same, it would take much more data for them to dynamically learn to use a feature less. The nuance here is the fact that given a new river system or a new intertidal dynamic, the balance between feature importance may change, and thus, the agility to conform to the changing dynamic is important.

Despite RF's strong performance in this study, its generalizability across ecosystems or longer timeframes still needs to be verified. Future work could test RF models on data from the same sites one year after initial sampling or from comparable but distinct estuarine systems. This would help validate the model's broader applicability.

3.5.1. Assessing the Predictive Power Over Temporal Variations

Investigating the impact of seasonality on predicting bed level changes, both RF and ANN models provide valuable insights. The assessment includes models trained with and without seasonal information, as well as season-specific models trained on individual subsets. In the baseline (non-seasonal) RF model, trained without explicit seasonal input using Dataset 3.A.1, tidal range emerged as the most important predictor of bed level change. This is consistent with prior studies emphasizing the critical role of tidal processes in estuarine sediment transport (Dyer, 1988; Fettweis & Van den Eynde, 2003; Baeye et al., 2011; Vanlede et al., 2015). The high R^2 and low error metrics on the test set align with earlier findings linking hydrodynamic drivers to sediment behavior (Winterwerp, 1998; Fettweis et al., 2006; Winterwerp et al., 2012).

Moreover, to examine the role of temporal variability more directly, seasonality was added as a categorical input using one-hot encoding in the extended RF model (Dataset 3.A.2). Including season slightly improved the model's predictive accuracy, with notable decreases in both MAE and MSE. Although the 'season' variable itself ranked low in feature importance, this likely reflects the model's ability to infer seasonal patterns from correlated variables such as SPM, velocity, and shear rate. These findings align with studies emphasizing the importance of accounting for seasonality in sediment transport modeling (Downing-Kunz & Schoellhamer, 2013; Horemans et al., 2020).

To isolate seasonal effects further, separate RF models were trained for each season using Dataset 3.A.3, excluding season as a feature. These models revealed that RF performance remained high across seasons, with consistently strong test R^2 values and low error rates. Tidal range remained the dominant predictor, while the relative importance of other variables varied seasonally. Shear rate (G) was particularly important in autumn, winter, and spring, reflecting increased resuspension under energetic flow conditions (Dyer & Manning, 1999; Winterwerp & van Kesteren, 2004). In contrast, mean floc size gained importance in spring and summer, corresponding to periods of stronger biological activity and particle aggregation (Passow, 2002; Fettweis et al., 2014; Verney et al., 2006; Maggi, 2009).

These results confirm the RF model's ability to capture both direct and indirect manifestations of seasonal variability. They also highlight its generalizability across seasons, suggesting that a model trained on multi-season data can robustly predict bed level changes under varied environmental conditions. This is particularly valuable for estuarine management, where efficient modeling is needed without exhaustive per-season retraining.

In comparison, the ANN model showed moderate performance in the non-seasonal case, with a test-set R^2 of 0.65. This indicates some predictive ability but notably lower accuracy than RF. The inclusion of season as a categorical feature in the ANN model (using Dataset 3.A.2) improved performance to an R^2 of 0.79 and reduced error metrics, confirming that ANN models benefit more from explicit temporal structuring. This is consistent with known ANN behavior: these models require more data and structured inputs to capture non-linear interactions effectively (Ouellet-Proulx et al., 2016; Zounemat-Kermani et al., 2020; Kisi & Yaseen, 2019; Francke et al., 2008). The ANN model's stronger response to season inclusion likely stems from the way categorical features help organize learning across time-dependent patterns, which might otherwise be difficult to extract from continuous variables alone. Season can serve as a proxy for underlying biological or physical changes not directly measured, such as EPS production or productivity cycles (Goodfellow et al., 2016; Cox et al., 2019).

To further explore seasonal dynamics, season-specific ANN models were trained using Dataset 3.A.3 (with no season variable). These models varied in performance, reflecting the complexity of environmental drivers across seasons. Spring yielded the best balance of accuracy and precision while summer showed the highest R^2 (0.90) but also the largest errors. This suggests the presence of stronger deviations or outliers in summer data—likely driven by elevated biological activity and dynamic floc behavior (Fettweis et al., 2022).

Together, these findings underscore the central role of seasonality in sediment dynamics and confirm that both RF and ANN models benefit from incorporating seasonal variation—either explicitly as a feature or implicitly through correlated physical drivers. RF models remain more data-efficient and robust across variable conditions, while ANN models require more structured inputs and careful tuning to match performance. The ability of both models to reflect seasonal trends aligns with broader ecological understanding and supports the use of ML in estuarine sediment forecasting.

3.5.2. Assessing the Predictive Power Over Spatial Variations

Both the RF and ANN models demonstrated strong performance across all monitoring sites, though accuracy varied depending on local environmental dynamics. At Lillo, model performance was consistently high. This brackish zone features a relatively stable hydrodynamic regime across seasons and exhibits a predictable coarsening of particle sizes during high SPM periods. Such conditions enhance model predictability. Maris et al. (2024) observed a slower rate of change in SPM concentrations at Lillo, supporting its classification as a low-variability zone—making it easier to model than more dynamic freshwater or saline areas.

In contrast, Branst exhibited more variability in sediment behavior, particularly linked to river discharge and seasonal flow patterns. The models captured this variability but with slightly reduced accuracy compared to Lillo. Zuidgors, by contrast, posed the greatest modeling challenge. High tidal energy and salinity introduced substantial turbulence, reducing model precision. These site-specific complexities are well documented in previous estuarine research (Dyer & Manning, 1999; Horemans et al., 2021; Eisma et al., 1980; Verney et al., 2009).

To improve model performance and more accurately capture the dynamics at these locations, the incorporation of additional parameters—such as seasonal biological influences, turbulent energy, and wave action—may be necessary to enhance model learning. These factors could help establish clearer trends and relationships between sedimentation, resuspension, and local environmental

forces as noted in Winterwerp & van Kesteren, 2004; Fettweis et al., 2014, providing deeper insight into the site-specific sediment dynamics across the estuary.

It is also important to note that in both RF and ANN models, season was included as a categorical input in the station-specific experiments. This allowed the models to conceptually integrate site-specific hydrodynamic behavior with seasonal variability, enhancing their ability to reflect underlying environmental dynamics even without explicit mechanistic programming. Even when season itself did not rank among the top features in RF importance scores, its inclusion improved performance by providing context for how continuous variables behave over time. In ANN models, in particular, season labels likely helped structure hidden-layer learning around recognizable environmental states, thereby improving accuracy in sites with higher variability. This strengthens the interpretation that season acts as a contextual layer that enhances spatial predictions by implicitly guiding model sensitivity to site-season interactions.

The RF model also provided consistent results across all sites in terms of feature importance. Tidal range consistently emerged as the most influential factor, playing a critical role in driving sediment transport dynamics throughout the estuary (Meire et al., 2021; Jiang et al., 2020). This finding aligns with historical observations that the tidal range has been increasing over time (Coen, 2008; Vandenbruwaene et al., 2020), with recent data further highlighting a rise in high water levels along the estuary (Barneveld et al., 2018). These tidal dynamics directly influence sediment transport, emphasizing the critical role of tidal forces in shaping bed level changes under both current and future sea-level rise conditions.

Following tidal range, mean floc size made notable contributions at all stations, highlighting the importance of particle aggregation processes in influencing sedimentation and resuspension (Chen et al., 2005; de Lucas Pardo et al., 2015). Floc size plays a key role in determining how particles settle and stabilize on the bed, as larger flocs are more effective at resisting resuspension during tidal fluctuations (Winterwerp & van Kesteren, 2004; Fettweis et al., 2014).

At Zuidgors, however, in addition to the above factors, SPM concentration also played a key role, further influencing sediment dynamics. This suggests that in saline environments, enhanced tidal energy and turbulence can break apart flocs, leading to increased sediment resuspension and higher SPM concentrations in the water column (Dyer & Manning, 1999; Nguyen Van Manh et al., 2015; Manh et al., 2014). These findings emphasize the complex interaction between salinity, tidal energy, and floc stability, with increased turbulence resulting in reduced floc cohesion and a greater tendency for sediment resuspension, thereby affecting sediment transport dynamics in saline zones (Fettweis et al., 2014; Passow, 2002). The relationships were effectively captured by the RF model, resulting in strong predictive accuracy across all zones.

Furthermore, as demonstrated in temporal experiments, it is encouraging that the RF model trained on all stations performed comparably to station-specific models, indicating a strong capacity for spatial generalization. This suggests that the model is not merely capturing local anomalies but is instead learning core physical processes that govern sediment transport across estuarine zones. One such process is the behavior associated with the Maximum Turbidity Zone (MTZ)—a dynamic region of elevated SPM concentrations formed through the interaction of tidal asymmetry, salinity gradients, flocculation, and estuarine circulation (Burchard & Baumert, 1998; Uncles et al., 2002). Although the MTZ was not explicitly modeled in the present study, its influence is inherently embedded in the behavior of key input variables such as SPM concentration, floc size (D50), shear rate (G), and current velocity. These variables collectively encode the processes that drive MTZ formation and variability, and also govern sedimentation and erosion dynamics—the primary focus of this research. This highlights the potential of data-driven modeling frameworks to capture emergent estuarine features through physically interpretable inputs, offering transferability to other systems with comparable sediment transport regimes.

3.5.3. Comparing RF and ANN Methods for Sediment Modeling

Evaluating Random Forests and ANN as predictive models for bed level changes in the Scheldt Estuary highlights their distinct strengths. Both models effectively capture seasonal and spatial variations, providing insights into the influence of seasonality and location on sediment dynamics. When adjusted for seasonal factors, Random Forest demonstrates superior predictive performance, excelling in capturing sediment transport dynamics and identifying key drivers such as tidal range, SPM concentration, and floc size. Similarly, ANN shows significant improvement with the inclusion of seasonal data, enhancing its predictive capabilities. Both RF and ANN perform well in spatial analysis, accurately modeling sedimentation across diverse intertidal zones. However, ANN's accuracy varies across different environments. This advanced modeling approach is crucial for estuarine management and policy development, particularly in addressing climate change. Studies by Kirwan and Megonigal (2013) and Temmerman et al. (2013) underscore the importance of these advancements for sustainable management and ecological preservation. Comparing the models in characteristics and performance, as outlined in Table 3.5, highlights their specific strengths and applications.

Table 3.5: Comparison between RF and ANN models across several criteria. R^2 values represent test set performance. Training times are based on Dataset 3.A.1 (~2 million rows) and averaged over three runs. Interpretability, tuning effort, and robustness were assessed qualitatively based on model behavior across all scenarios

Aspect	Random Forest	Artificial Neural Network
R^2 (test set)	High ($R^2 > 0.95$)	Varies (R^2: 0.65 to 0.90)
Sensitivity to data	Moderate	High (worse for smaller datasets)
Interpretability	High (provides feature importance)	Low (black-box model)
Training time	~9 hrs. (Less Efficient, Slower)	~1h (More Efficient, Faster)
Tuning needs	Minimal (automatic via OOB)	Moderate (manual tuning required)

- **Model Characteristics and Performance**

The RF and ANN models provide a nuanced understanding of sediment dynamics, each contributing insights and predictive power to estuarine sedimentology. The RF model is highlighted with high accuracy and effective identification of key variables like tidal range, crucial for understanding sediment dynamics in estuaries. This aligns with research by Dyer (1988) and Winterwerp and van Kesteren (2004), who noted the impact of tidal forces on sediment transport. The model's structured approach provides clear insights into environmental parameter-sediment behavior relationships, valuable for estuarine management and predictive modeling.

Conversely, the ANN model does not meet the performance of the RF model. However, with increased attention and investment in neural networks—including special hardware for efficient training and inference (prediction)—it is possible that with larger datasets, training time can be reduced, energy consumption better managed, and deployment on smaller devices enabled. In situations where reasonable accuracy is sufficient, ANN can offer a fast and efficient means to yield predictions. Moreover, as demonstrated in the largest training cases in this study, ANNs can outperform in scenarios involving extremely large datasets. Thus, if researchers intend to train very large models—e.g., combining multiple river systems or continuous long-term measurements—ANN may prove more efficient and potentially more accurate.

- **Seasonal Variations and Site-Specific Analysis**

In this study, both the RF and ANN models were applied to analyze seasonal variations and site-specific sediment dynamics. The RF model's detailed seasonal analysis shows how environmental factors fluctuate throughout the year, impacting sediment behavior (Cloern et al., 2016; Mudd et

al., 2004; Fettweis & Baeye, 2015). This provides insights into sediment deposition and erosion across different seasons, and predictive power that will be useful for future scenarios. However, studying specific seasons or locations usually means less data, and that is where ANN models are less applicable. As previously mentioned, the strength of ANN depends on the size of the data, more so than in RF models, and thus, local analyses are better approached with RF models first.

- **Training Times**

When comparing the training times of Random Forest and ANN models, it is essential to consider the influence of hyperparameters and the complexity of each model. RF models, which depend on the number of trees, often require more extended training times. In contrast, ANN models benefit significantly from GPU acceleration and other specialized hardware (e.g., on servers), resulting in faster training. The availability of specialized hardware for ANNs is due to two main factors: (1) their computational units consist of simple algebraic operations, making them ideal candidates to run on parallelized small GPU cores; and (2) the popularity of ANNs in other domains (like large language models) has incentivized the creation of additional specialized hardware (such as Google's TPUs). This efficiency gain was evident in the present study, where the ANN model, supported by a GPU-accelerated platform, completed training in an average of 65 minutes for the main dataset, compared to the RF model's approximately 9-hour training duration on a high-efficiency CPU. Additionally, the environmental impact of training models is a crucial consideration. ANNs, due to hardware and software optimizations, tend to be more energy-efficient and often use renewable energy sources in cloud computing servers, reducing their overall environmental footprint. This contrast in training times and efficiency highlights the need for careful model selection in research, balancing accuracy, computational resources, and environmental sustainability.

- **Practical Applications and Research Utility**

The RF model's clarity in identifying key features and its high predictive accuracy make it particularly suitable for broad-scope applications in estuarine management. This model excels in providing a macro-level perspective, which is crucial for formulating overarching management and conservation strategies. Its ability to pinpoint influential factors in sediment dynamics aids in making informed decisions at a larger ecosystem scale. RF models are able to achieve higher predictive accuracies using smaller datasets, making them ideal for in-depth studies of localized sediment behavior and local policy-making. This makes the RF model particularly beneficial for

focused conservation efforts and targeted environmental interventions, where understanding the unique characteristics of a specific area, as accurately as possible, is vital.

On the other hand, the ANN model's adaptability and flexibility make it a suitable tool for larger modeling efforts with an abundance of data. The strength of ANN lies in accommodating diverse environmental conditions when high volumes of data are available, being faster to train, potentially cheaper, and operable even on smaller devices if needed. ANNs can be used for localized testing and agile modeling when smaller datasets are available—provided that the highest accuracy is not essential—making them more appropriate for exploratory modeling and experimentation rather than for strong policy-making or highly nuanced predictions.

- **Model Selection Considerations**

Choosing between the RF and ANN models requires careful consideration of the study's objectives. The RF model is more appropriate for projects seeking comprehensive, generalizable, and dependable insights, especially where understanding the importance of various features is crucial. Its structured approach to feature analysis is beneficial for studies that aim to identify and prioritize influential environmental factors. In contrast, the ANN model is better suited for detailed, complex analyses of sediment dynamics, given vast amounts of data, or alternatively, agile experimentation for exploration and scientific purposes. Its strength in handling intricate interactions within diverse environmental settings makes it ideal for studies that require a deep dive into the complexities of a particular estuarine site, provided that sufficient data are available.

3.5.4. Machine Learning vs. Classical Models for Sediment Dynamics

While RF and ANN models demonstrate high predictive accuracy and effectively capture both spatial and temporal variability in sediment dynamics, it is essential to evaluate their performance against traditional numerical models commonly used in sediment transport studies. Classical numerical models—such as those based on finite difference, finite element, or finite volume methods—are well-established for simulating sediment transport and morphodynamic processes in estuarine systems. Tools like Delft3D, TELEMAC, MIKE21, and iFlow are frequently applied to model sediment transport in estuaries like the Scheldt.

These classical models are grounded in physical principles, such as the conservation of mass, momentum, and energy, and simulate sediment transport through deterministic equations (e.g., advection-diffusion equations as used by Boelens et al., 2020). They also rely on empirical

formulas for erosion and deposition (e.g., Partheniades, 1965; Krone, 1962), as demonstrated by Mulder & Udink (1991). This mechanistic foundation provides detailed insights into the underlying physical processes, offering explanations for how tides, waves, and estuarine circulation influence sediment transport. However, machine learning models like RF and ANN can adapt to data from diverse sources—whether high-precision or noisy—making them particularly valuable in environments where obtaining detailed physical data is challenging or when measurements are highly variable (e.g., multi-source data). While RF and ANN models excel in predictive accuracy, they lack the detailed process-based insights that classical models provide.

However, classical models typically require extensive calibration and validation based on field data, which can be time-consuming and resource-intensive. These models often depend on highly precise bathymetric data, current velocity measurements, and sediment properties, making their application in data-sparse regions difficult. Fettweis et al. (2007) and Van Kessel et al. (2011) highlighted the challenges of obtaining continuous, high-resolution measurements for calibration, which limits the accuracy of long-term predictions. In contrast, ML models naturally learn from the available data and capture patterns with fewer specific measurement requirements. Traditional models also struggle to capture non-linear relationships between environmental variables (e.g., SPM concentration, current velocity, and shear rate), particularly when faced with significant variability or noise in the data. As demonstrated by Dijkstra et al. (2019), process-based models may not fully capture the complexity of sediment dynamics under episodic events like channel deepening or extreme weather conditions.

In summary, both ML models (such as RF and ANN) and classical numerical models have distinct strengths and weaknesses. ML models offer superior predictive power, flexibility, and computational efficiency for short-term predictions and data-limited environments, while classical numerical models provide detailed insights into underlying physical processes and are better suited for long-term, broad-scale predictions. Given the complementary strengths of both approaches, future studies would benefit from integrating the two: using classical models to provide mechanistic understanding and long-term predictions, while leveraging ML models for refined, short-term forecasts and efficient analysis of large, heterogeneous datasets. This integration is particularly relevant as climate change and sea level rise may introduce divergences from classical understandings, exposing the more intricate dependencies across variables—a domain in which ML models excel.

3.6. Conclusions

This chapter assesses the impact of current and future intertidal zones on suspended sediment equilibrium within the Scheldt estuary by integrating key environmental factors, including current velocity, floc size, shear rate, tidal range, and seasonal variations. It evaluates how these factors influence sedimentation and erosion dynamics. Given the continuous nature of these variables, regression ML models are essential for accurate predictions. By effectively utilizing both RF and ANN to predict bed level changes, the study demonstrates the transformative potential of machine learning techniques in sediment dynamics.

The analysis underscores the pivotal role of seasonality in refining model accuracy. It reveals that both the RF and ANN models, when adjusted for seasonal factors, provide more accurate predictions. Notably, the RF model exhibits superior performance across various evaluation metrics. This superiority is attributed to its robust ability to capture the intricate dynamics of sediment transport, as evidenced by its exceptional predictive accuracy. The integration of seasonal data into the RF model significantly enhances error metrics, highlighting the indispensable role of temporal changes in sediment transport modeling. Moreover, the RF model's ability to provide feature importance adds another layer of insight, identifying tidal range, mean floc size, and SPM concentration as the dominant predictors across all models. This demonstrates that the RF model effectively captures the key drivers of sediment dynamics, further reinforcing its utility in sediment transport modeling.

In contrast, while the ANN models initially show more moderate predictive abilities, their performance markedly improves with the inclusion of seasonal factors. This improvement signals their potential utility in analyzing sediment behavior. Spatial analysis further distinguishes the RF model's adeptness at accurately modeling sedimentation behavior across diverse intertidal zones—an aspect crucial for informed coastal management and climate change adaptation strategies. Although the ANN models offer insightful spatial perspectives, their accuracy varies across different environments, reflecting the complex sediment dynamics in freshwater, brackish, and saline settings.

Therefore, this study demonstrates that ML models, specifically RF and ANN, are effective tools for predicting sediment dynamics, offering superior predictive power, flexibility, and computational efficiency. It is concluded that the RF model is a reliable method for formulating effective management and conservation strategies, due to its high accuracy and ability to identify crucial environmental factors. In contrast, the versatility of the ANN model makes it more suited for comprehensive, data-rich environmental studies. However, compared to classical numerical

models, they are limited in providing detailed mechanistic insights necessary for long-term and process-based predictions. Therefore, by integrating both approaches, future studies can create a more comprehensive and robust framework for sediment transport modeling.

Appendix 3.A: Interpolation Methods and Datasets Utilized in Modeling

The interpolation function is designed to fill missing values (NaNs) in an array through interpolation. The function begins by checking if the array contains at least two valid data points (non-NaN values), as interpolation requires a minimum of two data points. If this condition is met, the function first applies linear interpolation. It identifies the positions of the non-NaN values and constructs an interpolation function using these positions and their corresponding values. This function is then used to estimate and fill the NaN values within the array. If any NaN values remain, particularly at the boundaries where linear interpolation might fail, the function proceeds to use nearest-neighbor interpolation with extrapolation. Nearest-neighbor interpolation assigns the closest available data point's value to the missing values, while extrapolation ensures that NaN values at the array's edges are also filled. This approach ensures that missing data is replaced by plausible estimates based on surrounding values, enhancing the completeness of the dataset for further analysis.

The datasets used for this analysis are presented below. They include input parameters such as tidal range, current velocity, shear rate (G), SPM concentration, floc size (D50), and a categorical season indicator (e.g., spring, summer), all used to predict changes in bed level, which serves as the output variable. Therefore, although bed level change is not listed among the input variables in the tables below, it was included in every dataset as the regression target in this supervised modeling framework.

- Dataset 3.A.1 shows full non-seasonal measurements, with approximately 2 million datapoints interpolated to high frequency.
- Dataset 3.A.2 includes the same variables but encoded for seasonal analysis, with around 2 million datapoints distributed across all seasons.
- Dataset 3.A.3 represents approximately 0.5 million datapoints for a single season across all stations.
- Dataset 3.A.4 provides data for each of the three stations (Branst: ~0.7M, Lillo: ~0.8M, Zuidgors: ~0.4M datapoints) using measurements from all seasons.

Dataset 3.A.1: Full Non-Seasonal Measurements Across All Stations

D50 (µm)	SPM (mg.l^{-1})	Velocity (m.s^{-1})	Tidal Range (m)	G (s^{-1})
Approx. 2M datapoints representing measurements for all seasons and stations, interpolated to high frequency using the interpolation function described above.				

Dataset 3.A.2: Full Seasonal Measurements Across All Stations

D50 (µm)	SPM (mg.l^{-1})	Velocity (m.s^{-1})	Tidal Range (m)	G (s^{-1})	Autumn	Winter	Spring	Summer
Approx. 2M datapoints representing measurements for all seasons and stations, interpolated to high frequency using the interpolation function described above.					*Using one-hot encoding, each datapoint will have a 1 value in the season in which it belongs, and a 0 in other seasons.*			

Dataset 3.A.3: Individual Season Measurements for Autumn, Winter, Spring, and Summer Across All Stations

D50 (µm)	SPM (mg.l^{-1})	Velocity (m.s^{-1})	Tidal Range (m)	G (s^{-1})
Approx. 0.5M datapoints representing measurements for only one of the 4 seasons, across all stations, interpolated to high frequency using the interpolation function described above.				

Dataset 3.A.4: Seasonal Measurements for Branst, Lillo, and Zuidgors Stations with Detailed Data Per Station

D50 (µm)	SPM (mg.l^{-1})	Velocity (m.s^{-1})	Tidal Range	G (s^{-1})	Autumn	Winter	Spring	Summer
Datapoints representing measurements for only one of the 3 stations (Branst: approx. 0.7M, Lillo: approx. 0.8M, Zuidgors: approx. 0.4M), across all seasons, interpolated to high frequency using the interpolation function described above.					*Using one-hot encoding, each datapoint will have a 1 value in the season in which it belongs, and a 0 in other seasons.*			

Bibliography

1. Baeye, M., Fettweis, M., Voulgaris, G., & Van Lancker, V. (2011). *Sediment mobility in response to tidal and wind-driven flows along the Belgian inner shelf, southern North Sea*. Ocean Dynamics, 61, 611-622.
2. Barneveld, H., R. Nicolai, M. van Veen, S. van Haaster, T. Boudewijn, J. de Jong, K. van Didderen et al. "*Analyserapport: T2015-rapportage Schelde-estuarium*." Report PR3152. HKV Lijn in Water (Lelystad) 886 (2018).
3. Bashir, Z. (2016). *Modeling the influence of biological activity on fine sediment transport in the Dutch Wadden Sea* (Master's thesis, University of Twente).
4. Belgiu, M., & Drăguţ, L. (2016). *Random forest in remote sensing: A review of applications and future directions*. ISPRS journal of photogrammetry and remote sensing, 114, 24-31.
5. Boelens, T., Schuttelaars, H., Plancke, Y., & De Mulder, T. (2020). *Historical and future development of the tidally averaged transport of sandy sediments in the Scheldt estuary: a 2D exploratory model*. Ocean Dynamics, 70, 481-504.
6. Breiman, L. (2001). *Random forests*. Machine learning, 45(1), 5-32.
7. Brownlee, J. (2018). *Basics of linear algebra for machine learning*. Machine Learning Mastery.
8. Chen, M. S., Wartel, S., Eck, B. V., & Maldegem, D. V. (2005). *Suspended matter in the Scheldt estuary*. Hydrobiologia, 540, 79-104.
9. Cloern, J. E., Abreu, P. C., Carstensen, J., Chauvaud, L., Elmgren, R., Grall, J., ... & Yin, K. (2016). *Human activities and climate variability drive fast-paced change across the world's estuarine–coastal ecosystems*. Global change biology, 22(2), 513-529.
10. Coen, I. (2008). *De eeuwige Schelde? Ontstaan en ontwikkeling van de Schelde*. Technical Report D/2007/3241/203, waterbouwkundig laboratorium.
11. Cox, T. J. S., Maris, T., Soetaert, K., Conley, D. J., Van Damme, S., Meire, P., ... & Struyf, E. (2009). *A macro-tidal freshwater ecosystem recovering from hypereutrophication: the Schelde case study*. Biogeosciences, 6(12), 2935-2948.
12. Cox, T. J. S., Maris, T., Van Engeland, T., Soetaert, K., & Meire, P. (2019). *Critical transitions in suspended sediment dynamics in a temperate meso-tidal estuary*. Scientific reports, 9(1), 12745.
13. Cutler, D. R., Edwards Jr, T. C., Beard, K. H., Cutler, A., Hess, K. T., Gibson, J., & Lawler, J. J. (2007). *Random forests for classification in ecology*. Ecology, 88(11), 2783-2792.
14. De Brouwer, J. F. C., Ruddy, G. K., Jones, T. E. R., & Stal, L. J. (2002). *Sorption of EPS to sediment particles and the effect on the rheology of sediment slurries*. Biogeochemistry, 61, 57-71.
15. de Lucas Pardo, M. A., Sarpe, D., & Winterwerp, J. C. (2015). *Effect of algae on flocculation of suspended bed sediments in a large shallow lake. Consequences for ecology and sediment transport processes*. Ocean Dynamics, 65, 889-903.

16. Deng, H., Runger, G., Tuv, E., & Vladimir, M. (2013). *A time series forest for classification and feature extraction*. Information Sciences, 239, 142-153.
17. Dibike, Y. B., & Solomatine, D. P. (2001). *River flow forecasting using artificial neural networks*. Physics and Chemistry of the Earth, Part B: Hydrology, Oceans and Atmosphere, 26(1), 1-7.
18. Dijkstra, Y. M., Schuttelaars, H. M., & Schramkowski, G. P. (2019). *Can the Scheldt River Estuary become hyperturbid? A model analysis of suspended sediment concentrations and transport in response to channel deepening*. Ocean Dynamics, 69, 809-827.
19. Downing-Kunz, M. A., & Schoellhamer, D. H. (2013). *Seasonal variations in suspended-sediment dynamics in the tidal reach of an estuarine tributary*. Marine Geology, 345, 314-326.
20. Downing, J. A., Prairie, Y. T., Cole, J. J., Duarte, C. M., Tranvik, L. J., Striegl, R. G., ... & Middelburg, J. J. (2006). *The global abundance and size distribution of lakes, ponds, and impoundments*. Limnology and oceanography, 51(5), 2388-2397.
21. Dyer, K. R. (1988). *Fine sediment particle transport in estuaries. In Physical processes in estuaries (pp. 295-310)*. Berlin, Heidelberg: Springer Berlin Heidelberg.
22. Dyer, K. R., & Manning, A. J. (1999). *Observation of the size, settling velocity and effective density of flocs, and their fractal dimensions*. Journal of sea research, 41(1-2), 87-95.
23. Eisma, D., Kalf, J., & Veenhuis, M. (1980). *The formation of small particles and aggregates in the Rhine estuary*. Netherlands Journal of Sea Research, 14(2), 172-191.
24. Elliott, M., & Whitfield, A. K. (2011). *Challenging paradigms in estuarine ecology and management*. Estuarine, Coastal and Shelf Science, 94(4), 306-314.
25. Fettweis, M., & Baeye, M. (2015). *Seasonal variation in concentration, size, and settling velocity of muddy marine flocs in the benthic boundary layer*. Journal of Geophysical Research: Oceans, 120(8), 5648-5667.
26. Fettweis, M., & Van den Eynde, D. (2003). *The mud deposits and the high turbidity in the Belgian–Dutch coastal zone, southern bight of the North Sea*. Continental Shelf Research, 23(7), 669-691.
27. Fettweis, M., Baeye, M., Van der Zande, D., Van den Eynde, D., & Joon Lee, B. (2014). *Seasonality of floc strength in the southern North Sea*. Journal of Geophysical Research: Oceans, 119(3), 1911-1926.
28. Fettweis, M., Francken, F., Pison, V., & Van den Eynde, D. (2006). *Suspended particulate matter dynamics and aggregate sizes in a high turbidity area*. Marine Geology, 235(1-4), 63-74.
29. Fettweis, M., Nechad, B., & Van den Eynde, D. (2007). *An estimate of the suspended particulate matter (SPM) transport in the southern North Sea using SeaWiFS images, in situ measurements and numerical model results*. Continental Shelf Research, 27(10-11), 1568-1583.
30. Fettweis, M., Schartau, M., Desmit, X., Lee, B. J., Terseleer, N., Van der Zande, D., ... & Riethmüller, R. (2022). *Organic matter composition of biomineral flocs and its influence on suspended particulate matter dynamics along a nearshore to offshore transect*. Journal of Geophysical Research: Biogeosciences, 127(1), e2021JG006332.
31. Francke, T., López-Tarazón, J. A., & Schröder, B. (2008). *Estimation of suspended sediment concentration and yield using linear models, random forests and quantile regression forests*. Hydrological Processes: An International Journal, 22(25), 4892-4904.

32. Ghosh, A., Sharma, R., & Joshi, P. K. (2014). *Random forest classification of urban landscape using Landsat archive and ancillary data: Combining seasonal maps with decision level fusion.* Applied Geography, 48, 31-41.
33. Goodfellow, I., Bengio, Y., & Courville, A. (2016). *Deep learning*. MIT press.
34. Hastie, T., Tibshirani, R., Friedman, J. H., & Friedman, J. H. (2009). *The elements of statistical learning: data mining, inference, and prediction (Vol. 2, pp. 1-758)*. New York: springer.
35. Hillman, J. R., Stephenson, F., Thrush, S. F., & Lundquist, C. J. (2020). *Investigating changes in estuarine ecosystem functioning under future scenarios*. Ecological Applications, 30(4), e02090.
36. Horemans, D. M., Dijkstra, Y. M., Schuttelaars, H. M., Sabbe, K., Vyverman, W., Meire, P., & Cox, T. J. (2021). *Seasonal variations in flocculation and erosion affecting the large-scale suspended sediment distribution in the Scheldt estuary: the importance of biotic effects.* Journal of Geophysical Research: Oceans, 126(4), e2020JC016805.
37. Horemans, D. M., Meire, P., & Cox, T. J. (2020). *The impact of temporal variability in light-climate on time-averaged primary production and a phytoplankton bloom in a well-mixed estuary*. Ecological Modelling, 436, 109287.
38. Hyndman, R. J., & Koehler, A. B. (2006). *Another look at measures of forecast accuracy*. International journal of forecasting, 22(4), 679-688.
39. Jiang, L., Gerkema, T., Idier, D., Slangen, A., & Soetaert, K. (2020). *Effects of sea-level rise on tides and sediment dynamics in a Dutch tidal bay*. Ocean Science, 16(2), 307-321.
40. Kirilenko, A., & Hanley, R. S. (2008). *Reducing Uncertainty in Ecological Niche Models with ANN Ensembles*.
41. Kirwan, M. L., & Megonigal, J. P. (2013). *Tidal wetland stability in the face of human impacts and sea-level rise*. Nature, 504(7478), 53-60.
42. Kisi, O., Choubin, B., Deo, R. C., & Yaseen, Z. M. (2019). *Incorporating synoptic-scale climate signals for streamflow modelling over the Mediterranean region using machine learning models*. Hydrological Sciences Journal, 64(10), 1240-1252.
43. Kohavi, R. (1995, August). *A study of cross-validation and bootstrap for accuracy estimation and model selection*. In Ijcai (Vol. 14, No. 2, pp. 1137-1145).
44. Krone, R. B. (1962). *Flume studies of transport of sediment in estrarial shoaling processes*. Final Report, Hydr. Engr. and Samitary Engr. Res. Lab., Univ. of California.
45. Liaw, A., & Wiener, M. (2002). *Classification and regression by randomForest*. R news, 2(3), 18-22.
46. Maggi, F. (2007). *Variable fractal dimension: A major control for floc structure and flocculation kinematics of suspended cohesive sediment*. Journal of Geophysical Research: Oceans, 112(C7).
47. Maggi, F. (2009). *Biological flocculation of suspended particles in nutrient-rich aqueous ecosystems*. Journal of Hydrology, 376(1-2), 116-125.
48. Manh, N. V., Dung, N. V., Hung, N. N., Merz, B., & Apel, H. (2014). *Large-scale suspended sediment transport and sediment deposition in the Mekong Delta*. Hydrology and Earth System Sciences, 18(8), 3033-3053.

49. Manning, A. J., & Dyer, K. R. (1999). *A laboratory examination of floc characteristics with regard to turbulent shearing*. Marine Geology, 160(1-2), 147-170.
50. Maris, T., P. Gelsomini & J. Schoelynck, 2024. *Onderzoek naar de gevolgen van het Sigmaplan, baggeractiviteiten en havenuitbreiding in de Zeeschelde op het milieu*. Geïntegreerd eindverslag van het onderzoek verricht in 2023. *ECOSPHERE 024-RES023*. Universiteit Antwerpen, Antwerpen.
51. Mattei, F., Franceschini, S., & Scardi, M. (2018). *A depth-resolved artificial neural network model of marine phytoplankton primary production*. Ecological Modelling, 382, 51-62.
52. Meire, P., Plancke, Y., Govaerts, A., Cox, T., Gelsomi, P., Horemans, D., Meire, D., Meire, L., Zetsche, E. and Maris,T. (2021). *Synthesis note: SPM dynamics and trends in the Scheldt estuary*. ECOBE Report 021-R267 Universiteit Antwerpen, Antwerpen.
53. Meire, P., Ysebaert, T., Damme, S. V., Bergh, E. V. D., Maris, T., & Struyf, E. (2005). *The Scheldt estuary: a description of a changing ecosystem*. Hydrobiologia, 540(1), 1-11.
54. Mudd, S. M., Fagherazzi, S., Morris, J. T., & Furbish, D. J. (2004). *Flow, sedimentation, and biomass production on a vegetated salt marsh in South Carolina: toward a predictive model of marsh morphologic and ecologic evolution*. The ecogeomorphology of tidal marshes, 59, 165-188.
55. Mulder, H. P., & Udink, C. (1991). *Modelling of cohesive sediment transport. A case study: the western Scheldt estuary*. In Coastal Engineering 1990 (pp. 3012-3023).
56. Nakagawa, S., Takai, K., Inagaki, F., Chiba, H., Ishibashi, J. I., Kataoka, S., ... & Sako, Y. (2005). *Variability in microbial community and venting chemistry in a sediment-hosted backarc hydrothermal system: impacts of subseafloor phase-separation*. FEMS microbiology ecology, 54(1), 141-155.
57. Nichols, G. (2009). *Sedimentology and stratigraphy*. John Wiley & Sons.
58. Ouellet-Proulx, S., St-Hilaire, A., Courtenay, S. C., & Haralampides, K. A. (2016). *Estimation of suspended sediment concentration in the Saint John River using rating curves and a machine learning approach*. Hydrological Sciences Journal, 61(10), 1847-1860.
59. Pang, W., Zhou, X., Dai, Z., Li, S., Huang, H., & Lei, Y. (2021). *ADV-based investigation on bed level changes over a meso-macro tidal beach*. Frontiers in Marine Science, 8, 733923.
60. Partheniades, E. (1965). *Erosion and deposition of cohesive soils*. Journal of the Hydraulics Division, 91(1), 105-139.
61. Passow, U. (2002). *Transparent exopolymer particles (TEP) in aquatic environments*. Progress in oceanography, 55(3-4), 287-333.
62. Plancke, Y., & Vos, G. R. (2016, July). *Sediment transport in the Schelde-estuary: a comparison between measurements, transport formula and numerical models*. In Proceedings of the 4th IAHR Europe Congress, Liege, Belgium (pp. 27-29).
63. Prechelt, L. (1998). *Neural networks: Tricks of the trade*. Lecture notes in computer science, 1524, 53-67.
64. Ramesh, A., Pavlov, M., Goh, G., Gray, S., Voss, C., Radford, A., ... & Sutskever, I. (2021, July). *Zero-shot text-to-image generation*. In International Conference on Machine Learning (pp. 8821-8831). PMLR.

65. Rodriguez-Galiano, V. F., Chica-Olmo, M., Abarca-Hernandez, F., Atkinson, P. M., & Jeganathan, C. (2012). *Random Forest classification of Mediterranean land cover using multi-seasonal imagery and multi-seasonal texture*. Remote Sensing of Environment, 121, 93-107.
66. Rodriguez, J. D., Perez, A., & Lozano, J. A. (2009). *Sensitivity analysis of k-fold cross validation in prediction error estimation*. IEEE transactions on pattern analysis and machine intelligence, 32(3), 569-575.
67. Rosenblatt, F. (1958). *The perceptron: a probabilistic model for information storage and organization in the brain*. Psychological review, 65(6), 386.
68. Safak, I., Allison, M. A., & Sheremet, A. (2013). *Floc variability under changing turbulent stresses and sediment availability on a wave energetic muddy shelf*. Continental Shelf Research, 53, 1-10.
69. Sahin, C., Guner, H. A. A., Ozturk, M., & Sheremet, A. (2017). *Floc size variability under strong turbulence: Observations and artificial neural network modeling*. Applied Ocean Research, 68, 130-141.
70. Scardi, M. (2001). *Advances in neural network modeling of phytoplankton primary production*. Ecological Modelling, 146(1-3), 33-45.
71. Schwarz, C., Cox, T., Van Engeland, T., Van Oevelen, D., Van Belzen, J., Van de Koppel, J., ... & Temmerman, S. (2017). *Field estimates of floc dynamics and settling velocities in a tidal creek with significant along-channel gradients in velocity and SPM*. Estuarine, Coastal and Shelf Science, 197, 221-235.
72. Seo, H. J., Cho, M., & Yoon, H. D. (2020). *Data-driven analysis of stratified flow effect on suspended sediment concentration in an estuary*. Journal of Marine Science and Engineering, 8(8), 606.
73. Sequoia Scienti_c. (Sequoia Scientific. 2010). *How to compute the mean particle diameter from a LISST volume distribution*. Sequoia Scienti_c. ([Available online at http://www.sequoiasci.com/article/how-to-compute-the-mean-particle-diameter-from-a-lisst-volume-distribution-2/).
74. Son, M., & Hsu, T. J. (2011). *The effects of flocculation and bed erodibility on modeling cohesive sediment resuspension*. Journal of Geophysical Research: Oceans, 116(C3).
75. Temmerman, S., Meire, P., Bouma, T. J., Herman, P. M., Ysebaert, T., & De Vriend, H. J. (2013). *Ecosystem-based coastal defence in the face of global change*. Nature, 504(7478), 79-83.
76. Uchiyama, Y. (2005). *Modeling three-dimensional cohesive sediment transport and associated morphological variation in estuarine intertidal mudflats*. Report of the Port and Harbour Research Institute, 44(1).
77. Uncles, R. J., Bale, A. J., Stephens, J. A., Frickers, P. E., & Harris, C. (2010). *Observations of floc sizes in a muddy estuary*. Estuarine, Coastal and Shelf Science, 87(2), 186-196.
78. Uncles, R. J., Stephens, J. A., & Smith, R. E. (2002). *The dependence of estuarine turbidity on tidal intrusion length, tidal range and residence time*. Continental shelf research, 22(11-13), 1835-1856.
79. Van Kessel, T., Vanlede, J., & de Kok, J. (2011). *Development of a mud transport model for the Scheldt estuary*. Continental Shelf Research, 31(10), S165-S181.

80. van Leussen, W. (1994). *Estuarine macroflocs and their role in fine-grained sediment transport*. Ph. D. Thesis, University of Utrecht.
81. van Maanen, B., & Sottolichio, A. (2018). *Hydro-and sediment dynamics in the Gironde estuary (France): Sensitivity to seasonal variations in river inflow and sea level rise*. Continental Shelf Research, 165, 37-50.
82. Van Manh, N., Dung, N. V., Hung, N. N., Kummu, M., Merz, B., & Apel, H. (2015). *Future sediment dynamics in the Mekong Delta floodplains: Impacts of hydropower development, climate change and sea level rise*. Global and Planetary Change, 127, 22-33.
83. Vandenbruwaene, W., Stark, J., Plancke, Y., & Mostaert, F. (2020). *Agenda for the Future–Historical evolution of tides and morphology of the Scheldt estuary: subreport 5*. Synthesis. WL Reports.
84. Vanlede, J., Smolders, S., Maximova, T., & Teles, M. J. (2015, June). *The unstructured Scaldis model: a new 3D high resolution model for hydrodynamics and sediment transport in the tidal Scheldt*. In Proc., Scheldt Estuary: Physics and Integrated Management—Special Session on of the 36th IAHR World Congress (Vol. 11).
85. Verney, R., Brun-Cottan, J. C., Lafite, R., Deloffre, J., & Taylor, J. A. (2006). *Tidally-induced shear stress variability above intertidal mudflats in the macrotidal Seine Estuary*. Estuaries and coasts, 29, 653-664.
86. Verney, R., Lafite, R., & Brun-Cottan, J. C. (2009). *Flocculation potential of estuarine particles: The importance of environmental factors and of the spatial and seasonal variability of suspended particulate matter*. Estuaries and coasts, 32, 678-693.
87. Waterinfo.be (cited 2019). *Measurements and predictions of Waterinfo.be [data]*. [Available online at https://www.waterinfo.be/].
88. Widdows, J., Blauw, A., Heip, C. H. R., Herman, P. M. J., Lucas, C. H., Middelburg, J. J., ... & Verbeek, H. (2004). *Role of physical and biological processes in sediment dynamics of a tidal flat in Westerschelde Estuary, SW Netherlands*. Marine Ecology Progress Series, 274, 41-56.
89. Willmott, C. J., & Matsuura, K. (2005). *Advantages of the mean absolute error (MAE) over the root mean square error (RMSE) in assessing average model performance*. Climate research, 30(1), 79-82.
90. Winterwerp, J. C. (1998). *A simple model for turbulence induced flocculation of cohesive sediment*. Journal of hydraulic research, 36(3), 309-326.
91. Winterwerp, J. C., & Van Kesteren, W. G. (2004). *Introduction to the physics of cohesive sediment dynamics in the marine environment*. Elsevier.
92. Winterwerp, J. C., & Wang, Z. B. (2021). *Hydrosedimentological response to estuarine deepening: Conceptual analysis*. Journal of Waterway, Port, Coastal, and Ocean Engineering, 147(5), 04021023.
93. Winterwerp, J. C., Bale, A. J., Christie, M. C., Dyer, K. R., Jones, S., Lintern, D. G., ... & Roberts, W. (2002). *Flocculation and settling velocity of fine sediment*. In Proceedings in Marine Science (Vol. 5, pp. 25-40). Elsevier.
94. Winterwerp, J. C., Van Kesteren, W. G. M., Van Prooijen, B., & Jacobs, W. (2012). *A conceptual framework for shear flow–induced erosion of soft cohesive sediment beds*. Journal of Geophysical Research: Oceans, 117(C10).

95. Winterwerp, J. C., Wang, Z. B., Van Braeckel, A., Van Holland, G., & Kösters, F. (2013). *Man-induced regime shifts in small estuaries—II: a comparison of rivers*. Ocean Dynamics, 63, 1293-1306.
96. Zounemat-Kermani, M., Mahdavi-Meymand, A., Alizamir, M., Adarsh, S., & Yaseen, Z. M. (2020). *On the complexities of sediment load modeling using integrative machine learning: Application of the great river of Loíza in Puerto Rico*. Journal of Hydrology, 585, 124759.

Chapter 4

Integrating Scenarios into Predictive Models: Pathways to Conservation Strategies in Intertidal Sediment Dynamic

Abstract

The Scheldt estuary, like many estuarine systems, is highly sensitive to both human activities and climate change. Over recent decades, interventions such as dredging, channel deepening, and land reclamation, combined with sea-level rise (SLR), have significantly altered its tidal dynamics and sediment transport processes. Changes in tidal range can intensify hydrodynamic energy within intertidal zones, influencing sediment resuspension, deposition patterns, and the structural stability of flocs. Understanding how sedimentation and erosion processes may evolve under future conditions is essential for sustaining this vital ecosystem and requires models capable of capturing the complex interactions among key physical variables.

This chapter explored the potential of machine learning (ML) models to simulate estuarine sediment dynamics under tidal amplification scenarios. The main objective was to investigate how well these models capture the behavior of key physical variables—such as flow velocity, turbulent shear rate, suspended particulate matter (SPM) concentration, and floc size—and whether they can reproduce bed level change outcomes that reflect the expected spatial and seasonal variability based on these underlying drivers. The analysis focused on three representative intertidal sites along the estuary's salinity gradient: one each in the freshwater, brackish, and saline zones. By focusing on empirical relationships between these variables and bed level change, the framework aimed to reveal site- and season-specific sediment responses to future hydrodynamic forcing.

The projections showed that estuarine responses to tidal amplification are highly site- and season-dependent. Patterns of bed level change varied according to local hydrodynamic conditions, sediment availability, and floc stability, with model performance closely tied to the strength of empirical correlations. In systems where tidal range was strongly linked to sediment inputs—such as at the brackish site—projections aligned well with observed trends. In contrast, dynamic or floc-sensitive environments like the freshwater and saline sites exhibited greater uncertainty and nonlinear behavior.

Overall, the results demonstrate that while ML models cannot replace physical process models, they offer a valuable data-driven approach to exploring dominant controls on sediment behavior and identifying zones of vulnerability within estuarine systems. The findings underscore the importance of local context—particularly floc dynamics, sediment supply, and hydrodynamic conditions—in shaping future bed level responses. While the integration of high-resolution observations with data-driven modeling shows promises for advancing our understanding of sediment behavior under anticipated environmental changes, further work—especially involving

extended long-term datasets—is needed to improve model robustness and support future applications.

4.1. Introduction

Estuarine and tidal river systems, such as the Scheldt estuary, act as dynamic interfaces between terrestrial and marine environments. The interaction of water movement, sediment transport, and bed topography is crucial for their morphological evolution, which supports biodiversity, coastal defenses, and various ecosystem services (Chu et al., 2015; Bi and Toorman, 2015). A key factor in these systems is Suspended Particulate Matter (SPM), which significantly influences sediment dynamics, water quality, and ecological health. SPM behavior is largely governed by flocculation—a process in which suspended particles (flocs) aggregate and disintegrate. In estuarine environments, flocculation is central to regulating SPM dynamics, as it controls particle interactions and settling rates (Partheniades, 1993; Maggi, 2007; Mietta, 2010). Floc size and stability influence sedimentation and erosion patterns; larger, more cohesive flocs settle faster, whereas smaller or fragmented flocs are more easily resuspended (Chen et al., 2005; de Lucas Pardo et al., 2015). Additionally, seasonal variations in phytoplankton biomass and turbulence significantly affect floc behavior, leading to changes in floc size and stability, which in turn impact sediment dynamics. These variations depend on local environmental conditions such as hydrodynamic forces, salinity, and biological activity specific to each site, making accurate predictions of sediment transport processes more challenging in estuarine systems (Passow, 2002; Winterwerp & van Kesteren, 2004; Chen et al., 2005; Fettweis et al., 2014; Cox et al., 2019).

The intertidal zones of the Scheldt estuary serve as critical habitats that support a diverse array of species, thereby enhancing estuarine biodiversity. The sediment composition and tidal dynamics within these zones are vital to the ecosystem's functionality. Fine, organic-rich sediments facilitate the growth of algae, microphytobenthos and seagrasses as well as marsh vegetation, elevating primary productivity and promoting carbon sequestration. These biogeochemical processes not only sustain local biodiversity but also integrate into global carbon cycles, contributing to climate change mitigation strategies (Meire et al., 2005; Wolff, 2005; Van de Broek et al., 2018; Rios-Yunes et al., 2023; Alongi, 2018).

Tidal forces within the estuary regulate sediment dynamics, including transport, deposition, and erosion, which collectively maintain ecological equilibrium. Changes in sea level can influence tidal range responses, which may amplify or dampen depending on factors such as resonance, estuarine geometry, and friction in newly inundated areas (Jiang et al., 2020; Khojasteh et al., 2021). In the Scheldt estuary, reduced bottom friction in deepened upstream channels may

amplify tidal waves, whereas newly inundated zones downstream could increase energy dissipation, resulting in spatially variable tidal range trends (Van der Wegen et al., 2022). Moreover, in systems approaching resonance, even modest increases in water level can lead to tidal amplification, enhancing sediment resuspension and turbidity (Manh et al., 2014; Nguyen Van Manh et al., 2015). Understanding these dynamics is crucial for predicting estuarine responses to both natural and anthropogenic changes and informs future sediment system assessments (Temmerman et al., 2004; Kirwan et al., 2016).

In the context of accelerating global sea-level rise (SLR), estuarine systems worldwide are experiencing increasingly complex transformations. While SLR elevates baseline water levels, its impact on tidal dynamics is often nonlinear and site-specific. In some estuaries, SLR may enhance tidal asymmetry, altering the balance between flood and ebb dominance depending on local morphology, intertidal area, and sediment supply (Jiang et al., 2020). For instance, estuaries with diminishing intertidal storage capacity may become more ebb-dominant, as sediment export increases and morphological buffering declines. Similarly, Khojasteh et al. (2021) emphasize that deepening and reduced friction can amplify ebb dominance in certain systems. These dynamics highlight the complex interplay between SLR, morphology, and hydrodynamics, with implications for sediment transport and ecological stability that vary across systems.

In the Scheldt estuary, many of these global patterns appear to be unfolding, though their local expression is shaped by both natural and engineered modifications. Intertidal zones are increasingly inundated, and dredging, land reclamation, and channel deepening have collectively reshaped tidal behavior and sediment balance (Van Rijn et al., 2018; Cox et al., 2019; Dijkstra et al., 2019; Boelens et al., 2020). These changes may be contributing to a shift toward ebb dominance, which could enhance sediment export and intensify turbidity. Given the Scheldt's already high SPM concentrations (Cox et al., 2019), such shifts could destabilize aquatic habitats and complicate biodiversity conservation efforts. Preserving intertidal zones and closely monitoring sediment dynamics will be essential for maintaining ecological and geomorphological balance in the face of ongoing environmental pressures.

Despite the recognized importance of SPM in influencing sediment dynamics, there remains a need for approaches that can explore how interactions among physical variables shape sedimentation and erosion within estuarine intertidal zones. To address this, the current chapter applies machine learning (ML) models—developed and described in Chapter 3—to explore their potential to simulate sediment dynamics under tidal amplification scenarios. The main objective was to investigate how well these models capture the behavior of key physical variables—such as flow velocity, turbulent shear rate, SPM concentration, and floc size—and to evaluate whether their

learned relationships with bed level change reflect the expected variability across different estuarine zones and seasons. By using scenario-based inputs representing moderate and extreme increases in tidal range, the models were tested for their ability to generalize observed physical interactions under altered conditions. This approach contributes to a broader understanding of how data-driven models can complement traditional physical modeling in estuarine sediment research.

4.2. Material and Methods

4.2.1. Study Area

The Scheldt estuary, located in northern Belgium and southwestern Netherlands, comprises several distinct sections: the Western Scheldt in the Netherlands and the Sea Scheldt in Belgium, which is further subdivided into the Lower and Upper Sea Scheldt (Figure 4.1). The estuary is characterized by a funnel-shaped morphology and is well-mixed due to its relatively low freshwater discharge (Meire et al., 2005).

Additionally, the Scheldt estuary has experienced substantial long-term changes in tidal dynamics, characterized by a continuous increase in tidal range and tidal intrusion since the early Middle Ages (Coen, 2008; Vandenbruwaene et al., 2020). During 2018–2019, the mean tidal range at the Western Scheldt mouth in Vlissingen was approximately 3.7 m, increasing to about 5.4 m at Tielrode (100 km from the mouth) and then decreasing to roughly 2.6 m at Melle (150 km from the mouth) (Wang et al., 2019). Recent observations indicate a rise in high water levels along the entire estuary and a decrease in low water levels, particularly in the Upper Sea Scheldt (Barneveld et al., 2018).

Trend analyses, incorporating a linear increase SLR and a cyclical pattern representing natural tidal variations over an 18.6-year period, show a clear upward trend in high water levels, especially in Antwerp and Dendermonde (Depreiter et al., 2014). The relationship between freshwater discharge and tidal range has evolved over time, with the tidal range becoming more sensitive to discharge in recent years. This is reflected by a higher intercept and steeper slope in the relationship, indicating that even at lower discharges, the tidal range is now more affected by discharge. This increased influence is particularly noticeable in the upstream sections of the estuary (Meire et al., 2021).

Sediment transport plays a critical role in the estuary's dynamics. The annual SPM input at the upstream boundary ranges from 10^4 to 10^5 tons, closely linked to freshwater discharge variability

(Plancke et al., 2017; Dijkstra et al., 2019). Large volumes of sand and mud are continually dredged to maintain the fairway and ensure ship accessibility to the docks. These dredging activities, aimed at maintaining access to the Port of Antwerp, have significantly modified the estuary's morphology (Meire et al., 2005; Winterwerp et al., 2013; Dam et al., 2022). Dredged materials are often dumped back into the estuary, contributing to high SPM loads and increased turbidity, which negatively impact water quality, sediment balance, and ecological health (Dijkstra et al., 2019; Fettweis et al., 2019). During 2018–2019, annual dredging volumes were approximately 9.3 Mm^3/year in the Western Scheldt and 4.7 Mm^3/year in the Lower Sea Scheldt, with a significant proportion consisting of mud in the latter. These operations have contributed to a net sand import of 0.609 Mm^3/year into the Sea Scheldt from the Western Scheldt, highlighting the estuary's sediment dynamics and its dependence on active management (Cleveringa et al., 2014; Vandenbruwaene et al., 2017).

4.2.2. In Situ Observations

Three sites were selected as representative tidal flats for the respective zones of the Western Scheldt, Lower Sea Scheldt, and Upper Sea Scheldt in the Scheldt estuary (Figure 4.1). All locations are situated along the main Scheldt channel and are backed by tidal marshes representing different salinity gradients. The Branst site is located within the freshwater zone, approximately 105 km from the Scheldt mouth in the Upper Sea Scheldt. Lillo is situated in the mesohaline zone with a strong salinity gradient, approximately 65 km from the mouth in the Lower Sea Scheldt, and Zuidgors is located in the polyhaline zone, approximately 20 km from the mouth in the Western Scheldt.

Under local tidal conditions, the measurement frame containing the following instruments was placed at the elevation corresponding to 50% inundation time: for Branst, this location was at 2.63 m TAW; for Lillo, at 2.36 m TAW; and for Zuidgors, at 0.06 m NAP (2.39 m TAW). This frame included an OBS (Optical Backscatter Sensor; YSI type 6920 V2) mounted at 13 cmab (centimeters above bed) to measure turbidity and subsequently calculate SPM concentration. An ADV (Acoustic Doppler Velocimeter; Nortek Vector, 6 MHz) with its sampling volume at 12 cmab was used to measure current velocity and to determine bed level changes from the distance between the seabed and the ADV probe (DSP). Additionally, the turbulent shear rate (G) was calculated from the velocity obtained from the ADV. A LISST (Sequoia Scientific LISST-200X) equipped with a Path Reduction Module (PRM) at 13 cmab was used to measure particle size distribution and calculate median floc size (D50), which served as a proxy for floc size in this study. The same setup was used at all three locations in the estuary, with the frame oriented perpendicular to the main current.

Additionally, tidal range data were obtained from tidal gauges at Driegoten Tij/Zeeschelde for Branst, at Liefkenshoek for Lillo, and at Overflow van Hansweert for Zuidgors. Details about these instruments are provided in Chapter 2.

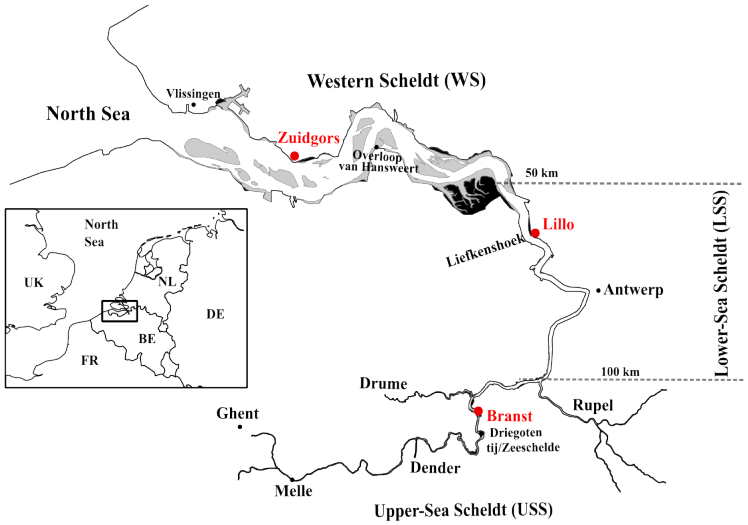

Figure 4.1: Map of the Scheldt Estuary showing the three intertidal measurement sites used in this study (red dots). Branst is located in the freshwater zone, Lillo represents the brackish zone, and Zuidgors is situated in the saline part of the estuary near the mouth. The sites were selected to capture spatial variability in sediment dynamics across the estuarine salinity gradient.

4.2.3. Model Setup

This section outlines the approach used to apply ML models, developed in Chapter 3, to predict bed level changes under different SLR scenarios in the Scheldt estuary. The Random Forest (RF) model was selected due to its higher predictive accuracy compared to the Artificial Neural Network (ANN) alternative. RF's robust structure—built on an ensemble of decision trees—allows it to capture the complex, non-linear interactions between variables that are essential for understanding sediment dynamics.

Three RF models were trained, one for each station (Lillo, Branst, and Zuidgors), using data that included observations from all seasons (Dataset 4.B.1 in the Appendix). A 70–30% training and testing random split was applied, with the training subset used to train the model, while the testing subset remained unseen by the model until the final evaluation. To maintain flexibility regarding unknown seasonal impacts, season-specific models were not created, and season was not included

as an input feature. Instead, each model was trained on multi-seasonal data, enabling it to learn patterns that could generalize across potential shifts in seasonal sedimentation dynamics.

Moreover, by training station-specific models with data from all seasons, the distinct environmental conditions and sedimentation patterns unique to each station were accounted for, while assumptions tied to current seasonal trends were avoided. This approach is considered valuable given the intricate relationships between sediment stability and factors such as floc composition and cohesion. As discussed in Chapter 2, these factors are influenced by seasonal activity and localized hydrodynamic forces, both of which may shift under changing estuarine conditions. Therefore, by capturing these variations, the models are better positioned to adapt flexibly to potential changes in seasonal patterns that may emerge under future conditions.

The input vector for the models consists of current velocity, turbulent shear rate (G), SPM concentration, median floc size (D50), and tidal range. Each of the three station-specific RF models was composed of 50 decision trees. The number of trees was treated as a hyperparameter and optimized to achieve a balance between predictive accuracy and generalization without overfitting. Additionally, the Out-of-Bag (OOB) error was used during training to validate the model's accuracy, resulting in a score of 98% for all three models (see Chapter 3 for more details).

Following training, the RF model's predictive performance was assessed on the training subset using the R^2 metric, with all three models achieving an R^2 accuracy of 98% at the Branst, Lillo, and Zuidgors stations. This level of accuracy aligns with results reported in Chapter 3, confirming the model's effectiveness in explaining bed level variability. Subtle variations in feature importance (ratios of input variables' contributions to model predictions) were observed across the stations, with tidal range consistently emerging as the dominant factor. Median floc size also contributed significantly at all stations. Notably, at Zuidgors, SPM concentration demonstrated a higher relative importance compared to other locations, indicating that it plays a more prominent role in model performance at this site.

To apply these models to future predictions of bed level changes, it is necessary to project the input parameters under hypothetical conditions defined by the respective scenarios. This step ensures that the model outputs reflect realistic changes in sedimentation and erosion dynamics. In the next section, the structured approach used to develop these projections is described, ensuring that they remain grounded in observed relationships and logical assumptions.

4.2.3.1. Model Input Parameters and Scenario-Driven Bed Level Modeling

The scenarios developed in this study are designed to simulate potential sediment dynamics under increased tidal range conditions. Constructing such scenarios requires a dataset that plausibly reflects variations in key input parameters under altered tidal forcing. As outlined above, these inputs include tidal range (TR), suspended particulate matter (SPM) concentration, flow velocity, turbulent shear rate (G), and median floc size (D50). Among these, tidal range is the most straightforward to project, as it has been well-documented in many estuarine systems. However, other parameters are more difficult to project due to limited documentation on their future behavior, necessitating a structured and systematic approach grounded in observed relationships to minimize assumptions.

Tidal range changes in estuarine systems result from a combination of natural and anthropogenic factors, including geomorphological configuration, hydrodynamic conditions, sediment dynamics, and SLR. The Scheldt Estuary has historically exhibited an increasing TR (Barneveld et al., 2018), although this trend has not been uniform across its spatial extent (Scheldecommissie et al., 2023). By 2020, observations indicated that the lower, more open part of the estuary (closer to the sea) had maintained a relatively stable TR since the 1970s. This stability is attributed to its wide morphology, which allows tidal energy to dissipate effectively. In contrast, the upstream section (further inland) has experienced a clear increase in TR over time. This tidal amplification results from the estuary narrowing inland, which naturally enhances tidal propagation. Human interventions, such as channel deepening and sediment management, have further intensified this effect. For instance, channel deepening reduces frictional resistance, thereby amplifying tidal wave propagation—a pattern documented by Jiang et al. (2020) and Khojasteh et al. (2021). Amplification is most pronounced in the mid-estuary and diminishes in the upper reaches, where river discharge counteracts incoming tidal energy.

Building on these spatially variable trends, it is important to recognize that TR evolution is influenced not only by past modifications but also by potential future changes in water levels. Among these, SLR is expected to modulate TR dynamics, although its effects remain strongly context dependent. Increased water depths may reduce bottom friction and enhance TR in confined sections of the estuary. However, in low-gradient zones, newly inundated areas can dissipate tidal energy and dampen TR. This duality, as discussed by Khojasteh et al. (2021), Friedrichs et al. (1990), and Pickering et al. (2017), underscores the need for estuary-specific assessments.

To reflect these complex and interacting drivers, a scenario-based approach was adopted, using +5% and +10% increases in TR to represent plausible future tidal amplification. These scenarios align with projections from earlier modeling efforts (Jiang et al., 2020; Van der Wegen et al., 2022) and represent realistic estimates under moderate SLR and ongoing morphological evolution. The projected seasonal TR increases under these scenarios range from 27–29 cm at Branst, 26–28 cm at Lillo, and 22–24 cm at Zuidgors.

To project other input parameters, a high-frequency observational dataset from 2018–2019 was used as the baseline, and regression relationships with TR were employed to guide projections for each station and season. The overall projection framework is outlined in Figure 4.2. The methodology for projecting the variables was adapted to the strength of their relationship with tidal range. These relationships were assessed by calculating R^2 values, which represent the proportion of variability in each dependent variable explained by changes in TR. An R^2 threshold of 0.2 was applied to distinguish between weak and moderate-to-strong correlations when evaluating the suitability of linear regression. This threshold was selected based on how projection outcomes respond to weaker or more uncertain relationships, aiming to balance sensitivity with model reliability. It is also consistent with practices commonly adopted in ecological modeling. As noted by Quinn & Keough (2002) and Legendre & Legendre (2012), lower R^2 values are frequently observed in ecological regression analyses due to system complexity. The chosen threshold ensures that moderate relationships are incorporated while minimizing over-reliance on weak correlations, thereby maintaining a practical yet robust approach to projecting future changes. To clarify how this balance was operationalized, the following criteria and methodological steps were applied based on the strength of the observed regression relationships:

- **Moderate to high R^2 values (≥ 0.2):** In cases where the R^2 value was equal to or greater than 0.2, the linear regression model was considered sufficiently robust to project these parameters directly based on TR. This approach is considered straightforward and reduces reliance on assumptions.
- **Low R^2 values (< 0.2):** For some parameters, the relationship with TR was identified as weak, as indicated by low R^2 values ($R^2 < 0.2$) in the regression analysis. In such cases, the regression equation was not considered reliable for projecting these parameters. Therefore, for future scenario projections, alternative machine learning models—specifically RF—were developed. The approach was defined as follows:
  - New RF models were applied only when at least three parameters (including TR) had strong regression relationships. This ensured a solid foundation for training the model.
  - The inputs included TR and the parameters with strong relationships (high R^2) to it. The output was the weakly correlated parameter. For example, if TR, SPM concentration, and G

showed strong relationships, but D50 did not, an RF model was trained using TR, SPM concentration, and shear rate G as inputs to predict D50 as the output.

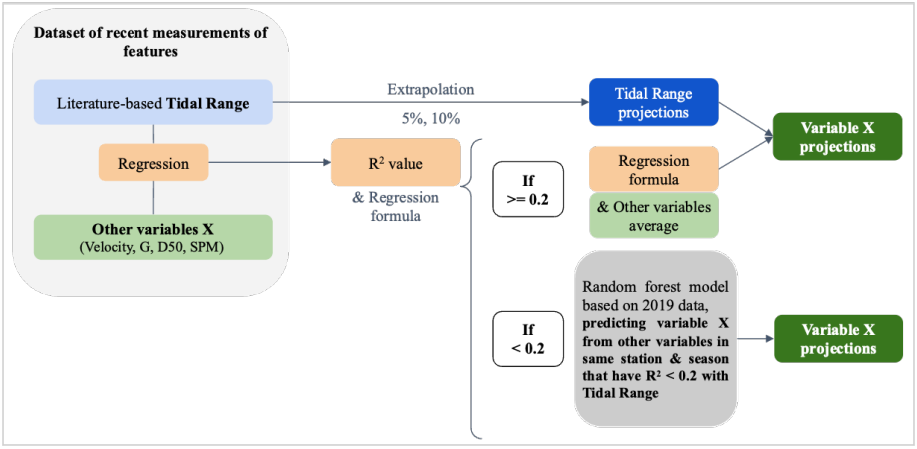

Figure 4.2: Scenario-building and variable projection pipeline used for modeling estuarine sediment dynamics under increased tidal range conditions. Tidal range (TR) was extrapolated by +5% and +10% based on literature-supported estimates to represent plausible future tidal amplification scenarios. Input parameters (velocity, turbulent shear rate G, SPM concentration, and floc size D50) were projected using one of two approaches depending on their observed relationship (R^2 value) with TR. When a parameter exhibited a moderate-to-strong correlation with TR ($R^2 \geq 0.2$), linear regression was used for projection. For parameters with weaker correlations ($R^2 < 0.2$), Random Forest models were trained using TR and other strongly correlated variables as inputs to predict the weakly related parameter

This approach enabled the logical and systematic projection of parameters that could not be directly linked to TR through regression alone. The method is directly aligned with the primary objective of the study—to improve understanding of the forces influencing sedimentation and erosion. For future modeling, rather than assigning arbitrary values to each parameter, a structured approach was employed to project them under future conditions. Accordingly, for each of the 12 season-station combinations, one of the following cases applies:

- **Case A, all 4 variables have usable regression with TR**: In such season-station combinations, TR-based projections were applied to all variables for scenario-based predictions.
- **Case B, fewer than 2 variables have usable regression with TR**: In these cases, scenario predictions were not performed due to insufficient predictive relationships.
- **Case C, two or three variables have usable regression with TR:** In these season-station combinations, as previously described, new RF models were trained to predict the remaining

one or two variables. The training dataset consisted of a 50% random sample of the data for the same season-station. The input features included the two or three variables with valid regression relationships, along with TR itself. If two variables required projection, two separate RF models were trained, each with a different target variable. The R^2 value for all RF models was verified to exceed 85%.

The detailed results of input vector development are presented in Appendix 4.A. Specifically, Tables 4.A.1, 4.A.2, and 4.A.3 provide the regression equations and coefficients for all parameters—velocity, turbulent shear rate (G), SPM concentration, and floc size—across the four seasons (Autumn, Winter, Spring, and Summer) at all stations, illustrating their relationships with TR.

Upon closer examination of the regression results, the relationships between parameters and TR display distinct patterns across stations and seasons. Based on these findings, season-station cases were classified into Case A, B, or C (Table 4). Figure 4.3 illustrates the regression coefficients with TR for each variable and season-station combination, with dots indicating the significance levels of the regressions.

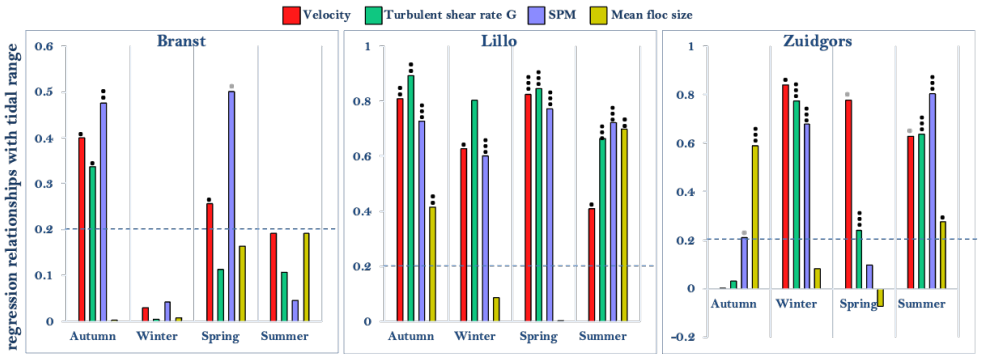

Figure 4.3: The plots show the regression of Velocity, Turbulent Shear Rate (G), SPM Concentration, and Floc Size (D50) against Tidal Range. P-values are reported for regressions with $R^2 > 0.2$ and refer to the statistical significance of the slope coefficient: one dot denotes $p < 0.05$ or near 0.05 (gray dot); two dots denote $p < 0.01$; three dots denote $p < 0.001$. When regression results indicated low $R^2 < 0.2$, RF models were employed to capture the relationships.

At Branst, regression results revealed considerable seasonal variability, with most parameters showing weak correlations with TR during winter and summer (Figure 4.3). In autumn, velocity, SPM concentration, and turbulent shear rate (G) demonstrated moderate relationships with TR

($R^2 > 0.2$), enabling their projection using linear regression (Case A, Table 4). However, floc size exhibited R^2 values below the threshold, necessitating the use of RF models for projection. In this case, velocity, SPM concentration, and G—all with strong R^2 values—were used as inputs alongside TR to predict D50 as the output (Case C, Table 4.1). A similar pattern was observed in spring: velocity and SPM concentration exceeded the R^2 threshold and were projected using linear regression (Case A), while RF models were required for G and D50 (Case C). For these RF models, TR, velocity, and SPM concentration served as inputs to predict both G and D50. In contrast, during winter and summer, none of the parameters achieved an R^2 above 0.2, making it unfeasible to reliably project any variable. These seasons were classified as Case B, where insufficient correlations led to exclusion from further analysis.

At Lillo, consistently strong relationships were observed between TR and the input parameters across most seasons, demonstrating suitability for linear regression-based projections. During autumn and summer, all parameters—velocity, G, SPM concentration, and D50—exhibited R^2 values well above 0.2, classifying these seasons as Case A. This enabled the straightforward application of regression equations to project all input parameters without the need for RF models. In winter and spring, while velocity, G, and SPM concentration maintained strong relationships with TR ($R^2 > 0.2$), floc size fell below the threshold. RF models were employed to project floc size for these seasons, with TR, velocity, SPM concentration, and G serving as inputs (Case C, Table 4).

At Zuidgors, the relationships between TR and the input parameters exhibited considerable seasonal variability, with no season displaying the consistent correlations observed at Lillo. During winter, velocity, G, and SPM concentration showed strong relationships with TR and were projected using linear regression (Case A). However, floc size demonstrated a weak correlation ($R^2 < 0.2$) and was projected using an RF model, with TR, velocity, G, and SPM concentration used as inputs (Case C). In spring, velocity and G retained R^2 values above 0.2 (Case A), while SPM concentration and floc size remained below the threshold and were projected using RF models (Case C), with TR, velocity, and shear rate G as inputs. In contrast, during autumn, velocity and G had R^2 values below 0.2, requiring the use of RF models with floc size and SPM concentration as inputs (Case C). During summer, all parameters—velocity, G, SPM concentration, and floc size—achieved R^2 values well above 0.2, placing the season in Case A.

Table 4.1 Overview of projection methods applied to key sediment parameters by season and station; This table details the projection methods used for key hydrodynamic and sedimentological parameters at different stations and seasons. The applied methods include linear regression for strong correlations ($R^2 > 0.2$) and Random Forest models for complex, weaker relationships ($R^2 < 0.2$), specifying relevant input variables where applicable.

Station	Season	Parameter	R^2	Projection Method	Case	RF Model Inputs (if applicable)
Branst	Autumn	Velocity [m.s^{-1}]	> 0.2	Linear Regression	Case A	N/A
		Turbulent Shear (G) [s^{-1}]	> 0.2	Linear Regression	Case A	N/A
		SPM concentration [mg.l^{-1}]	> 0.2	Linear Regression	Case A	N/A
		Floc Size (D50) [µm]	< 0.2	RF Model	Case C	TR, Velocity, SPM concentration, G
	Winter	All Parameters	< 0.2	No Projection Possible	Case B	N/A
	Spring	Velocity [m.s^{-1}]	> 0.2	Linear Regression	Case A	N/A
		Turbulent Shear (G) [s^{-1}]	< 0.2	RF Model	Case C	TR, Velocity, SPM concentration
		SPM concentration [mg.l^{-1}]	> 0.2	Linear Regression	Case A	N/A
		Floc Size (D50) [µm]	< 0.2	RF Model	Case C	TR, Velocity, SPM concentration
	Summer	All Parameters	< 0.2	No Projection Possible	Case B	N/A
Lillo	Autumn	All Parameters	> 0.2	Linear Regression	Case A	N/A
	Winter	Velocity [m.s^{-1}]	> 0.2	Linear Regression	Case A	N/A
		Turbulent Shear (G) [s^{-1}]	> 0.2	Linear Regression	Case A	N/A
		SPM concentration [mg.l^{-1}]	> 0.2	Linear Regression	Case A	N/A
		Floc Size (D50) [µm]	< 0.2	RF Model	Case C	TR, Velocity, SPM concentration, G
	Spring	Velocity [m.s^{-1}]	> 0.2	Linear Regression	Case A	N/A
		Turbulent Shear (G) [s^{-1}]	> 0.2	Linear Regression	Case A	N/A
		SPM concentration [mg.l^{-1}]	> 0.2	Linear Regression	Case A	N/A
		Floc Size (D50) [µm]	< 0.2	RF Model	Case C	TR, Velocity, SPM concentration, G
	Summer	All Parameters	> 0.2	Linear Regression	Case A	N/A
Zuidgors	Autumn	Velocity [m.s^{-1}]	< 0.2	RF Model	Case C	TR, SPM concentration, D50
		Turbulent Shear (G) [s^{-1}]	< 0.2	RF Model	Case C	TR, SPM concentration, D50
		SPM concentration [mg.l^{-1}]	> 0.2	Linear Regression	Case A	N/A
		Floc Size (D50) [µm]	> 0.2	Linear Regression	Case A	N/A
	Winter	Velocity [m.s^{-1}]	> 0.2	Linear Regression	Case A	N/A
		Turbulent Shear (G) [s^{-1}]	> 0.2	Linear Regression	Case A	N/A
		SPM concentration [mg.l^{-1}]	> 0.2	Linear Regression	Case A	N/A
		Floc Size (D50) [µm]	< 0.2	RF Model	Case C	TR, Velocity, SPM concentration, G
	Spring	Velocity [m.s^{-1}]	> 0.2	Linear Regression	Case A	N/A
		Turbulent Shear (G) [s^{-1}]	> 0.2	Linear Regression	Case A	N/A
		SPM concentration [mg.l^{-1}]	< 0.2	RF Model	Case C	TR, Velocity, G
		Floc Size (D50) [µm]	< 0.2	RF Model	Case C	TR, Velocity, G
	Summer	All Parameters	> 0.2	Linear Regression	Case A	N/A

The process of predicting bed level (BL) changes is carried out using a RF model, which utilizes projected inputs derived from three distinct cases (A, B, and C). These inputs are designed to reflect seasonal and spatial variability across three stations and four seasons, resulting in 12 unique case combinations. For each case, two projection scenarios are applied, generating 24 potential inputs. However, four specific cases—Branst winter and Branst summer—are excluded due to insufficient regression strength, yielding a total of 20 projection scenarios.

For each of scenarios, the input comprises the seasonal average values of five parameters, calculated for the corresponding season-station under plausible future tidal amplification scenarios. For example, in Branst during spring, the SPM concentration value represents the seasonal average and is used as an input for the RF model. Each station-specific RF model predicts an average BL change for the entire season based on these inputs. While intra-seasonal variations are not captured, this approach provides reliable predictions of average seasonal BL changes by leveraging the patterns and dependencies identified during model training.

This methodology ensures that model outputs remain robust, system-specific, and directly tied to seasonal and spatial dynamics, facilitating informed predictions of estuarine responses to future tidal amplifications scenarios. The structure of the dataset used by each RF model is provided in Dataset 4.B.1 (Appendix 4.B).

4.3. Results

As mentioned earlier, tidal range (TR) served as the primary variable for scenario-based projections, with +5% and +10% increases representing plausible future changes. Based on observed correlations, the variables (SPM, D50, G, velocity) were projected using either regression or Random Forest models, depending on their relationship with TR. This approach was grounded in empirical patterns from the 2018–2019 dataset, specifically correlations between TR and input variables, and between those inputs and bed level change (Appendix 4.A). Thus, the projections are not treated as black-box outputs but as extensions of observed sediment behavior under altered tidal conditions.

Figure 4.4 provides a visual synthesis of the predicted bed level change across station–season combinations. The following subsections analyze these projections season by season, comparing future bed level change (relative to present conditions) to the system's existing correlation structure. This approach highlights where model outputs are consistent with process-based expectations, and where they reveal potential shifts in the system's sedimentary behavior under future changes in tidal amplitude. These outcomes are further summarized in Tables 4.2 to 4.5,

which compare the expected sediment trends—based on observed controls such as floc size, SPM, and hydrodynamic conditions—with model projections at each site. This synthesis helps assess where projections align with empirical patterns, and where mismatches or threshold behaviors emerge.

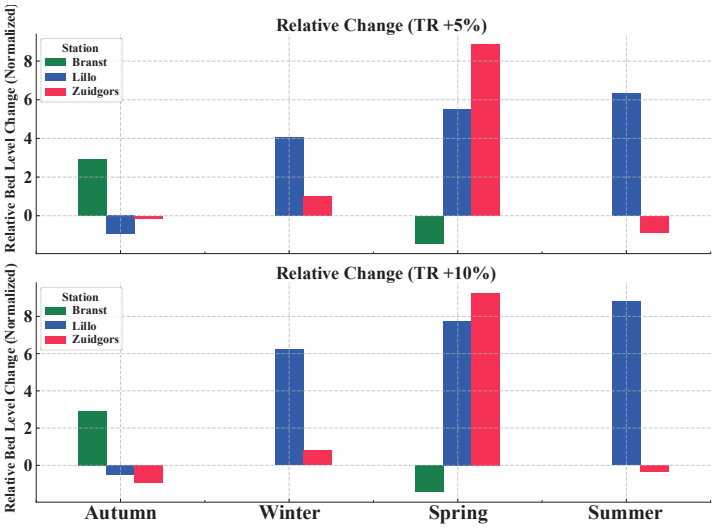

Figure 4.4. Projected relative changes in bed level across seasons and stations under tidal range increases of +5% (top) and +10% (bottom). Tidal amplification does not produce a uniform response across the estuary: Branst shows enhanced deposition in autumn but erosion n in spring; Lillo exhibits consistent sedimentation; Zuidgors alternates between mild erosion and strong accumulation. These patterns highlight the spatial and seasonal variability in sedimentary response, shaped by local differences in floc behavior, sediment availability, and hydrodynamic forcing.

At Branst in autumn, the model projected relative increases in bed level of +2.94 (TR +5%) and +2.91 (TR +10%). This aligns with the positive floc size–bed level correlation ($p < 0.001$), suggesting that flocs enhance sediment retention. Despite negative correlations between TR, velocity, and G with bed level, the model captures a regime where floc cohesion offsets resuspension. Positive TR–SPM and TR–G correlations indicate that increased sediment availability and mixing supported deposition under stable floc conditions.

At Lillo, the model predicted slight relative decreases in bed level (–0.94 at TR +5%; –0.50 at TR +10%). This aligns with the negative correlation between floc size and bed level ($p < 0.001$), implying that flocs are less stable under amplified tidal conditions. While TR, velocity, G, and SPM concentration were all positively correlated with bed level, their combined influence appears

insufficient to counterbalance the destabilization of flocs. The model thus reflects a setting where increased tidal energy reduces retention due to fragile sediment aggregates.

At Zuidgors, the model projected a shift toward relative erosion, with values of –0.15 (TR +5%) and –0.95 (TR +10%), indicating a threshold-like response to tidal amplification. This aligns with the negative TR–bed level correlation, suggesting intensified resuspension under higher energy. Yet, the positive floc size–bed level correlation ($p < 0.001$) indicates that deposition remains possible—if floc cohesion can resist fragmentation.

Table 4.2. Summary of model–observation alignment for autumn bed level projections. For each site, the table summarizes key empirical controls and the expected system response under increased tidal range (TR). The final column evaluates whether model outputs align with those expectations.

Station	Key Observed Relationships	Process-Based Expectation	Model Agreement
Branst	Floc size positively correlated with bed level; TR linked to higher SPM and G	Floc cohesion likely offsets resuspension under higher TR	Moderate deposition
Lillo	Floc size negatively correlated with bed level; TR associated with decreasing D50	Flocs likely destabilize and resuspend under stronger tidal energy	Slight erosion
Zuidgors	Floc size supports deposition; TR negatively correlated with bed level	Stable at moderate TR, but erosion likely under extreme TR due to floc fragmentation	Partial match

In winter, at Branst, no significant correlations were observed between tidal range and any of the key input variables (all $R^2 < 0.2$), including SPM, D50, velocity, and shear rate (G). This may reflect elevated variability or seasonal factors, such as hydrological forcing and biological activity, which may have limited the emergence of consistent TR–input relationships.

At Lillo, the model projected clear relative sedimentation, with predicted increases of +4.05 (TR +5%) and +6.23 (TR +10%). This aligns with strong SPM–bed level correlations and robust TR–SPM and TR–G relationships, indicating that tidal amplification enhanced both sediment supply and turbulence. The absence of a significant relationship between floc size and TR or bed level change further supports a supply-driven response dominated by SPM availability.

At Zuidgors, the model projected a transition from relative erosion to modest deposition, with predicted changes of +0.99 (TR +5%) and +0.79 (TR +10%). These gains align with the positive correlation between floc size and bed level change ($p < 0.001$), indicating that stable flocs support accumulation. However, the weak TR–D50 correlation suggests that accumulation was only maintained under limited turbulence, as reflected in the model's weaker response under higher TR.

Table 4.3. Summary of model–observation alignment for winter bed level projections. For each site, the table summarizes key empirical controls and the expected system response under increased tidal range (TR). The final column evaluates whether model outputs align with those expectations

Station	Key Observed Relationships	Process-Based Expectation	Model Agreement
Branst	No input variable showed significant correlation with TR ($R^2 < 0.2$)	No projection possible	Not modeled
Lillo	SPM positively correlated with bed level; strong TR–SPM and TR–G correlations; D50 not significant	Increased TR enhances sediment supply; system response is supply-driven	Sedimentation
Zuidgors	Floc size and SPM positively correlated with bed level; TR–D50 weak	Conditional sediment gains possible under moderate TR, but limited by turbulence	Modest deposition

In spring, at Branst, the model projected a relative trend toward erosion (approximately −1.44 under both TR scenarios), consistent with process-based expectations. A negative correlation between floc size and bed level change ($p < 0.001$) suggests that larger flocs became unstable under increased tidal energy. Although TR–SPM correlation was moderate and both SPM and velocity were positively correlated with bed level change, the resulting erosion points to the dominant role of floc stability in controlling sediment retention under tidal amplification.

At Lillo, the model projected notable relative sedimentation, with predicted increases of +5.51 (TR +5%) and +7.76 (TR +10%). This outcome aligns with a strong SPM–bed level correlation ($p < 0.001$) and a very strong TR–SPM relationship. The lack of a significant floc size effect further suggests that SPM availability, rather than floc cohesion, was the dominant driver of deposition under tidal amplification.

At Zuidgors, the model projected the highest springtime increase in relative bed level, with values of +8.87 (TR +5%) and +9.27 (TR +10%). This aligns with strong positive correlations between floc size and bed level change, and a strong TR–D50 relationship, suggesting that enhanced floc development and stability may tip the system toward deposition—an outcome the model effectively captured.

Table 4.4. Model–observation alignment for spring bed level projections across the estuary. The table summarizes key empirical controls and the expected sediment response under increased tidal range (TR). The final column evaluates whether model projections reflect these expectations.

Station	Key Observed Relationships	Process-Based Expectation	Model Agreement
Branst	Floc size negatively correlated with bed level; TR moderately increases SPM concentration	Increased TR may destabilize flocs, leading to erosion despite sediment supply	Shift from deposition to erosion
Lillo	SPM strongly correlated with bed level; TR–SPM very strong; floc size uncorrelated	Deposition may be primarily controlled by increased SPM availability	Substantial increase in deposition
Zuidgors	Floc size positively correlated with bed level; TR–D50 strong	Sediment accumulation can be promoted by floc stability and moderate energy	Highest deposition

In summer, as in winter, Branst was excluded from scenario modeling due to the lack of stable, predictive relationships between tidal range and sediment-related variables.

At Lillo, the model projected substantial relative sedimentation, with predicted increases of +6.36 (TR +5%) and +8.80 (TR +10%). These gains are supported by strong positive correlations between SPM and bed level change ($p < 0.001$), and a high TR–SPM relationship, indicating enhanced sediment supply. A strong TR–D50 correlation and a high floc size–bed level correlation further suggest that both floc cohesion and sediment availability contributed to accumulation.

At Zuidgors, slight relative erosion, with values of −0.87 (TR +5%) and −0.33 (TR +10%). This outcome corresponds with negative correlations between bed level change and all key variables—TR, velocity, G, SPM, and floc size. However, a positive TR–D50 correlation indicates that floc size tended to increase with tidal amplification. The combination of these patterns may explain the limited accumulation observed under both TR scenarios.

Table 4.5. Summary of model–observation alignment for summer bed level projections. Each site's observed correlation structure is used to infer the expected sediment response under increased tidal range. The final column evaluates whether the model projections reflect these dynamics.

Station	Key Observed Relationships	Process-Based Expectation	Model Agreement
Branst	No consistent correlation between TR and any input	No projection possible	Not modeled
Lillo	SPM and floc size both increased with TR and bed level	Sedimentation expected	Sedimentation
Zuidgors	all inputs negatively correlated with bed level	possibly erosion due to turbulence	Slight erosion

4.4. Discussion

By applying ML models under two tidal range (TR) increase scenarios—moderate (+5%) and extreme (+10%)—this study explored their potential to simulate sediment dynamics in estuarine intertidal zones. The primary objective was to investigate how well the models capture the behavior of key physical drivers—such as flow velocity, turbulent shear rate, SPM concentration, and floc size—and whether these relationships could be generalized to estimate bed level change across different spatial zones and seasonal conditions.

The outputs provided valuable insights and, in many cases, aligned with recent observational trends (Maris et al., 2024; Scheldecommissie, 2023). However, their interpretation requires caution due to constraints in data availability, assumptions in scenario design, and the complex, nonlinear nature of sediment–floc interactions. Still, this work offers a useful foundation for improving data-driven modeling approaches in estuarine sediment research.

A key finding was that tidal amplification does not yield uniform sediment responses across the estuary. Instead, outcomes varied depending on local hydrodynamic conditions, sediment availability, and seasonal biological activity. The agreement between modeled and observed trends highlights the promise of ML methods for identifying spatial vulnerabilities and dominant drivers of sediment change. However, more extensive long-term datasets are essential to improve model calibration, validate scenario outcomes, and better capture interannual variability.

The following sections evaluate model performance at three representative sites—Branst (freshwater), Lillo (brackish), and Zuidgors (saline)—and assess how seasonal projections compare with short-term field measurements and long-term system trends.

I. Branst [freshwater zone]

At Branst, located in the freshwater zone of the estuary, the machine learning model revealed a distinct seasonal shift in sediment dynamics under projected increases in TR, particularly in spring and autumn. While winter and summer were excluded due to insufficient correlation structure, the modeled seasons clearly indicated that floc characteristics were the dominant control on bed level change, mediating how the system responds even to modest tidal amplification.

In spring, the model projected a reversal from net sedimentation to net erosion under both moderate (+5%) and extreme (+10%) TR scenarios. This outcome aligned with empirical evidence: current observations already show a negative correlation between floc size and bed level change, indicating that flocs in spring are structurally vulnerable to shear forces. As TR increases,

associated turbulence (G) and velocity also rise, amplifying hydrodynamic stress and leading to floc disintegration and resuspension—a well-documented threshold in floc dynamics literature (Dyer & Manning, 1999; Winterwerp, 2002). The model reflects this transition effectively: as energy increases, flocs become smaller and weaker, making them more readily entrained than deposited.

In autumn, by contrast, the model captured positive floc–bed level correlations and projected moderate sedimentation. This pattern reflects a regime where lower hydrodynamic forcing and residual sediment supply support floc formation, aiding deposition. These results demonstrate that Branst functions as an energy-sensitive system, where both sediment availability and floc stability tightly govern sediment behavior.

The modeled seasonal responses are consistent with the historical behavior of the upper estuary, which has long fluctuated between net erosion and deposition due to interactions among river discharge, tidal asymmetry, and sediment supply (Meire et al., 2021; Vandenbruwaene et al., 2020). However, future changes in TR may destabilize this balance. The model's spring projections underscore this vulnerability: as tidal forcing increases, floc cohesion becomes a limiting factor, pushing the system beyond its natural thresholds of sediment accommodation. Even modest TR increases could exacerbate resuspension and trigger longer-term instability in this floc-dominated freshwater zone.

This forward-looking projection was supported by recent observational trends. Monitoring data from 2023 reported a decline in SPM concentrations (Maris et al., 2024) and a slowing of sedimentation rates in the upper estuary (Scheldecommissie, 2023). These findings reinforce the idea that as sediment supply diminished, the potential for floc formation—and thus deposition—also declined. Notably, Branst was historically identified as a naturally self-maintaining channel, with strong ebb-dominant flows that flushed sediment away (Scheldecommissie et al., 2023). Once loose sediment was depleted, erosion slowed because there was no fresh material to replace it. This may have led to a temporary balance in which neither sedimentation nor erosion dominated, and the system remained open yet stable. This case illustrates how floc availability and structural integrity critically determine sediment dynamics—a behavior that the model successfully captured.

II. Lillo [brackish zone]

At Lillo, located in the brackish zone, the model projected increased bed levels under most future scenarios—particularly during winter, spring, and summer—with weaker sedimentation in

autumn. This seasonal variability reflects supply-dominated sediment dynamics, shaped by both natural hydrodynamic processes and human intervention—most notably, continuous dredging carried out to maintain navigational depth.

Correlations calculated in this study showed that SPM concentrations were strongly and positively related to bed level change, alongside a robust relationship between tidal range (TR) and SPM. This indicates that sedimentation at Lillo is increasingly governed by sediment supply rather than sediment cohesion. Historical records support this interpretation: Lillo's channel tends to naturally infill and become shallower over time, a reflection of the system's inherently high SPM concentration (Scheldecommissie et al., 2023). However, to prevent navigational obstruction, this natural infilling is counteracted by frequent dredging, which has intensified over recent decades.

Such continuous dredging can disrupt the natural equilibrium by removing settled sediment, deepening the channel, and modifying near-bed hydrodynamics. Artificially increased water depth can reduce vertical mixing and weaken the flow gradients needed for efficient flocculation, diminishing the role of cohesive flocs in stabilizing the bed. This was evident in the present study: no significant relationships were found between floc size and either TR or bed level change. Instead, SPM concentration near the bed emerged as the most reliable predictor of sedimentation. The ML model captured this shift well, showing that as tidal energy increases, sedimentation no longer peaks in autumn but rather occurs more strongly during winter, spring, and summer, when supply conditions are more favorable.

This model behavior aligns with recent field observations. Since 2019, SPM concentrations at Lillo have gradually declined (Meire et al., 2024), and by 2023, the system began to show signs of stabilization, marked by reduced erosion and a persistent depositional trend (Scheldecommissie, 2023). These patterns suggest that SPM is no longer being continuously resuspended and transported by currents. As resuspension decreases, more sediment remains at the bed, reinforcing the area's inherent depositional tendency. This shift—characterized by lower surface transport, weaker resuspension, and naturally high sediment availability—has likely contributed to reduced net erosion and a gradual movement toward system stabilization.

III. Zuidgors [saline zone]

At Zuidgors, located in the saline zone, the machine learning model projected contrasting seasonal responses to increased tidal range. Spring exhibited the strongest net sedimentation, while autumn and summer showed erosion, and winter presented a more ambiguous response. These

outcomes reflect the site's high-energy, flood-dominant character, where strong tidal currents and persistent sediment redistribution shape bed level dynamics.

Correlation analyses highlighted the complex role of floc size in controlling sedimentation at Zuidgors. The relationship between tidal range (TR) and D50 varied across seasons, reflecting the dynamic response of floc formation to tidal energy. In winter and spring, TR–D50 correlations were weak, suggesting that floc characteristics were not directly modulated by tidal range. However, the positive correlation between floc size and bed level change in these seasons still supported deposition. The model reproduced this behavior, projecting sedimentation during both winter and spring.

In contrast, winter projections revealed some ambiguity. Observations during the measurement period showed erosion, yet the model predicted slight sedimentation. This discrepancy may result from moderate positive correlations between bed level change and variables such as shear rate (G), velocity, SPM, and TR, which likely influenced the model's output. This suggests that while the model reflects general empirical patterns, the system's real-time behavior may be influenced by unmeasured short-term turbulence or may require a longer observational dataset to confirm seasonal stability.

In summer, a similarly complex pattern emerged. TR–D50 correlations were positive, indicating that floc size increased with tidal energy; however, the D50–bed level correlation was negative, suggesting that larger flocs were not structurally stable enough to settle. The model responded accordingly, projecting slight net erosion. Moderate negative correlations between all key variables (SPM, G, velocity) and bed level change further underscore that hydrodynamic forcing exceeded floc cohesion, especially during this biologically favorable season for floc formation. Once again, the short observational window may obscure interannual variability, emphasizing the need for extended datasets.

Moreover, it has been documented that Zuidgors has experienced persistent erosion over recent decades. Although a brief period of sedimentation occurred between 1994 and 2005 due to disposal activity (Elias et al., 2023), erosion resumed afterward and continued through 2020 (Elias et al., 2023). Concurrently, Zuidgors has been naturally deepening over time (Scheldecommissie et al., 2023), coinciding with stable, ongoing dredging activities. This sedimentary behavior indicates that, despite flood-dominant tidal conditions enabling sediment import into the system, the imported sediment tends to accumulate unevenly. Strong tidal currents consistently redistribute sediment, causing localized buildup that necessitates continuous dredging.

The findings of this study reinforce this understanding, demonstrating that the influence of high tidal energy at Zuidgors is substantial, which may limit the extent to which modeled bed level changes reflect actual system behavior. Therefore, they should be interpreted with caution and in the broader context of long-term variability in key model input parameters—such as hydrodynamic forcing, SPM concentration, and floc size—to better capture their influence on sediment dynamics.

4.4.1. Model Strengths and Limitations

Estuarine sediment dynamics involve complex interactions among physical, chemical, and biological processes. Classical physically based numerical models—such as WAQUA-DELWAQ, Delft3D, and SCALDIS—are widely utilized to simulate sediment transport and morphological evolution in estuaries (Vanlede et al., 2015; Plancke & Vos, 2016). These models rely primarily on coupled differential equations and empirical parameterizations grounded in physical principles (Winterwerp, 2002; Vanlede et al., 2015). Despite their broad application, classical models frequently encounter difficulties in accurately representing nonlinear interactions, flocculation processes, and biologically mediated effects. These challenges may become even more complex in the future due to climate change, SLR, and associated increases in tidal range, which necessitate more data-driven approaches capable of capturing multi-parameter interactions and delivering closer predictions of sediment dynamics.

Recognizing these limitations, this study aimed to explore the efficacy of ML models, specifically Random Forest, as complementary, data-driven alternatives for capturing complex sediment dynamics in estuarine intertidal zones. Although ML has been extensively applied in other environmental modeling domains, its application to estuarine sediment transport—particularly in the context of biological and flocculation processes—remains relatively underexplored (Guégan et al., 2019; Zhou et al., 2021). Moreover, the intention was not to replace classical models but rather to leverage ML methods' strengths to enhance scenario-based sensitivity analyses. Specifically, the aim was twofold: (1) to evaluate whether ML models could replicate empirically observed relationships between floc characteristics, hydrodynamic conditions, and bed level change, and (2) to explore whether these models could provide site-specific, interpretable insights into estuarine sediment behavior under future tidal amplification scenarios.

4.4.1.1. Strengths of the Approach

A major strength of the ML approach lies in its ability to capture nonlinear, site-specific, and seasonally dynamic sediment behaviors that are difficult to represent using conventional modeling frameworks. Unlike physically based models that require fixed equations and often simplify flocculation or biological inputs, ML models such as RF can learn complex relationships directly from high-resolution field data. This flexibility allowed for a compound analysis of TR, current velocity, turbulent shear rate (G), SPM concentration, and floc size without imposing assumptions about functional forms or thresholds.

The model captured seasonal and site-specific sediment responses successfully, which were closely aligned with observational and historical records, thus providing confidence in their interpretive value. For example, in Lillo, the models effectively represented sedimentation processes dominated by sediment supply, accurately reflecting inherently high SPM concentrations, as reported by Scheldecommissie (2023) through long-term monitoring and recent field observations. Classical models, by contrast, typically require extensive recalibration through high-resolution data to reflect such shifting dynamics, especially under ongoing dredging interventions.

Moreover, ML models demonstrated their ability to identify threshold transitions—such as the shift from net deposition to erosion at Branst in spring—driven by floc disintegration under increased shear and velocity. These nonlinear shifts are difficult to resolve using fixed erosion/deposition rates but were more effectively captured by data-driven methods like ML models.

Further, RF models provided transparent feature importance analyses, highlighting critical variables such as tidal range and SPM concentration that consistently influenced sediment behavior. This interpretability is particularly valuable for management applications, offering clear, actionable insights into key sediment drivers that traditional modeling approaches often obscure within complex empirical formulations.

Another advantage of the ML approach in this study was its role in projecting input variables, particularly where linear regression failed to capture the complex, nonlinear interactions between TR and certain sediment parameters. For predicting variables with low direct dependency on TR, different RF models were trained when at least three input parameters exhibited strong correlations with TR. This selective application of RF provided two key advantages: first, it minimized overfitting by grounding projections in empirically linked parameters; second, it allowed for more robust projections of variables such as D50 or shear rate (G), whose dynamics are influenced by multiple interacting processes.

4.4.1.2. Limitations and Future Directions

Despite the strengths demonstrated by the ML approach, several limitations constrain the generalizability and predictive certainty of the presented results. Understanding these limitations is essential for interpreting the outcomes of this study and guiding future research and model development.

- **Empirical Nature and Temporal Constraint of Training Data**

A fundamental limitation of the current ML models lies in their reliance on empirical correlations derived from a single year (2018–2019) of field observations. While the dataset is rich in temporal resolution and spans multiple sites and seasons, it nonetheless represents a snapshot of present-day system dynamics. ML models, being data-driven, do not simulate processes from first physical principles but instead extract statistical patterns from the training data. As a result, their capacity to predict sediment behavior under novel or future conditions is inherently limited without retraining on updated datasets.

This limitation becomes particularly evident when the statistical relationships between input variables and bed level change are weak, inconsistent, or nonlinear outside the observed range. The scenario-based projections in this study are contingent on the strength and stability of these empirical correlations. For example, at Zuidgors, the model's projection of slight summer erosion was only partially supported by floc size behavior: the TR–D50 correlation was positive, but the D50–bed level relationship was negative—suggesting floc fragmentation under high turbulence, a nonlinear effect the model could not fully resolve. Similarly, at Branst, while the model captured springtime erosion well, it struggled in winter and summer due to weak inter-variable coherence. These examples highlight the need for caution when interpreting projections in contexts where statistical relationships are unstable or poorly understood mechanistically.

- **Uncertainty in the Assumed Increase in Tidal Range**

Another limitation arises from the assumption that tidal range (TR) will increase in the future. Although many studies support this link—particularly in estuaries undergoing deepening or reduced friction (Pickering et al., 2017; Khojasteh et al., 2021)—tidal responses to future conditions are not universally positive. In some systems, vertical accretion of intertidal flats or increased friction may dampen tidal energy or stabilize the tidal range (Friedrichs et al., 1990). In the Scheldt Estuary, historical observations indicate that TR has increased over time, but this trend

has not been spatially uniform (Barneveld et al., 2018; Scheldecommissie et al., 2023). By 2020, the lower estuary—characterized by a wider and more open morphology—had maintained a relatively stable TR since the 1970s, likely due to effective dissipation of tidal energy. In contrast, the upstream (narrower) section has experienced clear tidal amplification, with increased TR attributed to enhanced tidal propagation inland. These contrasting dynamics justify the use of TR as a projection driver in the upper estuary, though caution is warranted when generalizing this assumption across the entire system. Incorporating insights from morphodynamic simulations or presenting alternative scenarios with constant or damped TR could enhance the robustness of future projections.

- **Limited Scenario Granularity**

This study applied two discrete tidal range increase scenarios (+5% and +10%) to simulate moderate and extreme SLR-driven tidal amplification. While these levels reflect plausible bounds based on previous studies and observed TR changes in the Scheldt and other estuaries, they may not fully capture system sensitivity to incremental changes.

Even when an increase in TR is assumed, uncertainty remains regarding how the system responds to small versus large changes in tidal forcing. Estuarine sediment dynamics are often nonlinear, with abrupt shifts in erosion or deposition triggered by relatively minor changes in hydrodynamic conditions. A finer gradient of scenarios—such as 1%, 2%, 3%, etc.—could reveal inflection points or thresholds in sediment response that remain hidden within broader bracketing scenarios. While increased scenario resolution poses computational and interpretive challenges, it could enhance the robustness of future sensitivity analyses and support more nuanced, risk-informed management strategies.

- **Importance of Additional Environmental Drivers**

The current model includes key physical and sediment-related variables—such as SPM concentration, D50, current velocity, shear rate (G), and tidal range—but excludes environmental parameters like temperature and salinity, which are known to have substantial effects on estuarine sediment dynamics. Salinity affects flocculation by altering particle surface charge interactions and aggregation potential (Van Leussen, 1994), while temperature modulates biological activity, water viscosity, and microbial EPS production—each of which influences sediment cohesion and stability (Winterwerp et al., 2006; Mietta et al., 2009). Their inclusion in future modeling frameworks—alongside more refined projections of tidal energy—could significantly enhance

predictive performance and improve ecological interpretability of results, especially when considering seasonal and salinity-driven sediment variation.

4.5. Conclusion

The Scheldt Estuary has undergone significant transformations in recent decades due to anthropogenic interventions such as dredging, channel deepening, and land reclamation, combined with broader environmental pressures. These changes have altered tidal propagation, increased suspended sediment concentrations, and disrupted the estuary's sediment balance and ecological functioning. Changes in tidal range can intensify hydrodynamic energy within intertidal zones, influencing sediment resuspension, deposition patterns, and the structural stability of flocs. As a result, future shifts in tidal forcing may contribute to increasingly variable sedimentation and erosion dynamics across the estuary.

This chapter explored the potential of ML models to simulate estuarine sediment dynamics under tidal amplification scenarios. The main objective was to investigate how well these models capture the behavior of key physical variables—such as flow velocity, turbulent shear rate, SPM concentration, and floc size—and whether they can reproduce bed level change outcomes that reflect the expected spatial and seasonal variability based on these underlying drivers. In doing so, the analysis aimed to assess the reliability of this data-driven modeling approach for representing estuarine sediment behavior under future changes.

The results demonstrated that estuarine responses to tidal amplification are not uniform, but instead vary by site and season due to local hydrodynamic energy, sediment supply, and floc cohesion. At Branst (freshwater zone), the system showed high sensitivity to seasonal shifts in floc stability and shear stress, with increased tidal range often corresponding to a transition from net deposition to erosion—particularly in conditions where enhanced turbulence inhibited floc formation, such as in spring. At Lillo (brackish zone), sedimentation remained stable or increased under future scenarios, consistent with the site's strong TR–SPM correlations and supply-dominated sediment dynamics. At Zuidgors (saline zone), model results were more variable, with erosion prevailing during high-energy periods and floc-based sedimentation limited by turbulence—even when larger flocs were present. These outcomes reinforce that sediment behavior is strongly governed by both energy regimes and the structural integrity of flocs.

Importantly, the models captured key trends observed in recent field studies, but projections should be interpreted with caution given the limited temporal scope of input data and the absence of future validation datasets. While ML methods effectively characterized empirical sediment

behavior across diverse estuarine conditions, their application in predictive forecasting remains constrained by system complexity and data limitations.

In summary, this study highlights the value of integrating high-resolution field observations with data-driven modeling to investigate site-specific sediment responses under plausible future tidal conditions. While further refinement—such as the inclusion of long-term monitoring—is necessary to enhance model robustness, the results demonstrate the potential of machine learning approaches for advancing the understanding of estuarine sediment dynamics. As climate change continues to impact estuarine systems and their behavior becomes increasingly complex, maintaining system resilience will require more integrated, data-driven strategies that account for both natural variability and human influences.

Appendix 4.A: Measurement Periods

This appendix supplements Chapter 4 by presenting the full set of regression models linking tidal range to seasonal variability in key environmental parameters—velocity, turbulent shear rate (G), SPM concentration, and floc size (D50)—at the three intertidal monitoring stations: Branst (freshwater), Lillo (brackish), and Zuidgors (saline). For each station, regression outputs are presented for all four seasons (autumn, winter, spring, and summer) in a single composite table.

Each table contains the following information:

- **Regression equations** describing each environmental parameter as a function of tidal range.
- **Coefficient of determination (R^2)**, indicating the proportion of variability explained by the regression model.
- **Statistical significance** (p-values for both intercept and slope) to evaluate the reliability of regression parameters.
- **Correlation values** between each environmental parameter and observed bed level change under current conditions.
- **Parameter predictions** (velocity, turbulent shear rate (G), SPM concentration, and D50) under current tidal conditions, and for two scenario-based increases in tidal range (moderate and extreme), illustrating potential responses to changing tidal dynamics.
- **Bed level (BL) predictions** (where available), derived from modeled parameter values to indicate possible morphological responses.

Regression-based projections were applied where correlations with tidal range were sufficiently strong, whereas supplementary modeling (e.g., Random Forest) was used in cases with weaker correlations. These data support the scenario analysis in Chapter 4 by providing detailed insight into how sediment-related parameters respond to varying tidal forcing at each station.

The following tables (Table 4.A.1 to Table 4.A.3) present all seasonal regressions and scenario-based predictions for Branst, Lillo, and Zuidgors, respectively

Table 4.A.1: Seasonal Regression Models – Branst Station (Freshwater Zone)

Autumn	Equation (vs. TR)		p(a), p(b)	Correlation with bed level	current average	moderate scenarios	extreme scenarios
tidal range (m)	tidal range=tr	R2=1.00	-	-0.39	5.53	5.81	6.08
Velocity (m.s^{-1})	velocity=−0.0042+0.030×tr	R2=0.39	<0.05, <0.001	-0.25	0.16	0.17	0.18
G (s^{-1})	G=−0.14593+0.0913×tr	R2=0.33	<0.05, <0.001	-0.53	0.36	0.38	0.41
SPM concentration (mg.l^{-1})	SPM=−27.67+50.24×tr	R2=0.47	<0.05, <0.001	0.08	242.61	264.14	278.03
D50 (µm)	D50=143.912+1.506×tr	R2=0.002	-	0.21	151.32	85.90	86.56
BL Predictions (mm)	-		-	-	12.1	47.7	47.29
Winter	**Equation (vs. TR)**		**p(a), p(b)**	**Correlation with bed level**	**current average**	**moderate scenarios**	**extreme scenarios**
tidal range (m)	tidal range=tr	R2=1.00	-	0.29	5.56	5.84	6.12
Velocity (m.s^{-1})	velocity=0.277−0.0104×tr	R2=0.03	-	-0.36	0.22	0.22	0.21
G (s^{-1})	G=0.667+0.037×tr	R2=0.005	-	0.22	0.87	0.89	0.90
SPM concentration (mg.l^{-1})	SPM=454.30−16.85×tr	R2=0.04	-	0.22	356.63	355.90	351.22
D50 (µm)	D50=166.655−5.686×tr	R2=0.007	-	-0.36	132.41	133.45	131.87
BL Predictions (mm)	-		-	-	-	-	-
Spring	**Equation (vs. TR)**		**p(a), p(b)**	**Correlation with bed level**	**current average**	**moderate scenarios**	**extreme scenarios**
tidal range (m)	tidal range=tr	R2=1	-	0.04	5.61	5.89	6.17
Velocity (m.s^{-1})	velocity=0.20+0.0173×tr	R2=0.26	<0.05, <0.001	0.81	0.30	0.30	0.31
G (s^{-1})	G=0.938−0.06361×tr	R2=0.11	-	-0.12	0.57	0.97	0.98
SPM concentration (mg.l^{-1})	SPM=−99.03+60.05×tr	R2=0.50	0.073, <0.001	0.48	233.10	254.59	271.43
D50 (µm)	D50=−12.37+28.26×tr	R2=0.16	-	-0.54	135.46	105.53	105.53
BL Predictions (mm)	-		-	-	32.5	-14.428	-14.421
Summer	**Equation (vs. TR)**		**p(a), p(b)**	**Correlation with bed level**	**current average**	**moderate scenarios**	**extreme scenarios**
tidal range (m)	tidal range=tr	R2=1.00	-	0.58	5.66	5.95	6.23
Velocity (m.s^{-1})	velocity=0.0214+0.0348×tr	R2=0.19	-	0.10	0.21	0.23	0.24
G (s^{-1})	G=0.069+0.060×tr	R2=0.11	-	0.22	0.41	0.43	0.45
SPM concentration (mg.l^{-1})	SPM=109.411+5.905×tr	R2=0.04	-	0.36	142.90	144.52	146.19
D50 (µm)	D50=59.847+15.61×tr	R2=0.19	-	0.12	146.18	152.67	157.10
BL Predictions (mm)	-		-	-	-	-	-

Table 4.A.2: Seasonal Regression Models – Lillo Station (Brackish Zone)

Autumn	Equation (vs. TR)		p(a), p(b)	Correlation with bed level	current average	moderate scenarios	extreme scenarios
tidal range (m)	tidal range=tr	R2=1.00	-	0.32	5.31	5.58	5.84
Velocity (m.s^{-1})	velocity=−0.049+0.048×tr	R2=0.81	0.011, <0.001	0.50	0.21	0.22	0.23
G (s^{-1})	G=−1.135+0.398×tr	R2=0.89	0.001, <0.001	0.46	1.01	1.09	1.19
SPM concentration (mg.l^{-1})	SPM=−233.20+102.59×tr	R2=0.73	<0.001, <0.001	0.48	313.82	338.82	366.06
D50 (µm)	D50=184.75−12.50×tr	R2=0.41	0.001, <0.001	-0.48	118.30	115.04	111.72
BL Predictions (mm)	-		-	-	18.4	1.2	9.2
Winter	**Equation (vs. TR)**		**p(a), p(b)**	**Correlation with bed level**	**current average**	**moderate scenarios**	**extreme scenarios**
tidal range (m)	tidal range=tr	R2=1.00	-	0.79	5.39	5.66	5.93
Velocity (m.s^{-1})	velocity=−0.072+0.057×tr	R2=0.63	0.054, <0.001	0.72	0.22	0.25	0.27
G (s^{-1})	G=−1.89+0.54×tr	R2=0.80	0.001, <0.001	0.69	0.93	1.18	1.33
SPM concentration (mg.l^{-1})	SPM=−353.76+116.76×tr	R2=0.60	<0.001, <0.001	0.74	253.67	306.62	338.07
D50 (µm)	D50=177.31−9.55×tr	R2=0.087	-	-0.06	127.60	92.20	99.12
BL Predictions (mm)	-		-	-	1.3	6.7	9.6
Spring	**Equation (vs. TR)**		**p(a), p(b)**	**Correlation with bed level**	**current average**	**moderate scenarios**	**extreme scenarios**
tidal range (m)	tidal range=tr	R2=1	-	-0.78	4.63	4.86	5.09
Velocity (m.s^{-1})	velocity=−0.215+0.11×tr	R2=0.78	0.054, <0.001	-0.83	0.30	0.32	0.35
G (s^{-1})	G=0.8274+0.2687×tr	R2=0.24	0.001, <0.001	-0.23	2.06	2.13	2.20
SPM concentration (mg.l^{-1})	SPM=56.06+154.21×tr	R2=0.098	-	-0.40	779.13	329.22	309.22
D50 (µm)	D50=144.48+0.082×tr	R2=-0.071	-	0.31	143.39	155.97	159.97
BL Predictions (mm)	-		-	-	0.63	6.22	6.47
Summer	**Equation (vs. TR)**		**p(a), p(b)**	**Correlation with bed level**	**current average**	**moderate scenarios**	**extreme scenarios**
tidal range (m)	tidal range=tr	R2=1.00	-	0.63	5.41	5.68	5.95
Velocity (m.s^{-1})	Velocity=0.086+0.023×tr	R2=0.41	0.054, <0.001	0.07	0.21	0.22	0.22
G (s^{-1})	G=−0.38+0.198×tr	R2=0.66	<0.001, <0.001	0.38	0.70	0.74	0.79
SPM concentration (mg.l^{-1})	SPM=−117.08+61.30×tr	R2=0.72	<0.001, <0.001	0.56	215.00	231.13	247.71
D50 (µm)	D50=−457.92+128.74×tr	R2=0.70	0.001, <0.001	0.89	175.80	273.32	308.14
BL Predictions (mm)	-		-	-	-1.5	8.035	11.7

Table 4.A.3: Seasonal Regression Models – Zuidgors Station (Saline Zone)

Autumn	Equation (vs. TR)		p(a), p(b)	Correlation with bed level	current average	moderate scenarios	extreme scenarios
tidal range (m)	tidal range=tr	R2=1.00	-	-0.95	4.56	4.79	5.02
Velocity (m.s^{-1})	velocity=0.24+0.0023×tr	R2=0.0003	-	-0.24	0.24	0.50	0.51
G (s^{-1})	G=2.13−0.27×tr	R2=0.031	-	-0.06	0.98	2.60	2.68
SPM concentration (mg.l^{-1})	SPM=−45.27+96.69×tr	R2=0.21	0.179, <0.001	-0.58	386.60	417.77	439.81
D50 (µm)	D50=358.68−45.79×tr	R2=0.59	0.001, <0.001	0.59	144.30	139.40	128.96
BL Predictions (mm)	-		-	-	5.20	4.40	0.25
Winter	**Equation (vs. TR)**		**p(a), p(b)**	**Correlation with bed level**	**current average**	**moderate scenarios**	**extreme scenarios**
tidal range (m)	tidal range=tr	R2=1.00	-	0.80	4.59	4.82	5.05
Velocity (m.s^{-1})	velocity=−0.12+0.088×tr	R2=0.84	0.04, <0.001	0.71	0.29	0.31	0.33
G (s^{-1})	G=−1.42+0.66×tr	R2=0.77	0.001, <0.001	0.68	1.65	1.76	1.92
SPM concentration (mg.l^{-1})	SPM=−462.28+188.21×tr	R2=0.68	<0.001, <0.001	0.74	405.35	445.19	488.40
D50 (µm)	D50=49.12+13.49×tr	R2=0.084	-	0.45	108.98	141.00	141.00
BL Predictions (mm)	-		-	-	-30	-0.21	-6.21
Spring	**Equation (vs. TR)**		**p(a), p(b)**	**Correlation with bed level**	**current average**	**moderate scenarios**	**extreme scenarios**
tidal range (m)	tidal range=tr	R2=1.00	-	0.79	5.46	5.73	6.01
Velocity (m.s^{-1})	velocity=−0.026+0.045×tr	R2=0.82	<0.001, <0.001	0.72	0.21	0.23	0.25
G (s^{-1})	G=−0.711+0.296×tr	R2=0.84	<0.001, <0.001	0.72	0.85	0.99	1.07
SPM concentration (mg.l^{-1})	SPM=−352.77+112.17×tr	R2=0.77	<0.001, <0.001	0.63	239.16	290.30	320.92
D50 (µm)	D50=156.54−1.60×tr	R2=0.003	-	-0.03	145.49	115.94	119.96
BL Predictions (mm)	-		-	-	1.70	11.10	14.90
Summer	**Equation (vs. TR)**		**p(a), p(b)**	**Correlation with bed level**	**current average**	**moderate scenarios**	**extreme scenarios**
tidal range (m)	tidal range=tr	R2=1.00	-	-0.42	4.62	4.85	5.08
Velocity (m.s^{-1})	velocity=0.099+0.041×tr	R2=0.637	0.055, <0.001	-0.39	0.30	0.30	0.31
G (s^{-1})	G=−0.12+0.28×tr	R2=0.64	0.001, <0.001	-0.18	1.27	1.26	1.33
SPM concentration (mg.l^{-1})	SPM=−936.53+312.93×tr	R2=0.80	<0.001, <0.001	-0.21	548.65	580.06	652.28
D50 (µm)	D50=49.78+23.35×tr	R2=0.28	0.029, <0.001	-0.23	159.78	162.94	168.33
BL Predictions (mm)	-		-	-	42.20	5.48	28.28

Appendix 4.B: Datasets Utilized in Chapter 4

Dataset 4.B.1: Measurements for Branst, Lillo, and Zuidgors Stations with Detailed Data Per Station

D50 (µm)	**SPM concentration ($mg.l^{-1}$)**	**Velocity ($m.s^{-1}$)**	**Tidal Range (m)**	**G (s^{-1})**
Datapoints representing measurements for only one of the 3 stations (Branst: approx. 0.7M, Lillo: approx. 0.8M, Zuidgors: approx. 0.4M), across all stations-seasons, interpolated to high frequency using the interpolation function described above.				

Bibliography

1. Alongi, D. M. (2018). *Blue carbon: Coastal sequestration for climate change mitigation* (pp. 23-36). Cham, Switzerland: Springer.
2. Barneveld, H., R. Nicolai, M. van Veen, S. van Haaster, T. Boudewijn, J. de Jong, K. van Didderen et al. "*Analyserapport: T2015-rapportage Schelde-estuarium*." Report PR3152. HKV Lijn in Water (Lelystad) 886 (2018).
3. Bi, Q., & Toorman, E. A. (2015). *Mixed-sediment transport modelling in Scheldt estuary with a physics-based bottom friction law*. Ocean Dynamics, 65, 555-587.
4. Boelens, T., Schuttelaars, H., Plancke, Y., & De Mulder, T. (2020). *Historical and future development of the tidally averaged transport of sandy sediments in the Scheldt estuary: a 2D exploratory model.* Ocean Dynamics, 70, 481-504.
5. Chen, M. S., Wartel, S., & Temmerman, S. (2005). *Seasonal variation of floc characteristics on tidal flats, the Scheldt estuary*. Hydrobiologia, 540, 181-195.
6. Chu, A., Wang, Z., & De Vriend, H. J. (2015). *Analysis on residual coarse sediment transport in estuaries*. Estuarine, Coastal and Shelf Science, 163, 194-205.
7. Coen, I. (2008). *De eeuwige Schelde? Ontstaan en ontwikkeling van de Schelde*. Technical Report D/2007/3241/203, waterbouwkundig laboratorium.
8. Cox, T. J. S., Maris, T., Van Engeland, T., Soetaert, K., & Meire, P. (2019). *Critical transitions in suspended sediment dynamics in a temperate meso-tidal estuary*. Scientific reports, 9(1), 12745.
9. Dam, G., Van der Wegen, M., Taal, M., & Van der Spek, A. (2022). *Contrasting behaviour of sand and mud in a long-term sediment budget of the Western Scheldt estuary*. Sedimentology, 69(5), 2267-2283.
10. de Lucas Pardo, M. A., Sarpe, D., & Winterwerp, J. C. (2015). *Effect of algae on flocculation of suspended bed sediments in a large shallow lake*. Consequences for ecology and sediment transport processes. Ocean Dynamics, 65, 889-903.
11. Depreiter, D., Cleveringa, J., van der Laan, T., Maris, T., Ysebaert, T., & Wijnhoven, S. *Nota evaluatie van de Evaluatiemethodiek*. T2009 rapportage Schelde-estuarium.
12. Dijkstra, Y. M., Schuttelaars, H. M., & Schramkowski, G. P. (2019). *A regime shift from low to high sediment concentrations in a tide-dominated estuary*. Geophysical Research Letters, 46(8), 4338-4345.
13. Dyer, K. R., & Manning, A. J. (1999). *Observation of the size, settling velocity and effective density of flocs, and their fractal dimensions*. Journal of sea research, 41(1-2), 87-95.
14. Edzwald, J. K., Upchurch, J. B., & O'Melia, C. R. (1974). *Coagulation in estuaries*. Environmental Science & Technology, 8(1), 58-63.
15. Eisma, D., Kalf, J., & Veenhuis, M. (1980). *The formation of small particles and aggregates in the Rhine estuary*. Netherlands Journal of Sea Research, 14(2), 172-191.
16. Engel, P. A. (2009). *Spatial and temporal variability of tide-induced salt flux in a partially mixed estuary* (Doctoral dissertation, Massachusetts Institute of Technology).

17. Fettweis, J. M., Serrano, M. G., Brooks, J. P., Edwards, D. J., Girerd, P. H., Parikh, H. I., ... & Buck, G. A. (2019). *The vaginal microbiome and preterm birth*. Nature medicine, 25(6), 1012-1021.
18. Fettweis, M., Baeye, M., Van der Zande, D., Van den Eynde, D., & Joon Lee, B. (2014). *Seasonality of floc strength in the southern North Sea*. Journal of Geophysical Research: Oceans, 119(3), 1911-1926.
19. Fettweis, M., Schartau, M., Desmit, X., Lee, B. J., Terseleer, N., Van der Zande, D., ... & Riethmüller, R. (2022). *Organic matter composition of biomineral flocs and its influence on suspended particulate matter dynamics along a nearshore to offshore transect*. Journal of Geophysical Research: Biogeosciences, 127(1), e2021JG006332.
20. FitzGerald, D. M., Fenster, M. S., Argow, B. A., & Buynevich, I. V. (2008). *Coastal impacts due to sea-level rise*. Annu. Rev. Earth Planet. Sci., 36, 601-647.
21. Friedrichs, C. T., Aubrey, D. G., & Speer, P. E. (1990). *Impacts of relative sea-level rise on evolution of shallow estuaries*. Residual currents and long-term transport, 105-122.
22. Haigh, I. D. (2017). *Tides and water levels*. Encyclopedia of Maritime and Offshore Engineering, 1-13.
23. Horemans, D. M., Dijkstra, Y. M., Schuttelaars, H. M., Sabbe, K., Vyverman, W., Meire, P., & Cox, T. J. (2021). *Seasonal variations in flocculation and erosion affecting the large-scale suspended sediment distribution in the Scheldt estuary: the importance of biotic effects*. Journal of Geophysical Research: Oceans, 126(4), e2020JC016805.
24. Horemans, D. M., Meire, P., & Cox, T. J. (2020). *The impact of temporal variability in light-climate on time-averaged primary production and a phytoplankton bloom in a well-mixed estuary*. Ecological modelling, 436, 109287.
25. Jiang, L., Gerkema, T., Idier, D., Slangen, A., & Soetaert, K. (2020). *Effects of sea-level rise on tides and sediment dynamics in a Dutch tidal bay*. Ocean Science, 16(2), 307-321.
26. Khojasteh, D., Hottinger, S., Felder, S., De Cesare, G., Heimhuber, V., Hanslow, D. J., & Glamore, W. (2020). *Estuarine tidal response to sea level rise: The significance of entrance restriction*. Estuarine, Coastal and Shelf Science, 244, 106941.
27. Kirwan, M. L., Walters, D. C., Reay, W. G., & Carr, J. A. (2016). *Sea level driven marsh expansion in a coupled model of marsh erosion and migration*. Geophysical Research Letters, 43(9), 4366-4373.
28. Legendre, P., & Legendre, L. (2012). Numerical ecology (Vol. 24). Elsevier.
29. Leuven, J. R., Pierik, H. J., Vegt, M. V. D., Bouma, T. J., & Kleinhans, M. G. (2019). *Sea-level-rise-induced threats depend on the size of tide-influenced estuaries worldwide*. Nature Climate Change, 9(12), 986-992.
30. Maggi, F. (2007). *Variable fractal dimension: A major control for floc structure and flocculation kinematics of suspended cohesive sediment*. Journal of Geophysical Research: Oceans, 112(C7).
31. Manh, N. V., Dung, N. V., Hung, N. N., Merz, B., & Apel, H. (2014). *Large-scale suspended sediment transport and sediment deposition in the Mekong Delta*. Hydrology and Earth System Sciences, 18(8), 3033-3053.
32. Manning, A. J., & Schoellhamer, D. H. (2013). *Factors controlling floc settling velocity along a longitudinal estuarine transect*. Marine Geology, 345, 266-280.

33. Maris, T., P. Gelsomini & J. Schoelynck, 2024. *Onderzoek naar de gevolgen van het Sigmaplan, baggeractiviteiten en havenuitbreiding in de Zeeschelde op het milieu*. Geïntegreerd eindverslag van het onderzoek verricht in 2023. ECOSPHERE 024-RES023. Universiteit Antwerpen, Antwerpen.
34. Meire, P., Plancke, Y., Govaerts, A., Cox, T., Gelsomi, P., Horemans, D., Meire, D., Meire, L., Zetsche, E. and Maris,T. (2021). *Synthesis note: SPM dynamics and trends in the Scheldt estuary*. ECOBE Report 021-R267 Universiteit Antwerpen, Antwerpen.
35. Meire, P., Ysebaert, T., Damme, S. V., Bergh, E. V. D., Maris, T., & Struyf, E. (2005). *The Scheldt estuary: a description of a changing ecosystem*. Hydrobiologia, 540, 1-11.
36. Mietta, F. (2010). *Evolution of the floc size distribution of cohesive sediments*.
37. Partheniades, E. (1993). *Turbulence, flocculation and cohesive sediment dynamics*. Nearshore and estuarine cohesive sediment transport, 42, 40-59.
38. Passow, U. (2002). *Transparent exopolymer particles (TEP) in aquatic environments*. Progress in oceanography, 55(3-4), 287-333.
39. Passow, U., & De La Rocha, C. L. (2006). *Accumulation of mineral ballast on organic aggregates*. Global Biogeochemical Cycles, 20(1).
40. Pickering, M. D., Horsburgh, K. J., Blundell, J. R., Hirschi, J. M., Nicholls, R. J., Verlaan, M., & Wells, N. C. (2017). *The impact of future sea-level rise on the global tides*. Continental Shelf Research, 142, 50-68.
41. Plancke, Y. M. G., Vandebroek, E., Claeys, S., & Meire, D. (2017). *Sediment transport in the Schelde-estuary: The challenge of performing good measurements in challenging conditions*. Hydraulic Measurements and Experimental Methods 2017 Conference (HMEM 2017.
42. Quinn, G. P., & Keough, M. J. (2002). *Experimental design and data analysis for biologists*. Cambridge university press.
43. Rios-Yunes, D., Tiano, J. C., van Rijswijk, P., De Borger, E., van Oevelen, D., & Soetaert, K. (2023). *Long-term changes in ecosystem functioning of a coastal bay expected from a shifting balance between intertidal and subtidal habitats*. Continental Shelf Research, 254, 104904.
44. Sequoia Scienti_c. (Sequoia Scientific. 2010). *How to compute the mean particle diameter from a LISST volume distribution*. Sequoia Scienti_c. ([Available online at http://www.sequoiasci.com/article/how-to-compute-the-mean-particle-diameter-from-a-lisst-volume-distribution-2/).
45. Temmerman, S., Govers, G., Wartel, S., & Meire, P. (2004). *Modelling estuarine variations in tidal marsh sedimentation: response to changing sea level and suspended sediment concentrations*. Marine Geology, 212(1-4), 1-19.
46. TOEGANKELIJKHEID, L. V. E. (2014*). ECOTOPEN IN DE WESTERSCHELDE*.
47. Van de Broek, M., Vandendriessche, C., Poppelmonde, D., Merckx, R., Temmerman, S., & Govers, G. (2018). *Long-term organic carbon sequestration in tidal marsh sediments is dominated by old-aged allochthonous inputs in a macrotidal estuary*. Global change biology, 24(6), 2498-2512.

48. Van Manh, N., Dung, N. V., Hung, N. N., Kummu, M., Merz, B., & Apel, H. (2015). *Future sediment dynamics in the Mekong Delta floodplains: Impacts of hydropower development, climate change and sea level rise*. Global and Planetary Change, 127, 22-33.
49. Van Putte, N., Cox, T., Van Damme, S., & Maris, T. (2022). *IMMERSE: Modelling study on sediment management in estuaries*. Universiteit Antwerpen, Report, 3.
50. van Rijn, L., Grasmeijer, B., & Perk, L. (2018). *Effect of channel deepening on tidal flow and sediment transport: part I—sandy channels*. Ocean Dynamics, 68(11), 1457-1479.
51. Vandenbruwaene, W., Levy, Y., Plancke, Y., Vanlede, J., Verwaest, T., & Mostaert, F. (2017). *Integraal plan Boven-Zeeschelde: deelrapport 8*. Sedimentbalans Zeeschelde, Rupel en Durme. WL Rapporten.
52. Vandenbruwaene, W., Stark, J., Plancke, Y., & Mostaert, F. (2020). *Agenda for the Future–Historical evolution of tides and morphology of the Scheldt estuary: subreport 5*. Synthesis. WL Reports.
53. Verney, R., Lafite, R., & Brun-Cottan, J. C. (2009). *Flocculation potential of estuarine particles: The importance of environmental factors and of the spatial and seasonal variability of suspended particulate matter*. Estuaries and coasts, 32, 678-693.
54. Wang, Z. B., Vandenbruwaene, W., Taal, M., & Winterwerp, H. (2019). *Amplification and deformation of tidal wave in the Upper Scheldt Estuary*. Ocean Dynamics, 69, 829-839.
55. Waterinfo.be (cited 2019). *Measurements and predictions of Waterinfo.be [data]*. [Available online at https://www.waterinfo.be/].
56. Winterwerp, J. C., & Van Kesteren, W. G. (2004). *Introduction to the physics of cohesive sediment dynamics in the marine environment*. Elsevier.
57. Winterwerp, J. C., Wang, Z. B., Van Braeckel, A., Van Holland, G., & Kösters, F. (2013). *Man-induced regime shifts in small estuaries—II: a comparison of rivers*. Ocean Dynamics, 63, 1293-1306.
58. Wolff, W. J. (2005). *The exploitation of living resources in the Dutch Wadden Sea: a historical overview*. Helgoland Marine Research, 59, 31-38.

Chapter 5

Conclusion

In this thesis, the aim was to understand the role of the Scheldt estuary's intertidal areas as accommodation space for suspended sediment. The Scheldt estuary is an important ecosystem and economic waterway. With strong tidal forces and relatively small freshwater discharge, it supports a diverse range of species in a well-mixed environment (Meire et al., 2005). Over the past decades, the estuary has undergone significant changes due to both human interventions—such as dredging, land reclamation, and deepening of navigation channels—and sea-level rise (SLR) (Van Putte et al., 2022). These modifications have affected tidal dynamics, altered sediment transport, and led to elevated concentrations of suspended particulate matter (SPM). Annually, SPM loads at the upstream boundary of the estuary range from 10^4 to 10^5 tons, correlating with freshwater discharge (Plancke et al., 2017; Dijkstra et al., 2019).

Dredging activities, necessary to maintain shipping access to the Port of Antwerp, have deepened tidal channels and reduced intertidal zones. These changes disrupt natural sedimentation patterns, affecting habitats for benthic organisms and migratory birds (Meire et al., 2005; Winterwerp et al., 2013; Dam et al., 2022). Between 2018 and 2019, around 9.3 Mm^3/year of sediment was dredged in the Western Scheldt. Sediment budget studies also estimated a net import of 0.609 Mm^3/year of sand into the Sea Scheldt from the Western Scheldt, reflecting its sandy nature (Cleveringa, 2013; Vandenbruwaene et al., 2017). In the Lower Sea Scheldt, about 4.7 Mm^3/year of sediment was dredged during 2018–2019, including 3.4 Mm^3/year of mud, emphasizing its muddy character. The reintroduction of dredged material, particularly fine sediments, back into the estuary has increased SPM loads (Cox et al., 2019; Dam et al., 2016; Dijkstra et al., 2019).

This accumulation of SPM, influenced by dredging and low freshwater discharge, was found to have raised turbidity levels, creating persistent challenges for water quality and sediment balance (Fettweis et al., 2019; Maris et al., 2024). Additionally, the maximum turbidity zone (MTZ), where sediments tend to accumulate, was likely expanded due to dredging. Typically, the MTZ shifted seasonally, moving toward the saltwater zone in winter and the freshwater zone in summer, but its movement became more unpredictable in recent years (Cox et al., 2019).

The estuary experienced a consistent increase in tidal range in recent decades, with measurements showing higher high-water levels and lower low-water levels, especially in the Upper Sea Scheldt (Coen, 2008; Vandenbruwaene et al., 2020; Barneveld et al., 2018). These changes were suggested to have intensified hydrodynamic processes and altered tidal asymmetry, while an increased tidal range resulting from these changes was found to influence shifts between flood and ebb dominance. Such shifts depended on a complex interplay of factors, including sediment

availability, channel morphology, and intertidal area dynamics (Jiang et al., 2020; Van der Wegen et al., 2022).

In the Scheldt estuary, these global trends were evident. Rising sea levels inundated intertidal zones (Van der Wegen et al., 2022), while dredging, land reclamation, and channel deepening altered tidal dynamics and sediment balance (Van Rijn et al., 2018; Cox et al., 2019; Dijkstra et al., 2019; Boelens et al., 2020). Together, these changes pointed to a potential shift toward ebb dominance under future sea-level rise. This shift was expected to increase the estuary's sensitivity to river discharge fluctuations and reduce its capacity for sediment retention (Jiang et al., 2020; Meire et al., 2021). As a result, the estuary faced heightened risks of sediment erosion and reduced deposition, compounded by elevated turbulence and SPM levels. These conditions posed significant ecological threats, including reduced light penetration, degraded water quality, and adverse impacts on aquatic habitats and biodiversity (Cox et al., 2019; Dijkstra et al., 2019).

Given the estuary's ongoing sedimentation challenges, intertidal areas were recognized as crucial natural buffers for suspended sediments. They helped trap and stabilize sediments through processes such as flocculation and deposition (Ysebaert et al., 2002; Temmerman et al., 2013). These zones not only supported diverse ecosystems but also contributed to carbon sequestration, linking local ecological processes to global climate change mitigation (Chmura et al., 2003). Studying the intertidal areas provided insights into the estuary's capacity to accommodate rising SPM levels while preserving ecological balance. With the potential for the Scheldt estuary to shift toward a hyperturbid state, similar to the Ems estuary—where excessive sediment loads caused reduced light penetration and oxygen levels, harming aquatic life (De Jonge et al., 2014)—it was deemed essential to investigate the factors influencing sediment deposition and resuspension in the Scheldt's intertidal zones.

This thesis examined how hydrodynamic forces, flocculation dynamics, and SPM concentrations influenced sediment stability, as understanding these processes was considered key to addressing the estuary's sediment challenges and ensuring ecological resilience (Winterwerp & Van Kesteren, 2004; Fettweis et al., 2014; Horemans et al., 2021). To achieve these objectives, in situ observations were analyzed, collected during two weeks per season over the course of one year, to identify the key drivers of deposition-resuspension processes. A predictive machine learning model was developed to enhance understanding of sedimentation and erosion, and the model was applied to scenarios involving SLR to predict future bed level changes.

Figure 5.1 below repeated the outline of this thesis from Chapter 1 and presented the conclusions of the three main research questions in the following sections, each of which corresponded to one of the preceding chapters in this thesis.

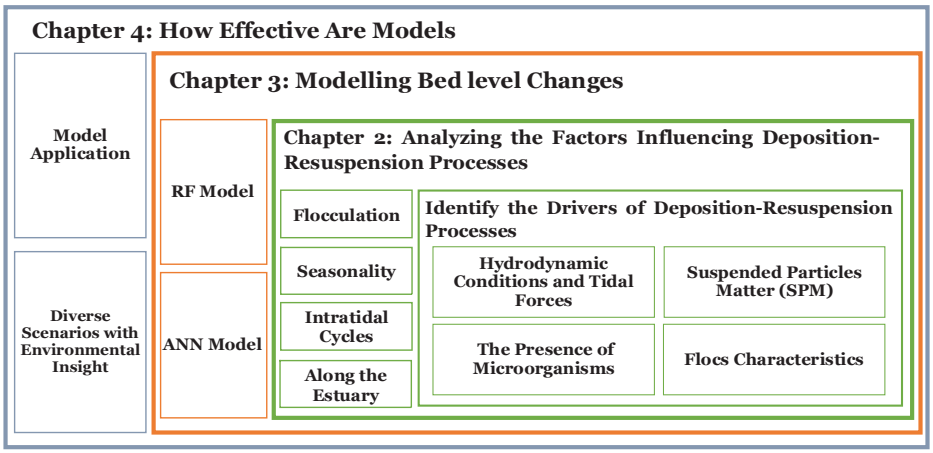

Figure 5.1: An overview of this thesis's structure exploring sediment dynamics in the Scheldt estuary. In Chapter 2, we investigated the drivers of deposition-resuspension processes in intertidal areas, examining how hydrodynamic forces, floc characteristics, and SPM concentrations influences sediment dynamics, considering seasonal, temporal, and spatial factors. In Chapter 3, we developed machine learning models to capture the complex, nonlinear relationships between variables such as SPM concentrations, current velocity, and turbulent shear rate, accounting for the highly variable and noisy nature of the data to assess temporal fluctuations in bed levels. Chapter 4 applied these models to predict bed level changes under future SLR scenarios.

5.1. How Do Factors Influencing Deposition-Resuspension Processes Affect Intertidal Areas as Accommodation Spaces?

In Chapter 2 of this thesis, the investigation focused on whether the intertidal zones in the Scheldt estuary effectively functioned as accommodation spaces for SPM, facilitating sediment deposition and contributing to the estuary's long-term stability. To address this question, high-frequency, biweekly observations were conducted over the course of a year (2018–2019) at three distinct intertidal sites: Branst (freshwater zone), Lillo (brackish zone), and Zuidgors (saline zone). The results indicated that the capacity of these zones to serve as accommodation spaces for SPM was highly site-specific and closely linked to the dynamics of floc formation and breakdown. These processes were, in turn, influenced by seasonal biological activity (Fettweis et al., 2022; Lai et al.,

2018; Cox et al., 2019) and localized hydrodynamic forces (Horemans et al., 2021; Dyer & Manning, 1999).

However, the short-term sedimentation and erosion patterns observed in this study deviated from the long-term morphological trends documented in the Scheldt estuary. The observed differences between short-term patterns and long-term trends emphasized that sedimentation and erosion in the Scheldt estuary were not only site-specific but were also shaped by a complex interplay of natural and anthropogenic factors. To contextualize these findings, Figure 5.2, adapted from Chapter 2, was included to illustrate the interconnected factors driving sedimentation and erosion in the Scheldt estuary.

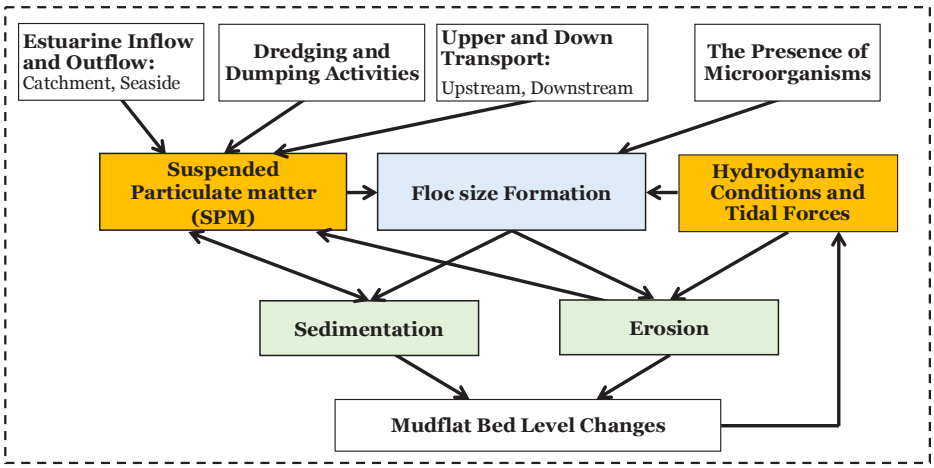

Figure 5.2. Conceptual diagram illustrating the processes influencing bed level dynamics in intertidal mudflats. SPM enters the system through multiple sources. It contributes directly to sedimentation, establishing a bidirectional relationship in which bed level changes also influence SPM behavior. SPM further promotes floc formation, particularly in the presence of microorganisms. The fate of these flocs, whether settling or remaining in suspension, is governed by hydrodynamic conditions such as tidal currents and turbulence. Changes in bed elevation, in turn, alter local hydrodynamics by modifying water depth, flow velocity, and turbulence, completing a feedback loop. Fully understanding mudflat evolution over time requires accounting for the combined influence of all these drivers, rather than isolating individual processes.

One of the key points in this figure was how SPM were influenced by various processes within the estuary. Estuarine inflow and outflow described the natural water movement caused by tidal cycles, which transported sediments in both directions. In addition, dredging and dumping activities, driven by human interventions to maintain navigable waterways, involved removing (dredging) and depositing (dumping) sediments, often disrupting the sediment balance.

Furthermore, upper and downstream transport reflected the movement of suspended sediments along the estuary, driven by tidal flows and riverine input. All these processes can influence sediment dynamics, and when they occur together, they create a complex system that makes predicting sediment behavior difficult.

In this study, the freshwater zone (Branst) exhibited the highest seasonal variability in bed-level dynamics, alternating between sedimentation in spring/autumn and erosion in summer/winter. These patterns were closely tied to seasonal river discharge variations, which controlled both sediment supply and turbulence levels (Temmerman et al., 2023; Cox et al., 2019; Horemans et al., 2021). Notably, summer erosion occurred despite the presence of large flocs and high macrofloc proportions, suggesting that these flocs were structurally fragile and prone to resuspension. In winter, increased SPM and positive SCI values confirmed mud-dominated suspensions, yet high turbulence prevented deposition. Over longer timescales, Branst remained relatively stable due to its ebb-dominant flow regime. However, decadal monitoring revealed a shift from slight erosion (pre-2015) to sedimentation (2016–2019) (Van Braeckel et al., 2019), showing that even morphodynamically stable zones could experience temporal shifts due to variations in sediment supply and river flow.

Lillo presented a relatively stable sediment regime throughout the year, with only minor erosion in summer. The site's moderate salinity helped enhance flocculation efficiency due to the charge-neutralizing effect of salt ions (Edzwald et al., 1974; Dyer, 1995; Winterwerp, 2002). Despite favorable conditions for floc formation, the correspondence between floc size and net bed-level change was weak—particularly in summer, when negative SCI values indicated structurally dense flocs behaving like sand. Long-term data revealed net erosion (~9 cm loss between 2009–2019) (Van Braeckel et al., 2019), largely attributed to repeated dredging activities, which disturbed bed structure, interfered with floc formation, and suppressed the stabilizing effects of biological processes. Thus, Lillo's apparent morphological stability concealed the reality of a heavily managed and artificially regulated sediment regime.

Zuidgors illustrated the challenges of maintaining sediment balance in high-energy, sand-rich intertidal zones. Although macroflocs were present year-round, especially in spring and summer, their structural fragility and the dominance of flood-driven tidal resuspension hindered long-term accumulation. Long-term trends showed persistent erosion, interrupted only by a temporary phase of sedimentation due to dredge spoil deposition (1994–2005) (Elias et al., 2023). Since then, net bed-level loss resumed, compounded by consistent dredging and a deepening channel profile (Scheldecommissie et al., 2023). SCI values further suggested that while flocs were present, they

might have been acoustically indistinguishable from compacted particles or sand—again raising concerns about their sedimentation potential under turbulent marine conditions.

In conclusion, the analysis in Chapter 2 demonstrated that the ability of intertidal areas to function as accommodation spaces was not a fixed property, but a dynamic outcome of biological cohesion, floc structure, hydrodynamic conditions, sediment availability, and anthropogenic disturbance. Branst, Lillo, and Zuidgors each exhibited distinct sediment behaviors that challenged the notion of static depositional or erosional zones. Understanding how short-term variability interacted with long-term trends was essential for predicting future sediment pathways and for managing estuarine morphology under continued environmental and human pressures

5.2. Is There a Model to Easily Assess the Relative Impact of Temporal Fluctuations on Bed Level Changes?

Chapter 3 of this thesis addressed the modeling of temporal fluctuations in bed level changes. To explore this, machine learning (ML) models were developed and evaluated—specifically, Random Forest (RF) Regression and Artificial Neural Networks (ANN)—to predict bed level changes in the Scheldt estuary based on key environmental variables. These model input variables (features) included SPM concentration, floc size, current velocity, turbulent shear rate (G), tidal range, and seasonal variations—parameters whose roles in sediment dynamics were discussed in the previous section. Tidal forces emerged as key drivers of sediment transport, with site-specific dynamics: flood dominance at Zuidgors promoted deposition under moderate conditions but led to erosion in winter; ebb dominance at Branst drove sediment export influenced by seasonal floc variations; and balanced asymmetry at Lillo stabilized coarser particle deposition during high SPM availability.

The goal of this modeling study was to better understand and predict sedimentation/erosion patterns in the Scheldt estuary, a highly complex and dynamic environment. Estuaries like the Scheldt were constantly influenced by various factors, including tides, currents, biological activity, and human interventions such as dredging (Winterwerp & van Kesteren, 2004; Elliott & Whitfield, 2011). These factors interacted in a mesh of complex dependencies, making it difficult to forecast how sediments would settle, erode, or move over time. Thus, a model was needed to effectively identify correlations between the parameters.

To achieve this, experiments were conducted by training and evaluating the models under different conditions: (1) comparing performance with and without season as a feature, (2) training

on individual seasonal data across all stations, and (3) assessing site-specific models trained on data from all seasons. The findings showed that while both models were able to predict bed level changes fairly well, the RF model consistently outperformed the ANN model. In non-seasonal models, RF identified tidal range as the key factor influencing sediment dynamics, aligning with findings from Dyer (1988) and Fettweis & Van den Eynde (2003). Furthermore, including seasonality improved RF accuracy, demonstrating its capacity to capture seasonal differences. Seasonal models revealed that turbulent shear rate (G) was critical in cooler months, highlighting the importance of high energy on sediment dynamics (Dyer & Manning, 1999), while floc size became more significant in warmer months due to seasonal factors affecting floc formation.

Moreover, the site-specific models showed that predictions at Lillo were more consistent, while greater variability was observed at Branst and Zuidgors, likely due to site-specific factors such as salinity and freshwater discharge. Notably, tidal range and floc size emerged as key factors influencing sediment transport, whereas SPM concentration played a more significant role at Zuidgors. These findings underscored RF's ability to generalize across sites, highlighting its potential for developing broader estuary prediction models, particularly in under-studied regions.

This study demonstrated that ML models, particularly RF, served as effective tools for predicting sedimentation patterns, offering more predictive power and flexibility compared to more classical sediment transport models. In contrast to classical models, which relied on simplified relationships and deterministic equations grounded in physical principles such as the conservation of mass and energy (Partheniades, 1965; Krone, 1962; Boelens et al., 2020), ML models learned from data, allowing them to capture more complex, nonlinear interactions. Classical models often required extensive field data gathering processes including calibration and validation, which were time-consuming and resource-intensive. By comparison, ML models did not depend on predefined equations but learned from data, potentially excelling at capturing complex, nonlinear interdependencies between multiple variables. Due to their inherent capability to learn generalized patterns, they proved particularly valuable when dealing with highly variable, noisy measurements or integrating data from multiple sources (Francke et al., 2008; Ouellet-Proulx et al., 2016). For example, sediment transport in the Scheldt estuary was influenced by hydrodynamic forces and biological activities affecting floc formation and breakdown. ML models like RF and ANN were capable of learning these intricate patterns and adjusting their predictions accordingly, making them effective for predicting short-term sediment behavior under various environmental scenarios.

However, despite their advantages, ML models lacked the mechanistic insight into physical processes that classical models provided. Classical models offered process-based understanding

rooted in fundamental physical laws, whereas ML models focused on identifying patterns from data. Thus, integrating ML models for short-term predictions with classical models for long-term, process-based understanding created a more comprehensive framework for sediment transport modeling. This combined approach was found to be especially valuable given the potential impacts of climate change and SLR, which could introduce new, complex, and nonlinear interactions—such as altered wave dynamics and shifting sediment supplies—that diverged from traditional expectations. ML models were particularly adept at capturing these intricate dependencies, making them essential for accurate predictions in evolving environmental conditions.

5.3. How Effective Is ML Modeling?

As discussed in the introduction, the Scheldt Estuary has undergone significant transformations in recent decades due to anthropogenic interventions such as dredging, channel deepening, and land reclamation, combined with broader environmental pressures. These changes have altered tidal propagation, increased suspended sediment concentrations, and disrupted the estuary's sediment balance and ecological functioning. Changes in tidal range can intensify hydrodynamic energy within intertidal zones, influencing sediment resuspension, deposition patterns, and the structural stability of flocs. As a result, future shifts in tidal forcing may contribute to increasingly variable sedimentation and erosion dynamics across the estuary.

Building on this context, Chapter 4 focused on understanding how sedimentation and erosion processes in the Scheldt Estuary might evolve under future conditions. Specifically, it evaluated whether the ML models, specifically RF models, captured the interactions among hydrodynamic conditions, floc characteristics, and SPM concentrations to predict sediment stability, providing insights for managing these challenges effectively. To achieve this, a scenario-based modeling framework was developed using high-frequency field data collected from three stations—Branst (freshwater), Lillo (brackish), and Zuidgors (saline)—across multiple seasons. Tidal range (TR) served as the primary variable for scenario-based projections, with +5% and +10% increases representing plausible future changes. Based on observed correlations, the variables (SPM, D50, G, velocity) were projected using either regression or Random Forest models, depending on their relationship with TR. This approach was grounded in empirical patterns from the 2018–2019 dataset, specifically correlations between TR and input variables, and between those inputs and bed level change. Thus, the projections are not treated as black-box outputs but as extensions of observed sediment behavior under altered tidal conditions.

The results demonstrated that estuarine responses to tidal amplification are not uniform, but instead vary by site and season due to local hydrodynamic energy, sediment supply, and floc

cohesion. At Branst (freshwater zone), the system showed high sensitivity to seasonal shifts in floc stability and shear stress, with increased tidal range often corresponding to a transition from net deposition to erosion—particularly in conditions where enhanced turbulence inhibited floc formation, such as in spring. At Lillo (brackish zone), sedimentation remained stable or increased under future scenarios, consistent with the site's strong TR–SPM correlations and supply-dominated sediment dynamics. At Zuidgors (saline zone), model results were more variable, with erosion prevailing during high-energy periods and floc-based sedimentation limited by turbulence—even when larger flocs were present. These outcomes reinforce that sediment behavior is strongly governed by both energy regimes and the structural integrity of flocs.

Importantly, the projections aligned well with both the empirical data and known long-term trends in estuarine morphology and sediment transport. The spatial variability in projected bed level change mirrored observed site-specific behaviors, reinforcing the value of RF models in capturing complex sediment dynamics. However, the analysis also highlighted limitations, particularly in scenarios with low correlation where projection accuracy was reduced. The chapter acknowledges that while RF models are powerful tools for identifying dominant controls on sediment dynamics, their reliability depends on the quality and representativeness of input data.

In conclusion, Chapter 4 highlights the value of integrating high-resolution field observations with data-driven modeling to investigate site-specific sediment responses under plausible future tidal conditions. While these models do not replace process-based physical models, they serve as valuable tools for screening scenarios, guiding monitoring efforts, and informing sediment management. As climate change continues to impact estuarine systems and their behavior becomes increasingly complex, maintaining system resilience will require more integrated, data-driven strategies that account for both natural variability and human influences.

5.4. General Conclusions

In this thesis, an investigation was conducted to determine whether the Scheldt estuary's intertidal zones could effectively accommodate SPM. The study began by focusing on how hydrodynamic forces, flocculation dynamics, and SPM concentrations influenced deposition and resuspension processes across different parts of the estuary's intertidal zones, which were characterized by distinct environmental conditions and salinity gradients. The primary findings revealed that sediment dynamics were closely tied to the formation and stability of flocs, which were driven by seasonal biological activity and localized hydrodynamic energy. Floc structure and cohesion were identified as critical factors determining whether sediments were deposited or resuspended, underscoring the complexity of sediment behavior in response to varying environmental forces.

To better predict these trends, ML models—RF and ANN—were developed, which effectively captured the complex relationships among the key variables influencing bed level changes. These models accounted for temporal fluctuations and site-specific conditions, providing valuable insights into the drivers of sedimentation and erosion, consistent with the primary findings and previous studies. The integration of ML approaches offered a robust tool for predicting short-term sediment behavior, addressing the limitations of classical process-based models, which often struggled with the complexity of highly variable estuarine environments.

By applying these models to future scenarios involving increased tidal ranges, potential changes in sediment dynamics under evolving environmental conditions were projected. The predictions effectively captured the key relationships governing sediment stability, demonstrating the models' utility for future projections. Moreover, a comparison of the results with other studies emphasized the importance of conducting longer and periodically augmented measurement campaigns to supply ML models with sufficient data, allowing them to capture various seasonal trends. For instance, this approach helped identify patterns such as gradual sediment accumulation or loss, which could significantly affect the estuary's morphology over time.

While these studies focused on the Scheldt intertidal areas, the methodology—based on capturing trends between key parameters—was found to be applicable to other intertidal zones as well. This adaptability highlighted the broader relevance of the approach in addressing sediment dynamics across different estuarine environments.

5.5. Implication For the Scheldt Estuary

In this section, several potential implications of the results for the Scheldt estuary are outlined.

5.5.1. Management

The findings from Chapter 2 revealed that sediment dynamics in the Scheldt estuary's intertidal zones were significantly influenced by flocculation processes, which depended on hydrodynamic forces and biological activity. This understanding implies that effective management can benefit from preserving conditions that promote floc stability and sediment deposition. For example, adjusting dredging schedules to avoid periods when biological activity enhances floc cohesion may minimize disruption to natural sedimentation processes. Additionally, conserving and restoring habitats that support floc-forming organisms, such as microphytobenthos, enhances the estuary's capacity to trap sediments. By aligning dredging and habitat management practices with the

natural sediment dynamics identified in this study, sediment retention can be improved, and the estuary's ecological health better maintained.

5.5.2. Monitoring

Chapter 3 demonstrated that ML models, particularly RF regression, were effective in predicting bed level changes by capturing complex relationships among environmental variables. This suggests that current monitoring programs should prioritize the collection of high-frequency, detailed data on key parameters such as SPM concentrations, floc sizes, current velocities, and turbulence levels. Implementing advanced monitoring equipment and establishing robust data management systems can improve the quality of data used in predictive models. By integrating these models into the monitoring framework, changes in sediment dynamics can be more accurately anticipated, allowing for proactive responses to potential erosion or sedimentation issues. Therefore, the findings support the enhancement of monitoring efforts to facilitate more informed and effective estuarine management.

5.5.3. Climate Change Adaptation

In Chapter 4, the application of predictive models to SLR scenarios indicated that increased tidal energy might alter sedimentation and erosion patterns in the estuary. This finding suggests that climate change adaptation strategies should focus on reinforcing and adapting intertidal zones to maintain their role in sediment accommodation under changing conditions. Practical measures include restoring and protecting intertidal habitats to enhance their resilience and sediment-trapping capacity. Infrastructure planning should incorporate adaptive designs that accommodate natural sediment processes, such as permeable structures that allow sediment flow and support habitat connectivity. By applying these insights, adaptation efforts can be more effectively targeted to preserve the estuary's ecological integrity and functionality in the face of climate change.

5.6. Opportunities For Further Research

In this section, ideas for further research are proposed that follow naturally from the results and would broaden the research scope of this thesis.

5.6.1. Long-Term Monitoring and Model Validation

The predictive models were based on data from 2018–2019, and discrepancies with more recent data highlighted the importance of continuous validation and refinement. Incorporating real-time data from ongoing monitoring efforts, such as those reported in recent studies, is expected to allow for more accurate predictions and improved responsiveness to changing conditions. Future research should prioritize establishing long-term monitoring programs that collect high-frequency data on key parameters such as SPM concentrations, floc characteristics, hydrodynamic conditions, and biological activity. This approach will improve model accuracy and enhance understanding of sediment dynamics over time, thereby supporting adaptive estuarine management.

5.6.2. Development of Dynamic and Adaptive Modeling Approaches

Building upon the findings of this study, there is a clear need to develop models capable of accommodating unexpected shifts in essential parameters, particularly SPM concentrations. The observed decrease in SPM levels in 2023, which contrasted with the sustained high concentrations assumed in the predictive scenarios, had significant implications for sediment stability, leading to increased erosion at key locations such as Branst and Lillo. This discrepancy highlights the limitations of static models and underscores the importance of integrating dynamic, adaptive mechanisms into modeling approaches.

Future research should focus on training models that account for fluctuations in SPM availability, driven by variable river discharge, upstream sediment management practices, and climatic variability. By incorporating these dynamics, models can more accurately simulate sedimentation and erosion processes across a range of environmental scenarios, enhancing their utility for estuarine management and policy development. Advancing modeling capabilities in this direction will not only improve predictive accuracy but also support proactive strategies to mitigate erosion and preserve the ecological integrity of the Scheldt estuary under evolving environmental conditions.

5.6.3. In-Depth Investigation of Flocculation Processes

Another important direction for future research is to deepen the understanding of how floc size, turbulent shear rate, and sediment dynamics interact under increasing tidal ranges due to SLR. While this study demonstrated that floc size significantly influenced whether net sedimentation or erosion occurred, the mechanisms governing floc formation and stability under variable hydrodynamic conditions remain only partially understood.

Future work should incorporate biological factors into models to enhance their predictive accuracy. High-resolution field measurements can be integrated with ML models to examine how biological processes—such as the production of cohesive organic substances—and physical forces like turbulence affect floc behavior. This knowledge will improve model performance and inform more effective sediment management strategies aimed at promoting floc stability and sediment retention—both of which are essential for mitigating erosion and safeguarding estuarine ecosystems like the Scheldt estuary.

5.6.4. Integration of Adaptive Management Strategies

Given the variability of environmental drivers—including climatic events, human interventions, and sediment management practices—there is a need to develop flexible modeling frameworks, such as ML-based approaches, that can adapt to evolving conditions. Future research should explore the integration of adaptive management strategies within these models to support timely and informed intervention decisions.

For example, while sediment disposal in areas near Zuidgors was observed to temporarily buffer against net sediment export by increasing SPM levels and promoting floc formation, rising tidal ranges and increased turbulence are expected to reduce its long-term effectiveness. Adaptive strategies could include optimizing disposal locations, improving sediment trapping mechanisms, and adjusting dredging schedules to maintain bed stability over time.

Bibliography

1. Barneveld, H., R. Nicolai, M. van Veen, S. van Haaster, T. Boudewijn, J. de Jong, K. van Didderen et al. "*Analyserapport: T2015-rapportage Schelde-estuarium*." Report PR3152. HKV Lijn in Water (Lelystad) 886 (2018).
2. Boelens, T., Schuttelaars, H., Plancke, Y., & De Mulder, T. (2020). *Historical and future development of the tidally averaged transport of sandy sediments in the Scheldt estuary: a 2D exploratory model.* Ocean Dynamics, 70, 481-504.
3. Chen, M. S., Wartel, S., & Temmerman, S. (2005). *Seasonal variation of floc characteristics on tidal flats, the Scheldt estuary*. Hydrobiologia, 540, 181-195.
4. Chmura, G. L., Anisfeld, S. C., Cahoon, D. R., & Lynch, J. C. (2003). *Global carbon sequestration in tidal, saline wetland soils*. Global biogeochemical cycles, 17(4).
5. Coen, I. (2008). *De eeuwige Schelde? Ontstaan en ontwikkeling van de Schelde*. Technical Report D/2007/3241/203, waterbouwkundig laboratorium.
6. Cox, T. J. S., Maris, T., Van Engeland, T., Soetaert, K., & Meire, P. (2019). *Critical transitions in suspended sediment dynamics in a temperate meso-tidal estuary*. Scientific reports, 9(1), 12745.
7. Dam, G., Van der Wegen, M., Labeur, R. J., & Roelvink, D. (2016). *Modeling centuries of estuarine morphodynamics in the Western Scheldt estuary*. Geophysical Research Letters, 43(8), 3839-3847.
8. Dam, G., Van der Wegen, M., Taal, M., & Van der Spek, A. (2022). *Contrasting behaviour of sand and mud in a long-term sediment budget of the Western Scheldt estuary*. Sedimentology, 69(5), 2267-2283.
9. de Jonge, V. N., Schuttelaars, H. M., van Beusekom, J. E., Talke, S. A., & de Swart, H. E. (2014). *The influence of channel deepening on estuarine turbidity levels and dynamics, as exemplified by the Ems estuary*. Estuarine, Coastal and Shelf Science, 139, 46-59.
10. Dijkstra, Y. M., Schuttelaars, H. M., & Schramkowski, G. P. (2019). *A regime shift from low to high sediment concentrations in a tide-dominated estuary*. Geophysical Research Letters, 46(8), 4338-4345.
11. Dyer, K. R. (1988). *Fine sediment particle transport in estuaries*. In Physical processes in estuaries (pp. 295-310). Berlin, Heidelberg: Springer Berlin Heidelberg.
12. Dyer, K. R., & Manning, A. J. (1999). *Observation of the size, settling velocity and effective density of flocs, and their fractal dimensions*. Journal of sea research, 41(1-2), 87-95.
13. Elias, E. P., Van der Spek, A. J., Wang, Z. B., Cleveringa, J., Jeuken, C. J., Taal, M., & Van der Werf, J. J. (2023). *Large-scale morphological changes and sediment budget of the Western Scheldt estuary 1955–2020: the impact of large-scale sediment management*. Netherlands Journal of Geosciences, 102, e12.
14. Elliott, M., & Whitfield, A. K. (2011). *Challenging paradigms in estuarine ecology and management*. Estuarine, Coastal and Shelf Science, 94(4), 306-314.
15. Fettweis, M., & Van den Eynde, D. (2003). *The mud deposits and the high turbidity in the Belgian–Dutch coastal zone, southern bight of the North Sea*. Continental Shelf Research, 23(7), 669-691.

16. Fettweis, M., Baeye, M., Van der Zande, D., Van den Eynde, D., & Joon Lee, B. (2014). *Seasonality of floc strength in the southern North Sea*. Journal of Geophysical Research: Oceans, 119(3), 1911-1926.
17. Fettweis, M., Riethmüller, R., Verney, R., Becker, M., Backers, J., Baeye, M., ... & Vereecken, H. (2019). *Uncertainties associated with in situ high-frequency long-term observations of suspended particulate matter concentration using optical and acoustic sensors*. Progress in Oceanography, 178, 102162.
18. Fettweis, M., Schartau, M., Desmit, X., Lee, B. J., Terseleer, N., Van der Zande, D., ... & Riethmüller, R. (2022). *Organic matter composition of biomineral flocs and its influence on suspended particulate matter dynamics along a nearshore to offshore transect*. Journal of Geophysical Research: Biogeosciences, 127(1), e2021JG006332.
19. Francke, T., López-Tarazón, J. A., & Schröder, B. (2008). *Estimation of suspended sediment concentration and yield using linear models, random forests and quantile regression forests*. Hydrological Processes: An International Journal, 22(25), 4892-4904.
20. Horemans, D. M., Dijkstra, Y. M., Schuttelaars, H. M., Sabbe, K., Vyverman, W., Meire, P., & Cox, T. J. (2021). *Seasonal variations in flocculation and erosion affecting the large-scale suspended sediment distribution in the Scheldt estuary: the importance of biotic effects*. Journal of Geophysical Research: Oceans, 126(4), e2020JC016805.
21. Jiang, L., Gerkema, T., Idier, D., Slangen, A., & Soetaert, K. (2020). *Effects of sea-level rise on tides and sediment dynamics in a Dutch tidal bay*. Ocean Science, 16(2), 307-321.
22. Krone, R. B. (1962). *Flume studies of transport of sediment in estrarial shoaling processes*. Final Report, Hydr. Engr. and Samitary Engr. Res. Lab., Univ. of California.
23. Maris, T., P. Gelsomini & J. Schoelynck, 2024. *Onderzoek naar de gevolgen van het Sigmaplan, baggeractiviteiten en havenuitbreiding in de Zeeschelde op het milieu*. Geïntegreerd eindverslag van het onderzoek verricht in 2023. ECOSPHERE 024-RES023. Universiteit Antwerpen, Antwerpen.
24. Meire, P., Plancke, Y., Govaerts, A., Cox, T., Gelsomi, P., Horemans, D., Meire, D., Meire, L., Zetsche, E. and Maris,T. (2021). *Synthesis note: SPM dynamics and trends in the Scheldt estuary*. ECOBE Report 021-R267 Universiteit Antwerpen, Antwerpen.
25. Meire, P., Ysebaert, T., Damme, S. V., Bergh, E. V. D., Maris, T., & Struyf, E. (2005). *The Scheldt estuary: a description of a changing ecosystem*. Hydrobiologia, 540, 1-11.
26. Ouellet-Proulx, S., St-Hilaire, A., Courtenay, S. C., & Haralampides, K. A. (2016). *Estimation of suspended sediment concentration in the Saint John River using rating curves and a machine learning approach*. Hydrological Sciences Journal, 61(10), 1847-1860.
27. Partheniades, E. (1965). *Erosion and deposition of cohesive soils*. Journal of the Hydraulics Division, 91(1), 105-139.
28. Plancke, Y. M. G., Vandebroek, E., Claeys, S., & Meire, D. (2017). *Sediment transport in the Schelde-estuary: The challenge of performing good measurements in challenging conditions*. Hydraulic Measurements and Experimental Methods 2017 Conference (HMEM 2017.
29. Temmerman, S., Govers, G., Meire, P., & Wartel, S. (2003). *Modelling long-term tidal marsh growth under changing tidal conditions and suspended sediment concentrations, Scheldt estuary, Belgium*. Marine Geology, 193(1-2), 151-169.

30. Temmerman, S., Horstman, E. M., Krauss, K. W., Mullarney, J. C., Pelckmans, I., & Schoutens, K. (2023). *Marshes and mangroves as nature-based coastal storm buffers*. Annual Review of Marine Science, 15(1), 95-118.
31. Temmerman, S., Meire, P., Bouma, T. J., Herman, P. M., Ysebaert, T., & De Vriend, H. J. (2013). *Ecosystem-based coastal defence in the face of global change*. Nature, 504(7478), 79-83.
32. Van Braeckel A., Elsen R & Van Ryckegem, G. (2019). *MONEOS monitoringsoverzicht en 1ste lijnsrapportage geomorfologie en diversiteit habitats*. Rapporten van het Instituut voor Natuur- en Bosonderzoek 2019 (33). *Instituut voor Natuur- en Bosonderzoek, Brussel*. DOI: doi.org/10.21436/inbor.16703072
33. Van Putte, N., Cox, T., Van Damme, S., & Maris, T. (2022). *IMMERSE: Modelling study on sediment management in estuaries*. Universiteit Antwerpen, Report, 3.
34. Van Ryckegem, G., et. al. (2023). *MONEOS - Geïntegreerd datarapport INBO: Toestand Zeeschelde 2022. Monitoringsoverzicht en 1ste lijnsrapportage Geomorfologie, diversiteit Habitats en diversiteit Soorten*. Rapporten van het Instituut voor Natuur- en Bosonderzoek 2023 (45). Instituut voor Natuur- en Bosonderzoek, Brussel. DOI: 10.21436/inbor.98471395
35. Vandenbruwaene, W., Stark, J., Plancke, Y., & Mostaert, F. (2020). *Agenda for the Future–Historical evolution of tides and morphology of the Scheldt estuary: subreport 5*. Synthesis. WL Reports.
36. Winterwerp, J. C., & Van Kesteren, W. G. (2004). *Introduction to the physics of cohesive sediment dynamics in the marine environment*. Elsevier.
37. Winterwerp, J. C., & Wang, Z. B. (2013). *Man-induced regime shifts in small estuaries—I: theory*. Ocean Dynamics, 63, 1279-1292.
38. Ysebaert, T. J., Herman, P. M. J., Hummel, H., Schaub, B., Sistermans, W. C. H., & Heip, C. H. R. (2002). *Monitoring and predictive modelling of estuarine benthic macrofauna and their relevance to resource management problems*. VLIZ Special Publication.

Acknowledgments

My Ph.D. journey would not have been possible without the unwavering support, trust, and kindness of so many people. Below, I would like to acknowledge some who particularly helped and inspired me during my Ph.D.

First and foremost, Patrick Meire, thank you for trusting me with this PhD and believing in the ideas I brought forward. Being given the freedom to pursue and shape my own research path was a great responsibility, and I am truly grateful for your support throughout.

To the jury members, your thoughtful feedback and encouragement sharpened my thinking and helped me approach my work with greater clarity. I learned a great deal from your insights—thank you.

My Ph.D. began on March 15, 2020, the first day of Belgium's COVID lockdown. I didn't even know if my flight would take off amidst the global uncertainty. In that moment, an email from Lotte Oosterlee arrived—asking for my flight details and offering to pick me up. That simple gesture lit up a confusing period, and so many more after. Throughout my PhD, whenever I was stuck, I knew I could always turn to you. Thank you for being my guide, support, and calm in the storm—always, without hesitation.

Dorian Bas, I still remember how we met just once before my PhD officially started—you helped me find my way to the bus station. I had no idea then that we would share an office for 4.5 years and go through all the ups and downs together. Thank you for being there every step of the way.

Sarah Hautekiet, I'll never forget our endless chats about absolutely everything. From post-BBQ strolls to our regular Komida breaks, every cinnamon chai latte will forever remind me of those fun, candid conversations with you. Thank you for always bringing joy and laughter into my PhD journey!

I also thank my wonderful colleagues for the meaningful discussions and warm memories. A special thank you to Mona Huyzentruyt, Ignace Pelckmans, Ken Schoutens, and Harvey Suello for making work life better in so many ways.

A heartfelt thanks to Tom Maris, Jonas Schoelynck, and Jean-Philippe Belliard for showing me what it means to be generous with your time, your knowledge, and your encouragement. Your mentorship set an example I hope to carry forward.

To my dear friend Sümeyra Akarçeşme, your dedication and strength in research have always inspired me. I'd love to share every "docop point" in life with you, because your presence makes even the toughest moments meaningful.

To my family, thank you for bearing the weight of distance throughout my immigration with such incredible strength and grace. Even in your hardest moments, you hid your pain just to ease mine—you never let me see your sadness and always reminded me to stay focused on my life. That quiet sacrifice, that unconditional love, was my anchor. I carry your strength with me every single day.

And finally, to my beloved husband, Morteza Behrooz, words will never fully capture what your love has meant to me. Thank you for your endless patience, listening to my countless stories, your quiet strength, and for believing in me even when I doubted myself. You stood by me through every challenge, celebrated every small victory, and lifted me when I fell. Whatever I have achieved, I achieved with you.

I hope that someday soon, the world will be a kinder and more beautiful place—a world where science lights the path, and every person has the chance to learn, grow, compete, and live with dignity.